Volume 67A
Number 1
Jan.–Feb. 1963

Physics and Chemistry

6

U.S. DEPARTMENT OF COMMERCE

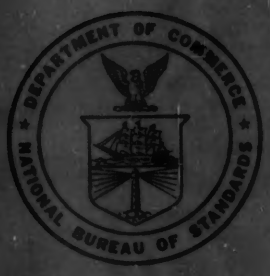

SECTION A

JOURNAL OF RESEARCH

NATIONAL BUREAU OF STANDARDS

Journal of Research

of the

National Bureau of Standards

A. Physics and Chemistry

JAN.–FEB. • 1963

VOLUME • 67A

NUMBER • 1

Editor: C. W. Beckett

Associate Editors: D. D. Wagman
J. M. Richardson

Publication dates:
Feb. 1, Apr. 1, June 1, Aug. 1, Oct. 1, Dec. 1, 1963.

JOURNAL OF RESEARCH

The National Bureau of Standards Journal of Research reports research and development in the fields of activity shown at right. Also included from time to time are survey articles on topics closely related to the Bureau's scientific and technical program.

The Journal is published in four separate sections as follows:

A. Physics and Chemistry

Contains papers of interest primarily to scientists working in these fields. Issued six times a year. Annual subscription: domestic, $4.00; foreign, $4.75.

B. Mathematics and Mathematical Physics

Presents studies and compilations designed mainly for the mathematician and the theoretical physicist. Issued quarterly. Annual subscription: domestic, $2.25; foreign, $2.75.

C. Engineering and Instrumentation

Reports research and development results of interest chiefly to the engineer and the applied scientist. Issued quarterly. Annual subscription: domestic, $2.25; foreign, $2.75.

D. Radio Propagation

Reports work in radio propagation, upper atmospheric physics and communications. Issued six times a year. Annual subscription: domestic, $4.00; foreign, $4.75.

Functions and Activities

The functions of the National Bureau of Standards are set forth in the Act of Congress, March 3, 1901, as amended. These include the development and maintenance of the national standards of measurement and the provision of means and methods for making measurements consistent with these standards; the determination of physical constants and properties of materials; the development of methods and instruments for testing materials, devices, and structures; advisory services to government agencies on scientific and technical problems; invention and development of devices to serve special needs of the Government; and the development of standard practices, codes, and specifications. The work includes basic and applied research, development, engineering, instrumentation, testing, evaluation, calibration services, and various consultation and information services. The Bureau also serves as the Federal technical research center in a number of specialized fields. The scope of activities of the National Bureau of Standards is suggested in the following listing of the divisions and sections engaged in technical work.

Washington, D.C.

Electricity. Resistance and Reactance. Electrochemistry. Electrical Instruments. Magnetic Measurements. Dielectrics. High Voltage.
Metrology. Photometry and Colorimetry. Refractometry. Photographic Research. Length. Engineering Metrology. Mass and Scale. Volumetry and Densimetry.
Heat. Temperature Physics. Heat Measurements. Cryogenic Physics. Equation of State. Statistical Physics.
Radiation Physics. X-ray. Radioactivity. Radiation Theory. High Energy Radiation. Radiological Equipment. Nucleonic Instrumentation. Neutron Physics.
Analytical and Inorganic Chemistry. Pure Substances. Spectrochemistry. Solution Chemistry. Standard Reference Materials. Applied Analytical Research. Crystal Chemistry.
Mechanics. Sound. Pressure and Vacuum. Fluid Mechanics. Engineering Mechanics. Rheology. Combustion Controls.
Polymers. Macromolecules: Synthesis and Structure. Polymer Chemistry. Polymer Physics. Polymer Characterization. Polymer Evaluation and Testing. Applied Polymer Standards and Research. Dental Research.
Metallurgy. Engineering Metallurgy. Microscopy and Diffraction. Metal Reactions. Metal Physics. Electrolysis and Metal Deposition.
Inorganic Solids. Engineering Ceramics. Glass. Solid State Chemistry. Crystal Growth. Physical Properties. Crystallography.
Building Research. Structural Engineering. Fire Research. Mechanical Systems. Organic Building Materials. Codes and Safety Standards. Heat Transfer. Inorganic Building Materials. Metallic Building Materials.
Applied Mathematics. Numerical Analysis. Computation. Statistical Engineering. Mathematical Physics. Operations Research.
Data Processing Systems. Components and Techniques. Computer Technology. Measurements Automation. Engineering Applications. Systems Analysis.
Atomic Physics. Spectroscopy. Infrared Spectroscopy. Solid State Physics. Electron Physics. Atomic Physics.
Instrumentation. Engineering Electronics. Electron Devices. Electronic Instrumentation. Mechanical Instruments. Basic Instrumentation.
Physical Chemistry. Thermochemistry. Surface Chemistry. Organic Chemistry. Molecular Spectroscopy. Molecular Kinetics. Mass Spectrometry.
Office of Weights and Measures.

Boulder, Colorado

Cryogenic Engineering. Laboratory. Cryogenic Equipment. Cryogenic Processes. Properties of Materials. Cryogenic Technical Services.

Central Radio Propagation Laboratory

Ionosphere Research and Propagation. Low Frequency and Very Low Frequency Research. Ionosphere Research. Prediction Services. Sun-Earth Relationships. Field Engineering. Radio Warning Services. Vertical Soundings Research.
Radio Propagation Engineering. Data Reduction Instrumentation. Radio Noise. Tropospheric Measurements. Tropospheric Analysis. Propagation-Terrain Effects. Radio-Meteorology. Lower Atmosphere Physics.
Radio Systems. Applied Electromagnetic Theory. High Frequency and Very High Frequency Research. Modulation Research. Antenna Research. Navigation Systems.
Upper Atmosphere and Space Physics. Upper Atmosphere and Plasma Physics. Ionosphere and Exosphere Scatter. Airglow and Aurora. Ionospheric Radio Astronomy.

Radio Standards Laboratory

Radio Physics. Radio Broadcast Service. Radio and Microwave Materials. Atomic Frequency and Time-Interval Standards. Millimeter-Wave Research.
Circuit Standards. High Frequency Electrical Standards. Microwave Circuit Standards. Electronic Calibration Center.

U.S. DEPARTMENT OF COMMERCE
Luther H. Hodges, Secretary

NATIONAL BUREAU OF STANDARDS
A. V. Astin, Director

Order all publications from the Superintendent of Documents
U.S. Government Printing Office, Washington 25, D.C.

Use of funds for printing this publication approved by the Director of the Bureau of the Budget (June 19, 1961).

JOURNAL OF RESEARCH of the National Bureau of Standards—A. Physics and Chemistry
Vol. 67A, No. 1, January–February 1963

Heat of Formation of Calcium Aluminate Monosulfate at 25 °C

H. A. Berman and E. S. Newman

(October 9, 1962)

The heat of formation of calcium aluminate monosulfate, $3CaO{\cdot}Al_2O_3{\cdot}CaSO_4{\cdot}12H_2O$, at 25 °C, and of less completely hydrated samples of the same compound, was determined by the heat-of-solution method, with 2*N* HCl as the solvent, and $3CaO{\cdot}Al_2O_3{\cdot}6H_2O$(c) and $CaSO_4{\cdot}2H_2O$(c), as the reactants. The results were as follows:

	ΔH, kj/mole	ΔH, kcal/mole
$3CaO{\cdot}Al_2O_3{\cdot}CaSO_4{\cdot}12H_2O$(c)		
Heat of formation		
from elements, ΔH_f°		−2100
from reactants and H_2O(l)		− 15.0
Heat of solution in 2*N* HCl	− 495.7	− 118.5
Change of heat of solution with H_2O content at $12H_2O$, per mole H_2O		
$\frac{d(\Delta H)}{dn}$		1.93

The heat of the reaction (ΔH)
$3CaO{\cdot}Al_2O_3{\cdot}CaSO_4{\cdot}12H_2O(c) + 2(CaSO_4{\cdot}2H_2O)(c) + 15H_2O(l) \rightarrow 3CaO{\cdot}Al_2O_3{\cdot}3CaSO_4{\cdot}31H_2O(c)$
is −134.4 kj/mole or −32.1 kcal/mole. The heat of the reaction (ΔH)
$3CaO{\cdot}Al_2O_3{\cdot}CaSO_4{\cdot}12H_2O(c) + 2(CaSO_4{\cdot}2H_2O)(c) + 16H_2O(l) \rightarrow 3CaO{\cdot}Al_2O_3{\cdot}3CaSO_4{\cdot}32H_2O(c)$
is −144.9 kj/mole or −34.6 kcal/mole.

Values reported earlier for the heat of formation of calcium aluminate trisulfate and of calcium aluminate monocarbonate should be revised by adding −0.9 kcal/mole to each reported ΔH value, with the following resulting values:

	ΔH from appropriate reactants kcal/mole	ΔH_f° kcal/mole
$3CaO{\cdot}Al_2O_3{\cdot}3CaSO_4{\cdot}31H_2O$(c)	−47.01	−4123
$3CaO{\cdot}Al_2O_3{\cdot}3CaSO_4{\cdot}32H_2O$(c)	−49.52	−4194
$3CaO{\cdot}Al_2O_3{\cdot}CaCO_3{\cdot}10.68H_2O$(c)	−19.77	−1957

Conditions for the formation of the monosulfate from solution, and its properties on exposure to moisture, are discussed.

1. Introduction

Calcium aluminate monosulfate, $3CaO{\cdot}Al_2O_3{\cdot}CaSO_4{\cdot}12H_2O$, also referred to as calcium monosulfoaluminate, is one of two complex salts that may be formed by the aggressive action of sulfate waters on portland cement. It is also an intermediate or a final product in the hydration of most portland cements, derived from the gypsum and tricalcium aluminate which they contain in the anhydrous state. Depending on the availability of the various reacting compounds, either the monosulfate or calcium aluminate trisulfate, $3CaO{\cdot}Al_2O_3{\cdot}3CaSO_4{\cdot}31$–$33H_2O$, may be formed [1, 2].[1]

The aluminate sulfates are representative, respectively, of two series of complex calcium aluminates, which may be represented by the general formulas $3CaO{\cdot}Al_2O_3{\cdot}CaX{\cdot}nH_2O$ and $3CaO{\cdot}Al_2O_3{\cdot}3CaX{\cdot}mH_2O$, where *X* is a divalent ion or two units of a monovalent ion, *n* is 10 to 12, and *m* is approximately 32. As with many compounds encountered in portland cement chemistry, the water content is not always definite. Some of the water in these compounds is tightly bound chemically; the remainder is more loosely bound and capable of variation with the ambient temperature or humidity.

As part of a continuing investigation of the thermochemical properties of substances occurring in hydraulic cements and their reaction products, the heat of formation of hydrated calcium aluminate monosulfate has been determined.

Measurements by the heat-of-solution method were made of the heat evolved at 25 °C in the reaction

$$3CaO{\cdot}Al_2O_3{\cdot}6H_2O(c) + CaSO_4{\cdot}2H_2O(c) + 4H_2O(l) \xrightarrow{\Delta H_1} 3CaO{\cdot}Al_2O_3{\cdot}CaSO_4{\cdot}12H_2O(c) \quad (1)$$

[1] Figures in brackets indicate the literature references at the end of this paper.

The heat of this reaction is the difference between the sum of the heats of solution of the reactants and the heat of solution of the product, in accordance with the following equations:

$$3CaO\cdot Al_2O_3\cdot 6H_2O(c)+12HCl(aq)\xrightarrow{\Delta H_2}[3CaCl_2+2AlCl_3+12H_2O](aq) \quad (2)$$

$$CaSO_4\cdot 2H_2O(c)+[3CaCl_2+2AlCl_3+12H_2O](aq)\xrightarrow{\Delta H_3}[3CaCl_2+2AlCl_3+CaSO_4+14H_2O](aq) \quad (3)$$

$$4H_2O(l)+[3CaCl_2+2AlCl_3+CaSO_4+14H_2O](aq)\xrightarrow{\Delta H_4}[3CaCl_2+2AlCl_3+CaSO_4+18H_2O](aq) \quad (4)$$

$$3CaO\cdot Al_2O_3\cdot CaSO_4\cdot 12H_2O(c)+12HCl(aq)\xrightarrow{\Delta H_5}[3CaCl_2+2AlCl_3+CaSO_4+18H_2O](aq) \quad (5)$$

The summation, equation 2+equation 3+equation 4−equation 5, results in equation 1. Similar summation of the ΔH values results in ΔH_1.

The heat of solution of each of the reactants and of the product was measured in $HCl\cdot 26.61H_2O$ (2.00N HCl at 25 °C). The heats of formation of the reactants were taken from Circular 500 [3] of the National Bureau of Standards.

All calculations in this paper are based on the 1961 atomic weight table [4] and on the thermochemical calorie, defined as exactly 4.184 joules. Differences between the 1961 and 1957 atomic weight tables are insignificant for this work, and the results obtained are therefore consistent with work published earlier on calcium aluminate monocarbonate [5] and calcium aluminate trisulfate [6], except for the revisions to this earlier work noted in sections 4.5 and 4.7.

2. Preparation and Analysis of Samples

2.1. Preparation

The calcium aluminate sulfates can be formed as white precipitates when aqueous solutions of calcium hydroxide, sulfate ion, and of compounds containing aluminum ion or aluminate ion are mixed.

At room temperature the trisulfate is the eventual product in all aqueous concentration ranges studied. Within a limited concentration range, however, the monosulfate can be formed first and may be isolated by filtration before conversion to the trisulfate takes place. The conditions for formation of the monosulfate and for producing the compound in adequate quantity are discussed in the appendix to this paper.

Eight preparations of calcium aluminate monosulfate were made. Details of the reaction mixtures and of the products obtained are given in table 1, together with details of some mixtures in which the trisulfate was formed. Preparations 1, 2, 3, 4, and 5 were made from saturated $Ca(OH)_2$ solution and calcium aluminate solution. The yields obtained in these batches were 9, 6, 7, 5, 11 g, respectively. Preparations 6, 7, and 8 were made from $Al_2(SO_4)_3$ solution and saturated $Ca(OH)_2$ solution by the alternate reaction-decantation technique described in the appendix, a technique which makes a larger yield of the monosulfate possible in the equipment available and within the time limits necessary to prevent conversion of the monosulfate to the trisulfate. Yields of batches 6, 7, and 8 were 16, 30, and 33 g respectively. The quantities obtained were about 75 percent of the theoretical yield, largely as a result of mechanical loss in the handling operations.

Preparation of the reagents, transfer of solutions, mixing, filtration, and other operations were performed in closed systems with precautions taken to exclude CO_2. Solutions were made with distilled water which had been boiled and then cooled in a current of CO_2-free air.

All batches were dried at 33 percent relative humidity in a desiccator over saturated $MgCl_2\cdot 6H_2O$ [7], except sample 8 which was dried at 12 percent relative humidity (saturated LiCl) [7]. Samples conditioned in this way are referred to hereinafter as "original" samples. Several portions of samples 2, 6, 7, and 8 were dried at 12 percent relative humidity, 5 percent relative humidity (23N sulfuric acid) [8], and 0 percent relative humidity (CaO). These samples are referred to as "dried" samples. Before placing the samples in the desiccators and after opening them at any time, the desiccators were evacuated to 2 to 4 cm Hg pressure and refilled with CO_2-free air which had been passed through the same conditioning solution as contained in the desiccator. Inasmuch as effective conditioning requires slow air flow, the desiccators were generally opened only once during a day, evacuated rapidly, and refilled overnight with conditioned air; thus, they were generally under vacuum most of this period. The desiccator containing CaO was kept under vacuum at all times, except when it was opened to remove a sample. When the loss on ignition of a preparation was constant, the material was ground and mixed in a sealed glass jar containing wood balls, and the ground material was stored in the appropriate desiccator.

Heat-of-solution determinations were made on all the "original" and "dried" preparations. Measurements were also made of the heats of solution of portions of sample 7 exposed for various periods of time to an atmosphere at 100 percent relative humidity. The latter environment was obtained by slowly passing dry CO_2-free air through CO_2-free distilled water and into a desiccator containing the samples to be exposed. The air was passed through water in two spiral gas-washing bottles and then through a delivery tube fitted with a fritted-glass opening immersed in a reservoir of water in the desiccator.

2.2. X-ray Diffraction and Chemical Analysis

X-ray diffraction patterns of the preparations were obtained by the powder method on a Geiger-counter diffractometer with copper Kα radiation. The principal peaks of the patterns are summarized in table 2. The samples conditioned at 33 percent relative humidity showed peaks of both the high-

TABLE 1. *Properties of the original preparations of calcium aluminate sulfates*

Sample designation	1	2	3	4	5	6	7	8	9	10	11
Original concentration of mixture:											
CaO, g/liter	1.088	1.047	1.051	0.983	1.025	[a]	[a]	[a]	0.914		
Al_2O_3, g/liter	.114	.226	.107	.075	.207	[a]	[a]	[a]	.253		
SO_3, g/liter	.239	.380	.225	.315	.358	[a]	[a]	[a]	.469		
Molar ratio:											
$CaO:Al_2O_3$	17.4	8.5	17.9	23.9	9.0	[a] 19.7	[a] 12.9	[a] 12.5	6.6	18.3	20.2
$SO:Al_2O_3$	2.7	2.2	2.7	5.4	2.2	2.9	2.9	2.9	2.4	3.0	3.0
$OH^-:Al_2O_3$	29.4	12.7	30.4	37.1	13.6	39.5	25.8	25.0	8.4	[b]	40.4
Final concentration of solution:											
CaO, g/liter	.850	.562	.846	.855	.624	[a] .910–.937	[a] .801–.811		.247	present	present
Al_2O_3, g/liter	.001	.000	.000	.001	.001	.000	.000		.058	absent	[c] absent
SO_3, g/liter	.168	.215	.182	.313	.253	[a] .144–.169	[a] .219–.253		.013	[c] absent	[c] present
Composition of product:											
Weight percent:											
CaO	36.03	36.15± .01	35.98± .03	35.48± .21	35.70± .06	36.20± .004	35.99± .02	37.35± .11			
Al_2O_3	16.40	16.76± .05	16.13± .02	16.14± .02	16.08± .01	16.35± .01	15.90± .02	16.88± .11			
SO_3	12.74	12.64± .11	12.65± .002	12.55± .02	13.07± .10	12.93± .02	13.56± .01	13.24± .11			
CO_2	.31± .02	.09± .004	.45± .004	[d]	.23± .01	.30± .000	.24± .01	.41± .000			
H_2O	[e] 34.52	34.19	34.77± .07	[d]	34.93± .03	34.25± .05	34.36± .04	32.02± .03			
Molar ratio:											
$CaO:Al_2O_3$	3.99_4	3.92_1± $.01_1$	4.05_8± $.00_5$	3.99_3± $.02_4$	3.89_9± $.00_7$	4.02_3± $.00_9$	4.11_4± $.00_3$	4.02_3± $.02_8$	[f] 6.2		
$SO_3:Al_2O_3$	$.98_5$	$.96_0$± $.00_9$	$.99_9$± $.00_7$	$.99_6$± $.00_1$	1.03_5± $.00_8$	1.00_7± $.00_1$	1.08_4± $.00_4$	0.99_9± $.01_0$	[f] 2.9		
$CO_2:Al_2O_3$	$.04_1$	$.01_2$± $.00_1$	$.06_1$± $.00_5$	[d]	$.03_3$± $.00_1$	$.04_3$± $.00_6$	$.03_5$± $.00_2$	$.06_0$± $.00_7$			
$H_2O:Al_2O_3$	11.91_2	11.54_5	12.20_0± $.02_8$	[d]	12.37_6± $.01_4$	11.85_6± $.01_9$	12.22_8± $.02_0$	10.73_4± $.07_1$			
Molar ratios of compounds present, to Al_2O_3:											
$3CaO·Al_2O_3·CaSO_4·nH_2O$	$.98_5$	$.96_0$± $.00_9$	$.99_9$± $.00_7$	$.99_0$± $.00_1$	$.89_5$± $.00_8$	1.00_0± $.00_6$	1.00_0± $.00_9$	$.99_8$± $.01_0$			[g]
where $n=$	12.01_1	11.82_8	12.21_7± $.02_8$	[d] 12.54	[h] 12	11.84_2± $.02_6$	12.05_6± $.02_1$	10.74_2± $.15_5$			
$3CaO·Al_2O_3·3CaSO_4·31H_2O$					$.04_6$± $.00_5$				[i]	[i]	
$CaCO_3$	$.03_8$	$.01_2$± $.00_1$	$.06_0$± $.00_6$	[d] .03	$.03_3$± $.00_1$	$.01_8$± $.00_1$	$.02_4$± $.00_6$	$.02_3$+ $.02_8$ − $.023$			
$Ca(OH)_2$		$.06_9$± $.01_8$									
$CaSO_4·2H_2O$						$.00_7$± $.00_1$	$.08_4$± $.00_4$				
$Al_2O_3·3H_2O$	$.01_1$	$.04_0$± $.00_9$		$.01_0$± $.00_2$	$.05_8$± $.03_5$			$.00_3$+ $.01_0$ − $.00_1$			
CO_2	$.00_6$			[d] .01		$.02_3$± $.00_1$	$.00_7$± $.00_8$	$.03$± $.02_8$			
Heat of solution of the sample:											
$-\Delta H$, (from table 5), cal/g	190.14	194.64	186.66	185.02	186.44	192.42	185.30	201.61			
standard error, cal/g±		.21	.19		.12	.12	.03				
Corrected heat of solution of the $3CaO·Al_2O_3·CaSO_4·nH_2O$											
$-\Delta H$, cal/g	190.5_1	191.4_4	187.6_5	185.2_9	197.7_3	193.5_2	191.0_2	202.5_8			
kcal/mole	118.6_3	118.5_8	117.5_3	117.1_5	123.0_9	119.9_2	119.0_9	121.5_2			

[a] 5-batch mixtures; concentrations variable. Molar ratios given are overall, for all 5 batches.

[b] CaO dissolved in sucrose.

[c] Absence of $SO_4^=$ in final solution is consistent with formation of $3CaO·Al_2O_3·3CaSO_4·mH_2O$; presence of $SO_4^=$ and simultaneous absence of Al_2O_3 is consistent with formation of $3CaO·Al_2O_3·CaSO_4·nH_2O$.

[d] Not determined because of insufficient sample. H_2O and CO_2 estimated.

[e] Calculated by difference. Insufficient sample for determination.

[f] Calculated from initial concentration of mixture and final concentration of solution.

[g] X-ray diffraction pattern showed peaks of $3CaO·Al_2O_3·CaSO_4·nH_2O$.

[h] Assumed to be $12H_2O$.

[i] X-ray diffraction pattern showed peaks of $3CaO·Al_2O_3·3CaSO_4·mH_2O$.

and low-humidity forms of the compound [9], except in the case of sample 3, which showed only the peaks of the high-humidity form at 8.8 and 4.4 A. There was some indication of a transformation of samples while on the machine, quick patterns sometimes showing a higher intensity of the 8.8 and 4.4 A peaks compared to the 8.2 and 4.0 peaks, respectively, of the low-humidity form, than long-term patterns run later on the same specimen. There is reason to believe, therefore, that samples taken for calorimetry contained more of the high-humidity form than the X-ray patterns indicate. Wet samples taken immediately after filtration showed the pattern characteristic of "wet-slice" calcium aluminate monosulfate [9] with the most intense lines at 9.8 and 4.9 A and an intermediate weaker line at 5.7 A. This pattern is consistently different in intensity relationships from the calcium aluminate trisulfate pattern, which has its most intense lines at 9.8 and 5.6 A and a weaker line at 5.0 A.

The oxide analyses of the preparations are given in table 1 and were obtained by replicate (2 to 5) measurements, except in the case of sample 1, for which material was available for only one measurement. The precision of the analyses and of the calculated mole ratios of the oxides (and of compounds calculated from the oxides) was determined. The estimates of standard error [2] for each oxide determination were calculated separately for each preparation, rather than by pooling the standard-error estimates for that particular determination for all preparations as had been done in earlier work [6]. This procedure is based on the assumption that, for a particular preparation, the calculated

[2] Standard error, formerly referred to as standard deviation of the mean,

$$= \sqrt{\frac{\Sigma x_i^2 - \frac{(\Sigma x_i)^2}{n}}{n(n-1)}}$$

where x_i is the result obtained for one measurement, and n is the number of measurements.

TABLE 2. *X-ray diffraction patterns of the calcium aluminate sulfates*

Preparation		Principal identifying lines								Pattern classification [a]
Designation	Conditioned at relative humidity	9.5-10.0A	8.8-9.3A	8.0-8.2A	7.5-7.8A	5.7A	4.7-4.9A	4.4-4.6A	3.8-4.1A	
	Percent									
2	33		5	4				4	3	Monosulfate Bc.
3	33		5					4	2½	Monosulfate B.
4	[c] 33		5	3				4	2	Monosulfate Bc.
5	[c] 33		5	3				5	2	Monosulfate Bc.
	[d] 33		4	4				2½	2½	Monosulfate bc.
	[e] 33		4	5				2	3	Monosulfate bC.
6	wet	5				2	5		2	Monosulfate A.
	[c] 33		5	3				4	3	Monosulfate Bc.
	[d] 33		5	3				4	2½	Monosulfate Bc.
	0			5			1	1	5	Monosulfate C.
7	wet	5				2	5		2	Monosulfate A.
	[c] 33		5	3				4	3	Monosulfate Bc.
	[d] 33		3	5			1	2	3	Monosulfate bC.
	[f] 100 (16 "H_2O")	4	5	4	4	3	1	4	2	Monosulfate Bc, trisulfate and monocarbonate.
	[f] 100 (17 "H_2O")	4	5	4	4	3	1	4	2	
	[f] 100 (20 "H_2O")	4		2	5	3	1	1	2	
	12	3	5	5		2	2	4	5	Monosulfate bC.
	5	1		5		2	2	2	5	Monosulfate C.
9	wet	5	1			5	4		5	Trisulfate.
10		5	1			5	4		5	Trisulfate.
11	wet	5					3		1	Monosulfate A.

[a] Letters refer to type of monosulfate pattern. Upper-case type indicates predominant pattern.
A—wet type of calcium aluminate monosulfate.
B—high-humidity type.
C—low-humidity type.
[b] Numbers refer to relative intensity of lines.
5—very strong.
4—strong.
3—medium.
2—weak.
1—very weak.
[c] Exposed to X-ray immediately after removal from conditioning chamber; pattern completed in 10 min.
[d] Exposed to X-ray some time after removal from conditioning chamber, but protected from atmosphere; pattern completed in 10 min.
[e] Same as d, but pattern completed in 40 min, following the 10-min pattern.
[f] 33 percent R.H.-conditioned samples, exposed to 100 percent R.H., for various lengths of time.

precision of the analysis is dependent on the uniformity of the preparation and not simply on the degree to which an analytical method can be reproduced. The calculated precision of the mole ratios of the compounds assumed to be present as impurities is an indication of the quantitative reliability of the impurity calculations. The designation of the compounds present as impurities was based on the chemical analysis, optical microscopic examination, and X-ray diffraction patterns.

The preparation of the gypsum and of the hydrated tricalcium aluminate has been discussed in reference [6].

3. Heat-of-Solution Measurements

The heats of solution were determined in $HCl{\cdot}26.61_4\ H_2O$ (2.00*N* HCl at 25 °C). The improved all-platinum calorimeter described in an earlier publication [5] was used, with platinum resistance thermometer, air jacket, and water bath controlled to ±0.005 °C or better. The calorimeter was stirred with the shorter of the two stirrers described, a 4-in. platinum stirrer with four-bladed propeller. Samples were introduced through a glass funnel. When the calorimeter temperature attained after the sample has dissolved is close to the temperature of the bath and the room, corrections for the heat capacity of the sample are minimized by the funnel-introduction technique.

Since it was inconvenient to prepare the calcium aluminate monosulfate in large quantities, 1-g samples of the compound were used with the normal quantity of acid (740 g) for the calorimeter. The quantities of $3CaO{\cdot}Al_2O_3{\cdot}6H_2O$ and $CaSO_4{\cdot}2H_2O$ required by the stoichiometry of eqs (1) to (5) are 0.61 and 0.28 g respectively (in 740 g HCl) corresponding to 0.49 and 0.22 g in 600 g HCl. The heat of solution of $3CaO{\cdot}Al_2O_3{\cdot}6H_2O$ was determined in earlier work [5, 6] in a platinum-lined calorimeter described by Newman [10] with samples ranging from 0.26 to 0.44 g in 600 g HCl, a sample-acid ratio slightly below the ratio required for this work. It has been shown, however, that there is no observable heat-of-dilution effect for samples of $3CaO{\cdot}Al_2O_3{\cdot}6H_2O$ in 2*N* HCl between 0.26 and 2.9 g [5, 11]. The determinations with the 0.26 to 0.44-g samples were therefore used for this work.

The heat of solution of 0.28 g of $CaSO_4{\cdot}2H_2O$ in 740 g of 2*N* HCl was separately determined for calculating the heat of reaction (eq (1)), in preference to the results of earlier determinations obtained with sample-acid ratios equivalent to 1.2 g and 0.53 g of $CaSO_4{\cdot}2H_2O$ in 740 g of acid. The heats of solution obtained with the 0.28-g samples were used because they were slightly higher than for the larger samples, but the differences (see sec. 4.1) are not considered sufficiently significant to suppose that a heat-of-dilution effect was actually observed. Although, according to eq (3), the gypsum should be added to the acid solution obtained from the dissolution of the tricalcium aluminate, it was actually added to the fresh acid. As has been shown [6], no measurable error is thereby introduced.

The heat effect of adding the 4 moles of H_2O appearing in eqs (1) and (4) was estimated as the partial molal heat content of H_2O in 2*N* HCl [3], neglecting the contribution of the small amounts of other solutes present.

TABLE 3. *Properties of the dried preparations of calcium aluminate monosulfate*

Conditioning agent	Saturated LiCl	23 *N* H_2SO_4				CaO		
Relative humidity, %	12	5	5	5	5	0	0	0
Original sample exposed	7	2	6	7	8	6	7	8
Time exposed, days	103	22	25	95	25	21	14	25
H_2O content, n, of the $3CaO \cdot Al_2O_3 \cdot CaSO_4 \cdot nH_2O$	11.83	10.67$_4$	10.66$_5$	10.56$_8$	10.62$_2$	8.77$_1$	8.60$_5$	8.61$_3$
Heat of solution of the sample, $-\Delta H$, cal/g	185.84	203.71	203.78	198.38	202.38	229.17	228.74	229.83
Corrected heat of solution of the $3CaO \cdot Al_2O_3 \cdot CaSO_4 \cdot nH_2O$, $-\Delta H$, cal/g	191.6$_1$	203.0$_7$	204.9$_9$	204.7$_5$	203.3$_6$	230.4$_8$	235.2$_1$	231.0$_7$
kcal/mole	118.7$_2$	121.5$_8$	122.6$_8$	122.1$_8$	121.5$_2$	130.0$_7$	132.0$_4$	129.7$_6$

4. Results and Discussion

4.1. Heats of Solution of the Preparations

The heats of solution obtained with the original preparations (samples 1–8) are shown in table 1. Those obtained with the dried preparations are shown in table 3. Both tables also show heats of solution of the pure calcium aluminate monosulfate, after correction for the impurities in the samples.

The heat capacities obtained in the calorimeter calibrations and the data from which these heat capacities were calculated, are listed in table 4. Detailed data from the heat-of-solution determinations are shown in table 5.

Determinations of the heat of solution of $CaSO_4 \cdot 2H_2O$ are shown in table 6, for sample-acid ratios of 0.0004, 0.0007, and 0.0017. For a range of ± 1 standard error the results for the lowest sample-acid ratio do not quite overlap those of the other two sets, but the gap is not great enough to be statistically significant. Perhaps a more precise determination of the heat of solution of $CaSO_4 \cdot 2H_2O$ at different sample-acid ratios would reveal a significant heat-of-dilution effect. In any event, the heat of solution obtained for the lowest ratio has been used, for the reason discussed in section 3.

TABLE 4. *Calibration of calorimeter with 740 grams 2N HCl*

Run	Time	I	E	Q	ΔR_c	Heat capacity
	sec	*amp*	*Volts*	*j*	*Ohm*	*j/ohm*
1	839.993	0.240711	16.6215	3360.793	0.117847	[a] 28,518.2
2	899.993	.238626	16.4756	3184.493	.111660	28,519.5
3	926.993	.237635	16.4076	3614.364	.126718	28,522.8
4	931.993	.234793	16.2123	3347.664	.124471	28,501.9
5	899.993	.240531	16.6060	3595.453	.126230	28,483.3
6	839.993	.241842	16.7005	3392.633	.119156	28,472.2
7	839.993	.240185	16.5849	3346.065	.117589	28,455.6
8	810.993	.246121	16.9946	3392.163	.119179	28,462.7
Mean heat capacity, j/ohm						[b] 28,492.0±9.59
Mean heat capacity, cal/ohm						6,809.7±2.29
1	1499.993	0.086368	6.65251	961.629	0.033684	[c] 28,548.5
2	1379.993	.086579	6.66773	888.609	.031169	28,511.3
3	1259.993	.086179	6.640233	804.697	.028218	28,517.1
4	899.993	.112554	7.77112	787.197	.027636	28,484.4
5	959.993	.112523	7.76940	839.261	.029422	28,524.9
6	910.493	.112549	7.77086	796.319	.027908	28,533.7
7	959.493	.112450	6.65251	838.128	.029442	28,467.0
Mean heat capacity, j/ohm						[c] 28,512.4±10.66
Mean heat capacity, cal/ohm						6,814.6±2.55

[a] It is not the authors' intention to imply that the heat-capacity values are either precise or accurate to the number of figures tabulated. These figures are carried through the calculations to facilitate the estimation of standard error. The heat-of-solution values obtained from them in tables 5 and 6 are rounded off.
[b] Long stirrer used. Temperature rise approximately 1 °C. Calibration used for determining heat of solution of samples 1 and 2.
[c] Short stirrer used. Temperature rise approximately 0.3 °C. Calibration used for determining heat of solution of samples 3, 4, 5, 6, 7, 8, and all dried and moist samples.

4.2. Correction for Impurities

The calculation of the composition of a sample and of the heat of solution of the pure calcium aluminate monosulfate present was performed as described in the appendices to references [5] and [6].

In general, X-ray diffraction patterns were useful only in revealing the major components, whereas optical microscopic examination was generally necessary to confirm the impurities suggested by the chemical analysis. In the case of samples exposed at 100 percent relative humidity, the X-ray pattern indicated breakdown of the aluminate monosulfate into compounds not detectable by chemical analysis (see sec. 4.8). Another useful indication of the nature of the impurities, also described in section 4.8, was the pattern of evolution of heat during the dissolution of the sample in the calorimeter.

As in earlier work on the heat of formation of calcium aluminate trisulfate [6], the presence of a small quantity of CO_2 not offset by CaO was a troublesome factor. (Note that in sample 6 the standard error of the free CO_2 was considerably smaller than the quantity of free CO_2 calculated, indicating a high confidence in its presence, whereas in sample 7 the standard error was almost as large as the quantity itself, indicating the reverse). This free CO_2, if actually present, is assumed to be sorbed much like free H_2O, and the quantity of heat it would liberate or absorb on dissolution of the compound is neglected. In reference [6], the heat of solution of hydrated alumina was also neglected, because this compound remained in suspension and did not contribute to the total heat evolved by the preparation. However, in these monosulfate preparations, clear solutions were obtained in the calorimeter, indicating that the hydrated alumina did dissolve (see sec. 4.7 for exceptions). Correction was therefore made for its heat of solution. Assarsson [12] points out that soluble hydrated alumina, obtained from precipitates that have digested for only a short time, contains between 3 and 4 moles of H_2O, and suggests that the additional H_2O is physically adsorbed on a particle that is chemically gibbsite, $Al_2O_3 \cdot 3H_2O$. Correction for the heat of solution of the hydrated alumina is

TABLE 5. *Details of heat-of-solution determinations on samples of calcium aluminate monosulfate*

Sample	Run	Corrected rise	Sample weight	Heat of solution, $-\Delta H$					
				Uncorrected	Correction for heat capacity of sample	Corrected	Std. error	Corrected	Std. error
		ohm	*g*	*j/g*	*j/g*	*j/g*	*j/g*	*cal/g*	*cal/g*
1 [a]		0.026628	0.9536	795.60	−0.07	795.53		190.14	
2 [a]	1	0.026372	0.9210	815.84	−0.26	815.58			
	2	.028594	1.0026	812.59	+.12	812.71			
	3	.029623	1.0353	815.24	−.38	814.86			
Mean, before correction for impurities						814.38	±0.86	194.64	±0.21
3 [b]	1	0.027118	0.9889	781.88	−0.10	781.78			
	2	.026801	.9792	780.39	−.20	780.19			
Mean, before correction for impurities						780.98	±.79	186.66	±.19
4 [b]		0.027587	1.0158	774.34	−0.23	774.11		185.02	
5 [b]	1	0.018405	0.6723	780.56	−0.20	780.36			
	2	.030042	1.0970	780.83	−.28	780.55			
	3	.027581	1.0101	778.54	+.04	778.58			
	4	.027295	0.9966	780.90	−.06	780.84			
Mean, before correction for impurities						780.08	±.51	186.44	±.12
6 [b]	1	0.028732	1.0143	807.67	−0.92	806.75			
	2	.028464	1.0067	806.18	−.85	805.33			
	3	.028248	1.0003	805.18	−.59	804.59			
	4	.028277	1.0033	803.60	−.07	803.53			
	5	.028342	1.0036	805.20	+.01	805.21			
Mean, before correction for impurities						805.08	±.52	192.42	±.12
7 [b]	1	0.027108	0.9973	775.01	−0.03	774.98			
	2	.027173	.9980	775.54	−.19	775.35			
	3	.027310	1.0035	775.96	−.36	775.60			
	4	.027494	1.0105	775.78	−.60	775.18			
Mean, before correction for impurities						775.28	±.13	185.30	±.03
8 [b]		0.029173	0.9870	842.75	+0.80	843.55		201.61	
6 (0% $R.H._i$) [b]		0.030891	0.9179	959.56	−0.70	958.86		229.17	
7 (0% $R.H._i$) [b]		.029708	.8845	957.66	−.62	957.04		228.74	
8 (0% $R.H._i$) [b]		.032505	.9636	961.81	−.19	961.62		229.83	
2 (5% $R.H._i$) [b]		.024698	.8256	852.96	−.65	852.31		203.71	
6 (5% $R.H._i$) [b]		.028828	.9640	852.65	−.03	852.62		203.78	
7 (5% $R.H._i$) [b]		.025596	.8786	830.65	−.64	830.01		198.38	
8 (5% $R.H._i$) [b]		.028965	.9761	846.09	+.65	846.74		202.38	
7 (12% $R.H._i$) [b]	1	0.027792	1.0173	778.94	−0.75	778.19			
	2	.027029	.9913	777.43	−.53	776.90			
Mean, before correction for impurities						777.54	±.65	185.84	±.15
7 (100% $R.H._i$) [b]									
16.1 "H_2O" [c]		0.02286	1.0450	623.7				[d] 149.1	
16.9 "H_2O" [c]		.02372	1.1483	589.0				[d] 140.8	
18.1 "H_2O" [c]		.01894	0.9910	544.9				[d] 130.2	
19.4 "H_2O" [c]		.02089	1.1918	499.8				[d] 119.4	
20.4 "H_2O" [c]		.02084	1.2398	479.3				[b] 114.6	

[a] Heat capacity of calorimeter 28,492.0$_5$ joules/ohm.
[b] Heat capacity of calorimeter 28,512.4$_7$ joules/ohm.
[c] See text for discussion of the composition of these samples.
[d] No correction was made for the heat capacity of these samples, because the sample temperature could not be measured in the short time between removal from conditioning chamber and introduction into calorimeter.

therefore calculated as a gibbsite correction. In samples 1, 2, 4, and 5, the uncertainty in the H_2O content of the gibbsite brings about a corresponding uncertainty in the H_2O content of the aluminate monosulfate: if the alumina is $Al_2O_3 \cdot 4H_2O$, this uncertainty ranges from 0.01 to 0.04 moles per mole monosulfate. The effect of this uncertainty on the heat of solution of the monosulfate is, however, only 1 part in 10,000 for $3CaO \cdot Al_2O_3 \cdot CaSO_4 \cdot 12H_2O$.

The mixture in which sample 5 was precipitated was on the border of the concentration range for formation of the monosulfate, under the experimental conditions of this work (see appendix, 7.1). Microscopical examination showed needles of calcium aluminate trisulfate with negative elongation, together with the usual needlelike "fibers" of the monosulfate which appear to have positive elongation because they are uniaxial negative plates observed

TABLE 6. *Heat-of-solution determinations on* $CaSO_4 \cdot 2H_2O$ *for different sample-acid ratios*

Sample weight	Acid weight	Corrected rise	Heat capacity of calorimeter	Heat of solution, $-\Delta H$					
				Uncorrected	Corrected for heat capacity of sample	Corrected	Std. error	Corrected	Std. error
g	*g*	*Ohm*	*j/ohm*	*j/g*	*j/g*	*j/g*	*j/g*	*cal/g*	*cal/g*
0.2768	740.0	−0.001370	28,512.4[7]	−141.12	−0.57	−141.69			
.2831		−.001372		−138.18	−.84	−139.02			
.2863		−.001438		−143.21	−.44	−143.65			
Mean						−141.45	±1.34	−33.81	±0.32
[a] 0.4340	600.0	−0.002398	[b] 24,479.9[6]	−135.26	+0.19	−135.07			
[a] .4285		−.002412		−137.80	+.09	−137.71			
[a] .4239		−.002431		−140.39	+.10	−140.29			
Mean						−137.69	±1.51	−32.91	±0.36
[a] 1.0171	600.0	−0.005708	[b] 24,479.9[6]	−137.38	+0.02	−137.36			
[a] 1.0060		−.005726		−139.34	+.03	−139.31			
[a] 1.0205		−.005742		−137.74	−.01	−137.75			
Mean						−138.14	±0.59	−33.02	±0.14

[a] These determinations were reported in abbreviated form in reference [6].
[b] See reference [5] for calibration details.

edgewise. Since both the monosulfate and the trisulfate have variable water contents, it was necessary to assume a distribution of H_2O molecules between the two. The H_2O balance most nearly corresponding to the analytical data was obtained by assuming $12H_2O$ for the monosulfate and $31H_2O$ for the trisulfate. The compound composition and corrected heat of solution shown in table 1 were then calculated. However, the point in figure 1 corresponding to this sample (open circle) shows the greatest deviation from the curve. Because of the uncertainties in the calculation of H_2O content and of other compounds and impurities for sample 5, this point was not included in establishing the curve.

Insufficient quantities of samples 1 and 4 made it necessary to assume water contents by subtraction of the total percentage of CaO, Al_2O_3, SO_3, and CO_2 from 100 percent. The CO_2 content of sample 4 was not determined, but was estimated from that of the other samples instead. Only one determination of major oxides could be made on sample 1. Although it was not possible, for this reason, to calculate standard errors for these analyses, the uncertainties in the final calculation of heat of solution and water content are not believed to be very great for these two samples. If the points in figure 1 corresponding to these samples were omitted, there would be almost no change in the curve.

The following values were used for the heats of solution of the various impurities:

$3CaO \cdot Al_2O_3 \cdot 3CaSO_4 \cdot 31H_2O$	$-\Delta H =$	74.94 kcal/mole [6]
$CaCO_3$		83.61 cal/g [5]
$Ca(OH)_2$		436.41 cal/g [13]
$CaSO_4 \cdot 2H_2O$		−33.81 cal/g from table 6
$CaSO_4 \cdot 1/2H_2O$		−7.64 cal/g [14]
$CaSO_4$ (soluble anhydrite)		10.31 cal/g [14]
$Al_2O_3 \cdot 3H_2O$		50.34 kcal/mole

The value for the heat of solution of $Al_2O_3 \cdot 3H_2O$ was derived by calculation from the heats of formation of gibbsite (hydrargyllite), $-\Delta H = 613.7$ kcal/mole [3]; α-Al_2O_3 (corundum), 399.09 kcal/mole [3]; $3H_2O$, 204.95 kcal/mole [3]; and the heat of solution of α-Al_2O_3 in 2.00*N* HCl, 59.95 kcal/mole [15]; with a small correction for the heat of dilution of HCl with the H_2O, estimated to be 0.05 kcal.

4.3. Heat of Solution of Calcium Aluminate Monosulfate

Figure 1 is a plot of the corrected heats of solution against the calculated water content of the pure compound. The points are derived from tables 1 and 3. The solid curve represents the following least-squares quadratic equation calculated from the points:

$$-\Delta H = 214.664 - 14.096n + 0.5069n^2 \qquad (6)$$

where

ΔH = heat of solution in kcal/mole calcium aluminate monosulfate
n = moles H_2O/mole calcium aluminate monosulfate

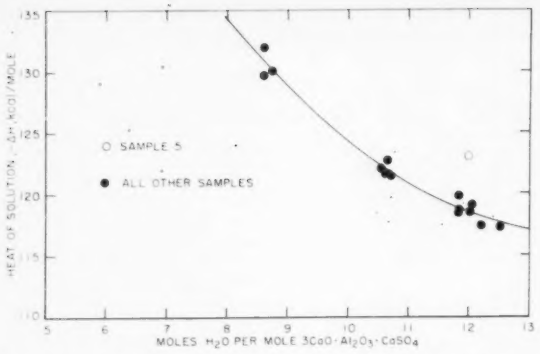

FIGURE 1. *Heat of solution of* $3CaO \cdot Al_2O_3 \cdot CaSO_4 \cdot nH_2O(c)$

This curve covers the range of 8 to $13H_2O$; that is, the samples conditioned at relative humidities of 33 percent and below. For reasons discussed in the preceding section, sample 5 (open circle) was omitted in calculating the equation. For the samples conditioned at 100 percent relative humidity, with water contents greater than $13H_2O$, see the discussion in section 4.8.

No correlation was apparent between the heats of solution and the various X-ray patterns characteristic of the monosulfate, except to the extent that the pattern showing the 9.0 and 4.5 A peaks was more prominent in the 33 percent relative-humidity-conditioned samples, which had the lower heat-of-solution values, and the 8.0 and 4.0 A peaks were more prominent in the dried samples, which had the higher heats of solution. One sample, No. 3, conditioned at 33 percent relative humidity, showed only the 9.0–4.5 A pair; one, No. 6 at 0 percent relative humidity, showed only the 8.0–4.0 A pair. All other patterns obtained (see table 2) were mixtures of the two basic patterns. There was no observable relation between the relative heights of the respective peaks and the heats of solution. However, the correlation between water content and heat of solution is definite. Since the X-ray specimens were not protected against room atmosphere while mounted on the diffractometer, it is uncertain whether the variation of heat of solution with water content is a function of water content alone or of the crystal-structure change reflected by the change in X-ray pattern as well.

From eq (6), the heat of solution of $3CaO \cdot Al_2O_3 \cdot CaSO_4 \cdot 12H_2O$ in $2.00N$ HCl (at a sample-acid ratio of 1:740) is $-\Delta H = 118.5$ kcal/mole. The change of the heat of solution with water content at this point, $d(-\Delta H)/dn$, is -1.93 kcal/mole per mole H_2O.

Corresponding values for the heats of solution of compositions containing less H_2O have been calculated from eq (6) and assembled in table 7.

4.4. Heat of Formation of the Product from the Reactants

The heat of the reaction represented by eq (1) is calculated from the heats of solution of the reactants and products. The heat effects of eqs (2), (3), (4), and (5) are added, as follows: (Note, however, that the tricalcium aluminate hydrate used as one of the reactants was actually $3CaO \cdot Al_2O_3 \cdot 5.859H_2O$ [6] and a further correction must be made later to correct for this departure from eq (2)). For

eq (2),	$-\Delta H = 139.163$ kcal/mole
(3)	-5.281
(4)	$+0.066$
(5)	-118.506
(1)	$+\Delta H = 15.44$

4.5. Correction for the Water Content of the Tricalcium Aluminate

The heat of solution of hydrated tricalcium aluminate was measured on a sample containing $5.859H_2O$ instead of $6H_2O$. It is therefore necessary to introduce a correction to the summation in section 4.4 based on the heat effect of the following equation:

$$3CaO \cdot Al_2O_3 \cdot 6H_2O(c) \rightarrow 3CaO \cdot Al_2O_3 \cdot 5.859H_2O(c) + 0.141H_2O(l) \quad (7)$$

In references [5, 6], the heat of this reaction was taken as 0.141/6.00 times the heat of hydration of anhydrous $3CaO \cdot Al_2O_3$ to the hexahydrate. This estimate was based on the assumption that the fraction hydrated to $6H_2O$ was 5.859/6.00, and that the remainder was anhydrous. From the measurements of Thorvaldson, Brown, and Peaker [11], the heat effect was calculated to be $-\Delta H = -1.36$ kcal/mole $3CaO \cdot Al_2O_3$. At this time, it seems to the authors

TABLE 7. *Thermodynamic properties of compositions of calcium aluminate monosulfate, for different water contents*

Moles H_2O per mole, n	8	9	10	11	12
Heat of solution in $2N$ HCl of $3CaO \cdot Al_2O_3 \cdot CaSO_4 \cdot nH_2O$ ΔH, kcal/mole	-134.3_4	-128.8_6	-124.3_9	-120.9_4	-118.5_1
Heat of formation from $3CaO \cdot Al_2O_3 \cdot 6H_2O$(c), $CaSO_4 \cdot 2H_2O$(c), and H_2O(l) ΔH, kcal/mole	$+0.9_2$	-4.5_8	-9.0_6	-12.5_3	-14.9_8
Heat of formation from the elements, $\Delta H°_f$, kcal/mole	$-1811._1$	$-1885._0$	$-1957._7$	$-2029._5$	$-2100._3$

more reasonable to adopt a figure for the heat effect of eq (7) derived from a continuous plot of the heat of formation of several hydrates of tricalcium aluminate against their water content. Data for such a plot between 0 and $11.6H_2O$ are also available from Thorvaldson, Brown, and Peaker's paper [11]. The points lie on a continuous curve, from which the heat effect of eq (7) may be estimated as $-\Delta H = -0.46$ kcal/mole, about one-third the figure previously used for this correction [5, 6].

If the heat of reaction calculated in section 4.4 is corrected for the heat effect of eq (7), the heat of reaction for eq (1) is then $-\Delta H = 15.44 - 0.46 = 14.98$ kcal/mole.

Heats of formation from the same reactants of compositions containing less H_2O, calculated in the same manner, are given in table 7.

4.6. Heat of Formation of Calcium Aluminate Monosulfate from the Elements

The heat of formation of calcium aluminate monosulfate is the sum of the heat effect of eq (1) and of the heats of formation of the reactants:

	kcal/mole
ΔH_f° $3CaO \cdot Al_2O_3 \cdot 6H_2O(c)$	$= -1329.$
ΔH_f° $CaSO_4 \cdot 2H_2O(c)$	$= -\ 483.06$
ΔH_f° $4H_2O(l)$	$= -\ 273.27$
ΔH eq (1)	$= -\ 14.98$
ΔH_f° $3CaO \cdot Al_2O_3 \cdot CaSO_4 \cdot 12H_2O(c)$	$= -2100._{31}$

The heats of formation of compositions with water contents less than $12H_2O$, similarly calculated, are shown in table 7 and figure 2. The heat effect of introducing H_2O into the compound at any stage of hydration can be determined from this figure.

4.7. Other Heats of Reaction

The revised correction for the heat of solution of tricalcium aluminate hexahydrate, described in section 4.5, must be applied to the heats of formation of calcium aluminate trisulfate and calcium aluminate monocarbonate, reported by the authors in references [5, 6]. To each of the reported values for ΔH_f, it is necessary to add the difference between 0.46 and 1.36, or -0.9 kcal/mole. The following revised values for the heats of formation are then obtained:

	ΔH from reactants [3] kcal/mole	ΔH_f° kcal/mole
$3CaO \cdot Al_2O_3 \cdot 3CaSO_4 \cdot 31H_2O(c)$	−47.01	−4123
$3CaO \cdot Al_2O_3 \cdot 3CaSO_4 \cdot 32H_2O(c)$	−49.52	−4194
$3CaO \cdot Al_2O_3 \cdot CaCO_3 \cdot 10.68H_2O(c)$	−19.77	−1957

The heat effects in the stepwise formation of the two complex calcium aluminate sulfates may be calculated from their heats of formation and summarized as follows:
The heat of the reaction

[3] Reactants for the trisulfate are the same as for the monosulfate. Reactants for the monocarbonate are $CaCO_3(c)$, $3CaO \cdot Al_2O_3 \cdot 6H_2O(c)$, and $H_2O(l)$.

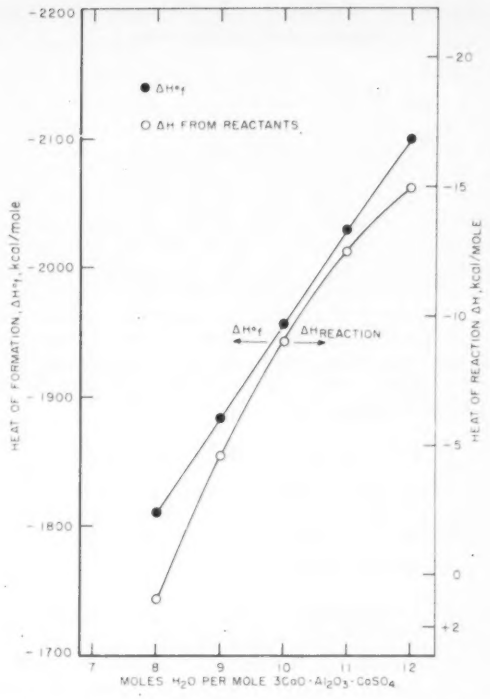

FIGURE 2. *Heat of formation of* $3CaO \cdot Al_2O_3 \cdot CaSO_4 \cdot nH_2O(c)$

Closed circles: ΔH_f° (from elements).
Open circles: ΔH from reactants $3CaO \cdot Al_2O_3 \cdot 6H_2O(c)$, $CaSO_4 \cdot 2H_2O(c)$, and $H_2O(l)$.

$$3CaO \cdot Al_2O_3 \cdot 6H_2O(c) + CaSO_4 \cdot 2H_2O(c) + 4H_2O(l) \rightarrow 3CaO \cdot Al_2O_3 \cdot CaSO_4 \cdot 12H_2O(c) \qquad (1)$$

is $\Delta H = -14.9_8$ kcal/mole

From the heats of reaction of $3CaO \cdot Al_2O_3 \cdot 6H_2O(c)$, $CaSO_4 \cdot 2H_2O(c)$, and $H_2O(l)$ to both the monosulfate (eq (1)) and the trisulfate (section 4.7 and ref. [6]), the heat of the reaction

$$3CaO \cdot Al_2O_3 \cdot CaSO_4 \cdot 12H_2O(c) + 2(CaSO_4 \cdot 2H_2O)(c) + 15H_2O(l) \rightarrow 3CaO \cdot Al_2O_3 \cdot 3CaSO_4 \cdot 31H_2O(c) \qquad (8)$$

is $\Delta H = -32.0_3$ kcal/mole

and for the reaction

$$3CaO \cdot Al_2O_3 \cdot CaSO_4 \cdot 12H_2O(c) + 2(CaSO_4 \cdot 2H_2O)(c) + 16H_2O(l) \rightarrow 3CaO \cdot Al_2O_3 \cdot 3CaSO_4 \cdot 32H_2O(c) \qquad (9)$$

is $\Delta H = -34.5_4$ kcal/mole.

4.8. Effect of Exposure of Calcium Aluminate Monosulfate to Moisture

Attempts to examine the effect of H_2O contents greater than $12.5H_2O$ on the heat of solution of the compound were not successful. Table 5 shows the heats of solution (in cal/g) and nominal water contents of portions of sample 7 exposed to 100 percent relative humidity for various lengths of time up to 2 months. If these values are plotted together with the corresponding values for the original and dried samples, the curve for the moist samples is not continuous with the curve for the others (fig. 3).

It is believed that the discontinuity observed is due to chemical decomposition of the monosulfate. Evidence obtained from X-ray diffraction data, chemical tests, and calorimetric observations suggests the following reaction:

$$3(3CaO{\cdot}Al_2O_3{\cdot}CaSO_4{\cdot}12H_2O)(c) + 3CO_2(g) + 10H_2O(l) \rightarrow Al_2O_3{\cdot}3H_2O(c) + 2CaCO_3(c) + 3CaO{\cdot}Al_2O_3{\cdot}CaCO_3{\cdot}11H_2O(c) + 3CaO{\cdot}Al_2O_3{\cdot}3CaSO_4{\cdot}32H_2O(c) \qquad (10)$$

The X-ray diffraction evidence includes a broadening of the peaks for the moist samples in the neighborhood of 9.0 and 8.0 A until they extended into the 7.5–7.8 A region, together with the appearance of a peak in the 9.5–10.0 A region. In the sample with the highest water content (about 20 "H_2O") the broad area separated into a distinct peak at 7.65 A, and a peak at 3.80 A was also evident. This trend is suggestive of the appearance of calcium aluminate monocarbonate, $3CaO{\cdot}Al_2O_3{\cdot}CaCO_3{\cdot}11H_2O$.

The 20 "H_2O" sample showed the peaks of calcium aluminate trisulfate at 9.8, 5.6, 4.7, 3.9, and 2.8 A. Although wet samples of the monosulfate show the first three peaks, it is possible to distinguish the two types of pattern by means of the relative peak intensities, as pointed out in section 2.2. It is apparent that the trisulfate was being formed during the exposure.

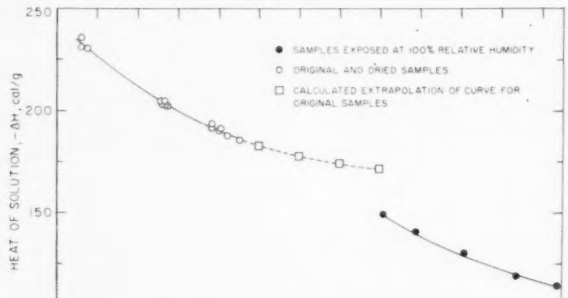
SAMPLES EXPOSED AT 100% RELATIVE HUMIDITY
ORIGINAL AND DRIED SAMPLES
CALCULATED EXTRAPOLATION OF CURVE FOR ORIGINAL SAMPLES
HEAT OF SOLUTION, -ΔH, cal/g
MOLE "H2O" PER MOLE 3CaO·Al2O3·CaSO4

FIGURE 3. *Heat of solution of calcium aluminate monosulfate samples exposed to 100 percent relative humidity, compared to that of the original and the dried preparations.*

Chemical tests showed a pickup of 29 percent of the original weight in a sample exposed to 100 percent relative humidity for 6 months. Of this weight increase, 11.9 percent was CO_2 and 17.1 percent was H_2O, quantities whose ratio is close to the H_2O: CO_2 ratio to be expected from eq (10), but which are greater in magnitude than the total weight pickup (17%) to be expected if that reaction went to completion. The pickup of CO_2 is definitely established.

The acid solutions obtained in the calorimeter from these exposed samples were turbid. The undissolved material was apparently hydrated alumina. It dissolved slowly in the acid during the determination, liberating heat slowly and producing a fictitious final rating period and an incorrect calculated thermal-leakage constant for the determination.

In order to obtain an accurate estimate of the heat of solution of these exposed samples, it was necessary to use the minute-to-minute heat-leakage correction described briefly in reference [5]. The initial rating period, the known heat-leakage constant of the calorimeter, and the initial temperature gradient between calorimeter and bath were used to determine the stirring energy. The total heat leakage was then determined for each 1- or 2-min reading interval by adding the stirring energy to the product of the heat-leakage constant and bath-calorimeter gradient for that interval. By subtracting the total heat leakage thus calculated from the observed temperature rise for the interval, a minute-to-minute record of the corrected temperature rise was obtained.

Figure 4 shows the trend of the corrected temperature rise for the exposed samples. For comparison, a similar plot for one of the 33 percent relative-humidity samples is shown, curve A. Note that curve A settles down to a constant value for the

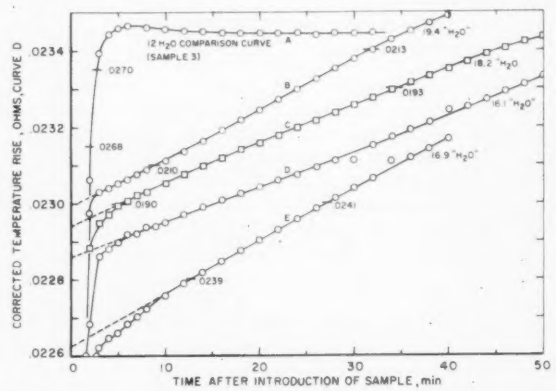

FIGURE 4. *Temperature rise in calorimeter (in ohms) versus time after introduction of sample, for samples conditioned at 100 percent relative humidity.*

A similar curve for an unexposed sample is shown for comparison. All curves are plotted to the same scale, but their ordinates represent different ranges of temperature rise. Ordinates at left are for curve D. Two ordinates are labeled on each of the other curves.

Curve A: Sample 3, conditioned at 33 percent relative humidity, shown for comparison.
Curve B: Sample 7, conditioned at 100 percent relative humidity to 19.4 "H_2O".
Curve C: Sample 7, similarly conditioned to 18.2 "H_2O".
Curve D: Sample 7, similarly conditioned to 16.1 "H_2O".
Curve E: Sample 7, similarly conditioned to 16.9 "H_2O".

corrected temperature rise after 12 min whereas the curves for the exposed samples show a rapid rise (representing solution of the aluminate sulfates) followed by a slower, almost linear rise (representing slow solution of the hydrated alumina). By extrapolating the slow-rise portion of the curve to zero time, the heat of solution of the rapidly dissolving constituents of the sample was obtained.

It should be noted that thermal equilibrium in the calorimeter is normally reached within about 5–6 min, whereas curve A becomes horizontal only after 12 min. The small drop in the curve between 7 and 12 min is not believed to represent a temperature lag. It is considered rather to reflect nonequilibrium endothermic release of CO_2 gas derived from solution of the small quantity of $CaCO_3$ in sample 3, as discussed in detail in reference [5]. A similar curve for sample 5, which was calculated to contain both $CaCO_3$ and $Al_2O_3 \cdot 3H_2O$, shows in succession a rapid temperature rise, a fall ($CaCO_3$), and finally a protracted rise ($Al_2O_3 \cdot 3H_2O$). This behavior of the temperature rise—time curve serves in several instances to confirm the impurities suggested by chemical analysis.

Calorimetric evidence is consistent with the reaction of eq (10) although it is not conclusive evidence of the reaction. Simple hydration of the monosulfate or physical water pickup would produce a curve either continuous with the 8–$12H_2O$ curve or higher than the right-hand curve of figure 3. If complete chemical reaction with H_2O alone had occurred, with transformation to the trisulfate, hydrated alumina, and $Ca(OH)_2$, the corresponding heat of solution of the mixture could not have been lower than 132 cal/g. The exposed samples, however, had heats of solution ranging from 150 to 115 cal/g. If eq (10) had gone to completion, the heat of solution would have been 99 cal/g. The calorimetric results are thus consistent with eq (10) provided the samples did not decompose completely during the exposure of 2 months or less. To reconcile the experimental heats of solution completely with the calculated values, it is necessary to assume that some of the weight picked up by the samples is sorbed H_2O. Calculations based on these heats of solution indicate further that a maximum of 70 percent conversion of the monosulfate to the products of eq (10) was approached during the 2-month period.

Further chemical evidence is apparent in the results of exposure to 100 percent relative humidity of a portion of sample 1 originally intended for a loss-on-ignition determination. After exposure to the moist air at several temperatures, the sample was reconditioned to constant weight at 33 percent relative humidity. Its loss on ignition at 1,000 °C after this treatment was 41.3 percent as compared with the original value of 34.5 percent. A sample of monosulfate completely converted according to eq (10) would have a loss on ignition of 44 percent; one 70 percent converted, 41 percent. In view of the speculative nature of this discussion, the close agreement between the experimental and calculated loss should be viewed with caution, but the similarity is nevertheless encouraging.

It is apparently difficult to protect samples of calcium aluminate monosulfate from CO_2 pickup in a moist atmosphere. Kantro, Copeland, and Anderson [9] report the same experience. A new approach is being made to the thermochemistry of samples of the compound containing more than $12H_2O$, by conditioning fresh wet pastes at 79 percent relative humidity (over saturated NH_4Cl). Wet pastes previously exposed at 100 percent relative humidity were nonuniform and difficult to handle in the calorimeter. It is expected that results based on this approach will be reported in a later publication.

5. Summary

Heats of formation of $3CaO \cdot Al_2O_3 \cdot CaSO_4 \cdot 12H_2O$(c), and of less completely hydrated samples of this compound ranging from 8 to $12H_2O$, have been determined by the heat-of-solution method, with 2*N* HCl as the solvent. Heats of reaction have been determined for the formation of $3CaO \cdot Al_2O_3 \cdot CaSO_4 \cdot 12H_2O$(c) from $3CaO \cdot Al_2O_3 \cdot 6H_2O$(c), $CaSO_4 \cdot 2H_2O$(c), and H_2O(l), and for the formation of $3CaO \cdot Al_2O_3 \cdot 3CaSO_4 \cdot 31$–$32H_2O$(c) from $3CaO \cdot Al_2O_3 \cdot CaSO_4 \cdot 12H_2O$(c), $CaSO_4 \cdot 2H_2O$(c), and H_2O(l).

The heat of solution of $3CaO \cdot Al_2O_3 \cdot CaSO_4 \cdot nH_2O$ in 2*N* HCl, in kcal/mole, may be expressed over the 8–$12H_2O$ range by a quadratic formula:

$$-\Delta H = 214.664 - 14.096n + 0.5069n^2.$$

The change of the heat of solution with H_2O content may be calculated from the expression:

$$-\frac{d(\Delta H)}{dn} = 1.0139n - 14.096$$

from which the rate at which the heat of solution of the $12H_2O$ hydrate varies with a small change in water content is

$$-\frac{d(\Delta H)}{dn} = -1.93 \text{ kcal/mole per mole } H_2O.$$

Calcium aluminate monosulfate is a metastable compound and can be formed from solution only within certain limits of the concentration ratios of the various reacting ions. If prepared and filtered within about 7 hr, a CaO/Al_2O_3 molar ratio of not less than 9 is necessary to prevent conversion to the trisulfate. The minimum CaO/Al_2O_3 molar ratio is significant because a high OH^- concentration favors formation and longer persistence of the monosulfate, and all or most of the CaO is obtained from $Ca(OH)_2$; from the mass-action law alone, a high CaO/Al_2O_3 ratio would be expected to produce the reverse effect.

In the presence of moisture and CO_2, evidence points to the probability that the monosulfate is converted to calcium aluminate trisulfate, calcium aluminate monocarbonate, calcium carbonate, and hydrated alumina. Although the evidence is not conclusive, an equation is suggested for this transformation.

6. Appendix. Conditions for the Formation and Stability of Calcium Aluminate Monosulfate

6.1. Effect of Reactant Concentrations

The $CaO—SO_3—Al_2O_3—H_2O$ system has been studied by Jones [16], D'Ans and Eick [17], and Eitel [18], who prepared equilibrium diagrams for two sets of products, a stable system in which the trisulfate is formed, and a metastable system in which the monosulfate is formed. However, detailed information on the conditions for forming the products of one or the other system is not generally available.

The concentration ratios necessary to produce either trisulfate or monosulfate within a given time limit bear no apparent relation to the stoichiometric ratios of the oxides in these compounds. Although the trisulfate exhibits a higher CaO/Al_2O_3 molar ratio (6:1) and a higher SO_3/Al_2O_3 ratio (3:1) than the monosulfate (4:1 and 1:1 respectively), the monosulfate was formed most readily in this work when the original mixture had a CaO/Al_2O_3 ratio greater than about 8, for SO_3/Al_2O_3 ratios ranging from 2.2 to 5.4 (see table 1). For CaO/Al_2O_3 ratios less than 8 or greater than about 50, the precipitate formed directly was either entirely or partly trisulfate. For CaO/Al_2O_3 ratios less than 6, a mixture of trisulfate and hydrated alumina tends to precipitate [2]. Unpublished work performed in this laboratory by Stearns [19] showed that, for SO_3/Al_2O_3 molar ratios between 2 and 3, the most stoichiometrically accurate precipitates of monosulfate were obtained at CaO/Al_2O_3 ratios of 20 to 24.

The apparent contradiction in the fact that formation of the complex sulfate with the lower CaO/Al_2O_3 ratio requires an original mixture of higher ratio may be resolved if it is considered that the source of the CaO is primarily calcium hydroxide. The preparations with the most $Ca(OH)_2$ had the highest OH^-/Al_2O_3 ratios in the original mixture, and would be expected to favor formation of a more basic precipitate, that is, the aluminate monosulfate in preference to the trisulfate. The viewpoint was tested by preparing a series of small-scale batches at several CaO/Al_2O_3 ratios, with varying additions of NaOH such that the OH^-/Al_2O_3 ratio was made to vary without corresponding changes in the CaO/Al_2O_3 ratio. Figure 5 shows the effect of OH^-/Al_2O_3 ratio (as calculated from concentrations in the original mixture) on the time required to initiate conversion of the monosulfate to the trisulfate, as well as the dependence of this time on the *p*H of the mother liquor. At any one CaO/Al_2O_3 ratio from 4 to 10, the time at which the trisulfate first appeared increased as the OH^-/Al_2O_3 ratio increased. For a constant OH^-/Al_2O_3 ratio, the CaO/Al_2O_3 ratio did not affect the time consistently, but in most instances higher CaO/Al_2O_3 ratio accelerated the conversion to the trisulfate, in accordance with the effect to be expected from the law of mass action. The conclusions of Lerch, Ashton, and Bogue [1] on the role of alkalinity are thus confirmed.

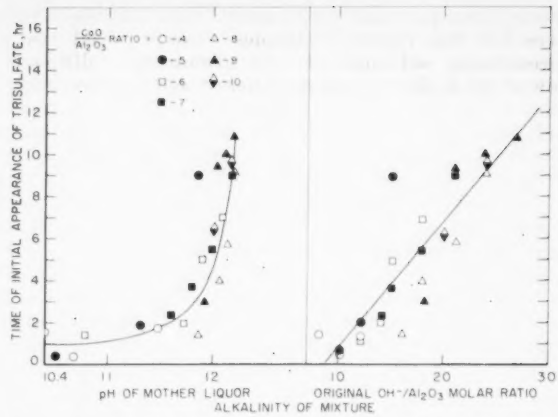

FIGURE 5. *Effect of alkalinity on time required for initial conversion of calcium aluminate monosulfate to calcium aluminate trisulfate.*

With extremely high CaO/Al_2O_3 ratios, the mass-action effect of the Ca^{++} ion may be stronger than the influence of OH^-, and trisulfate may be very readily precipitated at very high Ca^{++} concentrations.

The experience of other workers, who have been unable to prepare the monosulfate at room temperature, is possibly explained by these concentration-ratio requirements. For example, Kelly [20] attempted to prepare the monosulfate at room temperature from one liter of saturated $CaSO_4$ solution containing 3.06 g of $Al_2(SO_4)_3 \cdot 18H_2O$ and two liters of saturated $Ca(OH)_2$ solution. This mixture represents a CaO/Al_2O_3 molar ratio of 12, and an OH^-/Al_2O_3 ratio of 18. Although this is within the range of possible monosulfate formation based on consideration of the OH^-/Al_2O_3 ratio, it is near the low end of this range, and the OH^-/SO_3 ratio of Kelly's mixture was 3. In all the samples prepared in this work, the OH^-/SO_3 ratio was not less than 6, except for the preparation which turned out to be entirely trisulfate, sample 9, in which the OH^-/SO_3 ratio was 3.5.

6.2. Procedure for Preparation of Large Batches

Preparations 1, 2, 3, 4, and 5 were made from saturated $Ca(OH)_2$ solution, saturated $CaSO_4$ solution, and calcium aluminate solution. The calcium aluminate solution was prepared by shaking high-alumina cement (previously ignited at 1,000 °C to oxidize sulfides) with CO_2-free water for about 2.5 to 3 hr and rapidly filtering the supernatant liquid. (The calcium aluminate solution is metastable, and a precipitate appears unless it is used within a short time; if filtration is too slow, precipitation will occur during the filtration, but, once filtered, the solution is stable for several hours.) The calcium aluminate solution was added to the $Ca(OH)_2$ solution in a 12-liter flask while stirring; calcium sulfate solution was then added, and the entire mixture was stirred about 2 hr. The mixture was then filtered through a Buchner fritted-glass funnel, drained as free as possible of

mother liquor by suction, and transferred to a desiccator for conditioning to the desired H_2O content.

As a result of the limited range of concentrations in which the monosulfate precipitate may be preserved during the time required for the operations, the yield of the compound is low for a single batch prepared as described. The low solubility of $Ca(OH)_2$, 0.02 moles per liter, and the large CaO/Al_2O_3 molar ratio required, limits the quantity of Al_2O_3 that can be introduced, with the result that an individual 12-liter batch cannot theoretically yield more than 16 g of $3CaO{\cdot}Al_2O_3{\cdot}CaSO_4{\cdot}12H_2O$ under the most favorable conditions.

The yield cannot be increased by making several batches of the compound and mixing the filtered products because the precipitates obtained in different batches are slightly different in composition and the product, even if mixed, would not be uniform. The samples of the preparation taken for analysis might not have the same composition as the samples taken for calorimetry. The yield cannot be increased easily by increasing the volume of the mixture because excessively large reaction vessels would be needed. Potassium aluminate solution can be made more concentrated in Al_2O_3 than calcium aluminate solution, but large reaction vessels would still be required to maintain the CaO/Al_2O_3 ratio.

The following technique was therefore resorted to for producing larger batches (preparations 6, 7, and 8). About 140 to 230 ml of reagent $Al_2(SO_4)_3$ solution (0.08M) was added slowly to 11 liters of saturated $Ca(OH)_2$ solution. The mixture was stirred 5 to 10 min., allowed to settle 5 to 10 min., and 5 to 9 liters of the supernatant liquid was drawn off and discarded. Calcium hydroxide and aluminum sulfate solutions were then added in the same proportion as in the first addition and in quantity sufficient to replace the mother liquor removed. After stirring 5 to 10 min. and allowing to settle, 5 to 9 liters of the supernatant liquid was again drawn off and discarded. Three more additions of $Ca(OH)_2$ and $Al_2(SO_4)_3$ solutions were made by this alternate reaction-decantation technique. After the last addition, the entire remaining mass of precipitate produced was stirred for 15 min. and allowed to settle. Most of the supernatant liquid was withdrawn through the filter. The remainder was then stirred and the filtration completed. The total yield theoretically possible by this technique is about 40 g. The entire product is stirred at one time in mother liquor of the proper concentration. Analysis of the several mother-liquor batches showed no significant variations in concentration of CaO, but a steady increase in SO_3 content consistent with the formation of a precipitate containing less than the original mixture. The multiple addition-decantation technique cannot be continued indefinitely because the precipitate must be filtered before conversion to the trisulfate can take place.

7. References

[1] W. Lerch, F. W. Ashton, and R. H. Bogue, The sulphoaluminates of calcium, BS J. Research **2,** 715 (1929) RP54.

[2] O. M. Astreeva and L. Ya. Lopatnikova, The composition and properties of hydrated calcium sulfoaluminate (in Russian), Tsement **23,** No. 6, 11 (1957).

[3] F. D. Rossini, D. D. Wagman, W. H. Evans, S. Levine, and I. Jaffe, Selected values of chemical thermodynamic properties, NBS Circ. 500, U.S. Government Printing Office, Washington (1952).

[4] Compt. Rend. of the 21st Conference of the International Union of Pure and Applied Chemistry, Montreal (1961), Report of the Committee on Atomic Weights, pp. 284–327.

[5] H. A. Berman and E. S. Newman, Heat of formation of calcium aluminate monocarbonate at 25 °C, J. Research NBS, **65A** (Phys. and Chem.) No. 3, 197 (1961).

[6] H. A. Berman and E. S. Newman, Heat of formation of calcium trisulfoaluminate at 25 °C, Proceedings of the Fourth International Symposium on the Chemistry of Cement (Washington, 1960); NBS Mono. 43, pp. 247–257.

[7] A. Wexler and S. Hasegawa, Relative humidity-temperature relationships of some saturated salt solutions in the temperature range 0 to 50 °C, J. Research NBS **53,** 19 (1954), RP2512.

[8] R. H. Stokes and R. A. Robinson, Standard solutions for humidity control at 25 °C, Ind. Eng. Chem. **41,** 2013 (1949).

[9] D. L. Kantro, L. E. Copeland, and E. R. Anderson, An X-ray diffraction investigation of hydrated portland cement pastes, ASTM Proceedings **60,** 1020 (1960), Portland Cement Association Bulletin 128.

[10] E. S. Newman, Heat of formation of potassium calcium silicate, J. Research NBS, **62,** 207 (1950), RP2955.

[11] T. Thorvaldson, W. G. Brown, and C. R. Peaker, Studies on the thermochemistry of the compounds occurring in the system CaO-Al_2O_3-SiO_2, J. Am. Chem. Soc. **52,** 3927 (1930).

[12] G. Assarsson, Calcium aluminate. IV. The properties of aluminum hydroxide crystallized from calcium aluminate solutions, (in German), Z. anorg. allgem. Chem. **222,** 321 (1935).

[13] L. S. Wells and K. Taylor, Hydration of magnesia in dolomitic hydrated limes and putties, J. Research NBS **19,** 215 (1937) RP1022.

[14] J. C. Southard, Heat of hydration of calcium sulfates, Ind. Eng. Chem. **32,** 442 (1940).

[15] R. B. Peppler and E. S. Newman, Heats of formation of some barium aluminates, J. Research NBS **47,** 439 (1951), RP2269.

[16] F. E. Jones, The quaternary system CaO-Al_2O_3-$CaSO_4$-H_2O at 25 °C, J. Phys. Chem. **48,** 311 (1944).

[17] J. D'Ans and H. Eick, The system CaO-Al_2O_3-$CaSO_4$-H_2O at 20 °C (in German), Zement-Kalk-Gips **6,** 302 (1953).

[18] W. Eitel, Recent investigations of the system Lime-Alumina-Calcium Sulfate-Water, J. Am. Concrete Inst. **28,** No. 7, 689 (1957).

[19] Evelyn Stearns, NBS unpublished data, 1960.

[20] R. Kelly, Solid-liquid reactions amongst the calcium aluminates and sulphoaluminates, Can. J. Chem. **38,** 1218 (1960).

(Paper 67A1–188)

JOURNAL OF RESEARCH of the National Bureau of Standards—A. Physics and Chemistry
Vol. 67A, No. 1, January-February 1963

2,3-Dimethylpentane and 2-Methylhexane as a Test Mixture for Evaluating Highly Efficient Fractionating Columns*

Edwin C. Kuehner

(October 9, 1962)

A test mixture consisting of 2,3-dimethylpentane and 2-methylhexane was prepared and its relative volatility determined by a fractional distillation method. This test mixture was compared, experimentally and theoretically, with another test mixture commonly used for evaluating highly efficient fractionating columns.

1. Introduction

The development of more highly efficient fractionating columns has resulted in a greater need of test mixtures with lower relative volatilities than the ones commonly used in evaluating stills. The choice of components for such a test mixture is further limited to those which form ideal solutions and differ considerably from one another in a specific physical property, such as refractive index, by which the composition of mixtures of the components may be determined. The 2,2,4-trimethylpentane and *n*-heptane combination, with a normal boiling point difference of 0.812 °C, is an excellent test mixture for evaluating fractionating columns of medium efficiency. The separation of these components becomes sufficiently complete with fractionating columns of greatly increased efficiency, so that the number of theoretical plates, calculated by the Fenske equation [1],[1] becomes sensitive to small analytical errors.

Two isomers of heptane were selected for the components of a test mixture which might fulfill the requirements for evaluating very highly efficient fractionating columns. They are 2,3-dimethylpentane and 2-methylhexane, with normal boiling points [2] of 89.784 °C and 90.052 °C, respectively, a difference of 0.268 °C. The refractive index at 20 °C [2] of 2,3-dimethylpentane is 1.39196, and that of 2-methylhexane is 1.38485, a difference of 0.00711. This difference in refractive index is almost twice the difference in refractive index of 2,2,4-trimethylpentane and *n*-heptane.

2. Experimental Procedure

2.1. Apparatus

A random-packed still having a column 25 mm in diameter and 300 cm in height was used in this work. This vacuum-jacketed column was packed with chromel spirals (Helipak) and further insulated with aluminum-covered glass wool.

Also used was a precision-packed still similar to the Podbielniak Heligrid type, but having a packing made of precision wound platinum wire. This vacuum-jacketed column was 25 mm in diameter by 100 cm in height and further insulated with aluminum-covered glass wool.

A differential refractometer with a rotating cell block and vernier eye piece was used to determine mixture composition. A gas chromatograph, Perkin-Elmer Model 154, equipped with a hydrogen flame ionization detector and a capillary column with squalene substrate, was used for determining the presence of other isomers in each of the test mixture components.

2.2. Materials

The components for the *n*-heptane—2,2,4-trimethylpentane test mixture were obtained from Phillips Petroleum Company. They were distilled and redistilled in the 300-cm random-packed still until all traces of impurities detectable by analysis with the gas chromatograph and the differential refractometer were removed.

Of the two components of the 2,3-dimethylpentane—2-methylhexane test mixture, only the 2,3-dimethylpentane was obtainable in better than 90 mole percent purity from commercial sources. This material also contained about 5 mole percent of the second component in the test mixture, 2-methylhexane, which did not have to be removed. A distillation with the 300 cm still removed all of the other impurities which were detectable with the gas chromatograph.

Commercial grade isoheptane, obtainable from Phillips Petroleum Company, was the only commercial source of 2-methylhexane. This material contained both of the desired components of the test mixture, but in amounts of less than 20 mole percent of each. The presence of considerable amounts of close-boiling naphthenes in the commercial material was responsible for the difficulty in obtaining a test mixture from this material.

Several 4,000 ml charges of isoheptanes were distilled with the 300-cm random-packed still. With the aid of the gas chromatograph, the fractions having a high concentration of the desired two isomers were selected; these were combined and

* A portion of this work was uesd as a partial fulfillment of the requirements toward a M.S. degree from the American University.

[1] Figures in brackets indicate the literature references at the end of this paper.

redistilled. Only the fractions from this second distillation, which contained less than 2 percent naphthenes by chromatographic analysis, were combined for an attempt to purify further by azeotropic distillation. An equal amount of triethylamine was used as the azeotrope former, which was then separated from each fraction by subsequent extractions with ice water and dilute mineral acid. The fractions for which their respective chromatograms showed only two peaks, representing the desired isomers, were combined and percolated through silica gel to remove any remaining trace of triethylamine. By repeating this distillation procedure, 700 ml of 2,3-dimethylpentane—2-methylhexane test mixture, containing about 70 mole percent of 2-methylhexane, was obtained from 10 gallons of commercial isoheptanes.

Triethylamine was found to be more effective in removing traces of naphthenes than some of the other azeotrope formers that were tried, but complete removal was unsuccessful when more than 2 percent of naphthenes was still present in the isoheptanes after the second distillation.

The quantity of 2,3-dimethylpentane—2-methylhexane test mixture obtained by azeotropic distillation was sufficient for efficiency tests and relative volatility determination with the 100 cm precision packed still, but was insufficient for use in the 300-cm still having a greater hold-up in the column. Fortunately, a liter of synthetically prepared 2-methylhexane was obtained from the Chemistry Department of the Ohio State University. Because this material was of very high purity, further distillation was not necessary.

2.3. Calibration of Differential Refractometer

The determination of the composition of the test mixtures by gas chromatography was not possible because neither of the mixtures would separate completely, and the resulting peak areas could not be calculated with sufficient accuracy. The determination of composition by refractive index measurements, more precisely accomplished with a differential refractometer, was found to be the most expedient method of analysis.

Since the change in refractive index with change in composition of a test mixture is not entirely a linear relationship, it was necessary to calibrate the differential refractometer reading against a series of known compositions of the constituents for both test mixtures. Standard samples were used for this purpose, and the best equation of the curve was calculated by the method of least squares. The results, expressed as the difference between the refractive index of the mixture and one of their constituents, are as follows:

For 2,2,4-trimethylpentane and n-heptane Δ=ri(2, 2, 4-trimethylpentane)—ri (mixture) $=0.0030x+0.0008x^2$ where ri is the refractive index and x is the mole fraction of n-heptane.

For 2,3-dimethylpentane and 2-methylhexane Δ=ri(mixture)—ri(2-methylhexane) $=0.0073x-0.0002x^2$ where x is the mole fraction of 2,3-dimethylhexane.

2.4. Relative Volatility Determination

The relative volatility of the 2,3-dimethylpentane—2-methylhexane test mixture was determined by the fractional distillation method [3] and compared with the value calculated from vapor pressure data. By this method, the relative volatility of an unknown test mixture is determined with a still for which the efficiency was previously determined with a test mixture of known relative volatility. For the test mixture of known relative volatility, 2,2,4-trimethylpentane—n-heptane with a value of 1.0240 [4] was used. The 100-cm still was chosen to avoid exceeding the recommended maximum separation of 2,2,4-dimethylpentane and n-heptane [5]. This 100-cm still was charged with 700 ml of the 2,2,4-trimethylpentane—n-heptane test mixture and preflooded. Twenty-four hours later samples were taken of the distillate and of the returning material entering the still pot. The differential refractometer and the calibration equation for this test mixture were used to determine the composition of the samples. The number of theoretical plates n given in table 1 was calculated by means of the Fenske equation [1]. The average of seven determinations was used later to calculate the relative volatility of the 2,3-dimethylpentane—2-methylhexane test mixture.

TABLE 1. *Efficiency determination of 100 cm precision-packed still (2,2,4-trimethylpentane—n-heptane test mixture)*

Determinations	Boil-up rate	Mole fraction		Number of theoretical plates
		Distillate	Bottom	
	ml/min			
1	20.7	0.6997	0.3508	60.6
2	21.2	.7052	.3483	62.2
3	21.0	.6468	.3483	61.3
4	20.2	.6981	.3642	57.8
5	20.4	.7251	.3556	65.4
6	20.8	.7056	.3513	61.7
7	20.2	.7176	.3642	61.8
Average	20.6			61.5

The same procedure was employed with 700 ml of the 2,3-dimethylpentane—2-methylhexane test mixture. The same still was used under as nearly the same operating conditions as possible, and samples were taken and analyzed in a similar manner. The relative volatility α of this test mixture was calculated by the Fenske equation rearranged into the following form: $\log \alpha = \frac{1}{n} \log (x/1-x)(1-y/y)$ where x and y are the mole fractions of 2,3-dimethylpentane in the samples taken from the distillate and material returning to the still pot, respectively. The average of the three determinations (table 2) is in good agreement with the value calculated from the vapor pressure data [2,6] of 2, 3-dimethyplentane and 2-methylhexane at the temperature corresponding to the mean value of their normal boiling points. The value thus obtained should not be regarded as an absolute value for the relative volatility for this test mixture, but

as a sufficiently good approximation to show some of the merits of this test mixture from both experimental and theoretical considerations.

TABLE 2.—*Relative volatility determination of 2,3-dimethylpentane—2-methylhexane test mixture*

Determinations	Boil-up rate	Mole fraction		Relative volatility
		Distillate	Bottom	
	ml/min			
1	20.3	0.5876	0.4681	1.00774
2	19.9	.5916	.4671	1.00807
3	19.5	.5880	.4630	1.00790
Average	19.9			1.00790
Value calculated from vapor pressure data [2,6]				1.00795

2.5. Efficiency Test Runs

Efficiency test runs were performed, using the 300-cm random-packed still, with both the 2,2,4-trimethylpentane—*n*-heptane and the 2,3-dimethylpentane—2-methylhexane test mixtures. For each run, the still vaporizer was charged with 1,800 ml of one of the mixtures and preflooded. While operating at total reflux, samples of 2 ml each were taken of the distillate and the returning material at 24-hr intervals for a period of 7 days. During a run the rate of vaporization was controlled by a thermistor-actuated control device [7]. The composition of the samples was determined with the differential refractometer which was calibrated with known compositions of the two test mixtures. The number of equivalent theoretical plates was calculated from the composition of the samples of the distillate and material returning to the vaporizer by means of the Fenske equation. The values 1.024 [4] for the relative volatility of 2,2,4-trimethylpentane—*n*-heptane test mixture and 1.0079 for the 2,3-dimethylpentane—2-methylhexane test mixture were used in these calculations.

A standard deviation, σ_{ri} of 16 scale divisions or 0.000013 refractive index units, was determined with both test mixtures with the differential refractometer. By substituting the calibration equations for each test mixture into the standard propagation of error formula, equations for the standard deviation in terms of mole fraction were derived. For the 2,2,4-trimethylpentane—*n*-heptane test mixture the equations were $\sigma_x=\sigma_{ri}/(0.0030+0.0016x)$ and $\sigma_y=\sigma_{ri}/(0.0030+0.0016y)$. For the 2,3-dimethylpentane—2-methylhexane test mixture the equations were $\sigma_x=\sigma_{ri}/(0.0073-0.0004x)$ and $\sigma_y=\sigma_{ri}/(0.0073-0.0004y)$. The following equation was used to calculate the standard deviation, σ_n, in terms of the number of theoretical plates:

$$\sigma_n^2=\frac{1}{(\ln\alpha)^2}\left[\left\{\frac{\sigma_x}{x(1-x)}\right\}^2+\left\{\frac{\sigma_y}{y(1-y)}\right\}^2\right]$$

For both test mixtures, x and y are the mole fractions of the lower boiling constituents in samples taken from the top and bottom of the still respectively; σ_x and σ_y are the standard deviations of x and y respectively. The latter equation was derived from the Fenske equation and the standard propagation of error formula in which the correlation coefficient is zero.

Data on an efficiency run for each test mixture, including the standard deviations in terms of mole fraction and number of theoretical plates are given in table 3. These standard deviations were propagated entirely from analytical errors involved in reading the differential refractometer. Errors involved in taking boil-up rates and other errors peculiar to still operation, which are extremely difficult to determine, were entirely excluded in any of the calculations. The data given in table 3 should not be interpreted as an actual evaluation of the still at a definite boil-up rate, but as an indication of the effect an analytical error has on the calculated number of theoretical plates for the two test mixtures. For this reason, actual boil-up rates were not included in the data.

TABLE 3.—*Efficiency test runs on 300 cm random packed fractionation column*

Test mixture	Days after preflooding	x	σ_x [a]	y	σ_y [a]	n	σ_n
2,2,4 Trimethylpentane—*n*-heptane	1	0.9651	0.0029	0.1844	0.0040	202.7	3.2
	2	.9902	.0029	.1741	.0040	261.5	12.5
	3	.9938	.0029	.1690	.0040	281.2	19.6
	4	.9944	.0029	.1640	.0040	284.1	20.3
	5	.9942	.0029	.1584	.0041	287.3	21.0
	6	.9944	.0029	.1539	.0041	290.2	22.5
	7	.9944	.0029	.1490	.0041	291.9	22.5
2,3-Dimethylpentane—2-methylhexane	1	.6087	.0018	.2650	.0019	185.8	1.6
	2	.6760	.0018	.2587	.0019	227.2	1.6
	3	.6968	.0018	.2574	.0019	240.4	1.7
	4	.7003	.0018	.2584	.0019	242.0	1.7
	5	.7023	.0018	.2574	.0019	243.8	1.7
	6	.7196	.0018	.2538	.0019	256.8	1.7
	7	.7294	.0018	.2528	.0019	258.0	1.7

[a] Based on a σ_{ri} of 0.000013 refractive index units.

3. Discussion

As shown in table 3, a small error in reading the differential refractometer corresponds to a much greater error in the calculated number of theoretical plates when the 2,2,4-trimethylpentane—*n*-heptane test mixture is used for evaluating a highly efficient fractionating column than when the 2,3-dimethylpentane—2-methylhexane test mixture is used. This higher error occurs because the difference in boiling points of 2,2,4-trimethylpentane and *n*-heptane is large enough to result in such complete separation that the calculated number of theoretical plates is greatly affected by analytical errors. Also, the difference in their refractive indices is considerably less than that of 2,3-dimethylpentane and 2-methylhexane, resulting in a lower analytical precision.

In order to make a graphical comparison of the corresponding σ_n due to analytical errors over a wide range of theoretical plates n for both test mixtures, a common basis or condition was necessary. It has

been pointed out [5] that the effect of random analytical errors on n is least when the mole fraction of the material returning to the vaporizer y is equal to $(1-x)$, where x is the mole fraction of the lower boiling constituent in the distillate. This is sufficiently correct only when the magnitudes of the probable analytical errors of x and y are approximately equal. With this optimum condition imposed, the Fenske equation can be written as

$$n=\frac{2\log(x/1-x)}{\log\alpha}$$

and the standard propagation of error formula as

$$\sigma_n=\frac{(\sigma_x+\sigma_{(1-x)})^{\frac{1}{2}}}{x(1-x)(\ln\alpha)}$$

By calculating x for a series of n values and substituting these values into the propagation of error formula, a series of σ_n values was obtained. The σ_x and $\sigma_{(1-x)}$ used in the calculation were obtained by the use of the error formula for the calibration of the differential refractometer and a standard deviation, σ_{x1}, of 16 scale division or 0.000013 refractive index units. The calculated σ_n values are plotted against theoretical plates in figure 1 for both test mixtures. These curves show that, under the imposed condition, the 2,2,4-trimethylpentane—n-heptane test mixture is more desirable for evaluating stills developing less than 125 theoretical plates, but its desirability rapidly diminishes in evaluating stills greater than 125 plates. A still with 500 theoretical plates could be evaluated with the same standard deviation, σ_n, when the 2,3-dimethylpentane—2-methylhexane test mixture is used as when a 225-plate still is evaluated with the 2,2,4-trimethylpentane—n-heptane test mixture.

Only the analytical errors in reading the differential refractometer were considered in determining the curves in figure 1; the other factors would have approximately the same effect on both test mixtures, when the stills are operated under the same conditions.

The 2,3-dimethylpentane—2-methylpentane test mixture has the advantage of having a very low relative volatility and a large difference in refractive index of its components which greatly extends its usefulness in evaluating more highly efficient stills. A disadvantage in using this test mixture is the increased cost involved in the preparation and purification of its components over other readily obtainable test mixtures. Since it is possible to use a given volume of test mixture repeatedly for evaluating a number of fractionating columns, this initial cost may not seriously hamper its desirability as a test mixture, especially in evaluating very highly efficient fractionating columns in which the separation of components of other test mixtures becomes too great for precise analysis.

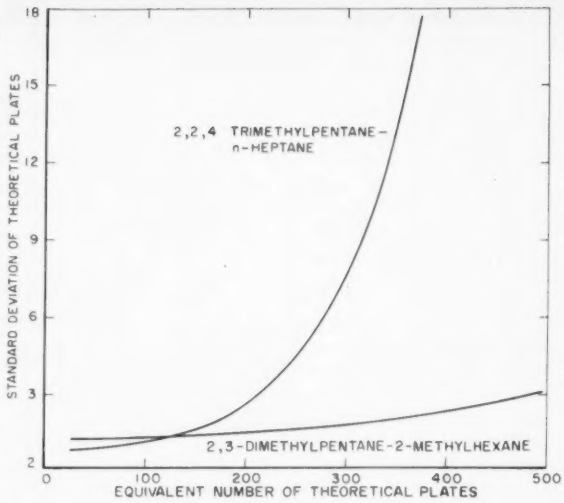

FIGURE 1. *Variation of standard deviation in number of theoretical plates with number of theoretical plates.*

Based on a standard deviation of 0.000013 refractive index units for both test mixtures and the condition that $y=(1-x)$.

The author thanks R. T. Leslie for helpful assistance and kind encouragement. Also, he acknowledges the kind encouragement of C. P. Saylor, NBS, F. L. Howard, NBS, and L. Schubert, The American University. The 2-methylhexane supplied by K. W. Greenlee, Ohio State University, is greatly appreciated.

4. References

[1] M. R. Fenske, Ind. Eng. Chem. **24,** 482 (1932).
[2] American Petroleum Institute Research Project 44, Selected Values of Properties of Hydrocarbons and Related Compounds (Carnegie Press, Pittsburgh, Pa., 1953).
[3] J. Griswold, Ind. Eng. Chem. **35,** 247 (1943).
[4] E. R. Smith and H. J. Matheson, J. Research NBS **20,** 641 (1938). RP1097.
[5] G. H. Miller and R. A. Woodle, General Papers presented before the Division of Petroleum Chemistry, 116th Meeting, A.C.S. Atlantic City, New Jersey, September 18–23, 1949.
[6] T. E. Jordan, Vapor Pressure of Organic Compounds, (Interscience Publishers, Inc., 1954).
[7] E. C. Kuehner and R. T. Leslie, Anal. Chem. **34,** 1155 (1962).

(Paper 67A1–189)

JOURNAL OF RESEARCH of the National Bureau of Standards—A. Physics and Chemistry
Vol. 67A, No. 1, January–February 1963

Phase Equilibrium Relations in the Sc_2O_3-Ga_2O_3 System

S. J. Schneider and J. L. Waring

(September 19, 1962)

The phase equilibrium diagram was determined for the Sc_2O_3-Ga_2O_3 system. A quenching furnace, wound with 60 percent Pt—40 percent Rh wire, was employed for experiments conducted at temperatures up to 1,800 °C. An induction furnace, having an iridium crucible susceptor, was used to obtain higher temperatures. Temperatures in the quenching furnace were measured with both an optical pyrometer and a 95 percent Pt—5 percent Rh versus 80 percent Pt—20 percent Rh thermocouple. The melting point of Ga_2O_3 was determined as 1,795 ±15 °C. Experiments at temperatures as high as 2,405 °C failed to melt Sc_2O_3. Two intermediate binary phases, a compound believed to be $6Sc_2O_3$·$5Ga_2O_3$ and a solid solution occur in the system. The solid solution phase appears as a single phase in the region roughly defined by the compositional limits of 55 to 73 mole percent Ga_2O_3 at the solidus. The 6:5 compound, stable only at high temperatures, melts incongruently at 1,770 ±15 °C and decomposes below 1,700 ±15 °C. The compound appears to have orthorhombic symmetry with a=13.85 A, b=9.80 A, and c=9.58 A. The indicated uncertainties in the melting points are a conservative estimate of the overall inaccuracies.

1. Introduction

A recent publication by Schneider, Roth, and Waring [1][1] outlined the general subsolidus phase relations for binary combinations of oxides of the trivalent cations. The paper was intended to provide a basis for subsequent detailed phase equilibrium studies of systems which might be representative of a particular group of systems. As part of a series of binary systems selected for study from those delineated in the previous work, the present investigation reports the phase equilibrium relations in the Sc_2O_3-Ga_2O_3 system.

Scandium sesquioxide (Sc_2O_3) is cubic with a=9.845 A [2] and has the C-type rare earth oxide structure (Tl_2O_3). It has no known polymorphs. The melting point of Sc_2O_3 has not been previously reported although it was estimated to be about 2,300 °C [3].

Several polymorphic forms of Ga_2O_3 are known to exist [4]. The only stable modification, commonly referred to as beta gallia, is monoclinic with a=12.23 A, b=3.04 A, c=5.80 A, and β=103.7° [5]. Goldschmidt and coworkers [6] estimated the melting point of Ga_2O_3 to be approximately 1,900 °C. Von Wartenberg and Reusch [7] reported a value of 1,740 °C. The latest melting point determination on Ga_2O_3 was that of Hill, Roy, and Osborn [8] who reported 1,725±15 °C.

2. Materials

The starting materials used in this study were found by general qualitative spectrochemical analysis [2] to have the following impurities:

Sc_2O_3—Y present in amounts less than 1.0 percent. La, Mn, Si, Yb, and Zr; each present in amounts less than 0.1 percent. Al, Ca, Cr, Cu, Fe, Mg, and Pb; each present in amounts less than 0.01 percent. Ag present in amounts less than 0.001 percent.

Ga_2O_3—Al and Si; each present in amounts less than 0.01 percent. Ca, Cu, Fe, Mg, Ni, Pb, and Sn; present in amounts less than 0.001 percent. Ag present in amounts less than 0.0001 percent.

3. Apparatus and Test Methods

A specially designed quenching furnace as well as an induction furnace were used in the present study. The quenching furnace is of interest because of its suitability for extended use at temperatures up to 1,800 °C.[3] It consisted essentially of two concentric alumina tubes encased in a "Transite" framework and insulated with alumina grain. The inner tube (o.d.—½ in., 24 in. long) and the outer tube (o.d.—2 in., 17 in. long) were wound nine turns per inch with 20 gage, 60 percent Pt–40 percent Rh wire, and 20 gage, 80 percent Pt–20 percent Rh wire, respectively. Separate power sources were used with each of the two windings. The power to the outer winding (booster) was supplied from a variable transformer. No attempt was made to control the temperature of the booster other than with approximate settings of the transformer. An a-c bridge type controller [10] in which the furnace winding was one arm of the bridge was used to obtain and control the temperature of the inner winding. As indicated by the thermocouple, temperatures in the hot zone of the furnace were easily controlled to ±3 °C.

[1] Figures in brackets indicate the literature references at the end of this paper.
[2] The spectrochemical analyses were performed by the Spectrochemistry Section of the National Bureau of Standards.
[3] All quoted temperatures referring to the present work are given on the International Practical Temperature Scale of 1948 (Text Revision 1960) [9].

The specimen was placed in a small (o.d.—3 mm, i.d.—2.6 mm, ½ in. long) 80 percent Pt—20 percent Rh tube which in turn was suspended from the quenching hooks in the hot zone of the inner tube by 0.005 in. diam 60 percent Pt—40 percent Rh wire. The hooks were made from 20 gage 60 percent Pt—40 percent Rh wire. A 90 percent Pt—10 percent Rh versus 100 percent Pt thermocouple was used to measure temperatures below 1,650 °C. For measurements between 1,650 and 1,800 °C, both a 95 percent Pt—5 percent Rh versus 80 percent Pt—20 percent Rh thermocouple and an optical pyrometer were used. It is noteworthy that it was necessary to shield the thermocouple with 90 percent Pt—10 percent Rh foil in order to reduce the pickup of induced emf at high temperatures. Even when the shielding was adequately grounded, the use of electronic equipment to record the output of the thermocouple was impossible. To overcome this problem, a high precision potentiometer and spot-light galvanometer were employed to measure the d-c emf of the thermocouple.

The optical pyrometer was sighted through a calibrated 45° glass prism using the bottom of the quenching hook-thermocouple assembly as the target. The platinum alloy tube could not be seen and thus approximate blackbody conditions probably prevailed. In every instance, the thermocouple and pyrometer values agreed to within 10 °C.

The essential features and characteristics of the induction furnace used in this work has been previously described [11]. In essence, the induction furnace simply consisted of an iridium crucible and cover which acted as the susceptor. The crucible with cover had the following overall nominal dimensions: height—¾ in., o.d.—7/16 in., and wall thickness—3/64 in. A small fragment of a sintered pellet was placed on a small iridium button which in turn was set inside the crucible. Temperatures were controlled manually and were measured with an optical pyrometer sighted through a calibrated 45° glass prism and the 3/64 in. diam hole in the crucible cover. As verified by calibration data, blackbody conditions were apparently obtained.

The temperature measuring systems of both the quenching furnace and the induction furnace were frequently calibrated against the melting points of Au (1,063 °C), Pd (1,552 °C), and Pt (1,769 °C).[4] In addition, the measuring system of the induction furnace was also calibrated against the melting point of Rh (1,960 °C). Temperatures measured in either furnace were considered to be accurate to at least ±5 °C below 1,650 °C and ±15° above. Precision of the measurements were better than ±5 °C.

Specimens were prepared from either 0.75 or 1 g batches of various combinations of Sc_2O_3 and Ga_2O_3. Calculated amounts of each oxide, corrected for ignition loss at 1,000 °C, were mechanically mixed, pressed at 10,000 lb/in.² into a ⅜ in. diam pellet and fired on Pt foil at 1,350 °C a minimum of 6 hr. The specimens were then ground in an agate mortar, remixed, again pressed into pellets and fired at 1,600 °C for 12 hr. The pellets, without regrinding, were again fired at 1,650 °C a minimum of 12 hr and in some cases as long as 30 hr.

Subsolidus as well as some melting point data were obtained by the familiar quenching technique. Following the preliminary heat treatments, the specimens were ground, placed in the platinum alloy tubes and fired at various temperatures for different periods of time in the quenching furnace. The tube containing the specimen was quenched into ice water and then examined by X-ray diffraction at room temperature using a high-angle recording Geiger-counter diffractometer and Ni-filtered Cu radiation. Equilibrium was assumed to have been attained when the X-ray pattern showed no change after successive heat treatments of a specimen or when the data were consistent with the results from a previous set of experiments.

Solidus temperatures were established using both the platinum alloy quenching furnace and the iridium crucible induction furnace. Because of the temperature limitations of the quenching furnace, melting points above 1,800 °C were determined exclusively with the induction unit. However, below 1,800 °C, some duplicate determinations were performed in each of the furnaces.

Solidus temperatures were determined by visual observation of quenched or rapidly cooled specimens which had been held at a given temperature approximately 30 to 60 sec. Powdered samples in platinum alloy tubes were used with the quenching furnace determinations while small fragments of a sintered pellet set directly on the iridium button were used as test specimens in the induction furnace. Melting of the specimen was indicated by a combination of evidence. A partially or completely melted specimen characteristically slumped very slightly and invariably adhered to the side of the platinum alloy tube or iridium button. In addition, the specimen had a translucent, pearly to clear appearance. Solidus temperatures, as recorded, are estimated to be accurate to ±15 °C.

Liquidus temperatures were practically impossible to determine because of the high viscosity of the liquid phase. In essence, the physical appearance of a partially melted specimen did not differ appreciably from that of a completely melted sample. X-ray patterns of melted specimens were extremely diffuse and difficult to interpret. A consistent correlation between the degree of melting and the X-ray pattern of a specimen could not be made.

4. Results and Discussion

The equilibrium phase diagram for a major portion of the Sc_2O_3-Ga_2O_3 system is given in figure 1. It was constructed from the data listed in tables 1 and 2. The solid circles represent the compositions and temperatures of experiments conducted in the quench furnace. Open circles indicates those studied in the induction unit. Triangles represent the boundary limits of solid solution areas as determined by the parametric method [12]. The liquidus curve given in the figure is considered to be a reasonable estimate of the true liquidus.

[4] The purity of the metals used for calibration purposes was better than 99.9 percent.

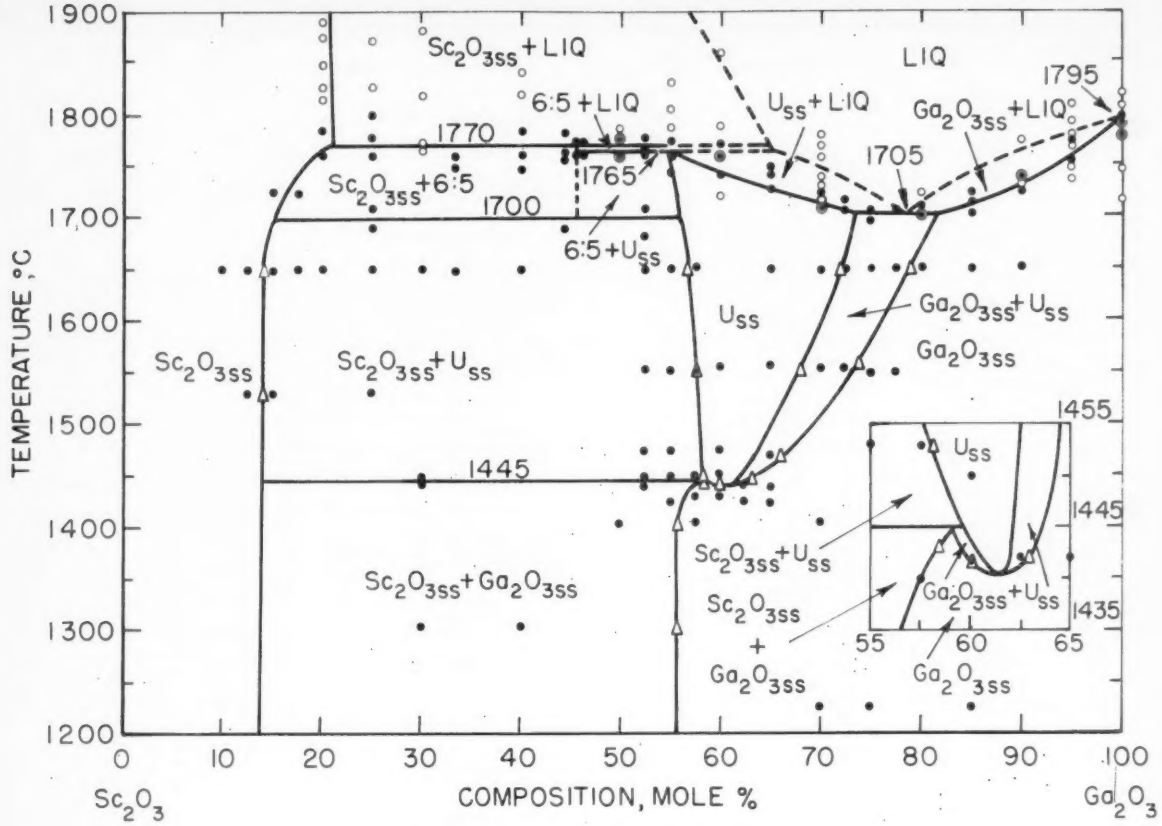

FIGURE 1. *Phase equilibrium diagram for the Sc_2O_3–Ga_2O_3 system*

[1] Insert shows expanded view of diagram from 55 to 65 mole percent Ga_2O_3 and from 1,485 °C to 1,455 °C.
Uss—Solid solution phase of unknown structure type.
Liq.—Liquid.
ss—Solid solution.
●—Compositions and temperatures of experiments conducted in the quench furnace.
○—Compositions and temperatures of experiments conducted in the iridium crucible induction furnace.
△—Boundary limits as determined by the parametric method.
⊙—Compositions and temperatures of experiments conducted in both the quenching and induction furnaces.

TABLE 1. *Experimental quenching data for compositions in the Sc_2O_3–Ga_2O_3 system*

Composition		Heat treatment [a]		X-ray diffraction analyses [b]	Remarks
Sc_2O_3	Ga_2O_3	Temp.	Time		
Mole%	*Mole%*	*°C*	*hr*		
90	10	1650	2	Sc_2O_{3ss}	
87.5	12.5	1530	6.5	Sc_2O_{3ss}	
		1650	2	Sc_2O_{3ss}	
85	15	1530	6.5	Sc_2O_{3ss}[c]	
		1650	2	Sc_2O_{3ss}[d]	U_{ss} not detected.
		1727	4.5	Sc_2O_{3ss}	
82.5	17.5	1650	2	$Sc_2O_{3ss}+U_{ss}$[c]	Similar results obtained on specimen furnace cooled from 1,650 °C.
		1727	4.5	$Sc_2O_{3ss}+6:5$	
80	20	1650	2	$Sc_2O_{3ss}+U_{ss}$[d]	Similar results obtained on specimen furnace cooled from 1,650 °C.
75	25	1530	6.5	$Sc_2O_{3ss}+U_{ss}$[c]	
		1650	2	$Sc_2O_{3ss}+U_{ss}$[c]	Similar results obtained on specimen furnace cooled from 1,650 °C.
		1692	4.5	$Sc_2O_{3ss}+U_{ss}$[c]	
		1709	3.5	$Sc_2O_{3ss}+U_{ss}+6:5$[c]	Reheat of 1,650 °C specimen nonequilibrium; 6:5 forming with U_{ss} decreasing in amount relative to previous heat.

Footnotes at end of t able.

TABLE 1. *Experimental quenching data for compositions in the Sc_2O_3–Ga_2O_3 system*—Continued

Composition		Heat treatment [a]		X-ray diffraction analyses [b]	Remarks
Sc_2O_3	Ga_2O_3	Temp.	Time		
Mole%	*Mole%*	*°C*	*hr*		
		1760	4	Sc_2O_{3ss}+6:5	
70	30	1304	64	Sc_2O_{3ss}+Ga_2O_{3ss}	
		1441	24	Sc_2O_{3ss}+U_{ss}	Nonequilibrium.
		1441	68	Sc_2O_{3ss}+Ga_2O_{3ss}+U_{ss}	Nonequilibrium; U_{ss} decreasing in amount relative to previous heat.
		1447	68	Sc_2O_{3ss}+U_{ss}[d]	
		1447	68	Sc_2O_{3ss}+U_{ss}+Ga_2O_{3ss}	Nonequilibrium; reheat of 1,304 °C specimen.
		1650	2	Sc_2O_{3ss}+U_{ss}[d]	
66.667	33.333	1747	3.5	Sc_2O_{3ss}+6:5+U_{ss}	Nonequilibrium.
		1757	4.5	Sc_2O_{3ss}+6:5+U_{ss}	Reheat of 1,747 °C specimen; nonequilibrium; U_{ss} decreasing in amount relative to previous heat.
		1642	5	Sc_2O_{3ss}+U_{ss}[c]	Reheat of 1,757 °C specimen.
60	40	1304	64	Sc_2O_{3ss}+Ga_2O_{3ss}	
		1650	2	U_{ss}+Sc_2O_{3ss}[d]	
		1747	4	6:5+Sc_2O_{3ss}+U_{ss}	Reheat of 1,650 °C specimen; nonequilibrium.
		1760	4	6:5+Sc_2O_{3ss}	Reheat of 1,747 °C specimen.
		1768	1	6:5+Sc_2O_{3ss}+U_{ss}	Nonequilibrium.
55.56	44.44	1758	4	6:5+U_{ss}+Sc_2O_{3ss}	Calcined only at 1,300 °C for 20 hr; nonequilibrium.
(5:4)		1763	9	6:5+U_{ss}+Sc_2O_{3ss}	Calcined only at 1,300 °C for 20 hr; nonequilibrium; U_{ss} and Sc_2O_{3ss} barely detectable.
		1689	3	U_{ss}+Sc_2O_{3ss}[d]	Calcined only at 1,300 °C for 20 hr; specimen heated first to 1,761 °C for 1 hr then cooled to 1,689 °C.
54.545	45.455	1761	10.5	6:5	Calcined only at 1,350 °C for 16 hr; may be small amount of U_{ss} present.
(6:5)					
53.846	46.154	1760	5	6:5+U_{ss}+Sc_2O_{3ss}	Calcined only at 1,350 °C for 20 hr; nonequilibrium.
(7:6)		1762	4.5	6:5+U_{ss}	Reheat of 1,760 °C specimen.
50	50	1405	16	Ga_2O_{3ss}+Sc_2O_{3ss}	Calcined only at 1,350 °C for 20 hr.
		1758	4	6:5+U_{ss}	Calcined only at 1,350 °C for 20 hr.
47.5	52.5	1443	6	Ga_2O_{3ss}+Sc_2O_{3ss}+U_{ss}	Nonequilibrium; U_{ss} present in very small amounts.
		1447	68	U_{ss}+Sc_2O_{3ss}	
		1471	21	U_{ss}+Sc_2O_{3ss}[d]	
		1555	2	U_{ss}+Sc_2O_{3ss}[c]	
47.5	52.5	1650	2	U_{ss}+Sc_2O_{3ss}[d]	Similar results obtained on specimen furnace cooled from 1,650 °C.
		1760	5	U_{ss}+6:5	
		1648	4	U_{ss}+Sc_2O_{3ss}[d]	Reheat of 1,760 °C specimen.
		1680	4.5	U_{ss}+Sc_2O_{3ss}[d]	Reheat of 1,760 °C specimen.
		1709	4	U_{ss}+6:5	Reheat of 1,760 °C specimen.
45	55	1423	66	Ga_2O_{3ss}+Sc_2O_{3ss}	
		1450	19	U_{ss}+Sc_2O_{3ss}	
		1471	21	U_{ss}+Sc_2O_{3ss}[d]	
		1555	2	U_{ss}+Sc_2O_{3ss}[d]	
		1650	2	U_{ss}+Sc_2O_{3ss}	
		1742	2	U_{ss}	
42.5	57.5	1405	16	Ga_2O_{3ss}	
		1429	18	Ga_2O_{3ss}	
		1440	19	Ga_2O_{3ss}+U_{ss}	Nonequilibrium.
		1453	19	U_{ss}+Sc_2O_{3ss}	
		1559	2	U_{ss}	
		1650	2	U_{ss}	
40	60	1429	18	Ga_2O_{3ss}	
		1442	220	Ga_2O_{3ss}+U_{ss}	
		1450	19	U_{ss}	
		1475	4	U_{ss}	
		1559	2	U_{ss}	
37.5	62.5	1423	156	Ga_2O_{3ss}	
		1442	220	Ga_2O_{3ss}+U_{ss}	
35	65	1423	156	Ga_2O_{3ss}	
		1442	220	Ga_2O_{3ss}	
		1471	21	Ga_2O_{3ss}+U_{ss}	
		1559	2	U_{ss}	
		1650	2	U_{ss}	
30	70	1227	94	Ga_2O_{3ss}	
		1402	2	Ga_2O_{3ss}	
30	70	1555	2	U_{ss}+Ga_2O_{3ss}	
		1650	2	U_{ss}	
27.5	72.5	1555	2	Ga_2O_{3ss}+U_{ss}	
		1650	25	U_{ss}+Ga_2O_{3ss}	
		1650	30	Ga_2O_{3ss}(I)+Ga_2O_{3ss}(II)+U_{ss}	Specimen not quenched; nonequilibrium. The Ga_2O_{3ss} phases have different unit cell dimensions.
25	75	1227	94	Ga_2O_{3ss}	
		1550	2	Ga_2O_{3ss}	
		1650	2	Ga_2O_{3ss}+U_{ss}	
		1650	24	Ga_2O_{3ss}(I)+Ga_2O_{3ss}(II)	Specimen not quenched; nonequilibrium. The Ga_2O_3 phases have different unit cell dimensions.
22.5	77.5	1550	2	Ga_2O_{3ss}	Reheat of 1,650 °C specimen.
		1650	2	Ga_2O_{3ss}+U_{ss}	
		1550	30	Ga_2O_{3ss}(I)+Ga_2O_{3ss}(II)	Specimen not quenched; nonequilibrium. The Ga_2O_{3ss} phases have different unit cell dimensions.
20	80	1650	2	Ga_2O_{3ss}	Same results obtained on specimen furnace cooled from 1,650 °C.
15	85	1227	94	Ga_2O_{3ss}	
		1650	2	Ga_2O_{3ss}	Same results obtained on specimen furnace cooled from 1,650 °C.
10	90	1650	2	Ga_2O_{3ss}	Same results obtained on specimen furnace cooled from 1,650 °C.

[a] Unless otherwise indicated, all specimens calcined at 1,350 °C for 6 hr, 1,600 °C for 12 hr and at 1,650 °C for a minimum of 12 hr prior to quenching experiment.

[b] Phases identified are given in order of amount present at room temperature: ss—solid solution: U—solid solution of unknown structure type; 6:5—compound having approximate composition of $6\,Sc_2O_3{:}5Ga_2O_3$.

[c] Extraneous X-ray peaks at d=2.7216 A and d=2.4212 A; probably represent nonequilibrium phase.

[d] Extraneous X-ray peak at d=2.7216 A; probably represents nonequilibrium phase.

TABLE 2. *Melting characteristics of the Sc_2O_3–Ga_2O_3 system*

Composition [a]		Temperature [b]	Furnace [c]	Observation [d]
Sc_2O_3	Ga_2O_3			
Mole %	*Mole %*	°C		
100	0	2345	I	Not melted.
		2405	I	Do.
90	10	1975	I	Do.
		2010	I	Do.
80	20	[e] 1760	Q	Do.
		1784	Q	Do.
		1814	I	Do.
		1828	I	Do.
		1849	I	Do.
		1874	I	Do.
		1890	I	Do.
		1970	I	Do.
		2030	I	Partially melted.
		2073	I	Do.
75	25	1760	Q	Not melted.
		1778	Q	Partially melted.
		[e] 1800	Q	Do.
		1825	I	Do.
		1870	I	Do.
70	30	[e] 1763	I	Not melted.
		1771	I	Partially melted.
		1819	I	Do.
		1882	I	Do.
60	40	1768	Q	Not melted.
		1786	Q	Partially melted.
		1818	I	Do.
		1842	I	Do.
55.56 (5:4)	44.44	[e] 1761	Q	Not melted.
		[e] 1763	Q	Do.
		1782	Q	Partially melted.
54.545 (6:5)	45.455	[e] 1761	Q	Not melted.
		1771	Q	Partially melted.
53.846 (7:6)	46.154	[e] 1762	Q	Not melted.
		1774	Q	Partially melted.
50	50	1757	I	Not melted.
		[e] 1758	Q	Do.
		1775	Q	Partially melted.
		1778	I	Do.
		1788	I	Do.
47.5	52.5	[e] 1760	Q	Not melted.
		1767	Q	Partially melted.
		1777	Q	Do.
		1778	Q	Do.
45	55	[e] 1760	Q	Not melted.
		1775	Q	Partially melted.
		1789	I	Do.
		1805	I	Do.
		1831	I	Do.
		1982	I	Completely melted?
40	60	1722	I	Not melted.
		1742	Q	Do.
		1758	Q	Partially melted.
40	50	1760	I	Partially melted.
		1771	Q	Do.
		1790	I	Do.
		1861	I	Completely melted?
35	65	1728	Q	Not melted.
		1741	Q	Partially melted.
		1748	Q	Do.
30	70	1708	Q	Not melted.
		1710	I	Do.
		1714	I	Partially melted.
		1727	Q	Do.
		1731	I	Do.
		1738	I	Do.
		1758	I	Completely melted?
		1768	I	Do.
		1779	I	Do.
27.5	72.5	1709	Q	Not melted.
		1715	Q	Partially melted.
25	75	1697	Q	Not melted.
		1707	Q	Partially melted.
22.5	77.5	1704	Q	Not melted.
20	80	1701	Q	Do.
		1703	I	Do.
		1707	Q	Partially melted.
		1724	I	Completely melted?
15	85	1703	Q	Not melted.
		1715	Q	Partially melted.
		1725	Q	Do.
10	90	1725	Q	Not melted.
		1730	I	Do.
		1735	Q	Partially melted.
		1737	I	Do.
		1785	I	Completely melted?
5	95	1736	I	Not melted.
		1749	I	Do.
		1754	Q	Do.
		1769	I	Partially melted.
		1771	Q	Do.
		1782	I	Do.
		1794	I	Completely melted.?
		1810	I	Do.
0	100	1717	I	Not melted.
		1748	I	Do.
		1775	I	Do.
		[e] 1775	Q	Do.
		1789	I	Do.
		1789	Q	Do.
		1793	I	Do.
		1797	Q	Completely melted?
		1799	I	Do.
		1809	I	Do.
		1820	I	Do.

[a] Specimens calcined at 1,350 °C for 6 hr, 1,600 °C for 12 hr, and at 1,650 °C a minimum of 12 hr prior to melting point experiment.

[b] Specimens furnace cooled except when indicated.

[c] Q—quenching furnace; I—induction furnace.

[d] Definite verification of complete melting could not be obtained.

[e] Specimen quenched.

Because of the temperature limitations of the equipment, only the melting point of Ga_2O_3 could be established. The melting point of Sc_2O_3 has been estimated to be between the melting points of BeO and Al_2O_3, about 2,300 °C [3]. However, all attempts to melt Sc_2O_3 in the present work at temperatures as high as 2,405 °C proved unsuccessful. The melting point of Ga_2O_3 was determined to be 1,795 ±15 °C. This value compares rather unfavorably with the 1,725 ±15 °C value reported by Hill, Roy, and Osborn [8]. The determination of Hill et al. [8], was made on a strip furnace which is generally subjected to considerable random errors. To verify that the melting point of Ga_2O_3 was at least above 1,769 °C, the melting point platinum, a small piece of Pt ribbon was imbedded in pure Ga_2O_3 and heated in the quench furnace to 1,775 °C. Upon examination, the platinum ribbon was completely melted while the Ga_2O_3 showed no signs of melting.

Two intermediate binary phases occur in the Sc_2O_3–Ga_2O_3 system. The first, a compound believed to be $6Sc_2O_3 \cdot 5Ga_2O_3$, melts incongruently at 1,770 ±15 °C. The compound has a fairly narrow region of temperature stability, decomposing to two solid phases at 1,700 ±15 °C. The compound could only be formed in appreciable amounts after heating appropriate compositions for at least 10 hr at temperatures between 1,760 °C and its melting point. It was necessary to quench the specimens from these temperatures in order to retain the phase at room temperature. Slow or even rapid cooling resulted in decomposition of the phase. Even these long time heats, a few degrees below the melting point, failed to produce completely single phase specimens. Due to either the inability to obtain equilibrium or to the failure to completely "quench in" the compound, residual amounts of other phases persisted. Possible compositions of the compound considered most likely were the Sc_2O_3:Ga_2O_3 molar

ratios of 5:4, 6:5, and 7:6 with the 6:5 ratio most probable. X-ray patterns of the three possible compositions indicated that the compound formed in the greatest amounts relative to the minor phases at the $6Sc_2O_3{:}5Ga_2O_3$ composition. It should be emphasized that the line in the phase diagram (fig. 1) representing the compound is dashed not because of uncertainty in the existence of the compound but because of uncertainty in its exact composition.

A literature search did not reveal any other compound or solid solution in binary combinations of trivalent oxides which were isostructural with the 6:5 compound. A comparison of the X-ray pattern of the 6:5 compound with that of Sc_2O_3 indicated that, because of similar positions and intensities of major reflections, a similarity in structure might exist. The X-ray pattern of the 6:5 compound, given in table 3, was indexed on an orthorhombic basis with $a=13.85$ A, $b=9.80$ A, and $c=9.58$ A. There is generally fair agreement between observed and calculated $1/d^2$ values. If the indexing given in table 3 represents the true indexing, the structure of the 6:5 compound apparently is an orthorhombic distortion of the cubic C-type structure where $a(6{:}5)\simeq\sqrt{2}a(Sc_2O_3)$.

TABLE 3. *X-ray diffraction powder data for* $6Sc_2O_3{:}5Ga_2O_3$[a] (CuKα radiation)

hkl[b]	*d*[c]	$1/d^2$		*I*/*I*$_0$[e]
		Obs	Calc[d]	
	Å			
002	4.80	0.0434	0.0436	5
320	3.354	.0888	.0885	18
401	3.257	.0943	.0943	7
103	3.109	.1035	.1032	3
222	3.058	.1070	.1061	15
402	2.805	.1271	.1269	100
040	2.4505	.1665	.1665	14
004	2.3956	.1742	.1742	23
403	2.3492	.1812	.1814	13
114	2.2956	.1898	.1899	3
233	2.1721	.2120	.2125	11
224	2.0535	.2371	.2367	4
404	1.9721	.2572	.2576	3
622	1.9132	.2732	.2728	2
350	1.8043	.3072	.3072	4
025	1.7859	.3135	.3139	4
252	1.7555	.3245	.3247	10
800	1.7326	.3331	.3334	23
542	1.7175	.3390	.3403	11
722	1.7134	.3406	.3405	34
044			.3408	
624	1.5736	.4038	.4035	7
116	1.5663	.4076	.4077	6
740	1.5396	.4219	.4218	4
360			.4217	
900			.4220	
803	1.5214	.4320	.4315	3
910			.4324	
605	1.4748	.4598	.4598	32
406	1.4507	.4752	.4754	20
804	1.4427	.5073	.5077	6
171	1.3780	.5269	.5262	3
017	1.3547	.5449	.5440	6
027	1.3196	.5742	.5742	3
080	1.2251	.6663	.6663	7
282	1.1703	.7301	.7306	3
672	1.1618	.7408	.7402	4

[a] Specimen not single phase; reflections due to phases other than $\simeq$6:5 compound are deleted.
[b] Orthorhombic Miller indices.
[c] Interplanar spacing.
[d] Based on orthorhombic cell, $a=13.85$ A, $b=9.80$ A, $c=9.58$ A.
[e] Relative intensity.

The X-ray pattern of the second intermediate binary phase found in the system has been previously reported by Schneider, Roth, and Waring [1]. It is a solid solution and may possibly have a structure similar to kappa alumina, a metastable polymorph of Al_2O_3 [1]. The X-ray pattern of this solid solution phase could not be indexed, so that verification of its possible kappa alumina-like-structure could not be obtained. This phase (labeled U_{ss} in fig. 1) occurs in the Sc_2O_3–Ga_2O_3 system from about 55 to 73 mole percent Ga_2O_3 at the solidus. Solidus temperatures in this region ranged between approximately 1,764 and 1,705 °C. The compositional area of stability decreases at lower temperatures, finally pinching out with a minimum at about 61.5 mole percent Ga_2O_3 and 1,440 °C. An expanded view of the minimum is given in the inset of figure 1.

The remainder of the system is comprised of solid solutions of the end member oxides as well as appropriate two phase areas. Solid solution of Ga_2O_3 in Sc_2O_3 (C-type structure) occurs from 0 to about 21 mole percent Ga_2O_3 at the solidus. Solidus temperatures in this area extend from the melting point of Sc_2O_3 (unknown) to 1,770 °C, the incongruent melting point of the 6:5 compound. The amount of Sc_2O_3 solid solution decreases to about 15 mole percent Ga_2O_3 at 1,300 °C.

X-ray patterns of specimens having compositions and heat treatments generally corresponding to the $Sc_2O_{3ss}+U_{ss}$ region (fig. 1) characteristically showed one, sometimes two diffraction peaks ($d=2.7216$ A, $d=2.4212$ A) which normally are not associated with those of the primary phases. The extraneous peaks were seemingly not related to experimental procedure; that is, longer heat treatment nor quenching or slow cooling of the specimens changed the intensities of the peaks. Furthermore, if the reflections represented a true equilibrium phase, they would follow the lever rule principle, increasing or decreasing with composition. This was not the case however. At present, the only possible explanation is that the extraneous reflections indicate the presence of some unidentified metastable phase.

Solid solution of Sc_2O_3 in Ga_2O_3 (beta-gallia structure type) occurs from about 82 to 100 mole percent Ga_2O_3 at the solidus. The solidus temperatures vary between 1,705 °C, the eutectic temperature, and 1,795 °C, the melting point of Ga_2O_3. Contrary to normal expectations, the amount of Ga_2O_3 solid solution increases at lower temperatures, extending to approximately 56 mole percent Ga_2O_3 at 1,405 °C. The unit cell dimensions of Ga_2O_3 solid solution at about 56 mole percent Ga_2O_3 and 1,405 °C were $a=12.70$ A, $b=3.16$ A, $c=5.92$ A and $\beta=102°18'$ in contrast to pure Ga_2O_3 where $a=12.23$ A, $b=3.04$, $c=5.80$ A, and $\beta=103.9°$ [5]. This large change in the cell dimensions of pure Ga_2O_3 due to solid solution resulted in the separation of normally unresolved X-ray diffraction peaks. Insofar as can be determined, the unit cell dimensions for the Ga_2O_3 solid solution are the largest thus far reported for a phase having the beta gallia structure type.

Specimens which normally should have contained only two phases, $U_{ss}+Ga_2O_{3ss}$, generally contained, upon slow cooling, an additional phase. This third phase was identified as Ga_2O_{3ss}, but having different unit cell dimensions than the true equilibrium Ga_2O_{3ss} phase. This phenomena of differential exsolution was common for specimens high in Ga_2O_3 content which had been slow cooled in the preliminary calcinations. To obtain the true equilibrium phases it was necessary to rely on the results obtained only from quenched specimens.

The exact compositions of the peritectic and eutectic points which occur in the system could not be determined accurately because of the inability to obtain complete liquidus data.

5. Summary

The equilibrium phase diagram for a major portion of the Sc_2O_3-Ga_2O_3 system was determined from a study of solid state reactions amd melting point relations. A specially designed platinum alloy quenching furnace was employed for subsolidus and melting point experiments conducted below 1,800 °C. A 95 percent Pt-5 percent Rh versus 80 percent Pt-20 percent Rh thermocouple and an optical pyrometer were used to measure temperatures between 1,650 and 1,800 °C. An inductively heated iridium crucible was used for the determination of solidus and liquidus temperatures above 1,800 °C. Phases were identified by examination of X-ray diffraction patterns.

The melting point of Ga_2O_3 was found to be 1,795 ±15 °C. The indicated uncertainty in the melting point is a conservative estimate of the overall inaccuracy. The melting point of Sc_2O_3 could not be determined because of temperature limitations of the equipment. However, it does not melt below 2,405 °C, the highest temperature attained in the present study.

Two intermediate binary phases were formed in the system. The first, a compound of approximately 6:5 molar ratio, melts incongruently at 1,770 °C and decomposes below 1,700 °C. Its X-ray pattern was indexed on the basis of an orthorhombic cell with $a=13.85$ A, $b=9.80$ A, $c=9.58$ A. This cell appears to be related to that of Sc_2O_3 with a (6:5) $\simeq\sqrt{2}\ a$ (Sc_2O_3). The second binary phase, a solid solution, exists from about 55 to 73 mole percent Ga_2O_3 at the solidus. The compositional range of stability decreases at lower temperatures, pinching out with a minimum at 61 mole percent Ga_2O_3 and 1,440 °C. The X-ray pattern of the solid solution phase could not be indexed.

6. References

[1] S. J. Schneider, R. S. Roth, and J. L. Waring, J. Research NBS **65A** (Phys. and Chem.) No. 4, 345–374 (1961).

[2] H. E. Swanson, R. K. Fuyat, and G. M. Ugrinic, NBS Cir. 539 **III,** 27 (1954).

[3] C. Barta, F. Petru, B. Hajek, Naturwissenschaften **45,** 36 (1958).

[4] R. Roy, V. G. Hill, and E. F. Osborn, Ind. and Eng. Chem. **45,** 819–820 (1953).

[5] S. Geller, J. Chem. Phys. **33** No. 3, 676–684 (1960).

[6] V. M. Goldschmidt, T. Barth, and C. Lunde, Pt. V Skrifter Norske Videnskaps-Akad. Oslo. I. Mat.-Natur. Kl. No. 7, 24 (1925).

[7] H. von Wartenberg and H. J. Reusch, Z. anorg. u. allgem. Chem. **207** [1] 1–20 (1932).

[8] V. G. Hill, R. Roy, and E. F. Osborn, J. Am. Ceram. Soc. **35,** 135–142 (1952).

[9] H. F. Stimson, J. Research NBS, **65A** (Phys. and Chem.) No. 2, 139–145 (1960).

[10] F. A. Mauer, Bridge-type furnace controller using Brown servoamplifier, informal communication; see also R. H. Bogue, Chemistry of portland cement, 2d ed. p. 311, (Reinhold Publishing Corp., New York, 1955).

[11] S. J. Schneider, Pt. III, J. Research NBS **65A** (Chem. and Phys.) No. 5, 429–434 (1961).

[12] C. S. Barrett, Structure of Metals, 1st ed., McGraw Hill Book Co., Inc., New York, 182–185 (1943).

(Paper 67A1–190)

JOURNAL OF RESEARCH of the National Bureau of Standards—A. Physics and Chemistry
Vol. 67A, No. 1, January–February 1963

Analysis of Two Infrared Bands of CH_2D_2*

Wm. Bruce Olson, Harry C. Allen, Jr., and Earle K. Plyler

(September 19, 1962)

Two infrared absorption bands of CH_2D_2 have been analyzed in the semirigid rotor approximation. These are the A-type band at 2671.67 cm^{-1} and the C-type band at 4425.61 cm^{-1}. The A-type band has previously been assigned as $\nu_3+\nu_9$, and the C-type band is tentatively assigned as $\nu_3+\nu_6$. The upper state of the A-type band is perturbed presumably by the close lying level $2\nu_5$. This interaction has not been investigated. The following values were found for the rotational constants of the ground vibrational state: $A_0=4.303$ cm^{-1}, $B_0=3.504$ cm^{-1}, $C_0=3.049$ cm^{-1}.

1. Introduction

The rotational-vibrational spectra of all the deuterated species of methane except CH_2D_2 have been well investigated [1]. [1]

Methane and CD_4 are spherical tops while CH_3D and CD_3H are symmetric rotors; on the other hand CH_2D_2 is an asymmetric rotor. It seemed of interest to determine the rotational constants of CH_2D_2 in order to have a set of constants for each of the species. Fortunately, high resolution spectra could be obtained for both an A-type and a C-type band for this molecule. As recently discussed [2], this is sufficient data to enable a good determination of the ground state constants using the complementary $\Delta F_2''$ values obtained from the two bands. These two bands have been analyzed in the semirigid approximation to yield good values of the ground state constants. Unfortunately a perturbation in the excited state of the A-type band introduces an uncertainty in the effective constants for this band that is larger than can be justified for the precision of the data. Only transitions involving levels with low values of the rotational quantum numbers have been used in the analysis in order to minimize the effect of centrifugal distortion.

2. Experimental Procedure

The spectra were recorded with the grating instrument of the Infrared Spectroscopy Section [3] using a 10,000 lines/in. grating with a ruled area of about 6×8 in. A cooled PbS photoconductive cell was used as the detector.

Both the A- and C-type bands were recorded using a multiple reflection cell with a total path length of 6 m, filled with CH_2D_2 to a pressure of 2 cm of Hg. The C-type band was observed in the second order of the grating and the A-type band in the first. The CH_2D_2 obtained from Merck & Co., Ltd., had a stated minimum purity of 98%.

The wavelengths of the lines were measured using higher order infrared emission lines of the rare gases as standards, and interpolating between them through the use of the fringes of a Fabry-Perot interferometer as previously described [4].

3. Theory

Preliminary to the actual analysis of the spectra the mean square values of the angular momenta about the three principal axes of inertia and the intensities were calculated.

Assuming tetrahedral geometry and identical bond lengths of 1.094 A for CH_2D_2 the moments of inertia, reciprocal moments in cm^{-1} units, and the asymmetry parameter κ were obtained.

For the calculated value of $\kappa=-0.27$, α, β, and γ, as defined by Allen [2], were obtained by linear interpolation in published tables [5] of $E(\kappa)$ for each energy level.

α, β, and γ may be shown to be identical with $\langle P_z^2\rangle$, $\langle P_x^2\rangle$, and $\langle P_y^2\rangle$, respectively, in an I^r representation [6]. The energy of a rotational level in a given vibrational state, neglecting centrifugal distortion, may be written as [2]:

$$E(J_{K_{-1},K_1})=\alpha A_v+\beta B_v+\gamma C_v,$$

and the difference between two rotational levels in the same vibrational state as:

$$\Delta F=\Delta\alpha A_v+\Delta\beta B_v+\Delta\gamma C_v.$$

The $\Delta\alpha$'s, $\Delta\beta$'s and $\Delta\gamma$'s for each of the ΔF_2's observable from strong transitions in the A- and C-type band were calculated.

The strong transitions for the A-type band are those which satisfy the selection rules:

$$\Delta J=0,\ \pm1 \qquad \Delta K_{-1}=0 \qquad \Delta K_1=\pm1,$$

and for the C-type band the strong transitions are those for which

$$\Delta J=0,\ \pm1 \qquad \Delta K_{-1}=\pm1 \qquad \Delta K_1=0.$$

* This work was supported in part by the Division of Chemistry, Atomic Energy Commission.

[1] Figures in brackets indicate the literature references at the end of this paper.

The relative intensities of the transitions were calculated by combining the Boltzmann factor, calculated using the estimated moments of inertia, and nuclear spin statistics with the appropriate line strengths from published tables [7].

The nuclear spins of the equivalent pairs of hydrogen and deuterium atoms in CH_2D_2 give rise to degeneracies of the rotational levels. For the ground vibrational state the statistical weight factors are 15 for the symmetric (A) rotational levels and 21 for the antisymmetric (B) levels.

The A-type band at 2672 cm^{-1} has been previously observed by Wilmshurst and Bernstein [8] who assigned it to the combination $\nu_3+\nu_9$. As the observed band type is consistent with this assignment and there should be no other bands of this type near 2670 cm^{-1}, there appears to be no reason to doubt the assignment.

The C-type band at 4425 cm^{-1} can best be assigned at $\nu_3+\nu_6$ as this seems to be the only combination which would give a C-type band in the region 4400–4500 cm^{-1}.

4. Analysis

As each of the bands was isolated from others of comparable intensity, initial assignments, with the aid of the calculated intensities, could be made by inspection. From the initial assignments ΔF_2 values were obtained, and with the calculated $\Delta\alpha$'s, $\Delta\beta$'s, and $\Delta\gamma$'s were used to refine the values of A, B, and C in the ground and upper vibrational states. From these values of A, B, and C, α's, β's, and γ's pertinent to the value of κ in each vibrational state were calculated as before.

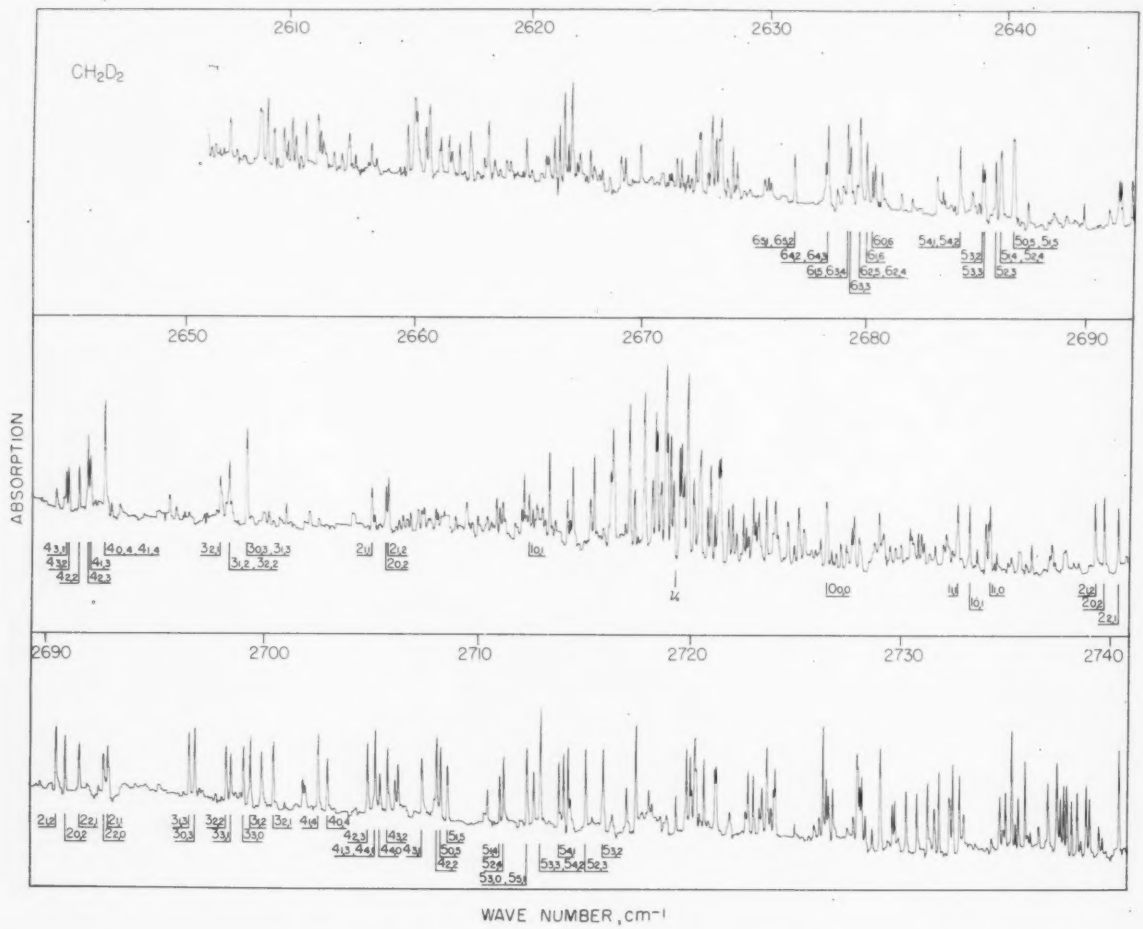

FIGURE 1. *The A-type band of* CH_2D_2 *at 2672* cm^{-1}.

The identification given is the ground state designation of J_{K_{-1},K_1} for $R_{0,1}$ transitions to the high wave number side of the band origin, and for $P_{0,\bar{1}}$ transitions to the low wave number side of the band origin.

A trial spectrum was then calculated from the expression:

$$\nu=\nu_0+\alpha' A_e+\beta' B_e+\gamma' C_e-\alpha A_0-\beta B_0-\gamma C_0.$$

From the trial spectrum and intensities more transitions could be assigned, enabling further refinement of the reciprocal moments of inertia.

While this iterative procedure worked well with the C-type band, Coriolis perturbations in the A-type band caused some difficulty in definitely locating some of the transitions.

The lowest observably perturbed level in the $\nu_3+\nu_9$ vibrational state is the 4_{13} level which is pushed down by 0.24 cm^{-1}. For $J=5$, the levels 5_{05}, 5_{14}, and 5_{23} are all perturbed, and for $J=6$ over half of the levels are perturbed.

This perturbation has not been investigated in detail. It probably arises through interaction with the vibrational state $2\nu_5$, the fundamental of which is theoretically inactive in the infrared, but appears to have been observed at 1329 cm^{-1} [8], the transitions becoming allowed through Coriolis perturbation. ν_5 has apparently been observed in the Raman also at 1333 cm^{-1} [9].

No account was taken of the effect of centrifugal distortion in this analysis. Since only levels with low J values were used in the analysis, the effect of this correction on the rotational constants was minimized. No systematic differences between the observed and calculated spectra were noticed until rather high J values were reached. In these regions of the absorption serious overlapping of transitions make the unique assignment of transitions to observed absorption peaks doubtful.

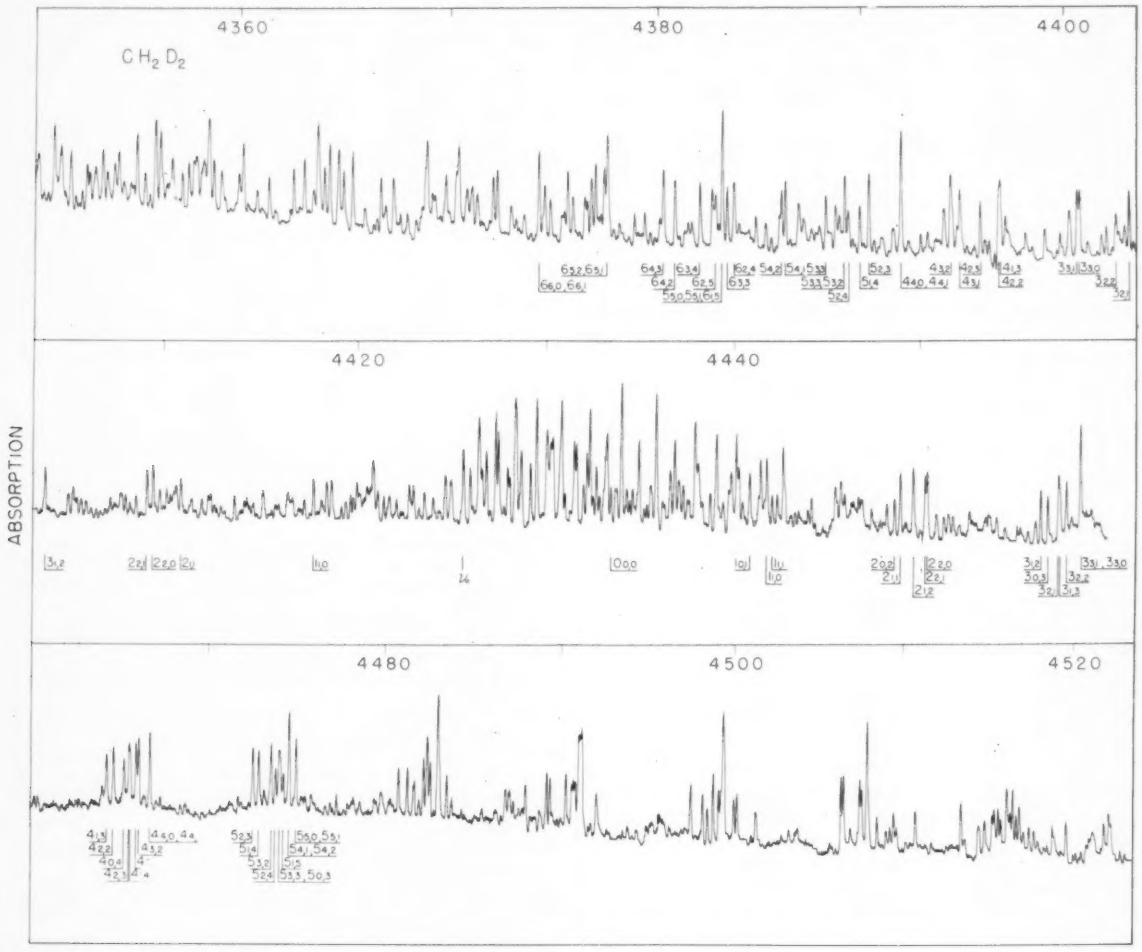

FIGURE 2. *The C-type band of* CH_2D_2 *at 4426 cm*$^{-1}$.

The identification given is the ground state designation of J_{K_{-1},K_1} for $R_{1,0}$ transitions to the high wave number side of the band origin, and for $P_{1,0}$ transitions to the low wave number side of the band origin.

Although no statistical analysis of the data was made, the excellent agreement between the observed and calculated ΔF_2 values for the ground state, and the sensitivity of the calculated ΔF_2 values to values of the rotational constants seem to indicate a probable error of the order of ± 0.002 cm^{-1} for each of the ground state constants. The agreement between the calculated and observed values of ΔF_2 for the ground state may be seen in table 1.

TABLE 1. *Ground state* $\Delta F_2''$

A-type band			C-type band		
$\Delta F_2''$	Calculated	Observed	$\Delta F_2''$	Calculated	Observed
	cm^{-1}	cm^{-1}		cm^{-1}	cm^{-1}
$0_{00}-2_{02}$	19.513	19.55	$0_{00}-2_{20}$	23.911	23.92
$1_{01}-3_{03}$	32.103	32.10	$1_{01}-3_{21}$	37.524	37.53
$1_{11}-3_{13}$	31.547	31.55	$1_{11}-3_{31}$	41.285	41.29
$1_{10}-3_{12}$	33.791	33.79	$1_{10}-3_{30}$	40.862	40.88
$2_{02}-4_{04}$	44.373	44.38	$2_{02}-4_{22}$	51.644	51.64
$2_{12}-4_{14}$	43.976	43.98	$2_{12}-4_{32}$	55.068	55.06
$2_{11}-4_{13}$	46.958	46.96	$2_{11}-4_{31}$	53.908	53.91
$2_{21}-4_{23}$	45.754	45.76	$2_{21}-4_{41}$	58.305	58.27
$2_{20}-4_{22}$	47.277	47.25	$2_{20}-4_{40}$	58.165	58.16
$3_{03}-5_{05}$	56.501	56.50	$3_{03}-5_{23}$	66.378	66.37
$3_{13}-5_{15}$	56.300	56.28	$3_{13}-5_{33}$	69.201	69.20
$3_{12}-5_{14}$	59.715	59.69	$3_{12}-5_{32}$	67.212	69.23
$3_{22}-5_{24}$	58.539	58.54	$3_{22}-5_{42}$	71.733	71.73
$3_{21}-5_{23}$	60.967	60.96	$3_{21}-5_{41}$	71.127	71.12
$3_{31}-5_{33}$	59.463	59.47	$3_{31}-5_{51}$	75.463	75.43
$3_{30}-5_{32}$	60.141	60.13	$3_{30}-5_{50}$	75.431	75.43
$4_{04}-6_{06}$	68.637	68.61	$4_{04}-6_{24}$	81.651	81.64
$4_{14}-6_{16}$	68.559	68.53	$4_{14}-6_{34}$	83.676	83.63
$4_{13}-6_{15}$	72.042	71.98	$4_{13}-6_{33}$	81.042	81.03
$4_{23}-6_{25}$	71.147	71.11	$4_{23}-6_{43}$	85.399	85.38
$4_{22}-6_{24}$	74.350	74.33	$4_{22}-6_{42}$	83.950	83.93
$4_{32}-6_{34}$	72.585	72.55	$4_{32}-6_{52}$	88.728	88.65
$4_{31}-6_{33}$	74.092	74.07	$4_{31}-6_{51}$	88.532	88.52
$4_{41}-6_{43}$	72.848	72.81	$4_{41}-6_{61}$	92.665	92.56
$4_{40}-6_{42}$	73.062	73.02	$4_{40}-6_{60}$	92.660	92.56

TABLE 2. *C-type band* $\Delta F_2'$

$A=4.255$ cm^{-1} $B=3.590$ cm^{-1} $C=3.151$ cm^{-1}

$\Delta F_2'$	Calc	Obs
	cm^{-1}	cm^{-1}
$0_{00}-2_{20}$	23.918	23.96
$1_{01}-3_{21}$	37.927	37.94
$1_{11}-3_{31}$	41.086	41.12
$1_{10}-3_{30}$	40.685	40.70
$2_{02}-4_{22}$	52.436	52.44
$2_{12}-4_{32}$	55.238	55.25
$2_{11}-4_{31}$	54.163	54.18
$2_{21}-4_{41}$	57.925	57.91
$2_{20}-4_{40}$	57.778	57.80
$3_{03}-5_{23}$	67.521	67.51
$3_{13}-5_{33}$	69.726	69.74
$3_{12}-5_{32}$	67.944	67.93
$3_{22}-5_{42}$	71.753	71.74
$3_{21}-5_{41}$	71.131	71.15
$3_{31}-5_{51}$	74.891	74.82
$3_{30}-5_{50}$	74.854	74.82
$4_{04}-6_{24}$	83.064	82.95
$4_{14}-6_{34}$	84.534	84.48
$4_{13}-6_{33}$	82.268	82.15
$4_{23}-6_{43}$	85.784	85.82
$4_{22}-6_{42}$	84.431	84.42
$4_{32}-6_{52}$	88.552	88.51
$4_{31}-6_{51}$	88.324	88.32
$4_{41}-6_{61}$	91.899	91.83
$4_{40}-6_{60}$	91.890	91.83

The constants for the excited states of these bands cannot be determined as precisely as those for the ground state with the available ΔF_2 values, but ± 0.005 cm^{-1} would seem to be a generous estimate of the probable error in the constants for these states. The calculated and observed ΔF_2 values for the excited states are compared in tables 2 and 3.

The constants determined for the three vibrational levels are given in table 4. The band origins were determined from the best fit between the observed and calculated spectra for low J values.

TABLE 3. *A-type band* $\Delta F_2'$

$A=4.254$ cm^{-1} $B=3.654$ cm^{-1} $C=3.019$ cm^{-1}

$\Delta F_2'$	Calc	Obs
	cm^{-1}	cm^{-1}
$0_{00}-2_{02}$	19.715	19.70
$1_{01}-3_{03}$	33.132	32.11
$1_{11}-3_{13}$	31.617	31.62
$1_{10}-3_{12}$	34.688	34.68
$2_{02}-4_{04}$	44.163	44.17
$2_{12}-4_{14}$	43.916	43.91
$2_{11}-4_{13}$*	47.748	47.51
$2_{21}-4_{23}$	46.516	46.54
$2_{20}-4_{22}$	48.979	48.96
$3_{03}-5_{05}$*	56.159	56.51
$3_{13}-5_{15}$	56.080	56.07
$3_{12}-5_{14}$*	60.078	59.35
$3_{22}-5_{24}$	59.144	59.11
$3_{21}-5_{23}$*	62.809	62.70
$3_{31}-5_{33}$	60.862	60.86
$3_{30}-5_{32}$	62.271	62.59

* Perturbed levels.

TABLE 4. *Rotational and vibrational constants*

	Ground state	$\nu_3+\nu_9$	$\nu_3+\nu_6$
	cm^{-1}	cm^{-1}	cm^{-1}
A	4.303	4.254	4.255
B	3.504	3.654	3.590
C	3.049	3.019	3.151
ν_0	-----	2671.67	4425.61

5. References

[1] Among the more recent high resolution analyses are those of: K. T. Hecht, J. Mol. Spectroscopy **5,** 355 and 390 (1960). M. A. Thomas and H. L. Welsh, Can. J. Phys. **38,** 1291 (1960). J. Moret-Bailly, Cahiers de Phys. **130–131,** 1 (1961). R. A. Olafson, M. A. Thomas, and H. L. Welsh, Can. J. Phys. **39,** 419 (1961). H. C. Allen, Jr., and E. K. Plyler, J. Research NBS **63,** 145 (1959). E. H. Richardson, S. Brodersen, L. Krause, and H. L. Welsh, J. Mol. Spectroscopy **8,** 406 (1962).

[2] H. C. Allen, Jr., Phil. Trans. Roy. Soc. London **A253,** 335 (1961).

[3] N. Gailar and E. K. Plyler, J. Research NBS **45,** 102 (1955).

[4] E. K. Plyler, L. R. Blaine, and E. D. Tidwell, ibid., **55,** 279 (1955).

[5] C. H. Townes and A. L. Schawlow, Microwave Spectroscopy, McGraw-Hill, New York, (1955).

[6] J. K. Bragg and S. Golden, Phys. Rev. **75,** 735 (1949).

[7] P. C. Cross, R. M. Hainer, and G. W. King, J. Chem. Phys. **12,** 210 (1944).

[8] J. K. Wilmshurst and H. J. Bernstein, Can. J. Chem. **35,** 226 (1957).

[9] G. E. MacWood and H. C. Urey, J. Chem. Phys. **4,** 402 (1936).

(Paper 67A1–191)

JOURNAL OF RESEARCH of the National Bureau of Standards—A. Physics and Chemistry
Vol. 67A, No. 1, January–February 1963

Precise Coulometric Titrations of Halides

George Marinenko and John K. Taylor

(September 19, 1962)

A method has been developed for the precise assay of halides by constant-current coulometric titration with silver ions generated at a silver anode. It is shown that a 4 milliequivalents sample of halide can be titrated with standard deviation of 0.005 percent.

1. Introduction

The determination of halides is of interest in many chemical investigations. For example, in a recent determination of the atomic weight of chlorine[1] [1] it was necessary to determine the chloride content of dilute solutions with high precision. For such applications, coulometric titration is particularly advantageous because it involves a minimum of manipulation. A further advantage is that the titrant is generated in situ in amount that is measured in terms of physical quantities.

Although a number of publications have been concerned with the coulometric determination of halides [2, 3, 4, 5] there seem to have been no attempts made to establish the conditions for high-precision titrations, i.e., better than 0.1 percent. Accordingly, the work reported in this paper was undertaken as part of a continuing program at the National Bureau of Standards to develop coulometric titrations of high precision and accuracy[6].

2. General Considerations

Coulometric generation of silver ion has been extensively studied. One of the more recent studies was done by D. N. Craig and coworkers [7, 8] in connection with the determination of the value of the faraday. The electrode reaction $Ag \rightarrow Ag^+ + e^-$ (or one equivalent thereto) proceeds at 100 percent current efficiency for current densities as high as 0.150 amp/cm² [7]. In the work reported in the present paper, the total area of the silver anode was about 20 cm² and the generation current was 100 ma; thus the current density did not exceed 0.005 amp/cm². At such low current densities, one is assured of having 100 percent current efficiency with respect to the generation of silver ion provided no less noble metals are present in the metallic silver. For this reason spectrochemically pure mint silver (stated purity, 99.999%) was utilized for constructing the generator anode. Nonoxidizable impurities in silver such as silica do not present any problems since the amount of silver ion produced by the electrochemical reaction is important rather than the weight loss of the anode. Accordingly, no need for further purification of silver was warranted at this time, since other uncertainties of the method were more significant.

[1] Figures in brackets indicate the literature references at the end of this paper.

All calculations were based on the 1961, C^{12} atomic weight scale. The molecular weights used for NaCl, NaBr, and KI were 58.442_8, 102.898_8, and 166.006_4, respectively.

The value of the faraday constant used was based on the determination of D. N. Craig et al. [7]. Using their electrochemical equivalent of silver, 1.117972 mg/coul, and the atomic weight of silver 107.870 g/mole on the new C^{12} scale, the value of the faraday is 96,487.2 coul/g-equiv.

3. Apparatus and Procedure

3.1. Apparatus

The design of the titration cell in this work was similar to that described in the previous communication of this series [6] except that the new cell was of smaller capacity. The anode and the cathode compartments were 180 ml electrolytic beakers connected horizontally by a 25 mm o.d. tube, approximately 10 cm in length, in which a coarse, a medium, and a fine porosity sintered glass disk were sealed. Each of the two intermediate compartments thus formed had a tube with a stopcock to enable filling and emptying, by applying vacuum or nitrogen pressure.

The anode was a heavy piece of silver 3 cm×3 cm and about ½ cm thick, made by melting together a number of thinner sheets of mint silver by placing them in a "sandwich" on a heavy plate of silver and applying heat with an oxygen torch. To permit mounting in the cell cover and to facilitate connection of the lead wire, the anode was attached to a 12 cm long cylindrical silver handle, 1 cm in diameter, fabricated from the same material. The anode thus formed was etched in dilute HNO_3 (1:10) to remove any surface impurities, and washed with large quantities of distilled water.

A piece of corrugated platinum foil (5 cm×16 cm) served as the cathode in the generation circuit. The large surface area thus obtained was necessary to minimize polarization of the cathode and to decrease current fluctuations due to variation in cell resistance as a consequence of the liberation of hydrogen gas.

The electrical circuit used in this work was the same as described in the previous communication [6].

The generation current for all titrations was 101 ma and its exact value was determined by the value of the standard resistor and the voltage of the satu-

rated Weston cell. Any small initial unbalance between the IR drop across the standard resistor and the standard cell was corrected quickly after which the IR drop across the standard resistor was maintained equal to the voltage of the Weston Cell. The value of the resistor used was 9.99994 ohms at 25.0 °C and its temperature was maintained constant in a thermostated oil bath. Nevertheless, the actual temperature of this resistor was measured before and after each titration with a mercurial thermometer, and corresponding corrections were applied, based on the mean value of temperature, by the use of the relation $R_t = R_{25}[1+\alpha(t-25)+\beta(t-25)^2]$ ohms.

In the course of a titration, the temperature of the standard resistor increased from the 25 °C bath temperature by as much as 1 °C. However, the correction for this difference amounted to only 7 ppm. Since the measurements of the temperature were made to a tenth of a degree the mean value of the resistor during the run was known to better than 1 ppm. The value of the saturated standard Weston cell used for the comparison of the IR drop of the standard resistor was 1.017875 v ± 0.8 μv at 34.099 °C. The temperature of the Weston cell was always maintained at that value in a specially built thermostated box.

Near the equivalence point of a titration, the current was passed incrementwise. It was found advantageous to use a commercially available constant-current coulometric titrator for this purpose, because the size of these increments can be conveniently and adequately controlled and reproduced using this instrument without any appreciable sacrifice of accuracy. The timing circuit and current of this instrument were calibrated and the It-product was found to be accurate to ±0.005 percent.

As in the case of acid and base titrations, it was found that a gel plug was necessary to eliminate the flow of electrolyte between the anode and the cathode compartments. In this work a silicic acid gel plug was used. It was conveniently prepared by mixing together 10 ml of 1:4 water diluted solution of technical grade sodium silicate (40 Be) with 5 ml of 1.0 M HNO_3. The resulting solution was poured onto the frit of the cathode compartment. Gelation of this solution occurred in approximately 2 min after initial mixing.

The amperometric indicator circuit consisted of two silver electrodes and a polarograph. The indicator cathode was a silver bead approximately 1 cm in diameter (3 cm^2 in area); the indicator anode was a bead approximately 0.5 cm in diameter (0.8 cm^2 in area). Both beads were made by melting the same silver as used for fabrication of the generator anode. These in turn were fused to pieces of platinum wire and the latter sealed into glass tubes to facilitate electrical contact. The polarograph was used as a source of the applied emf between these two electrodes and also as a recording microammeter, to measure the indicator current. The applied emf was 0.050 v.

All weighings were done on a 20-g capacity microbalance and were precise and accurate to ±0.003 mg. All weighings were corrected for air buoyancy.

3.2. General Procedure

The preparation of the coulometric cell consisted of thorough cleaning with fuming sulfuric acid followed by passage of large quantities of distilled water through the glass frits. Subsequently the cell was exposed to prolonged steam cleaning by forcing the steam to pass through the frits, followed again by several rinses with distilled water.

After such cleaning a silicic acid gel plug was poured onto the fine porosity frit of the cathode compartment.

The cell was surrounded by aluminum foil to shield the contents of the cell from light. About 100 ml of 0.1 M HNO_3 saturated with $NaNO_3$ were poured into the cathode compartment to which about 5 μeq of $AgNO_3$ solution were added to precipitate traces of halides or other impurities which form insoluble precipitates with silver. Otherwise, these could cause positive errors by migration into the anode compartment. A slight excess of silver ion would not cause any negative errors since the electrical migration forces would keep it from diffusing into the adjacent compartment.

For each titration 100 ml of anolyte were used. The anolyte was 1 M $NaNO_3$, 1 M acetic acid in 50 percent methanol. The methanol was added to suppress the solubility of silver halides [2].

The platinum cathode was placed in the cathode compartment and a Teflon-encapsulated magnetic stirring bar was lowered into the anode compartment by means of another magnet.

A polyethylene cover, supporting the generator anode and two indicator electrodes, was then secured on the anode compartment by means of a snugly fitting lock ring.

At this point the cell was placed on the platform of a magnetic stirrer, operated from a constant voltage transformer to insure constant stirring rate which is imperative for precise amperometric end-point detection.

Sufficient anolyte was permitted to flow into the intermediate compartments to just wet the bottom of each of the intermediate compartments, thus establishing electrical contact. About 10 μeq of halide were introduced into the anode compartment, through an opening in the cover, to facilitate pretitration.

At this point, a 6.43 ma current was passed incrementwise (1 μeq increments) with the coulometric analyzer. The indicator current was recorded after the passage of each increment. This pretitration was continued until the excess of silver ion was about 10 μeq or in terms of concentration $10^{-4}M$. The portion of the indicator current line, after the equivalence point, where the indicator current becomes a straight line function of the silver ion concentration, was extrapolated to zero current which was chosen to be the end point of both the pretitration and the final titration.

After the pretitration was completed, the intermediate compartments were completely filled with anolyte and the silver ion was generated using the

high-precision manually controlled constant-current circuit. The amount of silver which was generated at this point was a precalculated quantity, sufficient to react with about 99.5 percent of the halide expected to be found in a given sample.

Following the generation of silver ion the sample was introduced into the anode compartment, and the intermediate compartments were emptied by pressure until only the bottoms of these compartments were slightly wetted by the solution. At this point the titration was continued, using again the coulometric analyzer, until the indicator current passed a minimum and began to rise as the concentration of silver ion was increased. The titration was again stopped and the intermediate compartments were subjected to several successive rinsings with anolyte. From this point on, the titration was continued incrementwise in the same fashion as the pretitration. The amount of electrogenerated silver ion equivalent to the halide present is obviously the amount generated to the end-point plus the excess generated in the pretitration step.

It was found, in the preliminary part of the work, that in the case of large samples, e.g., 4 meq, erratic results were obtained if the sample was introduced into the cell before generation of silver ion, in that the generation current was very difficult to maintain constant after the generation of the first milliequivalent of silver ion. This phenomenon was caused by the dense precipitate deposited directly on the silver anode thus hindering the diffusion of the generated silver ion into the bulk of solution. This problem was solved by the above described procedure, that is, by pregeneration of the major portion of silver ion before the introduction of the halide sample into the cell. The amount of halide which still remained to be titrated after the introduction of sample was so small that the interference due to coating over of the electrode by the precipitate was eliminated.

Another problem which arose as a result of the pregeneration of silver ion was the delivery of sample. It was found that a solid sample could not be introduced directly into the silver ion solution because the halide crystals became instantaneously encapsulated by a film of silver halide precipitate and again inclusion errors were inevitable. Accordingly, the samples were either weighed into the cell in the form of solution or, in the case of solid-weighed samples, they were dissolved prior to delivery into the cell.

4. Titration of Sodium Chloride

4.1. Procedure

The sodium chloride which was used in this work was one purified by double recrystallization of a reagent grade salt by precipitation with HCl-gas from saturated solution and subsequent fusion in a platinum crucible. The large crystals of NaCl thus obtained were crushed in an agate mortar and dried at 110 °C. This material was stored in a desiccator until used. The spectrochemical analysis of this material showed the total metallic impurities did not exceed 0.004 percent.

Two sets of experiments were performed with sodium chloride, one involving the preparation of solutions which were later dispensed into the cell from polyethylene weighing bottles, and the second set involving weighing of sodium chloride as solid.

The solutions were prepared to be of such concentrations that the desired amount of chloride (1 meq or 4 meq) was contained in approximately 10 g of solution. The following were the concentrations of the two solutions on a vacuum-corrected basis: Solution A—0.1031324 meq/g; solution B—0.4202323 meq/g. The actual weight of a sample was obtained by difference in weight of the weighing bottle before and after the delivery of a sample.

Solid samples were weighed in a small boat also by the difference method. The crystals were delivered into a funnel, containing a Pyrex wool plug and leading into the anode compartment. After the generation of 99.5 percent of the silver ion required, as described above, the sample was washed down with 10 ml of distilled water. Near the end point the funnel was rinsed a number of times with anolyte withdrawn from the cell by means of a syringe to which a glass tube was attached in place of the customary needle.

TABLE 1. *Summary of results*

Determination number	NaCl solution A	NaCl solution B	NaCl weighed solid		NaBr weighed solid		KI weighed solid	
	1 meq assay	4 meq assay	1 meq assay	4 meq assay	1 meq assay	4 meq assay	1 meq assay	4 meq assay
1	99.970	99.990	100.018	100.003	100.156	100.172	99.910	99.972
2	99.979	100.007	100.012	100.016	100.122	100.163	99.905	99.960
3	99.997	100.005	99.954	99.994	100.187	100.170	99.923	99.960
4	100.026	100.000	99.960	99.997	100.226	100.177	99.976	99.975
5	100.029	100.007	99.943	100.000	100.133	100.188	99.881	99.976
6	100.022	100.008	99.974	100.001	100.191	100.169	99.921	99.965
7	99.999	100.010	99.983		100.133		99.940	
8	100.016	100.011	100.013		100.142			
9	99.994	100.056			100.211			
10		100.045			100.208			
11		100.070						
12		100.081						
Mean	100.004	[a] 99.996	99.986	100.002	100.171	100.173	99.922	99.968
Standard deviation	0.021	0.005	0.028	0.008	0.038	0.009	0.030	0.007

[a] The mean value of the assay corrected for the change in concentration of the solution with time.

663611—63——3

4.2. Results

The results obtained for a number of titrations over a period of several months are given in the table 1, columns 2, 3, 4, and 5. The agreement among these sets is remarkably good and well within the limits of standard deviation for each set. The precision for each of the sets is much better than could be obtained on the same size samples by conventional gravimetric or titrimetric methods.

It is apparent from the examination of the data that solution B of sodium chloride was increasing in concentration with time (fig. 1) even though both solutions were kept tightly closed in the ground glass stoppered bottles in water-vapor saturated bell-jars. In the case of solution A, this effect is not as pronounced as in the case of solution B. Two reasons account for this behavior. Firstly, the volume of solution A was 1,000 ml, while the volume of B was 200 ml. Thus for a given amount of water lost, the concentration change would be amplified by the factor of 5 in solution B over that of solution A. Secondly, the standard deviation for 1 meq samples is four times larger than for 4 meq samples; thus a trend in concentration change would be masked more in the case of solution A.

An equation of the form $A=A_o+bt$ was fitted to the data of solution B by the method of least squares to express the assay of solution at any time since the time of preparation. In this equation A is assay at any time, t, A_o is the assay of this solution at the time of preparation, b is the slope of this line expressed in precent day^{-1} and t is time elapsed since the preparation of solution in days. The solution of the above equation yields 0.00150 percent·day^{-1} for the slope b of this line, and 99.996 percent for A_o as indicated at the bottom of column 3, table 1. This value for the assay is in excellent agreement with both the expected value and the assays of the solid weighed samples of the same material.

5. Titration of Sodium Bromide

5.1. Procedure

The sodium bromide used for these experiments was a reagent grade salt. It was dried at 110° C and stored in a desiccator for use without any preliminary purification. The samples were weighed out as solid NaBr in the same manner as the solid NaCl samples.

5.2. Results

Two sample sizes, 1 meq and 4 meq, were investigated as in the case of NaCl and the results are given in columns 6 and 7 of table 1. The average value for the assay in both cases is in excellent agreement. The value of the assay appears to be 0.17 percent too high and undoubtedly is caused by the presence of chloride impurity since the amount of chloride in this salt is known to be of the order of 0.2 percent by weight. The standard deviations

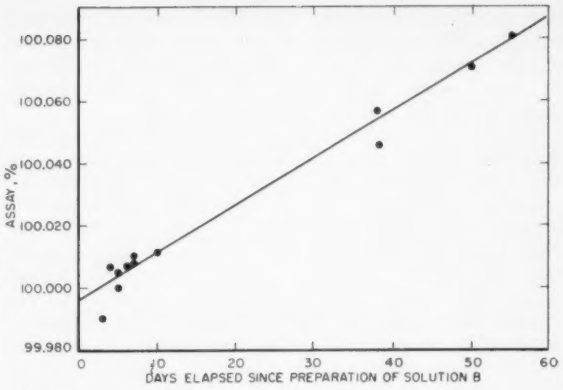

FIGURE 1. *Change of assay of solution B with time.*

for both the larger and the smaller samples are of the same order of magnitude as in the case of sodium chloride, 0.038 percent for 1 meq and 0.009 percent for 4 meq samples.

6. Titration of Potassium Iodide

6.1. Procedure

The potassium iodide was a reagent grade salt which was not subjected to any further purification. It was dried at 110 °C and stored in a desiccator before weighing. The choice of the potassium salt over sodium was made because sodium iodide is a very strongly hygroscopic material, which impairs accurate weighings.

In the vicinity of the end point of iodide titrations, the indicator current exhibited three inflection points, probably due to strong adsorption of the silver ion after the concentration of the latter reaches certain critical values. This, of course, indicated that several equilibria are to be satisfied, which brings in an uncertainty, or at least a doubt in the experimenter's mind as to the time to allow for equilibrium to establish. The problem was circumvented by the addition of 1 ml of 0.01 M solution of NaBr just as this end-point phenomenon occurred. The solution which was added was standardized previously by the coulometric technique and the number of milliequivalents in a 1-ml aliquot were subtracted from the total number of milliequivalents found in the sample. By this technique one in fact is determining the iodide by observing the bromide end point. In order to make the end point of the titration equivalent to the end point of the pretitration, a small amount of the same NaBr solution was added before the pretitration.

6.2. Results

The results for titration of 1 and 4 meq samples of potassium iodide are shown in columns 8 and 9 of table 1. Here again the precision for each set is of the same order of magnitude as in the case of the other two halides. The standard deviations for 1 and 4 meq samples are 0.030 and 0.007 percent

respectively. The mean value of the assay is larger for larger samples which can be caused by the adsorption of silver ions on the silver iodide precipitate.

7. Discussion

This work, similarly to the previous communication of the acidimetric titrations, shows the precise nature of coulometric titrations, with the attractive feature of utilizing a titrant the amount of which is based upon physical measurements rather than chemical standards of reference.

Needless to say, the experimenter must exercise extreme control over many factors such as weighing, delivery of sample, preparation of sample, current control, i.e., all factors which affect the precision and accuracy of any chemical analysis.

One factor which is especially important in these titrations and may very well apply to other precipitation titrations with amperometric end point detection, is the interference of the precipitate with the indicator electrode system. It was found that with large samples, the heavy precipitate which is formed may accumulate on the indicator electrodes, and in several instances it was found to form a bridge between the indicator anode and the indicator cathode. Such occurrence impairs the sensitivity of the indicator system by lowering the slope of the indicator current line. This condition, however, was simply eliminated by tapping the indicator electrodes before taking the final indicator current readings, to loosen the adhering precipitate.

At no time did the indicator current curves resemble those described by Lingane [9], even though the applied emf across the two indicator electrodes was 50 mv as he suggested. In all cases the indicator current was high before the end point, decreased as the end point was approached, passed through a minimum in the vicinity of the end point, and became a straight line function of the generated silver ion after the end point (fig. 2).

In view of the fact that a potential difference of only 50 mv was applied across indicator electrode system, it is very difficult to believe that a high indicator current before the end point was caused by the reduction of hydrogen ion at the indicator cathode. It may be explained by the reduction of the colloidal silver halides or silver halide complexes, since it is well known that silver chloride is appreciably soluble in high concentrations of chloride ion.

The pretitration procedure was devised to minimize uncertainty in the end-point location due to the absence of a well-defined residual current. By this technique the silver-halide equivalency is obtained from the difference between the end points, similarly determined, so that errors tend to cancel.

8. Conclusions

It has been shown that chlorides, bromides, and iodides can be titrated with high degrees of precision by coulometrically generated silver ion. In the case of sodium chloride, it has been shown that this method is accurate as well as precise. In the course of this work it has also been shown that it is rather difficult to maintain solutions of constant concentration. In working with solutions one is obliged to determine the rate at which the solution composition is changing to permit extrapolation of composition—time equation to time=0.

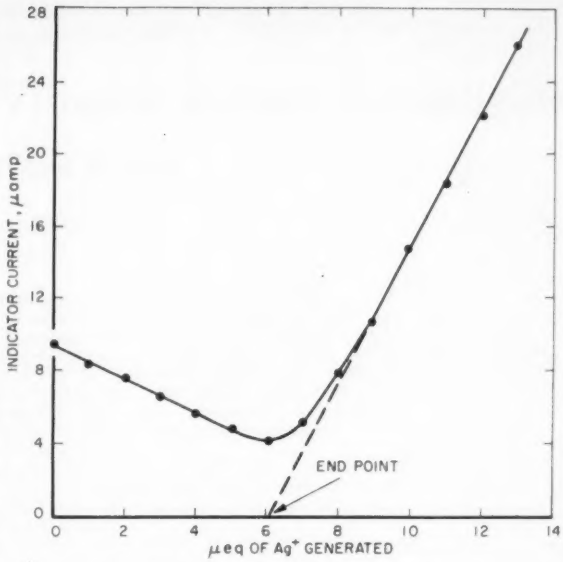

FIGURE 2. *Typical end-point determination.*

The authors are grateful to T. A. Willke of the Statistical Engineering Section for help in the statistical analysis of the data and especially for the statistical treatment of the data obtained for the sodium chloride solutions.

9. References

[1] W. R. Shields, T. J. Murphy, E. L. Garner, and V. H. Dibeler, J. Am. Chem. Soc. **84,** 1519 (1962).
[2] J. J. Lingane, Anal. Chem. **26,** 622 (1954).
[3] R. L. Kowalkowski, J. H. Kennedy, and P. S. Farrington, Anal. Chem. **26,** 626 (1954).
[4] D. D. De Ford and H. Horn, Anal. Chem. **28,** 797 (1956).
[5] E. P. Przybylowicz and L. B. Rogers, Anal. Chem. **28,** 799 (1956).
[6] J. K. Taylor and S. W. Smith, J. Research NBS **63A** (Phys. and Chem.) No. 2, 153 (1959).
[7] D. N. Craig, J. I. Hoffman, C. A. Law and W. J. Hamer, J. Research NBS **64A** (Phys. and Chem.), No. 5, 381 (1960).
[8] D. N. Craig, C. A. Law and W. J. Hamer, J. Research NBS **64A** (Phys. and Chem.), No. 1, 127 (1960).
[9] J. J. Lingane, Electroanalytical Chemistry (Interscience Publishers, Inc., New York, N.Y., 1958).

(Paper 67A1–192)

JOURNAL OF RESEARCH of the National Bureau of Standards—A. Physics and Chemistry
Vol. 67A, No. 1, January–February 1963

Radial Distribution Study of Vitreous Barium Borosilicate

G. J. Piermarini* and S. Block

(September 19, 1962)

An X-ray diffraction study of a barium borosilicate glass consisting of 24 mole percent barium oxide, 40 mole percent boric oxide, and 36 mole percent silicon dioxide has been performed. Resulting atomic radial distribution functions give the following average interatomic distances: Si-O, 1.6 A; Ba-O, 2.8 A; Ba-Ba, 4.7 A; and Ba-Ba, 6.8 A. From the 4.7 A Ba-Ba separation a Ba-O-Ba bond angle of about 115° has been calculated. The observed average barium separations are in partial agreement with that predicted by Levin and Block on the basis of a structural interpretation of immiscibility data. A proposed coordination change by Levin and Block for the barium atoms in the system has been confirmed, but the details of the coordination change mechanism have not.

Combining the results of the radial distribution study and immiscibility data on the barium borosilicate modifier-rich liquid at maximum barium oxide content has indicated that approximately 16.75 mole percent barium oxide is involved in the 4.7 A separation and 8.25 mole percent is associated with the 6.8 A separation.

A mechanism which allows the composition of the modifier-rich liquids in the ternary system to be calculated has been presented. The calculated composition has been found to agree well with the experimental value.

1. Introduction

A comprehensive structural interpretation of the immiscibility of alkali and alkaline-earth metal oxides in borate, silicate, and borosilicate systems has been proposed by Levin and Block [1].† Two models representing short-range structures, originated by Warren and Pincus [2], were adopted to enable the composition of the immiscibility limit to be calculated. The adopted models have been described previously [1,2] and are shown in figures 1 and 2.

For the binary barium borate system at the limit of maximum miscibility of barium oxide in the modifier-rich liquid, Levin and Block proposed that the average separation of barium atoms is 6.67 A resulting from type B coordination. Subsequent radial distribution analysis of the appropriate barium borate glass by Bienenstock, Posner, and Block [3] demonstrated that the proposed model was essentially correct. The average separation of barium atoms was found to be 6.8 A. This conclusion was based on the assumption that the structure of the modifier-rich liquid did not differ appreciably from the structure of the corresponding glassy state obtained by rapid quenching [4].

For the ternary system, barium borosilicate (part A, fig. 3), it was postulated that the configura-

*Taken in part from thesis submitted for degree of Master of Science, 1962; The American University, Washington, D.C.

† Figures in brackets indicate the literature references at the end of this paper.

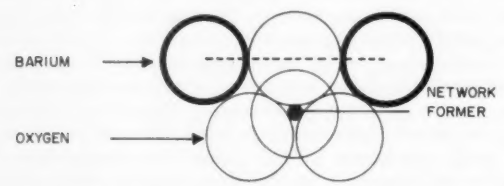

FIGURE 1. *Schematic representation of type A coordination.*

The network former is in either tetrahedral or triangular configuration. The calculated barium-barium nearest neighbor separation (dash line) is 5.50 Å.

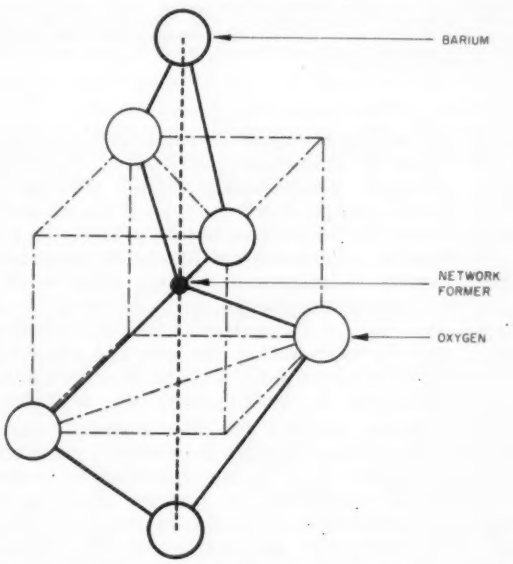

FIGURE 2. *Schematic representation of type B coordination.*

The network former is in tetrahedral configuration. The network former and barium polyhedra share edges. The calculated barium-barium nearest neighbor separation (dash line) is 6.67 Å.

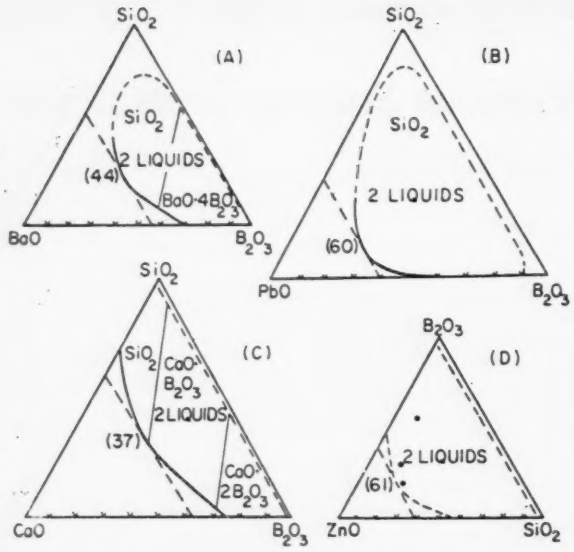

FIGURE 3. *Immiscibility regions (weight percent basis) in systems of type* $RO-B_2O_3-SiO_2$ *showing form of modifier-rich boundary curves.*

Numbers in parentheses, adjacent to intersection of solubility curves and tangents, indicate maximum solubility of modifier. To explain the form of these boundary curves, a change in coordination type for the modifier cation has been proposed by Levin and Block. Reproduced from E. M. Levin and S. Block, J. Am. Ceram. Soc. **40,** 95 (1957).

tion of the barium atoms in the modifier-rich liquids, at the limit of maximum miscibility of modifier oxide, changed progressively upon addition of silicon dioxide component from type B coordination, characteristic of the barium borate system, to type A coordination characteristic of the barium borosilicate system at maximum barium oxide content (see parenthetical number in part (A) of fig. 3 and related legend). Accompanied with the coordination change, a decrease in the average separation of barium atoms from 6.67 A (type B coordination) to 5.50 A (type A coordination) was postulated.

The primary purpose for this research was to compare the average barium interatomic separation in barium borate and barium borosilicate systems at maximum miscibility of barium oxide in the respective modifier-rich liquids in order to determine the mechanism accounting for the observed increase in the immiscible range of barium borosilicate. This paper describes the determination of average interatomic separations by means of a Fourier analysis of X-ray diffraction patterns of the appropriate barium borosilicate glass. It also presents a qualitative interpretation of the observed interatomic distances. With respect to the average barium separation, if the coordination change (B to A) postulated by Levin and Block is a physical reality, then the resulting atomic radial distribution curve should show the presence of a large maximum in the 5.5 A region and the absence of a peak of comparable magnitude in the 6.8 A range.

2. Experimental Procedures

The experimental procedures were essentially the same as those employed previously in the vitreous barium borate study [3]. Measurements were made with a Norelco X-ray diffractometer. Intensities were determined with a Norelco counting rate computer adjusted so that the probable intensity error did not exceed 2.4 percent. Monochromatization of the scattered radiation was achieved by means of the balanced filter technique [5]. Intensity correction due to air scatter was avoided by evacuating the volume defined by the scatter shield surrounding the specimen. The intensity data were automatically determined and recorded on a Brown strip-chart recorder at 0.05° intervals in 2Θ. Using Cu radiation, measurements were taken in the range 2° to 70° 2Θ. With Mo radiation, the intensity measurements were made in the range 20° to 60° 2Θ. Periodic checks were made to guard against significant variations in incident intensity. Further detail in the experimental procedure is given in reference 3.

The specimen, containing 24 mole percent barium oxide, 36 mole percent silicon dioxide, and 40 mole percent boric oxide, was obtained from G. W. Cleek and E. H. Hamilton of the National Bureau of Standards staff. The measured density of this specimen, determined by the method described by Glaze, Young, and Finn [6], is 3.35 g cm^{-3}. The normalized experimental intensities (A) corrected for polarization are shown in figure 4.

The coherent scattering factors, f, for barium, boron, silicon, and oxygen, in addition to the incoherent scattering factors for silicon, boron, and oxygen, were obtained from standard references [7]. The incoherent scattering factor for barium was calculated using [8]

$$I_{\text{inc}} = Z - f^2/Z.$$

The incoherent scatter was corrected with the Breit-Dirac factor [8]. The total independent scatter curve (B) in figure 4 is the sum of the coherent (C) and incoherent (D) scatter. Unlike the technique employed in the barium borate study [3], the experimental intensities corrected for polarization were put on an absolute scale (electron units per unit of composition) by adjusting the ordinates of the experimental intensity curve so that the experimental curve (A) matched the total independent scattering curve (B) at large s values. This procedure was followed because it appeared less likely to produce high frequency ripples in the distribution curve (assuming that systematic errors in intensity measurements and scattering curves have not been completely eliminated) which would interfere with the determination of peak positions. The method used here tends to push the error residue toward low s values thereby producing longer wavelength ripples which interfere less with the determination of peak positions. That high frequency ripples lead to inaccuracies in the distribution curve seems to be indicated in the barium borate study [3]. The normalized intensity curve (A) corrected for polarization is shown in figure 4.

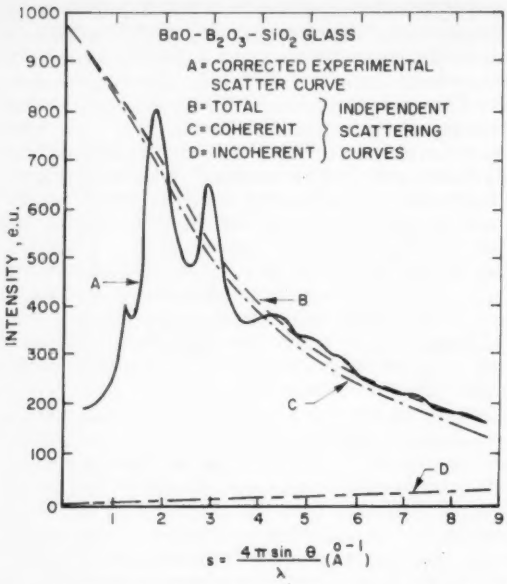

FIGURE 4. *Normalized experimental X-ray intensities (A) and independent scattering curves (B,C,D) for vitreous* BaO-B_2O_3-SiO_2.

Following essentially the same calculations employed in the previous barium borate study [3], the atomic radial distribution functions were determined. The weighted distribution is usually given by the relation:

$$\sum K_m 4\pi r^2 \rho_m(r) = \sum K_m 4\pi r^2 \rho_0 + \frac{2r}{\pi}\int_{s_{\min}}^{\infty} si(s) \sin sr\, ds,$$

where Σ indicates summation over the molecular composition. K_m is the effective number of electrons in atom m, and is defined as $K_m = f_m/f_e$. $4\pi r^2 \rho_m(r) dr$ is the number of atoms, each multiplied by its effective number of electrons, between distances r and $r+dr$ from atom m. ρ_0 is the average number of electrons per unit volume. s equals $(4\pi \sin\theta)/\lambda$, where θ is the Bragg angle of diffraction and λ is the wavelength of the radiation. $i(s)$ is the experimental amplitude function and is equal to $(I_{eu} - \Sigma f_m^2)/f_e^2$, where I_{eu} is the corrected experimental intensity of unmodified scattering in electron units per unit composition, f_m is the atomic scattering factor for atom m, and f_e is the average f per electron. That is, f_e equals $\Sigma f_m / \Sigma Z_m$, where Z_m is the atomic number of atom m. The reader is referred to reference 9 for further mathematical detail related to the above general equation.

The determination of the radial distribution function comprises two main steps: First, the numerical evaluation of the $si(s)$ function from experimental scattering data, and second, the evaluation of the summation

$$\frac{2r}{\pi}\sum_{s_{\min}}^{s_{\max}} si(s) \sin sr\Delta s.$$

These summations were performed on a high speed digital computer for 0.1 A intervals in r from $r=0$ to $r=9.9$ A over specified ranges in s, giving directly the differential radial distribution function,

$$\sum K_m 4\pi r^2 [\rho_m(r) - \rho_0],$$

from which, by adding the average radial atomic density, $\Sigma K_m 4\pi r^2 \rho_0$, the atomic radial distribution as a function of r is obtained.

3. Results

A fit at high s values of the corrected experimental intensity (A), derived from both the molybdenum and copper radiations, to the total independent scatter curve (B) is shown in figure 4. An atomic radial distribution function derived from the experimental intensity data is shown in figure 5. Several techniques were employed in determining the radial distribution function. For example, the series was terminated at various s values, the experimental scatter curve (A) was extrapolated to zero at $s=0$, the CuK_α and MoK_α intensity curves were fitted together in several ways, a number of normalization trials were made, and various temperature factors were applied to the $si(s)$ functions. Application of these techniques produced no significant change in the peak positions in the distribution curve shown in figure 5. However, the peak areas were affected. A temperature factor of $e^{-0.02s^2}$ was applied to the experimental amplitude function used in determining the distribution curve shown in figure 5. The intensity data covered the range 0.4 to 8.8 A^{-1} in s.

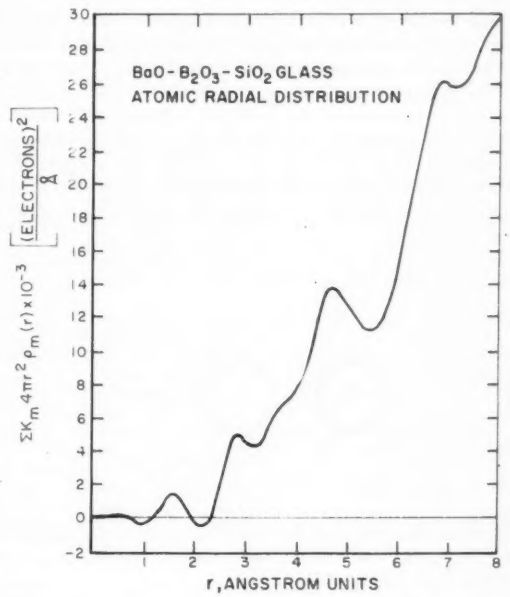

FIGURE 5. *Atomic radial distribution function of* BaO_2-B_2O_3-SiO_2 *glass.*

For the purpose of this study the more important features of the distribution function shown in figure 5 are the presence of two unexpected major peaks, one at 4.7 A, the other at 6.8 A, and the absence of an expected major peak in the 5.5 A region. The two observed peaks are attributed primarily to barium-barium interatomic separations, because the barium atom is the only one present in the glass having a large enough scattering factor to produce peaks of this magnitude.

The 4.7 A barium-barium separation is associated with a modified type A coordination wherein the barium-oxygen-barium bond angle is approximately 115, not 180° as postulated by Levin and Block. A schematic representation of modified type A coordination is shown in figure 6. If it is assumed that the barium atoms form, in general, a cubic array with an average edge of 4.7 A, then the face diagonal of this cube has a length of 6.65 A. Although the radial distribution function shows high atomic density in the region of 6.65 A, the maximum is at 6.8 A. This peak is primarily due to barium atoms in type B coordination, and the second nearest neighbor barium-barium separation arising from modified type A coordination. A similar barium separation (6.8 A) was found for type B coordination in the barium borate study by Bienenstock, Posner, and Block [3].

Further analysis of the distribution function indicates that the 1.6 A peak represents primarily the average silicon-oxygen nearest neighbor distance. The calculated distance is 1.62 A. By a similar radial-distribution study, Warren et al., obtained 1.62 A for the silicon-oxygen nearest neighbor distance in silica glass [9]. The 2.8 A peak represents the barium-oxygen nearest neighbor distance. The calculated separation is 2.8 A.

Coordination numbers calculated from the observed areas of maxima are rather doubtful due to systematic errors and the overlap of interatomic separations inherent in the technique. In addition, for complex glasses such as barium borosilicate, the calculation of coordination numbers is complicated.

Consider the 1.6 A peak. There are three interatomic separations contributing to the area of this peak. One is the previously mentioned 1.6 A silicon-oxygen separation, another is a 1.4 A boron-oxygen separation resulting from triangularly coordinated boron, and also present is a 1.5 A boron-oxygen separation arising from tetrahedrally coordinated boron [10]. The contributions of the two boron-oxygen separations to the area of this peak are indeterminate. However, compared with the contribution of the 1.6 A silicon-oxygen separation, the contributions due to the boron-oxygen separations are minor because of the low atomic number of boron. With due consideration for these facts, an estimated area of 400 (electrons)^2 is attributed to the 1.6 A silicon-oxygen separation. From this area a coordination number of 4.3 is calculated for the number of oxygen nearest neighbors about a silicon atom (see reference 3 for coordination number calculations). This value is consistent with the predicted value, 4.

The area of the 2.8 A peak has contributions from several interatomic separations as in the previous case. The primary contribution to this peak is from the barium-oxygen nearest neighbor separation. The area of the 2.8 A peak is estimated to be 2,500 (electrons)^2. If one were to assume 8-fold coordination for the oxygen nearest neighbors about a barium atom, then the calculated area is approximately 1,500 (electrons)^2.

The more important aspects of this research, the coordination change and estimate of percent of barium atoms in either coordination grouping, can be treated further. Continuing with the previous assumption that the barium atoms form a cubic array, an average barium separation of 5.58 A is calculated using the Warren and Pincus equation which states that the extent of immiscibility is inversely proportional to the cube of the modifier cation separation. The radial distribution function does not allow a determination of the relative amounts of barium atoms in type B and modified type A coordination but, as the contributing distances and average distance are known, the following calculation can be made to provide an estimate of the fraction of barium atoms in each coordination type.

Letting α equal the fraction of barium atoms involved in type B coordination and $(1-\alpha)$ the fraction involved in modified type A coordination, then

$$\alpha(6.8\text{ A})^3+(1-\alpha)(4.7\text{ A})^3=(5.58\text{ A})^3$$

$$\alpha=0.33.$$

Since the total amount of barium oxide in the modifier-rich liquid is 25 mole percent, then approximately 8.25 mole percent is associated with type B coordination and about 16.75 mole percent is involved in modified type A coordination.

The ratio of mole percents of barium oxide (16.4%) to boric oxide (83.6%) in the binary barium borate system at the limit of miscibility of barium oxide in the modifier-rich liquid is approximately 0.20. For this system the barium atoms have the type B configuration [3]. It is interesting to note that the

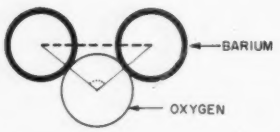

FIGURE 6. *Schematic representation of modified type A coordination depicting the short barium-barium separation, 4.7 Å, (dash line) and the small barium-oxygen-barium bond angle, 115°, (dot curve).*

The angle was calculated on the basis of a 2.8 A barium-oxygen separation and the 4.7 A barium-barium separation obtained from the radial distribution curve.

ratio of mole percents of barium oxide (8.25%) to boric oxide (40%) for the corresponding modifier-rich liquid in the ternary barium borosilicate system is 0.21, when only the calculated amount of barium oxide involved in type B coordination is considered. The similarity of ratios suggests that the amount of barium atoms in type B coordination remains constant as silica and barium oxide components are added, while the added barium atoms assume the modified type A coordination.

Using the oxygen-volume method [1] the composition of the maximum extent of miscibility of modifier oxide can be estimated. For barium borate in type B coordination, the relative mole percentages are: 16.1 BaO·83.9 B_2O_3 [1]. For barium silicate in modified type A coordination, the relative mole percentages are: 32.2 BaO·67.8 SiO_2. The combined compositions can be written as: 32.2 BaO (modified type A)·16.1 BaO (type B)·83.9 B_2O_3·67.8 SiO_2 or on a 100 percent basis as: 16.1 BaO (modified type A) · 8.0 BaO (type B) · 42.0 B_2O_3·33.9 SiO_2. This composition compares well with the experimental composition, 16.75 BaO (modified type A)·8.25 BaO (type B)·39 B_2O_3·36 SiO_2, where the relative amounts of each coordination type were determined by the calculation of α, the fraction of barium atoms involved in type B coordination.

4. Conclusions

The radial distribution functions reveal barium-barium separations at approximately 4.7 and 6.8 A. The unexpected 4.7 A distance is due to barium atoms in a modified type A coordination with a calculated barium-oxygen-barium bond angle of about 115°. The 6.8 A distance is due to barium atoms in type B coordination and the barium-barium second nearest neighbor separation due to modified type A coordination. The new factor as compared to the average barium separation in the barium borate glass is the 4.7 A separation. As postulated by Levin and Block, the increase of the immiscibility range in the ternary barium borosilicate system does occur by a coordination-change mechanism. However, the barium atoms are not involved solely in type A coordination. The factor which caused Levin and Block to assume 100 percent change to type A coordination is the good agreement observed between the average barium-barium separation (5.58 A) determined by using the Warren and Pincus immiscibility equation and the geometrical separation (5.50 A) due to the type A configuration with a 180° barium-oxygen-barium bond angle.

At the limit of miscibility in the binary barium borate system, the modifier-rich liquid contains 16.4 mole percent barium oxide with the barium atoms involved primarily in type B coordination. The corresponding barium borosilicate modifier-rich liquid contains 25 mole percent barium oxide [1]. Combining the results of the radial distribution study and the immiscibility equation indicates that approximately 16.75 mole percent barium oxide is involved in the modified type A configuration and 8.25 mole percent barium oxide is associated with type B coordination. In the barium borate modifier-rich liquid as silica and barium oxide components are added, it may be considered that the amount of barium atoms in type B coordination remains constant, while the additional barium atoms assume a modified type A coordination. Using the modified type A coordination model and the oxygen-volume method of calculating the extent of miscibility of modifier oxide [1] results in a final limiting composition of 16.1 BaO (modified type A)·8.0 BaO (type B)·42.0 B_2O_3·33.9 SiO_2 in mole percent.

Each coordination type, modified A or B, is not necessarily associated with a particular network former. One should consider the structure with type B coordination as having modifier cations separated primarily by the network former as described earlier in figure 2 and related legend. Thus, the modifier cations are bonded to different oxygens. The structure with modified type A coordination should be considered as having modifier cations bonded primarily to the same oxygen atom.

This study indicates the importance of determining whether the phenomenon of coexistence of type B and modified type A coordinations is limited to the ternary system. Research on relevant binary systems is presently being undertaken.

The authors are greatly indebted to A. Bienenstock for his valuable counsel in connection with many aspects of this study. In addition, thanks are due to H. M. Ondik of the National Bureau of Standards staff for developing a computer program for use in facilitating the calculations connected with this research.

5. References

[1] E. M. Levin and S. Block, J. Am. Ceram. Soc. **40,** 95 (1957).
[2] B. E. Warren and A. G. Pincus, J. Am. Ceram. Soc. **23,** 301 (1940).
[3] A. Bienenstock, A. S. Posner, and S. Block, J. Research NBS **64A** (Phys. and Chem.) No. 3, 229 (1960).
[4] K. Furukawa, Sci. Rep. RITU (Japan) **A–12,** 150 (1960).
[5] P. Kirkpatrick, Rev. Sci. Instr. **10,** 186 (1938); **15,** 223 (1944).
[6] F. W. Glaze, J. C. Young, and A. N. Finn, J. Research NBS **9,** 799 (1932) RP 507.
[7] H. Viervoll and O. Ogrim, Acta Cryst. **8,** 277 (1949); A. H. Compton and S. K. Allison, "X-rays in theory and experiment", 2d ed. (D. Van Nostrand Co., Inc., New York, 1935).
[8] R. W. James, "The optical principles of the diffraction of X-rays", vol. II, p. 462–3 (G. Bell & Sons, Ltd., London, 1954).
[9] B. E. Warren, H. Krutter, and O. Morningstar, J. Am. Ceram. Soc. **19,** 202 (1936).
[10] J. Biscoe and B. E. Warren, J. Am. Ceram. Soc. **21,** 287 (1938).

(Paper 67A1–193)

JOURNAL OF RESEARCH of the National Bureau of Standards—A. Physics and Chemistry
Vol. 67A, No. 1, January–February 1963

Dynamic Compressibility of Poly(Vinyl Acetate) and Its Relation to Free Volume

John E. McKinney and Harriet Vera Belcher

(September 19, 1962)

The complex bulk compliance (dynamic compressibility) of a commercial sample of poly(vinyl acetate), AYAT, was measured at frequencies from 50 to 1,000 cycles per second, temperatures from 0 to 100 °C, and static hydrostatic stresses from 0 to 981 bars (gage pressure) using an alternating hydrostatic stress generated and detected by piezoelectric transducers mounted in an essentially noncompliant cavity with dimensions small in comparison to a wavelength. The above temperature range was more than sufficient to cover the dispersion region in which an inflection in the storage compliance and a maximum in the loss compliance were observed. The data were reduced to functions of reduced variables using the WLF Equations extended to include static pressure with the "universal" WLF Constants and $dT/dP = 0.020$ °C/bar. The difference in limiting compliances at zero and infinite frequencies was larger than that predicted from the dT/dP shift using the free volume concept. A discussion is presented on possible processes that might contribute to an excessive value between limiting compliances.

1. Introduction

The free volume concept [1] [1] has been used frequently to explain the glass transition of polymers and glass forming liquids. To apply this concept it is postulated that the necessary and sufficient condition for a glass transition to occur in a polymer is that the free volume fraction reach the critical value necessary for continuously changing molecular arrangements, which account for the physical behavior typical of the liquid or rubbery state. This critical value of free volume fraction has been assumed to be independent of temperature and static pressure for a given material and nearly independent of the material (as long as it will undergo a glass transition under some conditions of state).

Measurements of the dynamic compressibility of vulcanized natural rubber-12 percent sulfur [2] were interpreted in terms of this concept, assuming that the compressibility observed at frequencies above (or temperatures below) the frequency-dispersion region corresponded to the compressibility of the occupied volume alone, and that the compressibility at frequencies below (or temperatures above) the dispersion region corresponded to the compressibility of the occupied plus the free volume. An extended WLF [1] equation including a linear dependence of free volume fraction on static pressure was used to reduce these observations to functions of a single variable. The "universal" WLF constants were found adequate to reduce the results at one atmosphere in terms of a single variable including frequency and temperature. The coefficient of pressure in the free volume fraction expression, evaluated empirically from the shifting of the dispersion region due to pressure, agreed with the isothermal compressibility difference calculated from the adiabatic difference in compressibility above and below the dispersion region.

For rubber-sulfur the shift in temperature with static pressure at constant free volume, 0.024 °C/bar, was nearly the same as that found for several other polymers investigated by different techniques: 0.025 for polyisobutylene [3], 0.027 for polyethylene [4], and 0.031 for polystyrene [5] hinting at the possibility that these numbers might be approximated by a "universal" constant as in the case of the WLF Universal Constants.

The purpose of this work was to investigate the effect of static pressure, temperature, and frequency on the dynamic compressibility of poly(vinyl acetate) in the vicinity of the glass transition in order to check on a different polymeric system the applicability of this free volume concept to explain the effects of pressure on mechanical properties and to evaluate the applicable constants.

2. Experimental Method

The dynamic bulk compliance [2] measurements were made with an apparatus described in previous publications [6, 7]. In this method the sample is contained, along with two PZT [3] ceramic volume expander transducers mounted on compliant copper springs, within a cylindrical cavity sufficiently small to make the acoustic pressure hydrostatic. The remaining air is displaced with a pressure transmitting fluid [*di*(2 ethyl hexyl) sebacate] whose adiabatic compressibility is known from previous PVT and heat capacity measurements. An a-c

[1] Figures in brackets indicate the literature references at the end of this paper.

[2] Compliance here is equivalent to compressibility in the usual acoustic usage. This follows the recommendations of the Committee on Nomenclature of the Society of Rheology [8].

[3] A solid solution of lead titanate and zirconium titanate supplied by the Clevite Research Laboratory, Cleveland, Ohio.

voltage is applied to one transducer and a corresponding signal is observed on the other. From the complex voltage ratio the complex bulk compliances may be calculated. The temperature is controlled by immersing the entire assembly in a thermostated bath and any desired static pressure in the range of 0 to 1,000 bars (gage pressure) may be superimposed upon the dynamic pressure using a hand operated pump.

The calibration procedure and the dynamic bulk compliance determinations on poly(vinyl acetate) were similar to those used on rubber sulfur [2]. All runs were made along an isobar with increasing temperature and the system was permitted to reach thermal equilibrium before each reading was recorded.

It is required that the specific volume of the sample be known as a function of temperature and pressure in order to calculate its dynamic bulk compliance from the transducer equations. Also such data yield useful information including the thermal expansivity, the isothermal compressibility, the glass transition temperature and its shift with pressure, all of which are useful in evaluating the parameters for a reduced variable formulation.

The specific volume of this sample of poly(vinyl acetate) was determined by using a glass dilatometer with mercury as a confining liquid. This was placed in a pressure cell with glass windows to view the height of the mercury column. The cell in turn was placed in a liquid thermostat. The pressure was limited to 500 bars to prevent collapse of the glass windows.

3. Samples

The poly(vinyl acetate) supplied through the courtesy of G. M. Powell of the Bakelite Company was a commercial sample designated AYAT for which the intrinsic viscosity in cyclohexanone at 20 °C was given as 0.69 dl/g. The polymer was received in the form of small pellets averaging about 0.6 cm in diameter. These were molded at about 100 °C into disks 1.5 cm in diameter and 3 mm thick. In order to determine if there were any significant swelling in the pressure transmitting oil [*di*(2 ethyl hexyl) sebacate], one of the disks was placed in the oil and weighed at approximately weekly intervals for six weeks. All of the weighings agreed within 2 parts in 10^4 indicating no significant swelling which could influence the bulk compliance determinations. In addition, the disk used in the bulk compliance determinations was weighed at frequent intervals to check for any effect of pressure on the swelling rate. Again the weighings agreed to within 2 parts in 10^4.

4. Results

4.1. Specific Volume Measurements

The specific volume, V_s, of PVAc as a function of temperature at several static pressures is shown on figure 1. All of the observations were taken along an isobar for each of the four runs. Measurements in the liquid region were independent of the direction of temperature change and reached equilibrium in about 15 min, which is about the time for the apparatus to reach equilibrium. In the glassy region about 1 hr was required to obtain apparent equilibrium [4] for each observation at constant pressure. It was found that the most reproducible measurements could be taken by commencing at some temperature above the transition region and then decreasing the temperature at constant pressure, allowing sufficient time to reach apparent equilibrium for each observation.

[4] The criterion adopted was that no further change in volume could be observed over a period of 1 hr within the precision of the experiment.

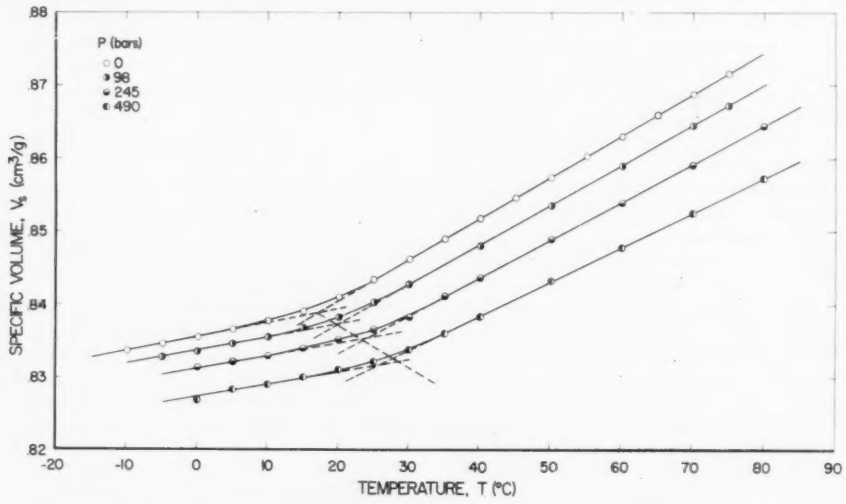

FIGURE 1. *Specific volume of PVAc plotted against temperature at several pressures.*

The dashed lines with positive slopes are extrapolated values of V_l, the specific volume established from volume-temperature relations in the liquid state, and V_g, established from volume-temperature relations in the glassy state. V_l and V_g were obtained by a least squares fit on the data, linear in T and quadratic in P, treating the liquid and glassy regions separately and ignoring the data in the transition region. The glass transition temperature, T_g, was obtained from the intersections of the extrapolations of V_l and V_g and was found to be 17 °C at 1 atm ($P=0$) and vary with pressure at a rate of about 0.020 °C/bar, as indicated by the dashed line with negative slope. As seems characteristic of poly(vinyl acetate), the glass transition temperature is poorly defined, since the thermal expansivity changes markedly over a temperature range of about 15°.

We had originally thought that our sample was a pure polymer, free of contaminant or very low molecular weight components; however, the value of T_g determined from this experiment is low in comparison with the generally accepted values of 25 to 32 °C. The low value obtained here may be partly attributed to the longer than usual times permitted for the specific volume observations to approach apparent equilibrium. On the other hand heating the sample in a vacuum at 70 °C for one week resulted in a loss of weight amounting to almost 2 percent. The presence of contaminant could lower the value of T_g and therefore contribute to the lower than usual value observed; thus, the data from our sample do not apply to pure PVAc, but to a sample with a small amount of contaminant. This uncertainty does not, of course, affect the validity of our results so far as our primary purpose is concerned.

Two additional thermodynamic quantities that are sometimes useful in evaluating some of the reduced variable parameters are the isobaric thermal expansivity,

$$\alpha=\frac{1}{V}\left(\frac{\partial V}{\partial T}\right)_P,$$

and the isothermal compressibility,

$$\beta=-\frac{1}{V}\left(\frac{\partial V}{\partial P}\right)_T.$$

The related reduced variable parameters are supposed to be the differences in the values of α and the values of β between the liquid and glassy states. Table 1 gives the thermal expansivities for the liquid state,

$$\alpha_l=\frac{1}{V_l}\left(\frac{\partial V_l}{\partial T}\right)_P,$$

for the glassy state,

$$\alpha_g=\frac{1}{V_g}\left(\frac{\partial V_g}{\partial T}\right)_P,$$

and the difference, $\Delta\alpha$, evaluated at $T=T_g$ for each observed pressure.

The compressibility, β, was difficult to determine due to the lack of data at different pressures, in particular those above 500 bars; hence, any attempted evaluation to obtain the desired difference, $\Delta\beta$, will be too uncertain to have any merit.

TABLE 1. *Thermal expansivities of PVAc for the liquid and glassy states evaluated at $T=T_g$ for each observed pressure*

P	T_g	$\alpha_l\times10^4$	$\alpha_g\times10^4$	$\Delta\alpha\times10^4$
Bars	°C	°C^{-1}	°C^{-1}	°C^{-1}
0	17	6.74	2.26	4.48
98	21	6.52	2.21	4.31
245	24	6.19	2.15	4.04
490	26	5.65	2.03	3.62

Values of V_g at pressures higher than 490 bars required for dynamic compressibility determinations (735 and 981 bars) were evaluated by linear extrapolation using slopes determined from values at 245 and 490 bars. Although the dependence of V_g on P is not exactly known at the higher pressures, this procedure is legitimate because of the small change in V_g with P. For example, an error in the slope of 10 percent will only produce a 0.2 percent error in V_g, which is smaller than other uncertainties involved.

4.2. Dynamic Bulk Compliance Measurements

Figure 2 shows the storage compliance, B', at 1,000 c/s as a function of temperature at different static pressures. At the higher pressures the data for some of the runs appear to be biased. That is, all of the values at one pressure appear to be in error by nearly a constant amount over a large temperature range. For example, the lower four curves were taken at equal pressure intervals; however, the compliance values, especially at high temperatures, do not decrease in a smooth fashion with pressure as would be expected. In particular the gap between the 490 and 736 bar curves appears to be excessive. This effect is attributed to variations in transducer response between the sample and calibration runs. The larger the temperature and pressure ranges that are covered, the less reproducible the measurements become, presumably because of irreversible changes in domain configuration within the transducers. For an isothermal run at 90 °C the response of B' with pressure was much smoother and, in particular, the excessive gap between the values of B' at 490 and 736 bars shown in figure 2 was not apparent.

Figure 3 shows the corresponding loss compliance. The temperatures for maximum B'' appear nearly the same as those for the inflections in B' in figure 2. For a single retardation time, or a symmetrical distribution of retardation times, these points appear at the same frequency when plotted against log frequency and would appear at the same temperature when these functions are plotted against temperature, except that there are slight displacements from the variation of ΔB, the difference between low and high frequency limiting compliances, with tempera-

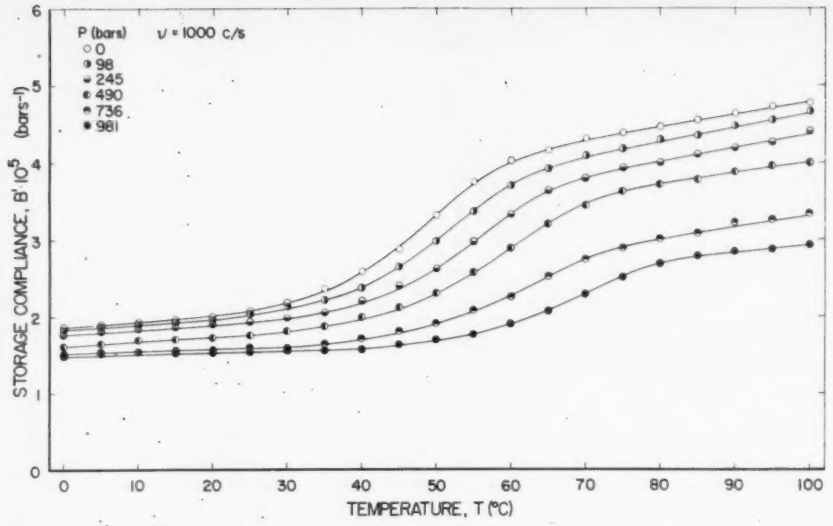

FIGURE 2. *Storage compliance at 1,000 c/s plotted against temperature at several pressures.*

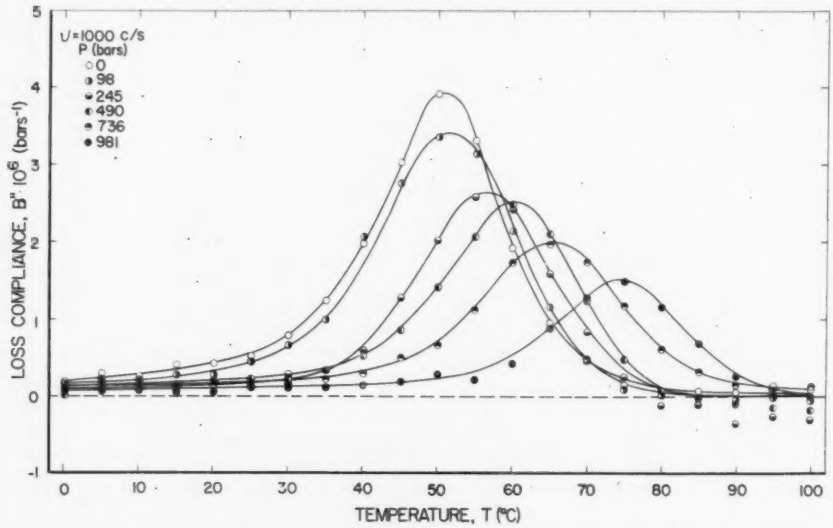

FIGURE 3. *Loss compliance at 1,000 c/s plotted against temperature at several pressures.*

ture. For an unsymmetrical distribution it can be shown [9] that the following inequalities hold, where τ_{max} is the time corresponding to the maximum of bulk retardation spectrum $L_v(\ln \tau)$ defined by the relation,

$$B^*=\int_{-\infty}^{\infty} L_v(\ln \tau)\,\frac{1}{1+i\omega\tau}\,d\ln\tau+B_\infty,$$

ω' is the angular frequency ($\omega=2\pi\nu$) of the inflection of B' versus $\ln\omega$, and ω'' is the frequency of max B'':

$$\omega''>\omega'>\frac{1}{\tau_{max}}$$

if $L_v(\ln\tau)$ falls off more rapidly for $\tau>\tau_{max}$ than for $\tau<\tau_{max}$, and

$$\omega''<\omega'<\frac{1}{\tau_{max}}$$

if $L_v(\ln\tau)$ falls off more rapidly for $\tau<\tau_{max}$ than for $\tau>\tau_{max}$.

The storage compliance at different frequencies for three different static pressures is shown in figure 4. The data at 1,000 c/s are identical to that shown in figure 2 under the same conditions. Scatter is higher at the lower frequencies, mostly because of a characteristic $1/\nu$ noise [10]. The data at $\nu=50$ and

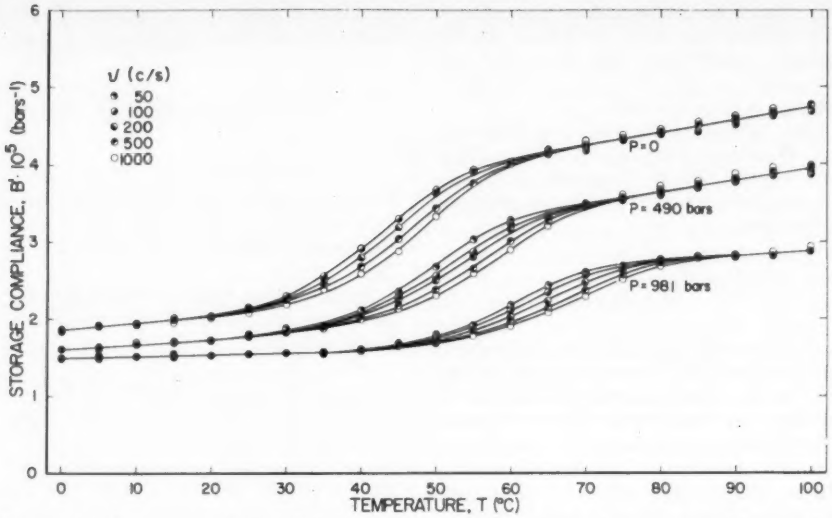

FIGURE 4. *Storage compliance plotted against temperature at several pressures and frequencies.*

$P=0$ were omitted entirely because of excessive scatter.

The corresponding loss compliance is given in figure 5. The maximum values of B'' at constant pressure generally increase slightly with frequency, which is consistent with the reduced variable formulation discussed in section 5. On the other hand the value of B''_{max} at $\nu=1{,}000$ and $P=0$ is about 25 percent greater than we would expect from extrapolating values at lower frequencies using the reduced variable formulation. A hint of this behavior is seen in figure 3 for $P=98$ bars also. Whether this behavior is real or an artifact of the experiment cannot be determined from these measurements.

5. Reduced Variables

The reduced variable formulation developed for the analysis of our earlier rubber-sulfur data [2] was used. In this treatment the complex bulk compliance,

$$B^*(T, P, \omega)=B_\infty(T, P)+\Delta B(T, P)\mathscr{B}^*(T, P, \omega) \quad (1)$$

is assumed to consist of two parts. The first, $B_\infty(T, P)$, is the adiabatic compliance,

$$-\frac{1}{V}\left(\frac{\partial V}{\partial P}\right)_s=-\left(\frac{\partial \ln V}{\partial P}\right)_s,$$

at infinite frequency. The second is the difference between the adiabatic compliances, $B_0(T, P)$ at $\omega=0$ and $B_\infty(T, P)$ at $\omega=\infty$, times a complex normalized dispersion function $\mathscr{B}^*(T, P, \omega)$, which goes to unity at $\omega\to 0$ and zero as $\omega\to\infty$.

Assuming that $\mathscr{B}^*(T', P', \omega')=\mathscr{B}^*(T, P, \omega)$ (equivalent to an invarient normalized retardation spectrum) when the data are shifted along a temperature, pressure, or log frequency axis, the final equation used to reduce the observed compliances to functions of reduced variables becomes

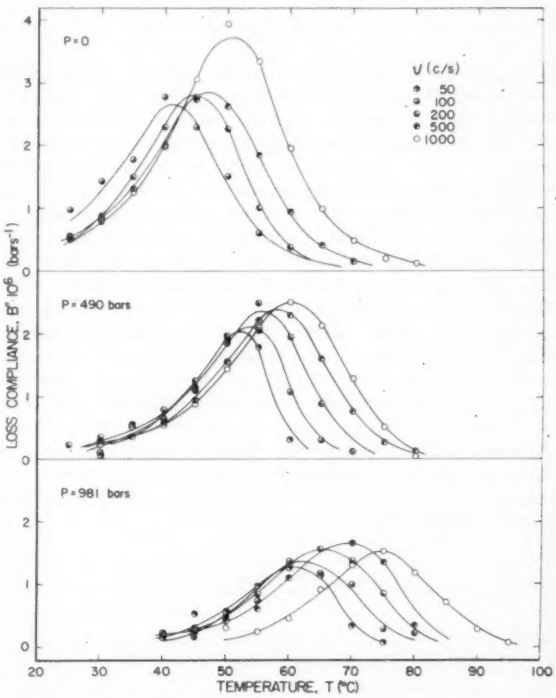

FIGURE 5. *Loss compliance plotted against temperature at several pressures and frequencies.*

$$B^*(T', P', \omega')=B_\infty(T', P')+\frac{\Delta B(T', P')}{\Delta B(T, P)}[B^*(T, P, \omega)-B_\infty(T, P)] \quad (2)$$

in which the primes designate either reduced variables or reference conditions. In a reduced variable

presentation only one of the independent variables is varied while the others are held constant at the arbitrary reference conditions. B_0 and B_∞ are evaluated empirically from the data in regions where frequency dispersion is insignificant.

The independent variables are reduced following the procedure of Williams, Landel, and Ferry [1] in the development of the WLF Equation with the addition of a linear pressure term in the expression for free volume fraction,

$$f(T,P)=f_g+\alpha_f(T-T_{g0})-\beta_f P \qquad (T\geq T_g \text{ or } P\leq P_g), \tag{3}$$

where T_{g0} is T_g at $P=0$ and P_g is the glass transition pressure, which may be defined as the break in the volume-pressure curve allowing sufficient time for significant variations to disappear. Frequency and viscosity are related by

$$\omega'=\omega\eta(T,P)/\eta(T',P'), \tag{4}$$

and viscosity and free volume fraction by

$$\eta=A\exp 1/f. \tag{5}$$

The viscosity used here is the steady flow shear viscosity. One can either assume explicitly that the retardation times determining bulk retardations are the same as those involved in shear motions or can look on these relations as defining a separate set of relations for bulk deformations, of the same form as those for shear, evaluating the constants empirically. The limited experimental information available seems to support the hypothesis that the retardation times governing dilatation are the same as those governing shear, except for the complications which may enter in due to the change in volume during the course of a given measurement [11]. In our case the alternating volume changes are too small to introduce any detectable effect of this type.

Equations (3), (4), and (5) are the basic equations necessary to develop the desired relations between the independent variables. Equation (3) written in terms of a viscosity at the arbitrary reference conditions, T_0 and $P_0=0$ (1 atm), is

$$\eta(T,P)=\eta(T_0,0)\exp\left[\frac{1}{f}-\frac{1}{f_0}\right], \tag{6}$$

where f_0 is the free volume fraction at the reference conditions. Substituting frequencies for viscosities in eq (6) by utilizing eq (4) with $\omega'=\omega_r$, the reduced frequency at the reference conditions, the ratio of corresponding frequencies is

$$\frac{\omega_r}{\omega}=\exp\left[\frac{1}{f}-\frac{1}{f_0}\right]. \tag{7}$$

Writing eq (7) in logarithmic form and using eq (3) to obtain explicit temperature dependence for f and f_0, the final equation for the reduced frequency in terms of the reduced variable parameters, the observed independent variables, T, P, and ω, and the arbitrary reference conditions, T_0 and $P_0=0$, becomes

$$\ln\omega_r=\ln\omega-\frac{\alpha_f(T-T_0)-\beta_f P}{[f_g+\alpha_f(T-T_{g0})-\beta_f P][f_g+\alpha_f(T_0-T_{g0})]}. \tag{8}$$

This reduces to the WLF Equation, if T_0 is taken as T_g and P set equal to zero, for which the "universal" constants correspond to $f_g=0.025$ and $\alpha_f=4.8\times10^{-4}$ °C^{-1}.

In a similar fashion the following equivalent expressions are found for a reduced temperature at $P_0=0$ and ω_0,

$$T_r=T-\frac{\beta_f}{\alpha_f}P+\frac{1}{\alpha_f}\frac{[f_g+\alpha_f(T-T_{g0})-\beta_f P]^2\ln(\omega_0/\omega)}{1-[f_g+\alpha_f(T-T_{g0})-\beta_f P]\ln(\omega_0/\omega)}, \tag{9}$$

and a reduced pressure at T_0 and ω_0,

$$P_r=P-\frac{\alpha_f}{\beta_f}(T-T_0)-\frac{1}{\beta_f}\frac{[f_g+\alpha_f(T-T_{g0})-\beta_f P]^2\ln(\omega_0/\omega)}{1-[f_g+\alpha_f(T-T_{g0})-\beta_f P]\ln(\omega_0/\omega)}. \tag{10}$$

In this formulation the free volume fraction, f, is in effect an empirical function of temperature and pressure. It is a free volume fraction related to the difference between V_l, the actual volume in the liquid region, and V_g, the volume obtained by linear extrapolation of the volume-temperature relation established in the glassy region. α_f is generally equal, or very close, to $\Delta\alpha$, the difference in isobaric thermal expansivities above and below T_g. If this is assumed,

$$\alpha_f=\left(\frac{\partial\ln V_l}{\partial T}\right)_P-\left(\frac{\partial\ln V_g}{\partial T}\right)_P=\left(\frac{\partial\ln V_l/V_g}{\partial T}\right)_P. \tag{11}$$

An analogous definition of β_f,

$$\beta_f=-\left(\frac{\partial\ln V_l/V_g}{\partial P}\right)_T, \tag{12}$$

involves the slopes of the isothermal volume-pressure curves below and above the glass transition pressure, P_g. A free volume fraction defined in a manner consistent with these definitions would be

$$f=f_g+\ln(V_l/V_g). \tag{13}$$

The logarithm of a variable may be expanded in two forms:

$$\ln x=\sum_{n=1}^{\infty}(-1)^{n+1}\frac{(x-1)^n}{n} \qquad 0<x\leq 2$$

and

$$\ln x=\sum_{n=1}^{\infty}\frac{(x-1)^n}{nx^n}. \qquad x>\frac{1}{2}$$

Representing the logarithm by the first term of the first expansion in eq (13) yields

$$f=f_g+\frac{V_l-V_g}{V_g} \tag{14}$$

and by the first term of the second expansion,

$$f=f_g+\frac{V_l-V_g}{V_l}. \tag{15}$$

The latter is the usual definition of the free volume fraction.

It turns out that $(V_l-V_g)/V_g$ is a better approximation to ln (V_l/V_g) for $V_l/V_g<1$ and $(V_l-V_g)/V_l$ for $V_l/V_g>1$. Since V_l/V_g is greater than one at temperatures above T_g, $(V_l-V_g)/V_l$ is the better approximation to ln (V_l/V_g). This justifies the choice of eq (15) rather than eq (14) as the appropriate approximation to the free volume fraction consistent with the definitions of α_f and β_f given by eqs (11) and (12).

6. Evaluation of the Reduced Variable Parameters

6.1. Limiting Compliances

The limiting compliances were evaluated as bilinear polynomials in T and P from a least square fit to the data at temperatures above and below the dispersion region, treating each region separately. Only the 1,000 c/s data were used because they contain the least experimental scatter. Using this procedure the limiting compliances in reciprocal bars are given empirically as:

$$B_0(T,P)\times10^5=2.919+1.905\times10^{-2}T -0.950\times10^{-3}P-1.011\times10^{-5}TP, \tag{16}$$

$$B_\infty(T,P)\times10^5=1.865+0.836\times10^{-2}T -0.433\times10^{-3}P-0.685\times10^{-5}TP, \tag{17}$$

with the difference,

$$\Delta B(T,P)\times10^5=1.054+1.069\times10^{-2}T -0.517\times10^{-3}P-0.326\times10^{-5}TP \tag{18}$$

in which T is in units of °C and P in bars.

ΔB cannot be measured directly due to the limted frequency range of the apparatus, hence it always involves an extrapolation of either B_0 or B_∞, and sometimes both. The assumption here is that eqs (16) to (18) are valid at all temperatures and pressures within the experimental range, although B_0 was determined from data at temperatures above the dispersion region and B_∞, at temperatures below.

6.2. Temperature-Frequency Relations

The range of frequencies covered in these measurements is too small to permit an accurate evaluation of the constants, f_g and α_f, particularly since the calculated shifts are rather insensitive to the exact values of these constants used in the WLF Equation. Our value of $\Delta\alpha$ at 1 atm is 4.5×10^{-4}, in good agreement with the value of 4.6×10^{-4} reported by Clash and Rynkiewicz [12]. Ferry [13] finds $\alpha_f=5.9\times10^{-4}$ and $f_g=0.028$ for poly(vinyl acetate), based on the temperature-frequency shifts required to reduce dynamic measurements. The difference between the values of α_f and $\Delta\alpha$ may be partly due to the fact that both are averages of a sort. α_f is an average value which gives good shifting factors for temperatures above T_g, whereas $\Delta\alpha$ is an average obtained by approximating two curves, one above and one below T_g, by straight lines.

For convenient reduction of our data we need a single set of constants for use over our whole temperature and pressure ranges. Ferry's $\alpha_f(5.9\times10^{-4})$ times the ratio of our $\Delta\alpha$ values at 490 bars (our median pressure) and 1 atm (for which pressure Ferry's α_f was found) gives 4.8×10^{-4} for the value of α_f at 490 bars. Since this corresponds to the "universal" value of α_f, it and the corresponding value for $f_g=0.025$ were used in reducing our data.

6.3. Evaluation of $(\partial T/\partial P)_f$

$(\partial T/\partial P)_f$ may be determined from the shift of characteristic temperatures (for constant $\mathscr{B}^*$) at constant frequency. If the actual frequency range were sufficient, this could be evaluated directly by observing the ratio $\Delta T/\Delta P$ necessary to maintain B''_{max} at constant frequency on the loss compliance-frequency plot. The equivalent shift when B'' is plotted against temperature is the shift of the characteristic temperature, T_1, with pressure at which the following relation (2) is satisfied:

$$\frac{1}{B''}\frac{\partial B''}{\partial T}=\frac{1}{\Delta B}\frac{\partial \Delta B}{\partial T}. \tag{19}$$

This is nearly the shift of the temperature of maximum B'' versus temperature with pressure. The value of $(\partial T/\partial P)_f$ obtained from the shift of the maximum usually agrees within 3 or 4 percent with that from eq (19).

Using the criteria of eq (19) on the curves of figure 3, the characteristic temperature, T_1, is nearly linear with pressure; however, the slope appears to increase slightly with pressure. A least squares fit of T_1 on P using all of the curves of figure 3 yields $(\partial T/\partial P)_f=0.024$ °C/bar, which is the same as that found for rubber-sulfur using the same criteria. Neglecting the 981 bar curve yields 0.021, which is nearly in agreement with 0.020 which produced the best fit on the reduced variable plots and is consequently used throughout the treatment of these data. It may be that 981 bars is too large for the linear dependence of free volume fraction on pressure assumed in eq (3). In recent work by

O'Reilly [14], $(\partial T/\partial P)_f$ was found to be 0.021 from PVT measurements and 0.022 from dielectric measurements (i.e., 0.06 to 10 kc/s).

α_f and β_f are in reasonable agreement with $\Delta\alpha$ and $\Delta\beta$ for many polymers. Differentiation of eq (3) at constant free volume fraction yields

$$(\partial T/\partial P)_f = \beta_f/\alpha_f, \tag{20}$$

which should correspond to $\Delta\beta/\Delta\alpha$. The data of figure 1 are not sufficiently reliable to establish $\Delta\beta$ as a function of pressure; however, ΔB should be equivalent except that it is assumed to be adiabatic. Table 2 is included to illustrate that although ΔB and $\Delta\alpha$ vary with pressure, the ratio, $\Delta B/\Delta\alpha$, is nearly constant when ΔB and $\Delta\alpha$ are evaluated at temperatures that shift with pressure at a rate of $(\partial T/\partial P)_f$. This ratio does, however, appear to increase slightly with pressure, which is in agreement with the slight increase in $\partial T_1/\partial P$ with pressure. The obvious distinction between the values of $\Delta B/\Delta\alpha$ in table 2 and $(\partial T/\partial P)_f = 0.020$ will be discussed in section 8.

TABLE 2. ΔB *at* T_1, $\Delta\alpha$ *at* T_g, *and* $\Delta B/\Delta\alpha$ *at various static pressures*

P	T_1	T_g	$\Delta B(T_1)\times 10^5$	$\Delta\alpha(T_g)\times 10^4$	$\Delta B(T_1)/\Delta\alpha(T_g)$
Bars	°C	°C	*Bars*$^{-1}$	°C^{-1}	°C/*bar*
0	50	17	1.59	4.48	0.035
98	51	21	1.53	4.31	.035
245	56	25	1.48	4.04	.037
490	60	26	1.34	3.62	.037
736	65	------	1.21	------	------
981	74	------	1.10	------	------

7. Reduced Variable Presentation

The following presentation includes the reduced data plotted as a function of reduced frequency, reduced temperature, and reduced pressure. The constants used were the WLF Universal Constants given in section 5 and $\beta_f/\alpha_f = 0.020$ bars^{-1}. All three representations are equivalent because $\mathscr{B}^*$ is held constant for each shift. They are all included, however, to illustrate the effect of varying each independent variable (T, P, or ω) while the others are held at the reference conditions.

The simplest reduced variables presentation is a reduced frequency plot referenced to $T=50$ °C and $P=0$ shown on figure 6. This is the only presentation in which the limiting compliances are constants. In figure 6 a distinct set of values of B' may be observed on the right which are about 5 percent above B_∞. These values are taken at different frequencies but all at 981 bars, which suggests that at 981 bars the linear dependence of B_∞ on pressure is no longer valid. This distinction may also be observed in the other reduced variable plots presented later. About eight decades are required to cover the dispersion region with a maximum $\mathscr{B}''=0.19$. The corresponding values for a single retardation time would be about 2 decades and $\mathscr{B}''_{\max}$ would be 0.5.

The reduced temperature plot referenced to $\nu=1{,}000$ c/s and $P=0$ is shown in figure 7. This is the most realistic presentation for our data because it involves the least shifting.

The reduced pressure plot referenced to $T=50$ °C

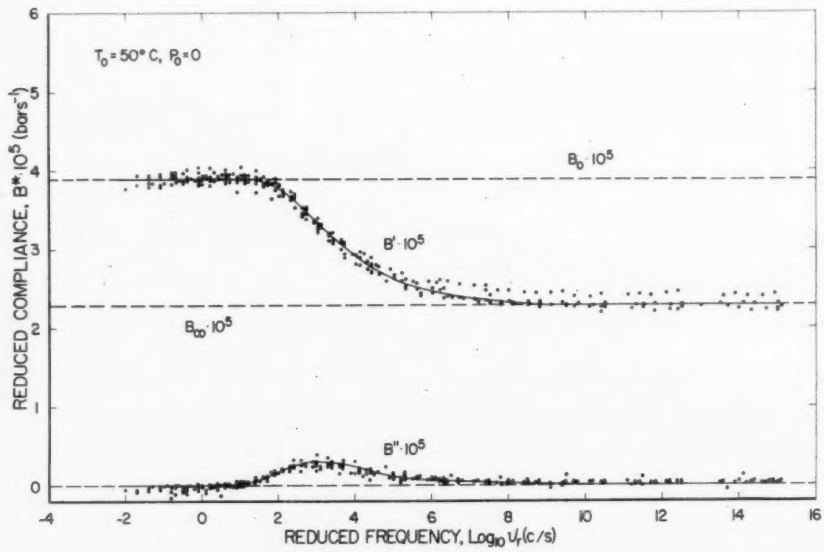

FIGURE 6. *Reduced compliance plotted against reduced frequency referenced to atmospheric pressure and 50 °C.*

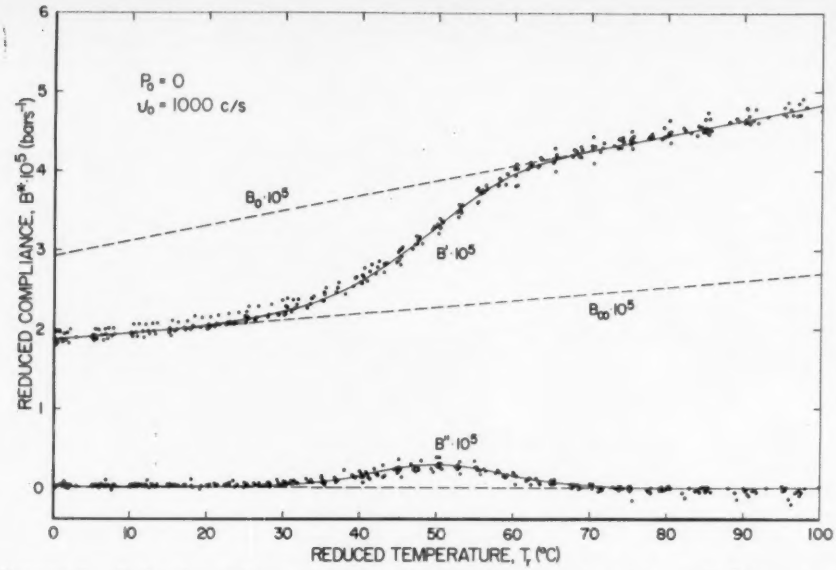

FIGURE 7. *Reduced compliance plotted against reduced temperature referenced to atmospheric pressure and 1,000 c/s.*

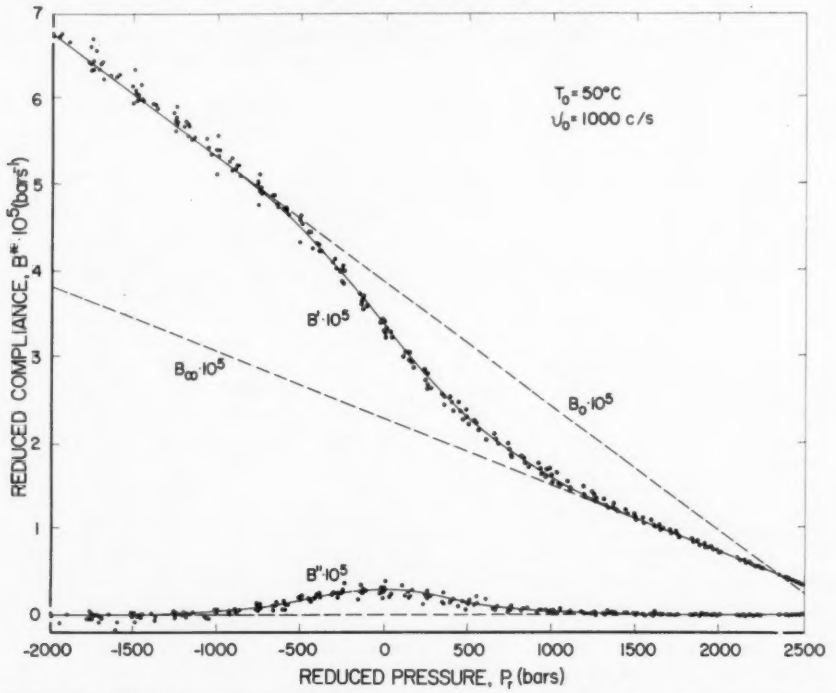

FIGURE 8. *Reduced compliance plotted against reduced pressure referenced to 50 °C and 1,000 c/s.*

and ν=1,000 c/s is shown on figure 8. This is not a realistic presentation in terms of actual pressure because of the excessive linear extrapolation of the limiting compliances, but does offer interesting suggestions as to the effect of static pressure of the dispersion. Several artifacts appear in this presentation, one being the existence of a negative pressure, which could be avoided by choosing T_0 sufficiently high. Also, the limiting compliances intersect at about 2,300 bars. This again may be due to excessive extrapolation, but does indicate the possible convergence of the limiting compliances at

a finite pressure. This would be equivalent to a complete collapse of free volume (at least f to f_g) at finite pressure above which frequency dispersion would not be observed.

8. Further Discussion

An implication of this free volume concept is that the difference between low and high frequency limiting compliances should be consistent with the horizontal shift of corresponding points, with static pressure, along a temperature plot at constant frequency. That is, the difference between limiting compliances, ΔB, should be equal to β_f evaluated from the horizontal shift

$$(\partial T/\partial P)_f=\beta_f/\alpha_f \tag{20}$$

except that ΔB is assumed to be adiabatic and β_f, isothermal. Although the observed compliances involve the ratio of alternating volume to alternating pressure, $(\partial T/\partial P)_f$ is a quasi-static phenomenon because it is evaluated from essentially an equilibrium temperature-pressure relationship. Since we have found only an average value for β_f, we should compare this with our ΔB evaluated at our median pressure, 490 bars, for which T_1 at 1,000 c/s is 60 °C. Substituting these conditions in eq (18) gives $\Delta B(60,490)=1.35\times10^{-5}$ bars^{-1}. The conversion of this to the corresponding isothermal value may be approximated by the addition of the term $\theta V_s\alpha^2/C_p$ [15] where θ is the absolute temperature and C_p is the specific heat at constant pressure, to each of B_0 and B_∞ before the difference is taken to obtain ΔB. Specific heat data for PVAc apparently do not exist in the literature for pressures other than 1 atm; however, reference 16 gives C_p over a temperature range from 20 to 50 °C at 1 atm for several different rates of heating. Extrapolating limiting heat capacities at slow and fast rates yields 0.43 and 0.32 cal/g °C, respectively. Although these values were not taken at 490 bars, they are considered to be sufficiently reliable to obtain the desired conversion, especially since α^2 is the dominant quantity. Since α_l and α_g change little with temperature, the values $\alpha_l=5.65\times10^{-4}$ and $\alpha_g=2.03\times10^{-4}$ °C^{-1} taken from table 1 are satisfactory. The observed value of $V_s=0.84$ cm^3/g at 60 °C and 490 bars taken from figure 1 was used in both cases because the time average of the specific volume during sinusoidal deformation is appropriate in this connection. Using these values gives for the conversions, $\delta B_0=4.95\times10^{-6}$ and $\delta B_\infty=7.6\times10^{-7}$. The difference between these added to $\Delta B=1.35\times10^{-5}$ gives 1.77×10^{-5} for the corresponding isothermal value. The value of β_f calculated from eq (20) using $(\partial T/\partial P)_f=0.020$ °C/bar and $\alpha_f=4.8\times10^{-4}$ °C^{-1} (490 bars) is 0.96×10^{-5}, which is even smaller than the adiabatic value, ΔB.

On the other hand, there was close agreement between β_f and the isothermal value corresponding to ΔB for vulcanized natural rubber-12 percent sulfur data [2] using nearly the same criteria for comparison. In this case β_f and the isothermal value corresponding to ΔB were 1.15×10^{-5} and 1.21×10^{-5} bars^{-1}, respectively.

Another distinction, which is probably related to that above, between PVAc and the rubber-sulfur is the proportion of the compliance of the free volume type to the total given by the ratio $\Delta B/B_0$. For PVAc this was found to be 0.41 compared to 0.25 for the rubber-sulfur, both evaluated at T_g+25 °C and $P=0$.

Although the presence of small amounts of impurities mentioned in section 4.1 influenced the value of the apparent glass transition temperature and possibly the magnitude of the bulk compliances to a slight extent, it is unlikely that the applicability of the free volume concept is strictly limited to very pure polymeric systems. It is conceivable, however, that the excessive value of ΔB in PVAc results from additional relaxation processes not present in the rubber-sulfur. For example, with some amorphous polymers, in addition to the alpha process involving changes in configuration of the polymer backbone and therefore associated with the glass transition, contributions to mechanical and dielectric response may result from a beta process involving rotation of side groups along the chain. For polymers that exhibit a beta process the corresponding dispersion region will occur at a lower temperature than that for the alpha process. At low frequencies the two regions of a temperature plot are usually very distinct; however, the different activation energies for the two processes are such that these regions merge at high frequencies and resolution becomes obscured. Since $(\partial T/\partial P)_f$ is a quasi-static phenomenon, one might expect that it would not depend upon the beta process, which would appear unfrozen over our entire experimental range at the long transient times involved, whereas, both dispersion regions might contribute to ΔB because of the possibility of these regions merging at the much shorter time scales (corresponding to $1/\omega$) of the alternating pressure.

With PVAc the beta process involves the rotation of the acetate group about the oxygen bond. Dielectric data of Veselovskii and Slusker [17] on PVAc show very distinct loss peaks near 1,000 c/s on a temperature plot for the alpha and beta process at 60 and −80 °C, respectively. These peaks do not appear to merge until well into the megacycle region. These data are fairly consistent with the recent dielectric data of Hikichi and Furichi [18] which give the corresponding temperature for the beta process at −58 °C and a constant apparent activation energy of 10 kcal/mole. Based on this evidence it would be inconsistent to attribute the excessive value of ΔB to a contribution resulting from an overlapping beta dispersion region obscured by the alpha process. Aside from the observation that the dispersion regions from the two processes do not merge until within the megacycle region, the beta process is unfrozen over the entire pressure, temperature, and frequency range of our experiment; therefore, its effect should not be observed here except, possibly, in a more complicated fashion than anticipated.

The data of Wada, Hirose, Asano, and Fukutomi [19] suggest a more probable interpretation of this anomaly. Two breaks were observed in their

volume-temperature curves for PVAc; one, the alpha or glass transition occurring at 28 °C and a secondary transition at 3 °C. Our volume-temperature data did not reveal the lower break, but it is possible that we did not go to low enough temperatures to include a low temperature change in slope. Wada and coworkers suggest that the low temperature transition is due to a sufficient loosening of free volume to permit rotation of chain ends. Many doubt the validity of such apparent breaks in volume-temperature curves at temperatures below T_g because of uncertainties resulting from the extremely long times required for the physical properties to reach equilibrium; however, even if this break is not real or completely separate from the one at T_g, the interpretation of Wada and coworkers may be justified because of the large temperature range of the glass transition region observed for PVAc.

Wada and coworkers have substantiated the existence of the low temperature transition by observing discontinuities in the complex shear modulus at 33 kc/s for both the 3 and 28 °C transition. Discontinuities in the temperature coefficients of the velocity of sound, dynamic storage moduli, and dynamic storage compliances are often observed with polymers at T_g. These discontinuities, as pointed out by Work [20], are manifestations of the sudden change of thermal expansivity with temperature at T_g. This behavior was, of course, not observed at T_g in our data because such a break would be obscured by the dispersion region. Higher frequencies are necessary to shift the dispersion region on a temperature plot far enough from T_g to observe such discontinuities in the slope of the storage compliance-temperature curve. For a more realistic reduced variable formulation B_∞ at temperatures above T_g should be evaluated from data at temperatures above T_g and below the dispersion region. Unfortunately this evaluation is not possible with our data for the reason mentioned above. Ultrasonic data on polymers and associated liquids [21] indicate that the slope of the compressibility-temperature curve increases slightly at T_g with increasing temperatures. The corresponding ΔB would then be more in agreement with β_f evaluated from $(\partial T/\partial P)_f$; however, since this correction was not necessary to obtain agreement for rubber-sulfur, it would undoubtedly not be large enough to eliminate the lack of agreement for PVAc.

On the basis of volume-temperature data for PVAc, which show the temperature range of the transition region so large that more than one rate process may be involved, it is conceivable that the dispersion region of the dynamic data is also complicated with additional mechanisms which could result in the large difference between limiting compliances as observed here.

The presence of additional dispersion mechanisms might appear to impose a serious limitation on the reduced variable treatment applied here because of the possibility of different activation energies associated with two or more processes. The assumption in our treatment is that $\mathscr{B}^*$ is associated with only one type of rate process, namely the alpha process, although many discrete retardation times may be involved. However, since many of the reduced variable parameters are evaluated empirically from the data and contributions from the additional processes are probably small, the treatment applied here is probably legitimate within the experimental error as apparent from a reasonable fit of data in the reduced plots.

After completion of the rubber-sulfur work, it was felt that the free volume concept and corresponding reduced variable treatment applied here was adequate to explain the dynamic compressibility behavior of polymers and possibly some associated liquids. Now that the poly(vinyl acetate) work is complete it is apparent that the reduced variable treatment needs certain refinements to make the parameters appearing in the formulation consistent with corresponding physical constants as postulated by theory. It is planned to continue this work on other systems in order to postulate a better model or make the necessary refinements on our present concepts.

The authors are indebted to R. S. Marvin and H. Leaderman for suggestions in preparation of the manuscript, to Fred Quinn and Gordon Martin for suggestions and technical assistance in static PVT measurements, and to Miss Mary C. Dannemiller for coding the equations for computer calculation.

9. References

[1] J. D. Ferry, Viscoelastic Properties of Polymers (John Wiley & Sons, Inc., New York, 1961) ch. 11.
[2] J. E. McKinney, H. V. Belcher, and R. S. Marvin, Trans. Soc. Rheology **4,** 347 (1960).
[3] H. Singh and A. W. Nolle, J. Appl. Phys. **30,** 337 (1959).
[4] S. Matsuoka, J. Polymer Sci. **57,** 569 (1962).
[5] S. Matsuoka and B. Maxwell, J. Polymer Sci. **32,** 131 (1958).
[6] J. E. McKinney, S. Edelman, and R. S. Marvin, J. Appl. Phys. **27,** 425 (1956).
[7] J. E. McKinney and C. S. Bowyer, J. Acoust. Soc. Am. **31,** 56 (1960).
[8] H. Leaderman, Trans. Soc. Rheology **1,** 213 (1957).
[9] R. S. Marvin, by private communication.
[10] See for example: V. C. Rideout, Active Networks (Prentice-Hall, Inc., New York) 1954, p. 437.
[11] A. J. Kovacs, Trans. Soc. Rheology **5,** 285 (1961).
[12] R. J. Clash, Jr., and L. M. Rynkiewicz, Ind. Eng. Chem. **36,** 279 (1944).
[13] Reference 1, Table 11–II, p. 219.
[14] J. M. O'Reilly, J. Polymer Sci. **57,** 429 (1962).
[15] See for example: M. W. Zemansky, Heat and Thermodynamics (McGraw-Hill Book Co., Inc., New York) 1957, p. 260.
[16] M. V. Volkenshtein, Structure of Glass, Vol. 2 (Consultants Bureau Translation, New York, 1961) p. 113.
[17] P. F. Veselovskii and A. I. Slusker, Zhur. Tekh. Fiz. **25,** 939 (1955); **25,** 1204 (1955).
[18] K. Hikichi and J. Furichi, Reports on Progress in Polymer Physics in Japan **4,** 69 (1961).
[19] Y. Wada, H. Hirose, T. Asano, and S. Fukutomi, J. Phys. Soc. Japan **14,** 1064 (1959).
[20] R. N. Work, J. Appl. Phys. **27,** 69 (1956).
[21] See for example: T. A. Litovitz and T. Lyon, J. Acoust. Soc. Am. **30,** 856 (1958).

(Paper 67A1–194)

JOURNAL OF RESEARCH of the National Bureau of Standards—A. Physics and Chemistry
Vol. 67A, No. 1, January–February 1963

An Investigation of the Constitution of the Mercury-Tin System[1]

Duane F. Taylor and Claire L. Burns

(October 9, 1962)

An investigation of the constitution of the mercury-tin system was made by a combination of three techniques: differential thermal analysis; diffusion and chemical analysis; and X-ray diffraction. The mercury-silver-tin system is of interest because it is the basis of dental amalgam, the most important single dental restorative material. Information as to the constitution of these alloys is incomplete for both the ternary system and the mercury-tin binary system. This study was devoted to the investigation of the mercury-tin system as a prerequisite to a study of the ternary alloys. The results obtained by the various methods are not in complete agreement. They indicate that the system is more complex than previously reported. Additional evidence for the beta phase as reported by Prytherich was found but the composition limits and eutectoid temperature remain to be confirmed. The gamma phase composition limits were found to differ from earlier values. Corroborative data for Gayler's delta phase and possible evidence for a previously unreported epsilon phase have been found by X-ray diffraction. The thermal analysis results indicate the possible existence of additional phases unconfirmed by other methods. A modified mercury-tin phase diagram based upon these findings is proposed.

1. Introduction

Dental amalgam has been developed to a stage where it is in many ways the best restorative material available to the dentist, and is used in more than three-fourths of all dental fillings. Nevertheless, it has certain undesirable properties which limit its usefulness, such as its tendency to flow under low compressive loads, and its susceptibility to brittle fracture at moderately high loading rates. The development of these alloys to date has been largely by empirical methods. Hope for further improvement appears to depend upon a better knowledge of the underlying metallurgy.

The mercury-silver-tin system, on which dental amalgams are based, has been studied by several workers since Joyner (1) [2] published the results of the first investigation of the system in 1911. However, progress in developing an understanding of the ternary alloys has been impeded by the lack of a well established diagram for the mercury-tin binary system. Portions of the diagram are incomplete and much of the remainder is in dispute. This study was undertaken with the purpose of improving the knowledge of the mercury-tin alloys as an essential first step toward the understanding of dental amalgams.

2. Previous Work

The number of published investigations of the mercury-tin system is small and many of them are confined to studies of portions of the system. The experimental difficulties occasioned by the low melting point of mercury, and the lack of interest caused by the limited commercial application of these materials, have combined to restrict the amount of effort devoted to the study of these alloys.

Figure 1 shows the currently accepted diagram for the mercury-tin system as given in the Metals Handbook [2]. It differs only in minor detail from that given by Hansen [3]. The liquidus is well established, having been investigated by several authors [4, 5, 6, 7]. Of these the work of van Heteren [6] was the most extensive and probably the most precise, but there is good agreement between his results and those of the others.

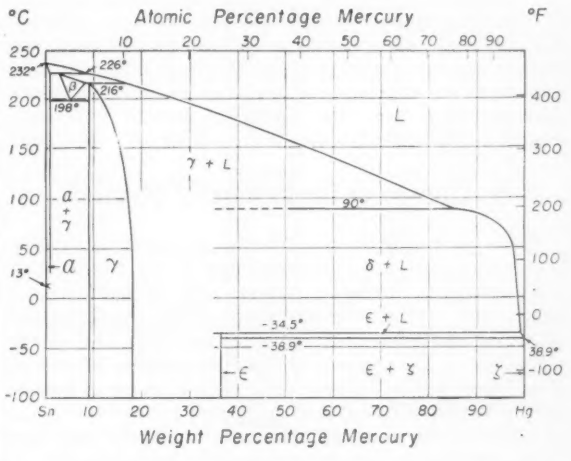

FIGURE 1. *The mercury-tin constitution diagram* [2].

[1] This article is based in part on a dissertation submitted to Georgetown University by Duane F. Taylor in partial fulfillment of the requirements for the degree of Doctor of Philosophy.

[2] Figures in brackets indicate the literature references at the end of this paper.

The solubility limit of mercury was determined from the electrode potential measurements of van Heteren [6] and the X-ray diffraction studies of Stenbeck [8]. The gamma phase was first identified by von Simson [9], who established the composition limits essentially as shown in figure 1. Stenbeck [8] confirmed her findings and reported evidence of an additional structure, presumably of higher mercury content.

The beta phase was discovered by Prytherch [10], whose work unfortunately has never been reported except to the extent that it was quoted by Gayler [11]. It appears that Prytherch's [10] diagram was based primarily upon thermal analysis data, showing an arrest at the beta peritectic temperature. The existence of the beta phase was confirmed by the high temperature X-ray diffraction studies of Raynor and Lee [12], although this finding is in apparent conflict with that of Schubert et al. [13], who concluded that the beta and gamma phases were identical.

The existence of a delta phase has been a matter of some dispute. Gayler [11] obtained a series of arrests in the course of thermal analysis of high mercury alloys, which she attributed to a proposed delta phase. Her observations on ternary alloys also appear to require the existence of such a phase. Troiano [14] also supported the existence of a delta phase, but his X-ray findings have been contested by Wainwright [15]. More recent work by Ryge, Moffett, and Barkow [16], Fairhurst and Ryge [17] and Dreiner [18] has produced no evidence for the existence of the delta phase. The uncertainty about the delta phase is indicated by the blank region in figure 1 where this phase would be expected to appear and by the inclusion of portions of the delta peritectic line.

The evidence for the epsilon phase as shown in the figure is almost equally weak. The indicated peritectic temperature is based upon van Heteren's [6] work, and appears well established, but the composition is dependent upon Prytherch's [10] unpublished findings.

The lack of agreement between the results obtained by different methods, and between those of different authors employing the same or similar methods, has caused any conclusions about the high mercury solid phases to be very speculative. This uncertainty is carried over to the silver-tin-mercury ternary diagram where the tin-rich corner is largely unknown.

3. Choice of Experimental Methods

From a number of possible methods of study, three were selected that appeared to be particularly well suited to the alloy system and to complement each other. These methods were differential thermal analysis, diffusion and chemical analysis, and X-ray diffraction. These methods had the added advantage that they would be similarly useful in an extension of the work to ternary alloys.

Differential thermal analysis, a traditional and basic approach, has several specific advantages. In the mercury-tin system, thermal analysis was the method used in the original detection of both the beta and delta phases. Its employment in this study offered a direct check on those findings. At the same time, it provided a tie-in to the well established liquidus data. The main drawback to this method is the susceptibility to suppression of certain phases in peritectic systems at heating and cooling rates normally employed. This tendency can be partially offset by the use of high-sensitivity differential techniques and low heating and cooling rates.

Diffusion and chemical analysis was chosen as a second method primarily because the diffusion can be performed isothermally and the prolonged retention of nonequilibrium phases formed at higher temperatures can be avoided. It also parallels the normal procedures in the use of dental amalgams and thus might shed some additional light upon the mechanisms of the amalgam setting reaction. The method is more effective in the determination of composition limits than in the determination of the range of temperature stability.

X-ray diffraction was selected as an adjunctive method to the thermal analysis and diffusion techniques. The ability of X-ray diffraction to identify individual crystal structures and thus demonstrate the presence of an individual phase in a mixture is of particular importance when used with diffusion specimens. As a separate method of identification it permits the confirmation or refutation of the phase sequence proposed by chemical analysis.

4. Materials Used

The compositions of the mercury and tin used in this study are given in tables 1 to 3. The mercury used was obtained from the Inorganic Chemistry Section of the National Bureau of Standards, where it was refined. The values of table 1 are maximum values from repeated analyses of various lots, rather than that for the particular lot used.

TABLE 1. *Composition of the mercury* used for the preparation of specimens*

Element	Maximum content
	ppm
Combined noble metals (Ag, Au, Ir, Os, Pt, Pd)	1.0
Combined base metals	0.1
Mercury	Balance

*Refined mercury, Inorganic Chemistry Section, National Bureau of Standards.

Two lots of tin were used. One lot consisted of Baker and Adamson Reagent Grade Tin Sticks produced by the General Chemical Division of Allied Chemical and Dye Corporation. This metal was used for a limited number of the early tin diffusion specimens. The manufacturer's reported analysis is given in table 2. The other lot of tin, which was used for all remaining diffusion specimens as well as

all thermal analysis and X-ray diffraction specimens, was Tadanac Brand Tin Shot obtained from the Consolidated Mining and Smelting Company of Canada Limited. The spectroanalysis of this tin, table 3, was performed by the Spectrochemistry Section of the National Bureau of Standards.

TABLE 2. *Composition of the tin* used for the preparation of initial diffusion specimens as reported by the manufacturer*

Element	Maximum content
	ppm
As	3
Cu	20
Fe	100
Pb	100
Zn	100
Sn	Balance

*Baker and Adamson Reagent Grade Tin sticks, lot G303.

TABLE 3. *Composition of the tin* used for the preparation of specimens as determined by spectroanalysis*

Element	Maximum content
	ppm
Ag	1
As	**40
Bi	1.5
Cd	1
Co	1.5
Cu	15
Fe	2
Mg	0.5
Ni	3
Pb	15
Sb	10

*Tadanac Brand High Purity Tin Shot, lot HPM 522.
**Approximate value only; an error of 20 to 50% of the indicated value is likely.

5. Differential Thermal Analysis

5.1. Equipment

The results of previous studies of the mercury-tin system that employed thermal analysis as a technique [5, 6, 10, 11] led to the expectation that the thermal effects of interest were apt to be small. In addition, the desirability of using low heating and cooling rates to permit closer approaches to equilibrium was expected to increase the problem of observing small heat effects. In order to obtain sufficient sensitivity, a differential method was employed using mercury as a reference substance. This method produces significant increase in sensitivity and is well suited to the detection of transformation in solid alloys [19].

The furnace used for this work was a vertical tube furnace, 11 inches in diameter and 21 inches in length with a lumen 1⅛ inches in diameter. The power supply to the furnace was provided by three transformers arranged in series. The first was a constant voltage transformer which served to suppress fluctuations in line voltage. The second and third transformers were variable transformers used to provide sensitive control of furnace temperature.

The specimens were assembled for insertion in the furnace as shown in figure 2. The temperature-indicating and differential thermocouples were inserted in the specimens, and both the experimental and reference specimens were placed in a Pyrex sheath. A Teflon spacer separating the two specimens was drilled and grooved to permit passage of the thermocouples. A similar spacer above the reference specimen served to hold the end of the porcelain thermocouple tube. This tube also passed through the flanged Teflon plug which closed the upper end of the sheath.

The assembly in turn fitted inside a heavy-wall copper tube which served to minimize the temperature gradient along the furnace. The flange on the Teflon plug substantially filled the inside diameter of the copper tube. When the copper tube and its contents were placed in the furnace, a plug rolled from sheet asbestos was placed around the thermocouple tube and slid down until it filled the furnace lumen just above the top edge of the copper. A flanged magnesite plug was then added to close the upper end of the furnace and to serve simultaneously as a support for the thermocouple tube. Under normal circumstances the copper tube was not removed from the furnace when the specimen was changed but was allowed to remain in the furnace as a liner.

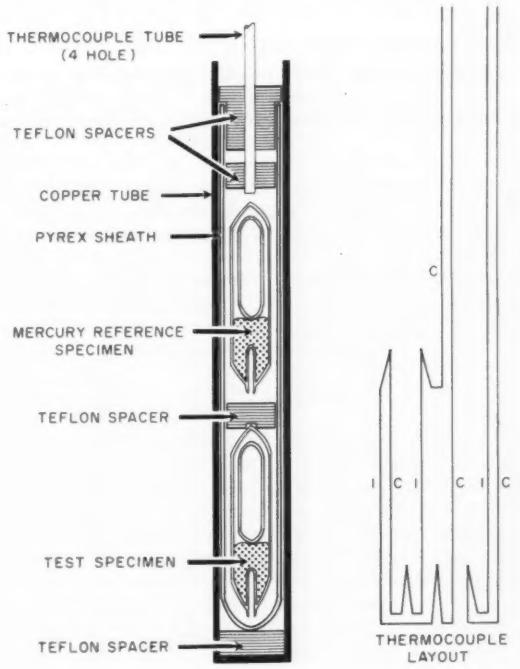

FIGURE 2. *Thermal analysis specimen arrangement.*

Figure 2 also shows a schematic drawing of the thermocouple arrangement. A 28-gage iron-constantan couple was used to measure the temperature of the specimen. The hot junction of this couple was located in the thermocouple well of the test specimen.

The temperature differential was measured by means of a two-junction iron-constantan thermopile arranged as shown in figure 2.

5.2. Specimen Preparation

The thermal analysis specimens were prepared in Pyrex tubes with reentrant thermocouple wells, similar in design to those employed by Murphy [20]. In order to maintain approximately constant areas for heat transfer, the specimens were prepared to constant volume rather than constant weight. The volume used was 3 ml, which produced a specimen about 30 mm long with the end of the thermocouple well approximately centered in the specimen. Weighed amounts of tin and mercury were placed in the tube and a sealed stuffer tube was added to fill most of the space below the intended seal. The tube was then repeatedly evacuated and flushed with dry hydrogen and was finally sealed with a residual hydrogen pressure of 2 to 5 mm of mercury. The alloys were then homogenized by heating to 250 °C and holding at that temperature for at least 1 hour, with repeated vigorous shaking. The tubes were then quenched in water at 20 to 25 °C and placed in an air bath at the selected annealing temperature.

The nominal composition of the mercury-tin alloys prepared for thermal analysis is given in table 4. The compositions are given in both weight and atomic percent; however, for convenience of discussion the specimens will normally be referred to only in terms of their composition in weight percent. A limited number of analyses indicated that the actual composition of specimens prepared by this technique did not differ significantly from the nominal values.

TABLE 4. *Nominal composition and liquidus temperatures of thermal analysis specimens*

Mercury content		Specimen	Liquidus temperature [a]
Weight %	*Atom %*		° *C*
0.00	0.00	67	231.9
2.00	1.19	28	230.1
5.02	3.03	27	222.9
7.00	4.26	26	219.3
10.00	6.17	65	218.4
12.01	7.47	76	216.0
14.00	8.78	77	214.4
16.01	10.14	78	212.8
17.97	11.47	24	208.3
18.00	11.50	79	208.4
20.00	12.89	23	204.0
21.97	14.28	22	203.2
23.96	15.71	21	199.5
27.00	17.96	72	197.5
29.90	20.15	20	191.6
39.99	28.28	73	176.1
50.00	37.17	19	157.5
60.00	47.02	74	139.0
70.00	57.99	18	118.9
80.00	70.30	75	99.0
100.00	100.00	66	----------

[a] The estimated uncertainty of these values ranges from 0.1 to 0.8 °C, with an average of about 0.5 °C.

5.3. Experimental Procedure

The individual specimen was removed from the annealing oven and assembled with a reference specimen of pure mercury, as shown in figure 2. No attempt was made to maintain the specimen at the annealing temperature during this process, although the operation was completed as rapidly as possible. In the case of specimens annealed at the higher temperatures (such as 85 °C) the necessity of manipulating the specimens resulted in their being cooled at least to a temperature where they could be readily handled. After the thermocouples had been inserted and both specimens positioned in the outer glass tube, the assembly was inserted into the furnace. The furnace temperature had been adjusted previously to an initial temperature at or below the annealing temperature so that the first test run in each instance was a heating run.

Most of the individual heating and cooling runs were made at a constant applied voltage. This resulted in a high initial heating or cooling rate as the temperature distribution within the furnace adjusted to the changed power input. After a transient period the rate was found to stabilize and almost any rate desired in the 200 °C range of interest could be obtained by the proper selection of the applied voltage. In a limited number of instances, where very slow rates seemed desirable, a clock drive was employed to vary the voltage.

Readings of the specimen temperature and of the differential temperature were made at regular intervals, normally every 2 min, except that at the higher heating and cooling rates 1-min readings were taken. In addition, an attempt was made to obtain extra readings at the maximum and minimum differential readings. With the heating rates most commonly employed, this procedure led to readings in intervals varying from 0.2 to 0.5 °C.

After the initial heating run and all subsequent heating and cooling runs, the specimen was held at a constant temperature for a period of time to permit the temperature distribution in the furnace to stabilize and to promote at least partial equilibrium of the specimen. In some cases in which substantial variation occurred between the results of annealed and nonannealed runs with the same specimen, it was returned to the oven for extended reannealing prior to additional tests.

5.4. Results

A total of 153 heating and cooling curves were run on the 18 experimental alloys and the pure mercury and pure tin calibration samples. A minimum of six test runs was made on each composition. Heating and cooling runs were customarily alternated with varying annealing times preceding each

heating curve. The results are divided into three groups for convenience of discussion: Liquidus determinations, low mercury alloys, and high mercury alloys.

a. Liquidus Determination

The liquidus temperature was determined for each composition studied by both heating and cooling curves. Table 4 presents the observed liquidus temperatures for the alloys studied. Since the liquidus was already reasonably well established, a change in technique to reduce the uncertainty did not appear justified. The observed values are in good general agreement with earlier values, though averaging slightly lower than those of van Heteren [6].

b. Low Mercury Alloys 0 to 18 Percent Mercury

The results from alloys containing 0 to 18 percent mercury are conveniently considered as a group. The alloys cover the alpha, beta, and gamma regions of the diagram (see fig. 1) and were chosen to study the relationship of those phases. Table 5 lists the temperature of each arrest found and the estimated uncertainty of the determination. It also indicates the composition range of the specimens for which the arrest was detected and, where possible, identifies the associated phases with the type of reaction causing the arrest.

TABLE 5. *Thermal analysis of mercury-tin alloys*

Observed arrests temperature	Estimated uncertainty	Composition range	Identification and comments
°C	°C	*wt* % Hg	
231.9	0.02	0 to 5	Tin liquidus
223.0	.5	2 to 10	Beta peritectic
213.9	.5	2 to 20	Gamma peritectic
203.5	1.0	18 to 22	Structural artifact
197.0	1.5	2 to 10	Beta eutectoid
196.0	1.5	24 to 27	Unidentified
188.0	2.0	7 to 27	Unidentified
160.0	4.0	27 to 40	Unidentified
118.0	0.5	18 to 70	Phase change
106.1	.5	18 to 70	Phase change
91.4	.5	18 to 80	Gayler's delta peritectic
67.1	2.0	30 to 70	Phase change—peritectic
55.5	2.5	18 to 70	Phase change—heating only

The results on the 0–18 percent mercury group of specimens appear to confirm most of Prytherch's [10] diagram for this composition range. Definite arrests were obtained at 223.0 ±0.5 °C and 213.9 ±0.5 °C. These values correspond closely to his peritectic temperature for the beta and gamma phases. Supercooling was a consistent problem in the cooling curves, particularly for the specimens containing 10 percent or less of mercury. The attainment of equilibrium in annealed samples prior to determining heating curves was also very difficult. Indeed some of the heating curves were more readily rationalized by an assumption of complete nonequilibrium conditions, that is, no interaction between phases. These observations are probably best substantiated by reference to an example.

Figure 3 presents the results of a heating run on specimen 27 (5% Hg, 95% Sn). The specimen had been annealed at 85 °C for 71 days prior to this test.

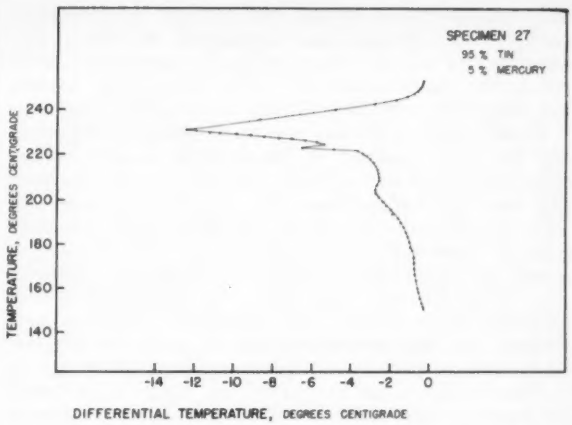

FIGURE 3. *Heating curve for 5% Hg 95% Sn alloy.*

This specimen, as well as the 0, 2, and 7 percent mercury specimens, showed no thermal effects below 150 °C on any heating or cooling run.

The main peak at 232.0 °C obviously coincides with the melting point of pure tin and the portion of the curve between there and 225 °C with the equilibrium between alpha and liquid. Similarly the very sharp peak at 222 to 223 °C represents the peritectic decomposition of the beta phase. The identification of the remainder of the curve becomes increasingly difficult as lower and lower temperatures are considered. It does not appear possible to reconcile these portions of the curve with figure 1.

c. High Mercury Alloys, 18 to 80 Percent Mercury

As a group, these alloys produced a surprising number and variety of thermal effects. Some of these were strong, routinely detected arrests, while others were much weaker and appeared much less consistently. Of these arrests, some are definitely associated with phase changes, but others may be artifacts or due to second order effects such as superlattice formation or even specific heat anomalies in a single phase. The stronger the arrest and the more often it was obtained, the more precisely can its temperature be determined.

5.5. Discussion

The results obtained on thermal analysis of the samples containing from 18 to 80 percent mercury indicate the occurrence of an unusually large number of arrests. To explain all of the observed arrests as phase changes would require an extremely complicated diagram, particularly when it is recognized that all of the required phases must almost certainly contain less than 30 percent mercury.

Of the arrests observed, four seem most likely to be identified with phase transformations, those at 118.0, 106.1, 91.4, and 67.1 °C. Each of these arrests are relatively strong, appear in both heating and cooling curves and in specimens over a consider-

able concentration range. In at least one instance each, these arrests have appeared as sharp discontinuities of the type normally associated with peritectic decompositions. The remaining arrests are deficient in one or more of these qualifications.

Cooling curve arrests are most pronounced when the phase of interest is the first or second formed from the liquid on cooling. Because of the shape of the mercury-tin liquidus this condition is met for this phase only in alloys of very high mercury content where the total amount of solid formed is small and the latent heat is thus reduced. Annealing to equilibrium just above the anticipated temperature of the arrest is the preferred method of procedure, but the annealing time required for the last of a series of peritectic phases can be very long.

The evidence for the arrest at 203.5 °C is based on heating curve evidence of the sort seen in figure 4. It has failed to appear in any of the cooling curves where it would be expected if it represents a peritectic temperature. It appears in many instances that when annealing conditions have been such as to produce a coarse structure, the phases formed during low temperature annealing tend to persist to their melting points, with little evidence of interaction below that point. The arrest at 203.5 °C is believed to be an artifact of this type.

The arrests observed in low mercury alloys appear to confirm the diagram for the high temperature regions as proposed by Prytherch [10], although the temperatures themselves are in better agreement with those of Hansen [3]. The results of the beta eutectoid temperature determinations may serve as confirmation of the reported value, but are probably inadequate as an independent determination. The liquidus values are in general agreement with earlier results.

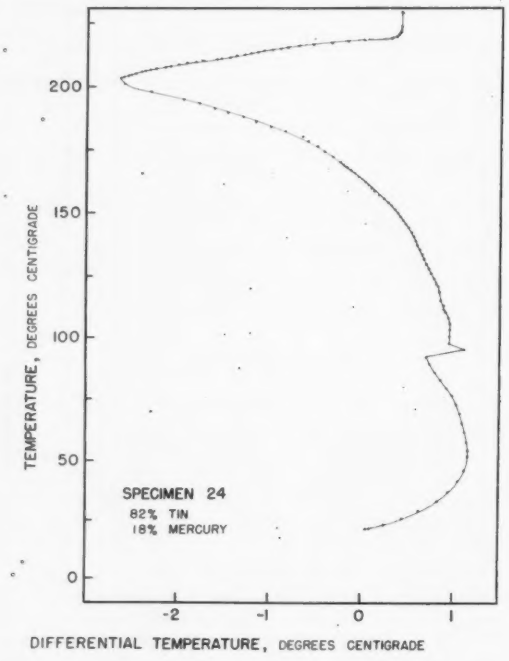

FIGURE 4. *Heating curve for 18% Hg 82% Sn alloy.*

6. Diffusion and Chemical Analysis

The use of diffusion and chemical analysis as an experimental method for the study of tin amalgams offers several advantages. This experimental technique avoids the metastable persistence of high temperature phases that is a common problem in peritectic systems. Murphy [20] in his study of the silver-mercury system, for example, found that the gamma phase was readily formed by the diffusion of mercury into finely divided silver, but that it was completely suppressed by cooling from the liquid state. Because of the high rates of diffusion of mercury into tin reported by Prügel [21] among others, this method appeared particularly suited to the study of the mercury-tin system.

With these advantages in mind, a series of experiments was performed in which ingots of tin were exposed to liquid mercury for varying periods, annealed and then serially sectioned and analyzed. The exposure temperature and time and the annealing time were varied systematically.

6.1. Specimen Preparation

The individual specimens used for the diffusion studies were small cylinders approximately 0.65 inch in diameter and 0.40 inch in length. They were machined from induction-melted ingots, slightly larger in diameter and 3 to 4 inches in length, cast under vacuum in Pyrex. All of the ingots were prepared from the high-purity tin with the exception of a limited number of the initial ingots which were made from Baker and Adamson Reagent Grade Tin Sticks, of the composition given in table 2. Under the conditions of the test no differences in behavior could be detected between specimens made from this metal and from the higher purity tin.

The cast ingots were turned in a lathe to remove any surface imperfections and were then cut into cylinders approximately 0.40 inch in length. Any cylinders showing signs of piping or porosity were rejected, and the remainder were weighed and measured as a means of detecting gross internal porosity. If the specimens were stored before exposure to mercury, their surfaces were cleaned immediately before use by a light polishing on 600-grit silicon carbide metallographic paper.

6.2. Experimental Procedure

The specimens were exposed to mercury by immersion at constant temperature. In order to avoid excessive initial dissolution of the specimens, saturated solutions of tin in mercury were prepared at each diffusion temperature. Four nominal temperatures were employed, 37, 60, 85, and 110 °C. It was found possible to reduce the variation in temperature of the specimen itself to less than ± 0.1

°C in all cases, by placing the beaker containing the immersed specimen within a vacuum desiccator, which was in turn placed within the oven.

After varying periods of immersion, the specimens were removed from the mercury and the excess liquid was blown from the surface with an air blast. This treatment did not remove all of the liquid, but did reduce the quantity to a thin film adhering to the surface. Some of the specimens were then sectioned immediately, while others were returned to the oven for an additional annealing period before sectioning.

All sectioning was done on a lathe. The specimen was held in a collet and the lateral surface turned down until unreacted tin was exposed. A series of samples was then taken from the mercury-containing layer remaining on the end of the specimen. Figure 5 shows a schematic representation of a specimen after immersion in mercury. Views (A) and (B) are transverse and axial sections and indicate mercury penetration as well as characteristic location of expansion cracks. View (C) is an axial section of a specimen as it would appear after the reduction of the lateral surface preparatory to the taking of samples as serial sections from the end. The depth of cut used in taking the samples varied from specimen to specimen, being adjusted so as to provide minimum sample of 80 mg. These samples were then stored at room temperature until analyzed for their mercury content.

Mercury analysis was performed by a modification of the technique of Crawford and Larson [22], employing an evacuated closed system rather than a carrier gas stream. The tube was evacuated to a total pressure of 5 to 10 mm of mercury and then flushed repeatedly with dry nitrogen before the valve was finally closed with the tube in the evacuated condition. The furnace was maintained at a temperature of 500 °C at the location of the combustion boats, and the samples were left in the furnace for 1½ hours. At the end of this period the Pyrex tube was slid from the furnace and allowed to cool to room temperature before the vacuum was relieved. The mercury distilled from the specimens condensed on the cool portion of the tube remaining outside of the furnace, and was removed mechanically before the combustion boats were withdrawn for reweighing. This procedure retained the advantage of the Crawford and Larson [22] technique in that the mercury content was determined as weight loss in the specimen rather than requiring the collection and determination of the mercury driven off. At the same time it minimized oxidation problems due to either leakage or trace contamination of the carrier gas.

Table 6 shows the conditions of test for all the specimens studied with the exception of calibration runs, specimens tested during the development of the methods, and some few specimens lost due to experimental error. The immersion and annealing temperatures were the same for all tin specimens annealed at 37 and 60 °C. Attempts to immerse a tin specimen for any extended period at either 85

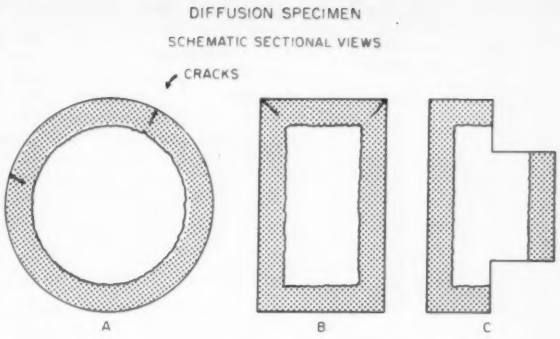

FIGURE 5. *Schematic sectional views of diffusion specimen.* Dark areas indicate diffusion of mercury.

or 110 °C led to the rapid conversion of the specimen and mercury to a slushy mass of platelike crystals dispersed in the remaining liquid. These specimens were therefore immersed at 37 °C prior to annealing at the higher temperature.

6.3. Results

The results of the analyses for specimen 20 are presented in figure 6. It exhibits many features common to all of the specimens and in particular of those sectioned immediately after removal from immersion. Each point on the diagram represents the result of an analysis of one entire sample and is plotted at the mean depth of the sample. The diameter of the points approximates the uncertainties of measurement of each value. The range of depth involved in each sample is indicated by the short bars near the lower margin of the figure.

The curve as drawn through the experimental points shows, as expected, a continual decrease of mercury content with depth. It also appears to consist of four distinct sections which are lettered

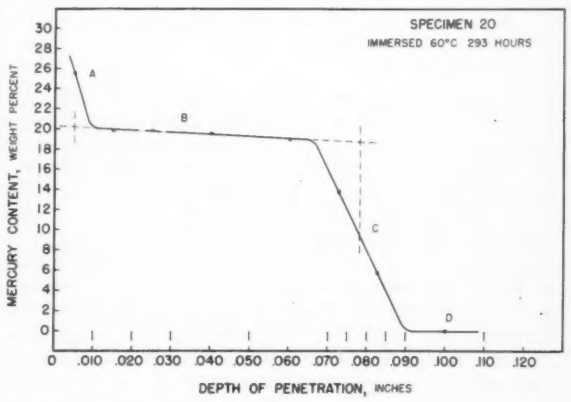

FIGURE 6. *Concentration-depth curve for specimen 20.*

TABLE 6. *Composition limits for the observed tin-mercury phases for individual diffusion specimens*

Specimen	Conditions				Weight percent mercury content of three phases						Depth at 10% mercury
	Immersion		Annealing		Lowest		Intermediate		Highest		
	Temp	Time	Temp	Time	Min	Max	Min	Max	Min	Max	
	°C	hr	°C	hr	% Hg	% Hg	% Hg	% Hg	% Hg	% Hg	in.
1	37	65							21.10 (13.66)	22.30 (14.52)	0.023
2	37	72							21.00 (13.59)	23.00 (15.02)	.029
3	37	73	37	41			19.00 (12.19)	20.05 (12.92)			.037
4	37	73	37	611			19.00 (12.19)	20.50 (13.24)			.038
5	37	124	37	242	18.35 *(11.74)	18.50 (11.84)	19.15 (12.29)	19.50 (12.54)			.048
6	37	124	37	338	17.80 (11.36)	18.80 (12.05)					.049
7	37	144					19.20 (12.33)	20.20 (13.03)	21.50 (13.95)	22.05 (14.34)	.042
8	37	144	37	130	17.95 (11.46)	18.50 (11.84)	18.95 (12.15)	19.35 (12.43)			.050
9	37	165							21.30 (13.80)	22.60 (14.73)	.047
10	37	170							20.90 (13.52)	21.90 (14.23)	.046
11	37	264							20.80 (13.45)	22.20 (14.44)	.089
12	37	264	37	768	17.90 (11.43)	18.65 (11.94)					.089
13	37	336							20.90 (13.52)	22.20 (14.44)	.079
14	37	336	37	168			19.20 (12.33)	20.20 (13.03)			.077
15	37	366							20.80 (13.45)	22.00 (14.28)	.076
16	60	114	60	75			19.30 (12.40)	20.05 (12.92)	21.20 (13.73)	22.20 (14.44)	.070
17	60	114	60	510	17.80 (11.36)	18.70 (11.98)	18.95 (12.15)	19.00 (12.19)			.071
18	60	125	60	240	18.60 (11.91)	18.70 (11.98)	19.00 (12.19)	19.05 (12.23)			.054
19	60	125	60	1,536	17.75 (11.32)	18.65 (11.94)					.041
20	60	293					18.90 (12.12)	20.15 (12.99)			.077
21	60	293	60	721	17.80 (11.36)	18.65 (11.94)					.113
22	60	356					19.40 (12.47)	26.10 (17.29)			.100
23	60	356	60	606	17.75 (11.32)	18.55 (11.88)	18.90 (12.12)	20.05 (12.92)			.142
24	37	222	85	258	Samples lost						
25	37	222	85	335			19.00 (12.19)	20.15 (12.99)			.096
26	37	222	85	3,931	17.50 (11.15)	18.50 (11.84)	18.90 (12.12)	19.65 (12.64)			.110
27	37	222	110	332	Samples lost						
28	37	222	110	526	17.55 (11.19)	18.60 (11.91)					.092
29	37	222	110	672	Samples lost						
30	37	222	110	794	17.50 (11.15)	18.80 (12.05)					.096

*Equivalent atomic percentages.

A through D on the figure. Section A indicated a surface layer of high but rapidly decreasing mercury content. It is readily interpreted as a mixture of the equilibrium surface phase with the adherent mercury film. Section B indicates a thick layer of very slowly decreasing mercury content. Such steps in diffusion curves are commonly taken as indicating a one-phase layer. Section C, indicating a layer of rapidly decreasing mercury content probably represents a mixture of the phase of section B with that of section D. Section D, which here consists only of portions of zero mercury content, normally will include the unreacted core material and also the solid solution region of the same structure.

Considering the curve as a whole, it seems to show the presence of one intermediate tin-mercury phase. The composition limits of this phase may be estimated by extrapolation of the straight line of section B to the middepths of the transition zones. Such an extrapolation (as indicated by the dotted lines in fig. 6) leads to an estimated maximum mercury content of 20.3 percent and a minimum of 18.8 percent. A similar procedure can be followed for the estimation of the maximum solubility of mercury in tin, by extrapolation of the line in section D, in those cases where more than one nonzero point occurs in that section.

Caution must be exercised in reaching such conclusions, since several possibilities for error exist.

It has been demonstrated radiographically by Gunther and Jehmlich [23] that the initial penetration of mercury into tin is intergranular; thus the possibility exists that the mercury content of the points in section B is too high because of the inclusion of such intergranular mercury. The possibility also exists that there might be one or more undetected solid phases in section C which remained undetected because a low diffusivity or narrow composition limits kept the layer thickness too small to be detected by the sectioning technique employed. Although the individual layers may be extremely thin, it is generally held that a separate layer must be formed for each intermediate phase. Rhines [24], for example, states that, "In binary systems, when diffusion occurs at substantially constant temperature and pressure, the layers formed correspond in kind and in order of their occurrence to the single-phase regions, . . . no two-phase regions appear." If such phases exist undetected in section C of figure 6, then the proper limit for the extrapolation of the line of section B is to the midpoint of the transformation to the first such phase.

The curves for all specimens sectioned immediately after removal from mercury at 37 or 60 °C were similar, each showing a single flat. In the specimens immersed at 37 °C, however, the extrapolated composition limits were approximately 22.3 and 21.0 percent mercury. Figure 7 shows the results for one such 37 °C specimen, specimen 1.

One specimen, specimen 16, immersed and annealed for a short time at 60 °C, produced a diffusion curve showing two flats. As can be seen from figure 8 the composition limits for the two phases agree well with those found in figures 6 and 7

Protracted annealing at either 60 or 37 °C resulted in the production of curves with a third set of indicated limits of mercury content, figure 9. The relatively short immersion time and long annealing time used for specimen 19 resulted in a complete transformation to the third observed phase. Slightly longer immersion and a short anneal produced steps characteristic of both the second and third phases in specimen 8, figure 10.

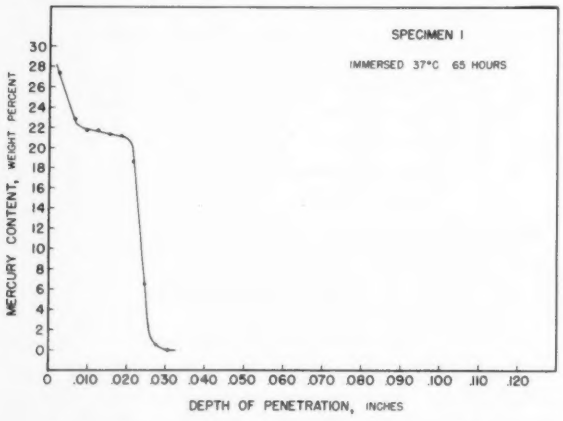

FIGURE 7. *Concentration-depth curve for specimen 1.*

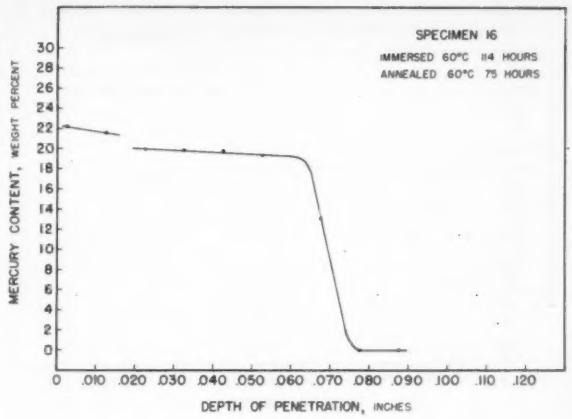

FIGURE 8. *Concentration-depth curve for specimen 16.*

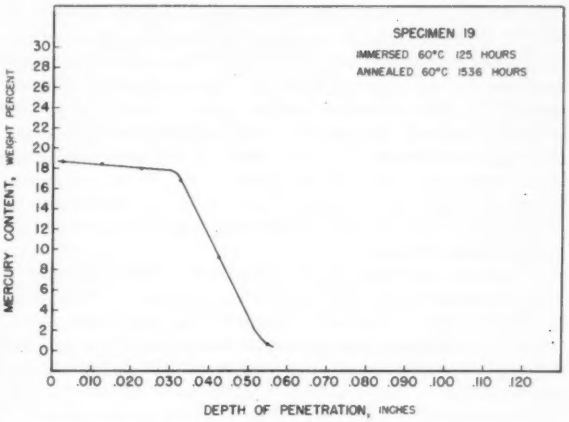

FIGURE 9. *Concentration-depth curve for specimen 19.*

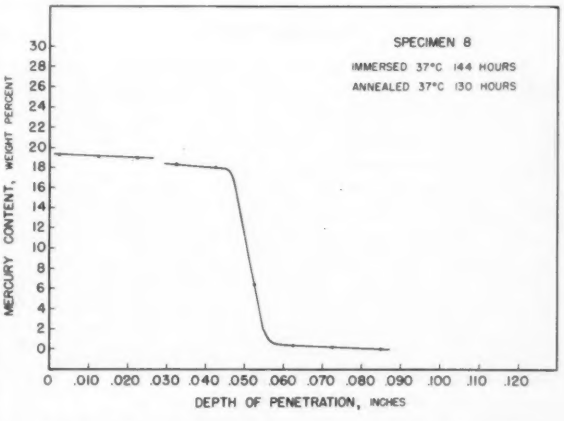

FIGURE 10. *Concentration-depth curve for specimen 8.*

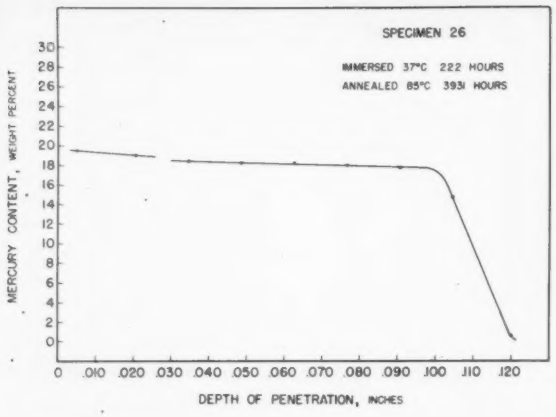
SPECIMEN 26
IMMERSED 37°C 222 HOURS
ANNEALED 85°C 3931 HOURS
MERCURY CONTENT, WEIGHT PERCENT
DEPTH OF PENETRATION, INCHES
0 .010 .020 .030 .040 .050 .060 .070 .080 .090 .100 .110 .120
0 2 4 6 8 10 12 14 16 18 20 22 24 26 28 30

FIGURE 11. *Concentration-depth curve for specimen 26.*

Whereas specimens annealed at 37 °C would be "dry" within 24 hours, the specimens annealed at 85 °C showed liquid on their surfaces after 11 days. The specimens annealed at 110 °C showed persistent surface liquid up to 14 days. Even then the liquid mercury disappeared only after machining had exposed a fresh tin surface with which it could react. Further evidence of a low rate of diffusion at these temperatures is given in figure 11. When sectioned after 5½ months of annealing at 85 °C, specimen 26 still showed layers of the second and third mercury-containing phases.

Table 6 summarizes the results for all of the individual tin-mercury diffusion specimens. The composition limits for each observed flat were calculated by the extrapolation procedure used in figure 8 and are tabulated here in accordance with the presumed occurrence of three intermediate tin-mercury phases. Also included is the total depth to the point at which the mercury content is 10 percent. The composition limits reported in this table should be considered as saturated values only when the equilibrium phase was also present in the specimen.

6.4. Discussion

The method of constant temperature diffusion followed by serial sectioning and analysis appears to be well suited to the study of the tin-mercury system. The results indicate the formation of three intermediate tin-mercury phases at 37 °C.

The phase of lowest mercury content appears to correspond to the gamma phase of existing diagrams, since even protracted annealing does not cause the appearance of any phase intermediate in composition between it and tin. The phase with the next higher mercury content appears to correspond to the delta phase reported by Gayler [11] and decomposes at an appropriate temperature for such identification. The remaining phase is previously unreported but is here tentatively designated epsilon.

Table 7 presents the composition limits for these phases as determined at each experimental temperature. As shown in the table, these phases all have narrow and closely spaced zones of solid solubility. The most noteworthy finding is the unexpectedly high minimum content found for the gamma phase. This is in sharp contrast to previously reported limits for this phase which indicated minimum mercury contents of the order of 8 percent as seen in figure 1.

This previous solubility limit appears to be based primarily on the X-ray diffraction work of von Simson [9] and Stenbeck [8], with some indirect evidence being provided by the results of Løvold-Olsen [25], Schubert et al. [13], and Raynor and Lee [12]. It is very difficult in most of these instances to determine what was the previous thermal history of the specimens used. Almost certainly in the case of the work of both von Simson [9] and Stenbeck [8] and apparently in most of the other work, the annealing times were inadequate to cause the precipitation of tin from the gamma phase formed on cooling from the liquid. As a result, the composition limits of the gamma phase based on their findings are more indicative of the composition range over which the gamma phase is formed at elevated temperatures than of its equilibrium extent at room temperature. The one possible exception to the charge of insufficient annealing is a specimen of Raynor and Lee's [12] which was annealed for 2 weeks at 150 °C. This specimen contained 7.193 atomic percent of mercury (approximately 11.5 weight percent), and apparently consisted entirely of gamma. While their paper does not deny the presence of tin lines in the X-ray pattern neither does it report them as it presumably would had they been observed. Possibly even this annealing time is inadequate or the amount of grain size of the precipitated tin was too small to detect. If not, a rather rapid widening or displacement of the gamma region must occur above 110 °C to accommodate this observation.

TABLE 7. *Composition limits for the gamma, delta, and epsilon tin-mercury phases as a function of diffusion temperature*

Temperature	Mercury content					
	Gamma phase		Delta phase		Epsilon phase	
	Min	Max	Min	Max	Min	Max
°C	wt % Hg	wt % Hg	wt % Hg	wt % Hg	wt % Hg	wt % Hg
37	17.9	18.8	19.0	20.1	20.9	22.3
	*(11.4)	(12.05)	(12.2)	(13.0)	(13.5)	(14.5)
60	17.8	18.6	19.0	20.1	**21.2	**22.2
	(11.4)	(11.9)	(12.2)	(13.0)	(13.7)	(14.4)
85	17.5	18.5	18.9	20.1		
	(11.2)	(11.8)	(12.1)	(13.0)		
110	17.5	18.6				
	(11.2)	(11.9)				

*Equivalent atomic percentages.
**Found in only one specimen at 60 °C diffusion temperature.

7. X-ray Diffraction

7.1. Specimen Preparation

X-ray diffraction patterns were obtained on a total of 20 mercury-tin specimens with mercury contents ranging from 5.0 to 22.1 percent. The specimens were prepared by two different techniques;

14 of them were derived from diffusion specimens while the remaining 6 were fused and annealed.

The technique employed in the preparation of the specimens by diffusion was identical with that by which the samples were obtained for mercury analysis. The samples used for the diffraction studies were selected, on the basis of the analyses of other samples from the same diffusion specimen, to provide evidence about the structures of the phases found in diffusion studies. The mercury content of these specimens was determined by interpolation of the composition-depth results from adjacent analyzed samples.

The remaining 6 specimens were prepared by sealing weighed portions of the component metals in a Pyrex tube in vacuum or an inert gas atmosphere. The alloy was fused at 250 °C, and quenched. The ingot was then annealed for a short period in the tube. After removal from the Pyrex tube the specimen was reduced to a coarse powder by turning on a lathe.

This procedure was intended to correspond approximately to the specimen preparation techniques used by previous investigators, although, as noted above, the information as to the exact techniques they used is often incomplete. The annealing times used in this study appear to exceed those of Stenbeck [8] and von Simson [9] but are less than those used by Raynor and Lee [12].

The composition and source of the X-ray diffraction specimens produced by diffusion are listed in table 8. The composition and heat treatment of the X-ray diffraction specimens produced by fusion are given in table 9.

TABLE 8. *Observed X-ray diffraction patterns as a function of mercury content in diffusion specimens*

Mercury content	Specimen	Source		Observed pattern
		Diffusion specimen	Sample depth	
wt %			*in.*	
22.10+ (14.37)*	1	7	0.0025	Complete hexagonal
21.94 (14.26)	7	1	.0075	Complete hexagonal
21.83 (14.18)	2	7	.0125	Complete hexagonal
21.72 (14.10)	3	11	.0250	Complete hexagonal
20.00 (12.89)	6	****15	Surface	Complete hexagonal
19.88 (12.80)	8	1	0.0375	Transition**
19.78 (12.73)	9	22	.0500	Complete hexagonal
19.27 (12.38)	12	26	.0135	Transition
19.20 (12.33)	4	8	.0075	Transition
18.72 (11.99)	10	21	.0500	Transition
18.29 (11.70)	13	26	.0555	Incomplete hexagonal***
18.19 (11.63)	5	8	.0375	Incomplete hexagonal
18.07 (11.54)	14	28	.0550	Incomplete hexagonal
12.58 (7.85)	11	21	.1075	Incomplete hexagonal

*Equivalent atomic percentages.
**Ratio of 001 and 100 peak height less than 0.8.
***001, 002, and 003 lines absent.
****This specimen was annealed for 168 hours at 37 °C after removal from the mercury, in addition to the treatment indicated in table 6.

TABLE 9. *Observed X-ray diffraction patterns as a function of mercury content in cast specimens*

Mercury content	Specimen	Annealing		Observed pattern
		Temp	Time	
wt %		*°C*	*hr*	
21.75 (14.12)*	15	70	2	Transition**
17.83 (11.38)	16	70	2	Transition***
12.51 (7.80)	17	160	2	Incomplete hexagonal
12.45 (7.76)	18	160	4	Incomplete hexagonal
10.23 (6.32)	19	150	2	Incomplete hexagonal-tin trace
4.95 (2.99)	20	150	2	Incomplete hexagonal-tin

*Equivalent atomic percentages.
**Ratio of 001 to 100 peak height 0.75.
***Ratio of 001 to 100 peak height 0.30.

7.2. Experimental Procedure

All of the diffraction patterns were obtained on a Norelco X-ray Spectrograph using copper Kα radiation. This instrument is equipped with a goniometer having an auxiliary rotating device which rotates the specimen about an axis perpendicular to its surface throughout the test. This rotation produces more uniform curves when the specimen is small, as were the majority of those used in this study.

The specimens were prepared for the tests by sprinkling the particles onto a thin layer of petroleum jelly spread on the surface of the plastic mount. The diffraction curve was run over the range from 20° to 165° 2 θ at a rate of 1° 2 θ per minute, with a chart speed of ½ inch per minute. This scanning rate and chart speed were found to produce very satisfactory curves with good resolution. Even at 2 θ angles as low as 65°, the α_1 and α_2 peaks were normally resolved on the curves from specimens prepared by diffusion. At 2 θ angles above 110° they were often resolved to the background level. The resolution was somewhat poorer on cast specimens with the α_1 and α_2 lines routinely resolved only above 80° 2 θ.

7.3. Results

The results of the X-ray diffraction tests on the specimens produced by diffusion correlate closely with the mercury content. Those specimens having mercury content between 21.0 and 22.2 percent mercury, that is specimens selected from the highest mercury content phase regions of diffusion specimens, uniformly produced curves of the type shown in figure 12. This curve was obtained from specimen number 3 and is readily indexed as a simple hexagonal structure with the parameters reported by Raynor and Lee [12] for the gamma mercury-tin phase. The individual peaks in figure 12 are labeled on this basis. (Lines labeled M are from the resin used as a specimen support.)

Although the diffraction curves were run from 20° to 165° 2 θ, only the portions between 25° and 80°

663611—63——5

are reproduced here. Most of the changes of interest occur within this interval.

All of the specimens taken from the phase with the lowest mercury content of the diffusion specimens (17.8 to 18.6% mercury) gave diffraction patterns similar to figure 12 except for the almost complete suppression of the 001, 002, and 003 peaks. Minor changes occur in the peak heights of other lines but those mentioned are the most characteristic. All of the lines which are present appear at the same angles as in figure 12.

Specimens having mercury contents between 18.6 and 21.0 percent gave patterns in which the ratios of the 001, 002, and 003 lines to the 100, 200, and 300 lines, respectively, increased approximately in proportion to mercury content.

Figure 13 shows a curve derived from specimen 10 which contained 18.72 percent mercury. Even this small amount of mercury in excess of the 18.6 percent limit has caused the reappearance of the 001 peak, although the 002 peak cannot be distinguished from the diffuse peak due to the support. More mercury increased the relative height of these peaks but in no instance did the 001 or 002 line of an intermediate mercury content phase specimen exceed 80 percent of the peak height of the 100 or 200 line. In contrast, in all of the highest mercury content phase specimens the 001 and 002 lines were stronger than the associated 100 and 200 lines.

Table 8 presents a summary of the X-ray diffraction findings on diffusion samples with the specimens arranged in order of mercury content. Only three specimens appear to merit further comment. Specimen 9 appears out of place. Its composition and source place it as an intermediate mercury content phase specimen, but its X-ray diffraction pattern showed 001, 002, and 003 lines among the strongest found. The cause of this conflict is not known.

The mercury content of specimen 6 similarly appears to be too low for the observed pattern. In this case, however, the mercury content is probably at fault. This specimen was the only one tested without sectioning, so that the pattern was obtained from the surface of the intact specimen rather than from a powdered layer. The mercury content was estimated from the composition-depth curve for the opposite end of the ingot.

On the basis of its composition and the shape of the diffusion curve, tin lines were expected in the pattern of specimen 11. They were not found. In-

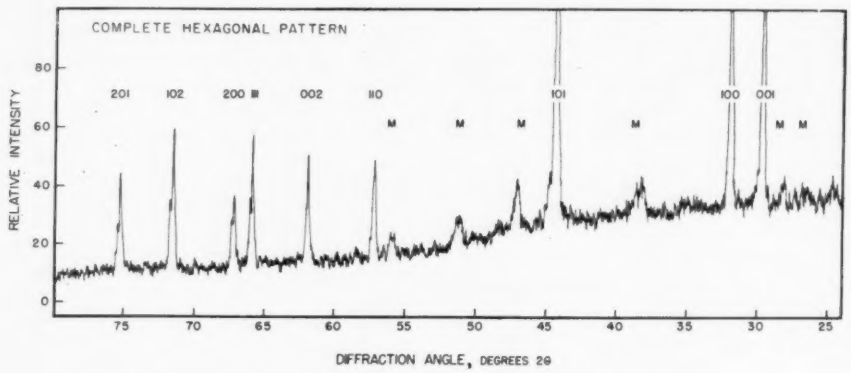

FIGURE 12. *"Complete hexagonal" X-ray diffraction pattern.*

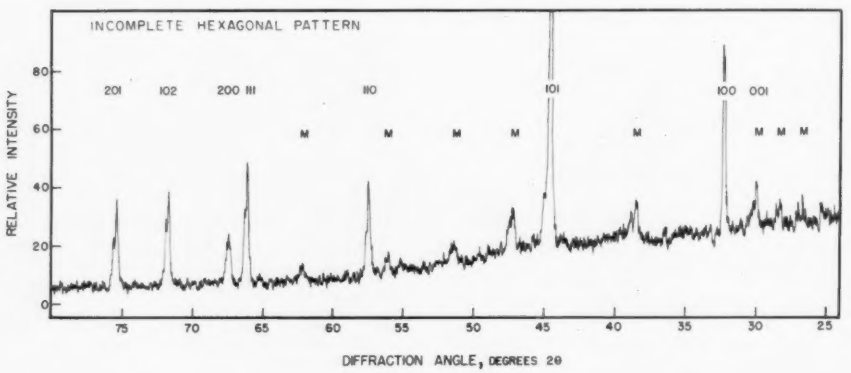

FIGURE 13. *"Incomplete hexagonal" X-ray diffraction pattern.*

spection of the sample showed it to consist of two obviously different types of particles, one fine and granular, and gray in color; the other small, curled chips more nearly white in color. The mercury content of the mechanically separated chips was found to be about 4 percent. If this mercury were distributed as a thin surface layer of a tin-mercury phase, it might cover the tin and explain the absence of tin lines.

The X-ray diffraction patterns from the cast and annealed specimens showed a somewhat similar dependence upon mercury content as shown in table 9. In no instance was the pattern of the cast specimens of the type which has been called "complete hexagonal" in the diffusion specimens. It is believed that the short time at a low annealing temperature was inadequate to resolve a mixture of phases produced on cooling.

7.4. Discussion

The X-ray diffraction results appear to indicate the occurrence of two phases between 17.8 and 22.2 percent mercury in the mercury-tin system at normal room temperatures. These findings are in disagreement with previous X-ray investigations of this system and only partially corroborate the diffusion test results of this study. The nature of the observed patterns, however, are such that they may permit a reconciliation of the otherwise contradictory data.

The structure found for diffusion specimens with 21.0 to 22.2 percent mercury is readily indexed as a simple hexagonal structure with one atom per unit cell as reported by von Simson [9]. So also are most of the structures containing 18.7 to 21.0 percent mercury which were labeled "transition" structures. But the structure in equilibrium with tin at room temperature, the "incomplete hexagonal" in which the OOX lines are missing, cannot be explained with such a simple structure.

One possibility that must always be considered in regard to patterns in which particular lines appear to be suppressed is preferred orientation. The method of specimen preparation employed in these tests makes this an unlikely cause in this instance. The samples were reduced to a powder which was stored at room temperature for a considerable period of time before the patterns were taken. The sharpness of the lines in the patterns, showing no evidence of strain broadening, indicates that recrystallization probably occurred in the particles during this time. The specimens were prepared for the diffraction test by sprinkling the powder onto a layer of petroleum jelly spread on the surface of the mount. Even if preferred orientation did occur in the individual chips as a result of the machining operation, it seems unlikely that the particles could all be so alined after transfer to the mount. No alternate structure is proposed, but it is possible that some structure more complex than the one atom simple hexagonal is required to account for the suppression of the missing lines. *If* the patterns in figures 12 and 13 represent two different phases corresponding to the highest mercury content and lowest mercury content phases of the diffusion specimens, the "transition" pattern is easily explained as a mixture of the two. The X-ray diffraction results fail to confirm the existence of the intermediate content phase of the diffusion.

Although several specimens were tested with compositions in the immediate vicinity of that for which Stenbeck [11] reported a line doubling, which he attributed to an orthorhombic structure, no evidence of such a structure was found. Since the gamma phase is reported to extend to much lower mercury contents at elevated temperatures, it is conceivable that his results were the product of lattice parameter variations caused by variation in mercury content in unannealed specimens. He does not report any annealing treatment for his specimens.

The problem remains as to why other investigators have found the structure in equilibrium with tin to be a simple hexagonal if the 00X lines are truly absent. A possible explanation in the case of cast specimens is incomplete annealing. As seen in specimen 16, a composition (17.8%) which in a diffusion specimen would result in the complete absence of the 00X lines, does not do so in a cast specimen even after a short anneal. Cast specimens containing 8 to 14 percent mercury as von Simpson's [9] did, might well produce at least some of the phase responsible for these lines and show a "transition" pattern. It is of interest to note that she reports the 001 line as weak and that she found the 002 line on only one side of the film.

Raynor and Lee [12] investigated a specimen with 7.193 atomic percent mercury (11.5 wt %) which was annealed for 2 weeks at 150 °C. They do not report the absence of the 00X lines or the occurrence of tin lines. This specimen lies between specimens 17 and 19 in composition and was annealed at approximately the same temperature for a considerably longer time. No previous investigator seems to have studied a specimen in the narrow range of 17.8 to 18.6 percent mercury. Even so, extended annealing would apparently be required to produce a uniform structure in cast specimens.

The X-ray results do little to substantiate the tin saturated boundary of the gamma region as inferred from the diffusion study. Only three specimens, 17, 18, and 19, have compositions and annealing temperatures that would make them of use for this purpose. The annealing times are certainly too short to assure equilibrium if allowance is made for the slow rate of diffusion found at elevated temperatures. (See fig. 11). The identification of weak tin lines in specimen 19 in spite of the very short anneal is, however, partial confirmation that the boundary does shift to higher mercury contents at lower temperatures. It is possible that specimens 17 and 18 fall within the gamma region and would not show tin lines even after extended annealing.

The failure to obtain tin lines from specimen 11 raises some doubt as to whether the method is suitable for the determination of this boundary.

As mentioned before, the sample at the time of sectioning appeared to contain two distinct phases, one of which appeared to be tin. After standing at room temperature for some time before the X-ray pattern was determined, the specimen showed no tin lines even though chips of low mercury content were readily separated mechanically from the sample. This behavior can be explained if portions of the phase that was present with the tin has mercury contents higher than the equilibrium value as the result of a low rate of diffusion. After sectioning, these portions would be brought in direct contact with the tin chips and mercury transfer could occur, producing a layer of product on the surface of the tin chips and thus masking the tin lines. Such a mechanism could operate in any instance when equilibrium has not been attained prior to sectioning, but should at least in part be offset by determination of the diffraction pattern as soon as possible after sectioning.

If the gamma region is as curved as the diffusion results indicate, the appearance of tin lines in a diffraction pattern obtained at room temperature might be the result of precipitation from what was a homogenous structure at the annealing temperature. In a more general sense, the same possibility of transformation between the annealing temperature and the diffraction test temperature might be invoked to explain the appearance of only two phases where the diffusion tests indicate three. If provision were made for adequate annealing, elevated temperature diffraction tests would seem to offer the best hope of clarifying the boundaries of the gamma phase. Annealing times much longer than those of Schubert et al. [13] would be required.

8. Proposed Tin-Mercury Diagram

The proposed tin-mercury diagram based upon the findings of this study is shown in figure 14 and an enlargement of the tin rich end of the diagram is shown in figure 15. In drawing the boundaries in the diagram an attempt has been made to reconcile the results from various test methods and investigators. Where conflicts occur between the different sources, an attempt has been made to allow for the relative uncertainty of the individual findings.

The liquidus curve essentially follows that of van Heteren [6] except that it has been lowered slightly in the alpha+liquid and beta+liquid regions where he had no observations. This lowering is based on the thermal analysis results of this study and appears to agree with Prytherch's [10] results in the same region. The alpha phase boundaries are based mainly on those as drawn by Hansen [3]. The maximum solubility of mercury in tin has been indicated to be 1 percent by van Heteren's [6] electrode potential measurements, and the thermal analysis and metallographic results of this investigation confirm that this limit must be less than 2.0 percent mercury. There appear to be no other applicable data.

The existence of beta phase at elevated temperature appears to be well established. Our thermal analysis studies confirm Prytherch's [10] finding of a peritectic arrest although the value obtained is slightly lower than that of figure 1. The only evidence against the occurrence of this phase was the work of Schubert et al. [13], which apparently was in error because of inadequate annealing of the specimens. In a note added in publication, they acknowledge that Raynor and Lee's [12] results were conclusive. Although the existence of this structure is quite certain, the composition limits are unsupported by experimental data. As drawn in figures 14 and 15, they merely follow figure 1 for lack of any better information. The limits appear reasonable and are not contrary to theory.

The beta eutectoid temperature is very poorly established, although the thermal analysis results appear to confirm that the 198 °C value of figure 1 is approximately correct. If reliance is placed upon the presence or absence of experimental points in Prytherch's [10] diagram, as noted in the comments on Gayler's [11] paper, this temperature was never established experimentally. For lack of other evidence, it is indicated here at 197 °C on the basis of our thermal analysis results.

The gamma peritectic temperature of 213.9 °C also is based on thermal analysis results and agrees well with Hansen's [3] value of 214 °C. The composition of the gamma peritectic is set at 9 percent mercury primarily on the basis of X-ray results of von Simson [9] and Stenbeck [8] although, since their results can be reconciled with the present findings only on the basis of incomplete annealing at low temperature, it is perhaps risky to assume that their specimens were at equilibrium above 200 °C. From the liquidus values it is obvious that this point must be at 14 percent mercury or less, but there is no evidence for a location other than the one indicated.

The remainder of the gamma region has been considerably altered. The tin-saturated boundary has been moved to agree with the results of the diffusion studies below 110 °C, as has the mercury-saturated boundary. Between 110 and 197 °C the tin-saturated boundary has been drawn to allow for the X-ray diffraction results on cast specimens. The mercury-saturated boundary above 110 °C has been drawn on the basis of heating curve indications of the start of melting. These data, however, showed considerable variation with annealing and the curve should be considered as approximate.

The overall picture of the gamma region as a narrow band swinging to higher mercury contents at lower temperatures is somewhat unusual because of the size of the swing relative to the width of the region. This construction serves nicely, however, to explain certain heat absorptions that occur in low mercury content thermal analysis specimens. In many instances the specimen has been annealed at an elevated temperature for a while before the start of the run. Portions of the specimen should thus have consisted of gamma saturated with tin. If the proposed diagram is correct, these portions would soon be heated across the gamma region and liquid would start to form with an absorption

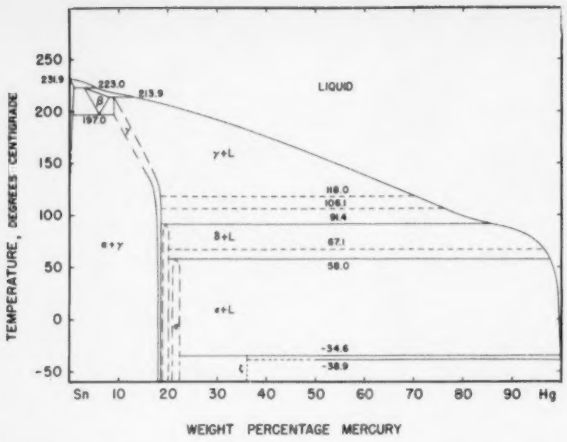

FIGURE 14. *Proposed tin-mercury constitution diagram.*

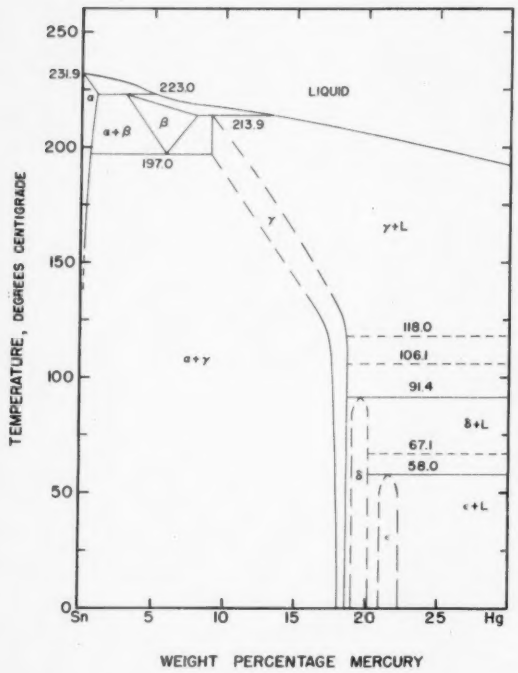

FIGURE 15. *Enlarged tin-rich portion of proposed constitution diagram.*

of heat. One example of this type of reaction is seen in figure 3.

Two additional peritectic phases labeled delta and epsilon are shown on the diagram. They are located on the basis of the combined thermal analysis and diffusion results. The delta phase was present in 85° diffusion specimens but not in 110 °C specimens. It is thus readily associated with the 91.4 °C arrest observed on thermal analysis. This thermal arrest is very strong and coincides with that found by Gayler [11].

The epsilon phase composition limits are similarly set from the observed composition range for the phase with the highest mercury content in diffusion specimens, and are even more certain than those of the delta region. The peritectic temperature is not so definitely known. The arrest found on thermal analysis at 67.1 °C is strong and well defined and seems certainly to represent a peritectic temperature. If this temperature is associated with the epsilon phase, however, highest mercury content phase layers should have routinely appeared in the 60 °C diffusion specimens but were detected in only one out of the eight specimens immersed at 60 °C.

The next lower arrest that might logically be associated with the highest mercury content phase structure occurred at 55.5 °C. This arrest is less well defined than the other, since it was found on heating curves only, and has an uncertainty of 2.5 °C. Considering that in a single instance this structure appeared in a specimen nominally annealed at 60 °C, the actual peritectic temperature would have to lie near the top of the uncertainty range even if maximum allowance is made for possible variation in the annealing temperature. As a result the peritectic temperature of the epsilon phase is indicated at 58 °C.

The peritectic phase at −34.6 °C found by van Heteren [6] and placed by Prytherch [10] at $HgSn_3$ has not been investigated and is merely reproduced as previously stated. It is designated here as zeta.

This leaves three strong thermal arrests at 67.1, 106.1, and 118 °C to be explained. On the basis of the thermal data alone, these arrests would definitely appear to represent peritectic phase formations but no other affirmative evidence for such phases has been found. Such a closely spaced series of phases seems quite unlikely, and these arrests may instead represent second order transformations rather than phase changes. For these reasons these arrests are merely indicated by dashed lines in the figures.

One additional possibility, which is entirely speculative, is that the gamma region as shown in figure 15 is in reality two separate regions. One phase, stable at high temperatures, would form as indicated at the 213.9 °C peritectic temperature and would decompose on cooling at a 106.1 °C eutectoid. The other phase having the composition limits discovered in the diffusion tests would then be associated with a 118.0 °C peritectic temperature. Such a construction would account for two of the unidentified arrests and would simultaneously eliminate the need for the unusual variation in the composition limits of the gamma region with temperature. The tests as performed provide neither support nor refutation for such a construction. The findings of Günther and Jehmlich [23] seem to support the existence of some such complex series of phases although they do not identify any of the corresponding compositions.

9. Conclusions

The results of this investigation have indicated that the mercury-tin system is more complicated than was previously reported. Additional evidence for the existence of the beta phase has been found by determination of the separate peritectic temperatures of the beta and gamma phases as indicated by Prytherch [10]. The composition limits and eutectoid temperature of the beta phase remain to be confirmed. This appears best approached by a series of elevated temperature X-ray diffraction patterns. A set of specimens annealed in the beta range and tested at successively lower temperatures should provide the needed information. The data from thermal analysis studies and X-ray results suggest that the limits of the gamma phase should be shifted as indicated in figure 14 and 15. Corroborative evidence for Gayler's [11] delta phase has been found by thermal analysis and diffusion methods. Possible evidence for an additional epsilon phase has also been found.

10. References

[1] Joyner, R. A., Amalgams containing silver and tin. J. Chem. Soc. **99,** 195–208 (1911).

[2] Metals Handbook, American Society for Metals (Cleveland, 1948).

[3] Hansen, M., Constitution of binary alloys (McGraw-Hill Book Co., Inc., New York, N.Y. 1958).

[4] Puschin, N. A., Chem. Z. **24,** 950 (1900) as referenced in van Heteren [6].

[5] Heycock, C. T., and Neville, F. H., The molecular weights of metals when in solution, J. Chem. Soc. **57,** 376–393 (1890).

[6] van Heteren, W. J., Die Zinnamalgame. Z. anorg. Chem. **42,** 129–173 (1904).

[7] Tamman, G., Zur Konstitution der Legierungen, Z. physik Chem. **3,** 441–449 (1889).

[8] Stenbeck, S., Röntgenanalyse der Legierungen von Quecksilber mit Silber, Gold, und Zinn, Z. anorg. Chem. **214,** 16–18 (1933).

[9] von Simson, C., Röntgenuntersuchungen an Amalgamen, Z. physik Chem. **109,** 183–192 (1924).

[10] Prytherch, W. E., unpublished work; the diagram proposed is shown in J. Inst. Metals **60,** 381, 403 (1937).

[11] Gayler, M. L. V., The constitution of the alloys of silver, tin and mercury, J. Inst. Metals. **60,** 379–406 (1937).

[12] Raynor, G. V., and Lee, J. A., The tin-rich intermediate phases in the alloys of tin with cadmium, indium and mercury, Acta Metallurgica **2,** 616–620 (1954).

[13] Schubert, K., Rösler, U., Mahler, W., Dörre, E., and Schütt, W. Strukturuntersuchungen an einigen Valanzelektronen-armen Legierungen Zwischen B-Metallen, Z. Metallkunde **45,** 643–647. (1954).

[14] Troiano, A. R., An x-ray study of dental amalgams, J. Inst. Metals **63,** 247–263 (1938).

[15] Wainwright, C., J. Inst. Metals **63,** 260 (1938). Discussion of [14].

[16] Ryge, G., Moffett, J. C., and Barkow, A. G., Microstructural observations and x-ray diffraction studies of silver-tin amalgams, J. Dental Research **32,** 152–167 (1953).

[17] Fairhurst, C. W., and Ryge, G., The tin-mercury phase in dental amalgam. Paper presented at a meeting of the International Association for Dental Research, March, 1961.

[18] Dreiner, Rudolf, Rontgenographische Untersuchungen über den Abbindevorgang bei Silber-Zinn-Amalgamen. Von der Fakultät für Bergbau und Hüttenwesen der Rheinisch-Westfälischen Technischen Hochschule Aachen zur Erlangung des akademischen Grades eines Doktor-Ingenieurs genehmigte Dissertation (Dec. 1958).

[19] Hume-Rothery, W., Christian, J. W., and Pearson, W. B., Metallurgical equilibrium diagrams, Institute of Physics, London (1952).

[20] Murphy, A. J., The constitution of the alloys of silver and mercury, J. Inst. Metals **46,** 507–522, 528ff (1931).

[21] Prügel, K., Die Diffusion von Quecksilber in Zinnfolien, Z. Metallkunde **30,** 25–27 (1938).

[22] Crawford, W. H., and Larson, J. H., Residual mercury determination process, J. Dental Research **34,** 313–317 (1955).

[23] Günther, F., and Jehmlich, G., X-ray investigation of diffusion in the system tin-mercury, Z. Metallkunde **50,** 288–293 (1959).

[24] Rhines, F. N., Diffusion coating of metals, Symposium on surface treatment of metals, 122–165, Amer. Soc. for Metals (1941).

[25] Løvold-Olsen, L.; see Vegard, L., Skrifter norske videnskaps-akad, Oslo, Mat. Naturv. Kl. **2,** 32–37 (1947); quoted from Structure Repts. **11,** 163 (1947–1948).

(Paper 67A1-195)

JOURNAL OF RESEARCH of the National Bureau of Standards—A. Physics and Chemistry
Vol. 67A, No. 1, January–February 1963

Effect of Methyl Bromide Additions on the Flame Speed of Methane

Carl Halpern

(September 5, 1962)

The effect of small quantities of methyl bromide, up to 0.5 percent by volume, on the flame speed of methane-air mixtures has been determined. Maximum flame speeds, at given experimental conditions, are reduced proportionately to the amount of methyl bromide added. Flame speeds of rich mixtures are reduced much more than are flame speeds of lean mixtures. Reaction zone thickness of methane-air flames is increased by the addition of methyl bromide and the thickness increases with the amount of methyl bromide.

1. Introduction

Halogenated hydrocarbons have long been used to extinguish fires, and the effect of these combustion inhibitors on various combustion parameters has been the subject of many investigations [1–10].[1] Limits of flammability, quenching distance, and laminar flame speed all have been found to be affected by these inhibitors. Effect of inhibitors on the limit of flammability has been the chief topic of these investigations. The effect on flame speed has been little studied and what work that has been published usually treats of the effects of several inhibitors on a given fuel; description of the effects of other experimental conditions are usually lacking [1,2,9, 10]. It was felt that a study of the effect of one inhibitor on flame speed under controlled experimental conditions would be of interest and of value. Methane was chosen as the fuel since we have had considerable experience in the determination of the flame speed of methane-air mixtures. Methyl bromide was chosen as the inhibitor.

2. Apparatus and Procedure

A description of the apparatus and method used to measure flame speeds has been presented earlier [14]. Briefly, the apparatus consists of drying and metering systems for air and fuel, and a nozzle, the exit of which is the burner port. Means are provided to control the temperature of the combustible mixture issuing from the nozzle. Flame speeds are determined by a total-area method, which is based on the measurement of the area of an enlarged photograph of the schlieren image of the flame.

It was decided to prepare mixtures of air and methyl bromide of the desired strength and to meter these mixtures, rather than to set up a third metering system for the small quantities of methyl bromide that would be required. Some error is introduced in the metering of these mixtures, since the sharp-edged orifice used was calibrated for air. However, since the maximum amount of methyl bromide added was only 0.5 percent by volume of the air, it was considered that the error would be tolerable.

The mixtures of methyl bromide and air were prepared in a 120 gallon (16 ft^3) steel tank. The tank was evacuated to a pressure of several microns and the methyl bromide admitted from its container. Rise in pressure was measured on a mercury manometer, read to 0.01 in. Air from a compressor was dried by passing first through a column of activated alumina and then through a cold trap immersed in a slush of dry ice in a mixture of equal parts by weight of chloroform and carbon tetrachloride. Water content of the air is thus kept at 0.03 percent by volume. The dried air was admitted slowly to the tank, and the final pressure, generally 130 psig, was read on a calibrated Bourdon gage to 0.1 psig.

The products of combustion, which contain hydrogen bromide and bromine, were drawn from the enclosure surrounding the burner by a large capacity vacuum pump. Air currents, set up by the pump, so disturbed the flames that the pump was shut off when photographs were taken.

Mixtures of 0.1, 0.2, 0.3, 0.4, and 0.5 percent by volume of methyl bromide in air were prepared. For each mixture, the variation of flame speed with mixture ratio, by weight, of methane to air plus methyl bromide was determined, gas velocity at the exit of the nozzle being constant. The ratio, by weight, of methane to air plus methyl bromide was varied from 0.054 to 0.072, and the gas velocity at the port of the nozzle was varied from 3 to 6 fps. Control of the temperature of the combustible mixture was such that the maximum change in temperature during a single run of about 3 hr duration was 3.7 °F. Actual gas temperatures ranged from about 90 °F in the summer to about 75 °F in the winter. The variation of flame speed with temperature was determined using a mixture ratio of methane to air of 0.060 (the air contained 0.2% methyl bromide), and a gas velocity of 4 fps; the temperature range in this determination was from 70 to 95 °F. Variation of flame speed with temperature was found to be 0.00328 fps per °F, and this value was used to correct

[1] Figures in brackets indicate the literature references at the end of this paper.

all flame speeds to a constant temperature of 75 °F. It is not expected that the rate of change of flame speed with temperature will differ appreciably with the relatively small amounts of methyl bromide added. Some previously unpublished data in our possession shows that the rate of change of flame speed with temperature is unaffected by changes in mixture ratio.

3. Results

Combustion of methane with air to which methyl bromide had been added proceeded smoothly. The outer mantle of the flames was colored brown by the formation of free bromine and the odor of bromine was noticeable. At lean conditions, the brown color began close to the base of the flame and extended to the tip. As flames became richer in fuel, the normal blue-green color of the inner cone appeared and the brown color was seen only near the tip of the outer mantle. As the concentration of methyl bromide was increased, the brown color became more intense, but in rich flames was visible only near the tip of the outer mantle. It is probable that hydrogen bromide is the original product and is converted to bromine by the overall reaction: $4\ HBr + O_2 \longrightarrow 2\ Br_2 + 2\ H_2O$. Apparently there is insufficient oxygen in a rich flame for complete conversion of hydrogen bromide.

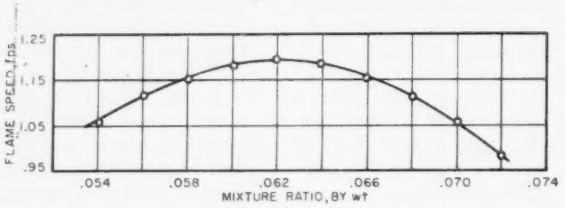

FIGURE 1. *Variation of flame speed of methane with mixture ratio.*

The variation of flame speed with mixture ratio for a methane-air flame is shown in figure 1. This is taken from our previous work [14] with the values of flame speed corrected to 75 °F. The maximum flame speed is 1.196 fps, at a fuel-air ratio of 0.062. At a fuel-air ratio of 0.054, flame speed is 1.057 fps, and at a fuel-air ratio of 0.072, flame speed is 0.980 fps.

Results of addition of methyl bromide are shown in figures 2 through 6. It should be noticed that gas mixtures described as having the same mixture ratio but with different amounts of methyl bromide added do not have exactly the same ratio of fuel to air. As the amount of additive increases, the amount of air decreases, and the ratio between fuel and air increases; but this increase is only a matter of about a tenth of a percent. However, these facts should be remembered when comparing results. Figure 2

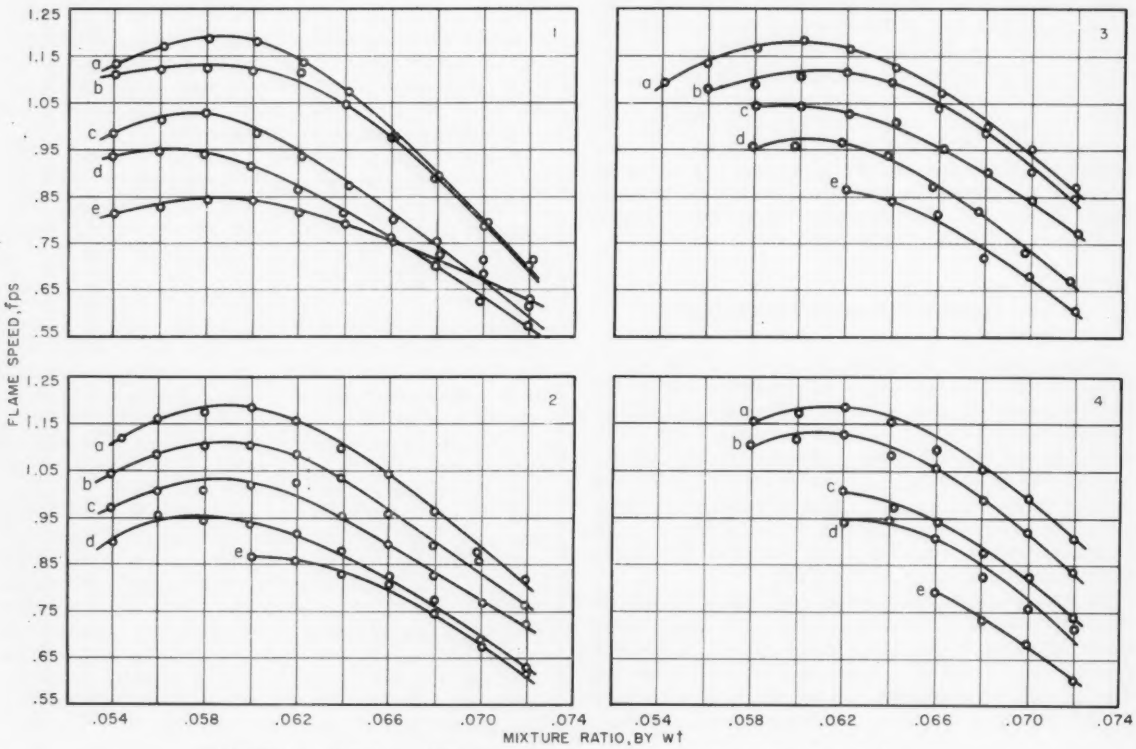

FIGURE 2. *Effect of addition of methyl bromide on the flame speed of methane.*

Percentage methyl bromide added: a=0.1; b=0.2; c=0.3; d=0.4; and e=0.5. Gas velocity=1, 3 fps; 2, 4 fps; 3, 5 fps; and 4, 6 fps.

shows the variation of flame speed with mixture ratio, by weight, of methane to air plus methyl bromide, when 0.1, 0.2, 0.3, 0.4, and 0.5 percent by volume, respectively, of methyl bromide is added to air, and at gas velocities of 3, 4, 5, and 6 fps.

For each addition of methyl bromide and at each gas velocity, there is found one value of mixture ratio at which flame speed is greatest. Maximum flame speed for a methane-air flame occurs at mixture ratio 0.062; addition of methyl bromide causes maximum flame speed to shift to leaner conditions, especially at the lower gas velocities. (Stoichiometric for a methane-air flame is equivalent to a mixture ratio of 0.0583.) Table 1 lists the maximum flame speeds and the experimental conditions at which they were observed.

TABLE 1. *Maximum flame speeds*

Flame speed	Wt CH_4 / Wt air+CH_3Br	Percent CH_3Br added to air	Flame speed / Flame speed CH_4-air	Gas velocity
fps				*fps*
1.196	0.062	0	----------	6
1.186	.058	0.1	0.992	3
1.125	.058	.2	.941	3
1.029	.058	.3	.860	3
0.945	.056	.4	.790	3
.843	.060	.5	.704	3
1.186	.060	.1	.992	4
1.103	.060	.2	.922	4
1.029	.062	.3	.860	4
0.958	.056	.4	.801	4
.864	.060	.5	.722	4
1.185	.060	.1	.991	5
1.117	.062	.2	.934	5
1.047	.058	.3	.875	5
0.967	.062	.4	.806	5
.867	.062	.5	.724	5
1.186	.062	.1	.992	6
1.127	.062	.2	.942	6
1.006	.062	.3	.841	6
0.945	.064	.4	.790	6
[a].790	.066	.5	.661	6

[a] Blow-off occurred at 0.064.

Flash-back which represents the rich limit of operation of the burner was not encountered at any of the experimental conditions used. Blow-off which represents the lean limit of operation was rather frequent especially at gas velocities of 5 and 6 fps. No cases of blow-off were encountered at 3 fps and only one at 4 fps; this occurred at mixture ratio of 0.058 with 0.5 percent CH_3Br added to the air. Table 2 lists the conditions at which the leanest flame could exist before blow-off occurred. It can be noted that as the amount of methyl bromide increases, the lean limit shifts toward fuel-rich conditions, while the flame speed becomes less. Rich flames are thus stabilized when methyl bromide is present.

Theoretically, the velocity with which combustible gas issues from a burner should have no effect on the flame speed. In practice, some variation of flame speed with gas velocity is noted [14]. In this present work, a small decrease of flame speed with increasing gas velocity, amounting to about 2 percent of the average value over the gas velocity range covered, was found at mixture ratios yielding maximum flame

TABLE 2. *Lean limit of operation of burner*

Percent CH_3Br added to air	Wt CH_4 / Wt air+CH_3Br	Gas velocity	Flame speed
		fps	*fps*
0.1	0.058	6	1.156
.2	.056	5	1.084
.2	.058	6	1.103
.3	.058	5	1.047
.3	.062	6	1.006
.4	.058	5	.958
.4	.062	6	.941
.5	.060	4	.864
.5	.062	5	.867
.5	.066	6	.790

speeds, and at leaner conditions. At rich conditions, flame speed increased with gas velocity, and the variation amounted to as much as 15 percent of the average value. Rich flames, however, are very tall as the flame speed is very low, and tall flames are very susceptible to disturbances. It is possible, therefore, that the increased variation of flame speed with gas velocity may be due to these disturbances.

The addition of methyl bromide to the combustion air reduces the maximum flame speed and the more methyl bromide added, the greater is the reduction in flame speed. Flames burning at mixture ratios greater than that at which maximum flame speed occurred are more affected by methyl bromide than are those burning at leaner conditions. At 0.1 percent methyl bromide addition, for example, and at a gas velocity of 3 fps, the maximum flame speed is 1.186 fps at a mixture ratio of 0.058. At a mixture ratio of 0.072 flame speed is 0.718 fps which is 60.6 percent of the maximum, while at mixture ratio 0.054, flame speed is 1.134 fps which is 95.6 percent of the maximum. The corresponding percentages for the methane-air flame are 82.0 percent at mixture ratio 0.072 and 88.4 percent at mixture ratio 0.054. The addition of 0.1 and 0.2 percent of methyl bromide even increases the flame speed at lean conditions. At a gas velocity of 3 fps, the flame speed at mixture ratio 0.054 is 1.134 fps for a 1 percent addition and 1.120 fps for 0.2 percent addition. For a methane-air flame, flame speed is 1.057 fps at mixture ratio 0.054 and a gas velocity of 6 fps.

In figure 3, flame speed is plotted against the percent of methyl bromide added to the combustion air. Mixture ratio is 0.062 and gas velocity is 5 fps. Flame speed decreases as the percentage of methyl bromide increases, and the data points fall along a straight line. For all experimental conditions of mixture ratio, gas velocity and methyl bromide addition, similar results were found. Hence, it may be deduced that the reduction in flame speed is directly proportional to the amount of methyl bromide, at least in the range of addition used in this work. In figure 4, the maximum flame speed at each addition of methyl bromide, at constant gas velocity, is plotted against the percentage of methyl bromide, and again the data points fall on a straight line, and the slopes of these lines are of similar magnitude.

The reduction in maximum flame speed is directly proportional to the amount of methyl bromide added and amounts to 0.0828 fps for each tenth percent of methyl bromide added.

In the method used for determining flame speeds, photographs of the schlieren and visible images of the flame are taken simultaneously on the same film. The schlieren image which depends on the change in density and thus on the change in temperature marks the position where chemical reactions begin in the flame [15]. The visible image indicates the region in the flame where reactions are completed [16] except for equilibrium changes. Hence, the separation between the schlieren and visible images is a measure of the thickness of the reaction zone. However, since both images in an enlarged photograph are rather diffuse, these measurements cannot be considered exact.

It is found that the thickness of the reaction zone varies with the flame speed; the greater the flame speed, the less is the thickness of the reaction zone. Figure 5 shows the variation of reaction zone thickness with mixture ratio at constant gas velocity; 0.2 percent methyl bromide was added to the air and the gas velocity was 4 fps. Similar curves are obtained for all the other experimental conditions. Figure 6 shows the variation of reaction zone thickness with added methyl bromide at constant mixture-ratio and at constant gas velocity. Mixture ratio was 0.070 and gas velocity was 6 fps. Zone thickness increases with the amount of methyl bromide added, and similar results were obtained at all other experimental conditions of mixture ratio and gas velocity. From some previously unreported experiments, it is found that the reaction zone thickness of a methane-air flame at fuel-air ratio of 0.070 and gas velocity of 6 fps was 0.0180 in. Minimum thickness was 0.015 in. and occurred at mixture ratio 0.062.

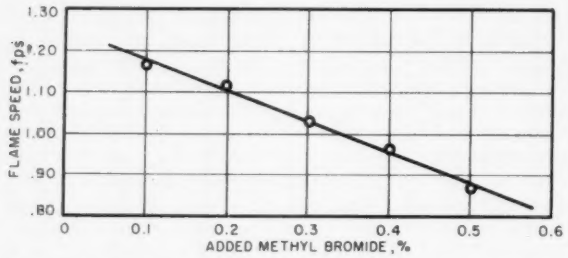

FIGURE 3. *Variation of flame speed with added methy bromide.*

Mixture ratio, by weight, =0.062. Gas velocity=5 fps.

The mechanism of combustion inhibition by halogenated hydrocarbons is not fully understood [5, 9, 11, 12]. Since the combustion of hydrocarbons in air involves the propagation of chain reactions by free radicals, it is plausible to assume that the presence of halogen results in the deactivation of one or more of the chain carrying radicals. Since deactivation would effectively decrease the rate of reaction, the general effect of chemical inhibitors in decreasing flame speeds would be explained. The increased reaction zone thickness which results on the addition of methyl bromide may also be explained by the effective decrease in reaction velocity.

The increase in flame speed noted at lean conditions at additions of 0.1 and 0.2 percent methyl bromide cannot be so explained. Since there is more oxygen in a lean flame, it may be that methyl bromide acts as a fuel rather than an inhibitor at this condition and the reaction mechanism is different. If methyl bromide acts as a fuel, then the mixture ratio should be expressed as $\frac{\text{wt methane + wt methyl bromide}}{\text{wt air}}$, in which case the

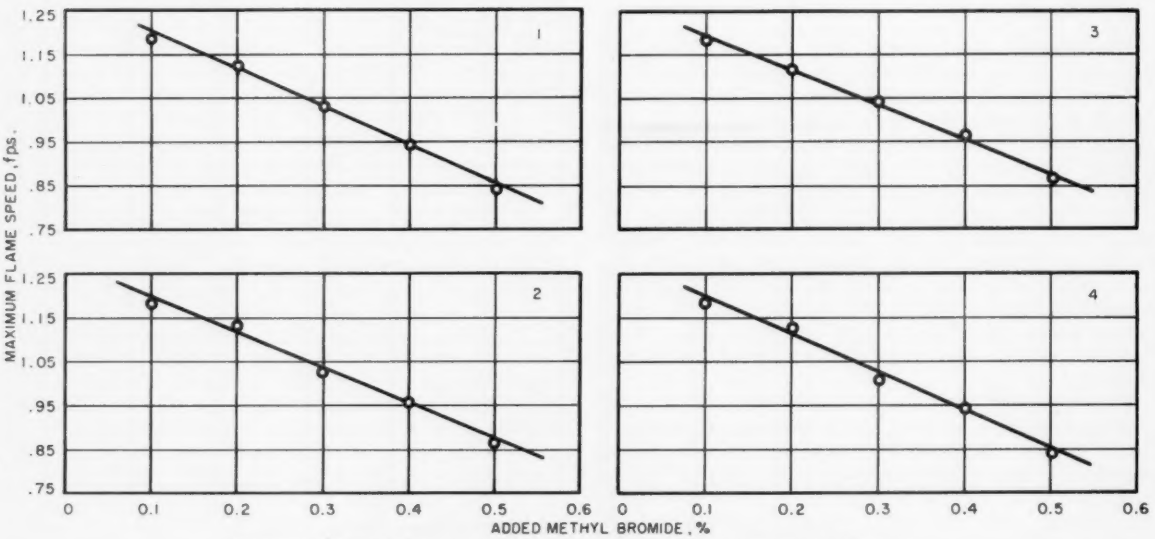

FIGURE 4. *Variation of maximum flame speed with added methyl bromide.*

Gas velocity—1, 3 fps; 2, 4 fps; 3, 5 fps; and 4, 6 fps.

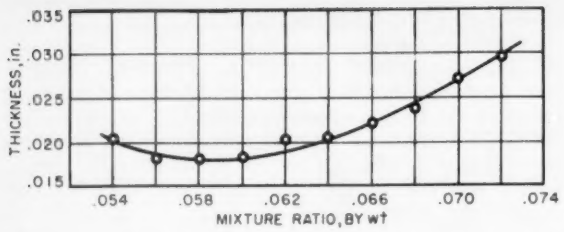

FIGURE 5. *Variation of reaction zone thickness with mixture ratio.*

0.2 percent methyl bromide added. Gas velocity=4 fps.

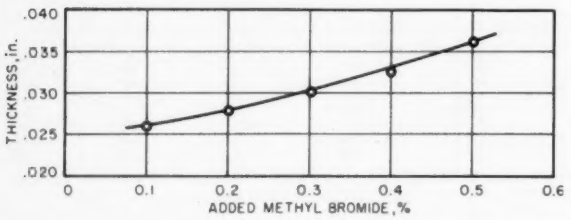

FIGURE 6. *Variation of reaction zone thickness with added methyl bromide.*

Mixture ratio 0.070. Gas velocity=6 fps.

value is 0.057 instead of 0.054, and 0.059 instead of 0.056 for the addition of 0.1 percent methyl bromide. Then if we superpose the curve for flame speed versus mixture ratio at 0.1 percent methyl bromide addition, using the new values of mixture ratio, on the curve for methane-air, the two curves agree for values of mixture ratio less than that at which maximum flame speed occurred.

4. Experimental Observations

Table 3 presents in detail observations on the effect of some variables on the flame speed and reaction zone thickness.

TABLE 3. *Effect of some variables on flame speed*

A. 0.1% CH_3Br added to air

Wt CH_4 / Wt air+CH_3Br	Reaction zone thickness	Gas temperature	Flame speed	Flame speed corrected to 75° F
1. Gas velocity=3 fps				
	in.	*°F*	*fps*	*fps*
0.05407	0.0155	91.3	1.187	1.134
.05608	.0146	91.4	1.224	1.170
.05807	.0168	90.0	1.234	1.186
.06013	.0165	90.6	1.236	1.185
.06216	.0168	90.9	1.190	1.138
.06410	.0190	91.2	1.127	1.074
.06610	.0200	91.3	1.032	.979
.06800	.0223	91.4	.944	.891
.07013	.0257	91.4	.834	.780
.07214	.0305	91.3	.771	.718

TABLE 3. *Effect of some variables on flame speed*—Continued

Wt CH_4 / Wt air+CH_3Br	Reaction zone thickness	Gas temperature	Flame speed	Flame speed corrected to 75° F
2. Gas velocity=4 fps				
	in.	*°F*	*fps*	*fps*
0.05436	0.0192	89.6	1.168	1.120
.05592	.0172	87.8	1.203	1.167
.05794	.0179	88.3	1.217	1.174
.05992	.0202	88.9	1.232	1.186
.06189	.0191	89.2	1.203	1.156
.06387	.0195	89.6	1.143	1.094
.06594	.0219	89.6	1.090	1.042
.06794	.0235	89.3	1.014	.967
.06989	.0272	89.3	.923	.876
.07196	.0295	89.3	.866	.818
3. Gas velocity=5 fps				
0.05409	0.0198	86.6	1.133	1.094
.05593	.0191	87.1	1.174	1.135
.05808	.0203	87.0	1.207	1.168
.06010	.0191	84.8	1.217	1.185
.06204	.0224	85.8	1.201	1.167
.06406	.0228	86.1	1.162	1.126
.06604	.0218	86.6	1.108	1.070
.06809	.0238	87.0	1.050	1.011
.07006	.0267	86.9	.991	.952
.07204	.0284	87.0	.904	.864
4. Gas velocity=6 fps				
0.05807	0.0190	86.1	1.192	1.156
.06003	.0203	86.2	1.208	1.171
.06200	.0192	85.6	1.223	1.186
.06402	.0212	84.9	1.186	1.153
.06601	.0225	85.4	1.129	1.095
.06800	.0238	86.0	1.092	1.056
.07003	.0260	86.1	1.027	.991
.07198	.0287	86.3	.943	.906

B. 0.2% CH_3Br added to air

1. Gas velocity = 3 fps				
	in.	*° F*	*fps*	*fps*
0.05406	0.0217	74.5	1.109	1.110
.05601	.0202	74.8	1.121	1.120
.05803	.0201	75.2	1.126	1.125
.05998	.0181	75.2	1.120	1.120
.06206	.0207	75.5	1.115	1.113
.06402	.0221	75.3	1.049	1.048
.06599	.0236	76.0	.983	.980
.06794	.0251	75.6	.890	.889
.07000	.0279	75.2	.787	.786
.07202	.0328	75.1	.706	.706
2. Gas velocity = 4 fps				
0.05394	0.0203	77.7	1.053	1.044
.05591	.0182	75.8	1.088	1.085
.05794	.0182	75.8	1.105	1.103
.05996	.0183	75.9	1.106	1.103
.06197	.0203	76.1	1.092	1.088
.06391	.0205	76.4	1.038	1.033
.06594	.0220	76.9	.966	.960
.06787	.0237	77.2	.899	.892
.06994	.0272	77.4	.859	.851
.07197	.0295	79.5	.778	.764
3. Gas velocity = 5 fps				
0.05600	0.0190	77.2	1.091	1.084
.05800	.0178	77.5	1.098	1.090
.05998	.0198	76.7	1.115	1.110
.06199	.0200	76.6	1.122	1.117
.06396	.0207	76.6	1.102	1.097
.06597	.0218	76.8	1.043	1.037
.06801	.0230	76.9	.995	.989
.06999	.0258	77.1	.912	.906
.07198	.0278	77.2	.882	.874

TABLE 3. *Effect of some variables on flame speed*—Continued

Wt CH_4 / Wt air+CH_3Br	Reaction zone thickness	Gas temperature	Flame speed	Flame speed corrected to 75° F
	4. Gas velocity = 6 fps			
	in.	*°F*	*fps*	*ps*
0.05798	0.0195	77.8	1.112	1.103
.05994	.0212	77.8	1.126	1.117
.06199	.0207	78.7	1.139	1.127
.06397	.0207	76.2	1.087	1.083
.06597	.0230	76.7	1.064	1.058
.06804	.0247	77.2	.996	.989
.06995	.0278	77.6	.931	.922
.07197	.0295	77.8	.844	.836
	C. 0.3% CH_3Br added to air			
	1. Gas velocity = 3 fps			
	in.	*°F*	*fps*	*fps*
0.05391	0.0237	80.6	1.004	0.985
.05602	.0253	80.0	1.029	1.013
.05799	.0220	79.6	1.044	1.029
.06019	.0234	79.8	1.001	.985
.06210	.0258	80.3	.956	.939
.06414	.0237	80.4	.892	.874
.06610	.0258	80.2	.817	.800
.06810	.0295	80.6	.747	.729
.06997	.0349	79.2	.701	.687
.07196	.0395	79.3	.631	.617
	2. Gas velocity = 4 fps			
0.05390	0.0203	78.3	0.984	0.973
.05594	.0200	77.3	1.016	1.008
.05796	.0190	76.5	1.013	1.008
.05996	.0228	76.7	1.024	1.019
.06193	.0217	77.1	1.036	1.029
.06393	.0252	78.3	.965	.954
.06596	.0240	79.1	.909	.896
.06794	.0260	78.9	.839	.827
.07002	.0299	77.9	.778	.769
.07196	.0297	77.2	.729	.722
	3. Gas velocity = 5 fps			
0.05804	0.0210	77.4	1.055	1.047
.06000	.0222	76.6	1.045	1.040
.06211	.0207	77.5	1.037	1.029
.06410	.0215	76.2	1.013	1.009
.06613	.0242	76.8	.959	.953
.06807	.0270	77.2	.913	.906
.07006	.0300	77.0	.847	.840
.07203	.0350	76.5	.757	.752
	4. Gas velocity = 6 fps			
0.06196	0.0232	77.8	1.015	1.006
.06418	.0247	77.4	.981	.974
.06607	.0272	78.9	.955	.942
.06804	.0283	77.3	.884	.877
.07006	.0300	77.4	.833	.825
.07198	.0345	77.8	.749	.740
	D. 0.4% CH_3Br added to air			
	1. Gas velocity=3 fps			
	in.	*°F*	*fps*	*fps*
0.05391	0.0203	72.5	0.930	0.938
.05593	.0207	73.9	.941	.945
.05795	.0209	75.0	.942	.942
.05993	.0218	75.4	.918	.917
.06194	.0225	75.8	.872	.869
.06393	.0248	74.6	.811	.812
.06596	.0270	72.7	.745	.752
.06790	.0315	72.9	.708	.701
.06988	.0372	74.6	.628	.623
.07195	.0408	75.3	.576	.575

TABLE 3. *Effect of some variables on flame speed*—Continued

Wt CH_4 / Wt air+CH_3Br	Reaction zone thickness	Gas temperature	Flame speed	Flame speed corrected to 75° F
	2. Gas velocity=4 fps			
	in.	*°F*	*fps*	*fps*
0.05395	0.0228	74.8	0.895	0.896
.05591	.0227	75.1	.958	.958
.05790	.0205	75.2	.945	.944
.05995	.0217	74.8	.935	.936
.06193	.0237	74.7	.916	.917
.06395	.0248	74.7	.877	.878
.06600	.0280	74.7	.804	.805
.06798	.0303	74.8	.770	.771
.07000	.0360	75.2	.677	.676
.07196	.0397	75.4	.628	.627
	3. Gas velocity=5 fps			
0.05795	0.0225	75.3	0.959	0.958
.05978	.0227	75.3	.957	.957
.06177	.0237	74.8	.967	.967
.06375	.0258	73.2	.934	.940
.06578	.0272	74.5	.872	.873
.06775	.0300	75.2	.822	.821
.06978	.0340	75.1	.730	.730
.07175	.0393	74.2	.672	.674
	4. Gas velocity=6 fps			
0.06202	0.0233	84.6	0.972	0.941
.06399	.0248	82.8	.971	.945
.06598	.0260	83.0	.934	.908
.06801	.0297	81.0	.843	.823
.07001	.0325	81.6	.778	.757
.07204	.0380	82.9	.741	.716
	E. 0.5% CH_3Br added to air			
	1. Gas velocity=3 fps			
	in.	*°F*	*fps*	*fps*
0.05399	0.0248	80.1	0.830	0.814
.05602	.0235	79.7	.844	.829
.05802	.0233	79.9	.858	.842
.06003	.0238	76.8	.849	.843
.06200	.0240	77.6	.826	.818
.06397	.0250	78.3	.801	.790
.06596	.0265	78.6	.773	.761
.06797	.0282	78.6	.769	.757
.07001	.0328	80.0	.734	.718
.07204	.0370	79.6	.629	.614
	2. Gas velocity=4 fps			
0.06000	0.0230	78.7	0.876	0.864
.06192	.0232	79.3	.871	.856
.06396	.0252	79.7	.844	.829
.06594	.0278	80.0	.811	.794
.06798	.0307	80.5	.761	.743
.07002	.0330	80.7	.706	.688
.07194	.0387	81.0	.633	.614
	3. Gas velocity=5 fps			
0.06196	0.0275	75.0	0.867	0.867
.06398	.0275	75.4	.841	.840
.06593	.0311	74.6	.813	.814
.06793	.0325	75.5	.719	.718
.06994	.0377	75.6	.682	.679
.07199	.0422	75.6	.604	.603
	4. Gas velocity=6 fps			
0.06599	0.0293	76.4	0.795	0.790
.06801	.0323	75.5	.735	.733
.06999	.0362	76.0	.684	.681
.07200	.0415	75.8	.603	.601

5. Conclusions

Small amounts of methyl bromide added to methane-air mixtures have a large effect on the flame speed. Maximum flame speed is reduced proportionately to the amount of methyl bromide added. Flame speed of rich mixtures is much more reduced than that of lean mixtures. Reaction zone thickness is increased by the presence of methyl bromide.

6. References

[1] R. F. Simmons and H. G. Wolfhard, Trans. Faraday Soc. **51,** 1211 (1955).

[2] F. H. Garner, R. Long, A. J. Graham, and A. Badakhshan, Sixth Symposium (International) on Combustion, p. 802, Reinhold Pub. Corp., N.Y. (1957).

[3] M. C. Burdon, J. H. Burgoyne, and F. J. Weinburg, Fifth Symposium (International) on Combustion, p. 647, Reinhold Pub. Corp., N.Y. (1955).

[4] J. H. Burgoyne and G. Williams-Leir, Proc. Roy. Soc. **A193,** 525 (1948).

[5] F. E. Belles and C. O'Neal, Jr., Sixth Symposium (International) on Combustion, p. 806, Reinhold Pub. Corp., N.Y. (1957).

[6] F. E. Belles, Nat. Advisory Comm. Aeronaut. Tech. Note 3565 (1955).

[7] J. E. Malcolm, Department of the Army, Engineering Research and Development Laboratories, Fort Belvoir, Va., Rept. 1177 (Aug. 18, 1950).

[8] E. C. Creitz, J. Research NBS **65A** (Phys. and Chem.) No 4, 389 (1961).

[9] W. A. Rosser, H. Wise, and J. Meller, Seventh Symposium (International) on Combustion, p. 175, Butterworths Scientific Pub., London (1959).

[10] G. Lask and H. G. Wagner, Eighth Symposium (International) on Combustion, p. 432, Williams and Wilkins, Baltimore, Md. (1962).

[11] R. Friedman and J. B. Levy, Wright Air Development Center Tech. Rept. 56–568 (1957).

[12] R. Friedman, Fire Research Abstracts and Reviews **3,** 128 (1961).

[13] A. Levy, J. W. Droege, J. Tighe, and J. F. Foster, Eighth Symposium (International) on Combustion, p. 524, Williams and Wilkins, Baltimore, Md. (1962).

[14] C. Halpern, J. Research NBS **60,** 535 (1958) RP2867.

[15] J. J. Broeze, Third Symposium (International) on Combustion, p. 146, Williams and Wilkins, Baltimore, Md. (1949).

[16] A. G. Gaydon and H. G. Wolfhard, Flames, their structure, radiation, and temperature, p. 96, Chapman and Hall, Ltd., London (1960).

(Paper 67A1–196)

JOURNAL OF RESEARCH of the National Bureau of Standards—A. Physics and Chemistry
Vol. 67A, No. 1, January–February 1963

Publications of the National Bureau of Standards*

Selected Abstracts

Reliability of a system in which spare parts deteriorate in storage, G. H. Weiss, *J. Research NBS* **66B** (*Math. and Math. Phys.*) *No. 4, 157 (Oct.–Dec. 1962). 75 cents.*
The problem considered is that of determining the failure statistics for a system consisting of a single part and n spares, in which it is assumed that that failure occurs at different rates in use and in storage. The resulting equations can be solved explicitly when both types of failures follow a Poisson law. Otherwise algorithms are given for the calculation of the failure probabilities.

Laguerre expansions for successive generations of a renewal process, G. H. Weiss, *J. Research NBS* **66B** (*Math. and Math. Phys.*) *No. 4, 165 (Oct.–Dec. 1962). 75 cents.*
It is shown that the coefficients in the Laguerre expansions for successive generations in a renewal process are related by an algebraic convolution. Thus the calculations are easily mechanized for computation.

An application of information theory to the analysis of contingency tables, with a table of $2n \ln n$, $n=1(1)10{,}000, S. Kullback, M. Kupperman, and H. H. Ku, *J. Research NBS* **66B** (*Math. and Math. Phys.*) *No. 4, 217 (Oct.–Dec. 1962). 75 cents.*
In this paper we present a number of useful tests for contingency tables in conjunction with a useful table to assist in the necessary computations. A consistent and simple approach based on the notions of information theory is used in developing the various test procedures and the results are analyzed in the form of analysis-of-information tables. Beginning with tests of hypotheses for a one-way table, tests of hypotheses of specified probabilities, independence, conditional independence, homogeneity of classifications, symmetry, and interaction are developed or indicated for contingency tables of two, three, four, and higher order classifications. Extension of these procedures to certain tests for Markov chains is indicated. Worked examples are given throughout the paper. A table of $2n \ln n$ for $n=1(1)$ 10,000 is appended for use in computation.

Use of surface refractivity in the empirical prediction of total atmospheric refraction, W. R. Iliff and J. M. Holt, *J. Research NBS* **67D** (*Radio Prop.*) *No. 1 31 (Jan.–Feb. 1963). 70 cents.*
The use of a 1.9-cm radio sextant capable of precise tracking of the sun has produced accurate measurements of total atmospheric microwave refraction. These data are used to verify the high correlation of such refraction with surface refractivity for low altitude angles. The values of the correlation coefficients obtained vary from 92.2 percent at 16 degrees to 98 percent at 2 degrees. An empirical predictor is developed, based on this correlation, which satisfactorily accounts for the observed refraction. The mathematical form of the predictor is given, and suggestions are made for its use.

Composition of reflection and transmission formulae J. Heading, *J. Research NBS* **67D** (*Radio Prop.*) *No. 1 65 (Jan.–Feb. 1963). 70 cents.*
An integral equation for the electric field in a continuously stratified ionized medium is derived; this is then manipulated to yield equations for the reflection and transmission coefficients, at the same time being susceptible to physical interpretation. The equations are solved by successive approximations, the first terms being a Fresnel-type coefficients. Various applications of the results are discussed.

Titheridge coefficients for the polynomial method of deducing electron density profiles from inograms A. R. Long and J. O. Thomas, *J. Research NBS* **67D** (*Radio Prop.*) *No. 1 79 (Jan.–Feb. 1963). 70 cents.*
Sets of Titheridge polynomial coefficients suitable for the conversion into electron density profiles of smooth virtual height frequency curves, such as those observed regularly at night, are presented for a series of values of the magnetic dip angle and gyrofrequency. These magnetic conditions have been chosen so that the coefficients are suitable for the analysis, to a reasonable degree of accuracy, of ordinary and extraordinary ray records obtained anywhere in the world. The coefficients may be used for the analysis of topside-sounder data to a first order of accuracy if the plasma frequency at the satellite is small.

Chemistry of cement. Proceedings of the Fourth International Symposium, Washington, 1960, *NBS Mono. 43, Vol. I (Aug. 31, 1962), $5.75; Vol. II (Sept. 27, 1962), $5.50. The two volumes are available at $11.25 a set.*
This two-volume Monograph contains the complete texts of all papers given at the Fourth International Symposium on the Chemistry of Cement, held in Washington, D.C., October 2–7, 1960. The publication represents one of the most complete reference works available on the subject, and presents the latest information in most of the fields of cement chemistry research. Topics covered, divided according to session titles: Volume I, Chemistry of clinker, chemistry of hydration of cement compounds, and chemistry of hydration of portland cement; Volume II, Properties of cement paste and concrete destructive processes in concrete, chemical additions and admixtures, and special cements.

Tables of Eisenstein functions. Vibrational contributions to the thermodynamic functions, J. Hilsenrath and G. G. Ziegler, *NBS Mono. 49 (July 12, 1962) $2.75.*
Tables are presented for the contribution of a harmonic oscillator to the free energy function, enthalpy function, entropy, and heat capacity of gases. Dimensionless values of the Planck-Einstein functions are given as a function of $x=Hc/kT$ for $x=0.0010(.0001)$ $0.1500(.001)$ $4.000(.01)$ $10.00(.2)$ 16.0. A second table which gives the contributions in cal/mole °K directly as a function of frequency μ, and temperature T, was computed using the values 1.43880 for the second radiation constant hc/k, and 1.98717 for the universal gas constant R. The arguments for the latter table are spaced at 10 wave number intervals from 100 cm^{-1} to 4000 cm^{-1}.

Bibliography on atomic transition probabilities, B. M. Glennon and W. Wiese, *NBS Mono. 50 (Aug. 1, 1962) 35 cents.*
A bibliography on atomic transition probabilities is presented. The papers are arranged according to elements and stages of ionization, and the method employed and class of transitions are indicated behind each reference. Only articles on discrete transitions, both permitted and forbidden, are listed. Also included is a supplementary list of papers dealing with transition probabilities from a general point of view, a table showing the availability of numerical material on the individual atoms and ions, and a table of conversion factors.

Experimental transition probabilities for spectral lines of seventy elements, C. H. Corliss and W. R. Bozman, *NBS Mono. 53 (July 20, 1962) $4.25.*
Relative intensities of 39,000 spectral lines with wavelengths between 2000 and 9000 angstroms have been determined on a uniform energy scale for seventy elements. The light source was an arc between copper electrodes to which a single element was added in the ratio of one atom of element to

1000 atoms of copper. The temperature of the arc was determined, by comparison of the observed intensities with published relative *gf*-values, to be 5100 ± 110°K. The degree of ionization of eleven elements in the arc was determined by comparison of intensities in spectra of neutral and ionized atoms with known absolute *gf*-values. With the aid of Saha's ionization equation, the electron density in the arc was found to be 2.4×10^{16}cm^{-3}. The ionization of seventy elements separately added to the arc was then calculated with Saha's equation. A correction was made for diffusion of atoms from the arc stream. With this information, relative values of *gf* on a uniform scale can be computed for the 25,000 lines which have been classified. By calibration with known absolute *gf*-values, the scale is put on an absolute basis. Absolute transition probabilities for 25,000 lines of 112 spectra have been calculated in this way and the results are tabulated by spectrum. The wavelength in angstroms, energy levels to the nearest kayser, *g*A in 10^8 per second, *gf*, and the log *gf* are given for each line.

Systems of electrical units, F. B. Silsbee, *NBS Mono. 56 (Sept. 20, 1962) 30 cents.*
The various systems of measurement, with their respective sets of units, used in the literature on electricity and magnetism are described in detail. Their historical development is summarized. The manner in which each is derived from either of the two alternative points of view of the experimentalist and the theoretician is compared and contrasted. The desirability of recognizing both points of view in international standardization, particularly when discussing rationalization, is pointed out. The present status of the absolute measurements on which all electrical units are based is reported, and tables are included for the conversion of equations and numerical values from one system to another.

A tabulation of the thermodynamic properties of normal hydrogen from low temperatures to 540 °R and from 10 to 1500 psia, Supplement A (British units), J. W. Dean, *NBS Tech. Note 120A (June 1962) 45 cents.*
Pressure, volume, temperature, internal energy, enthalpy, and entropy of normal hydrogen gas have been tabulated along isobars in 2 °R temperature steps. The range covered is from the saturation temperature to 540 °R and from a pressure of 10 to 1500 psia. The source of data is Research Paper 1932 of the National Bureau of Standards Journal Of Research. The method is described by which the data presented in Research Paper 1932 is reduced to properties directly useful for engineering calculations. A method is also described for estimating the effects of ortho-para compositions upon the tabulated properties.
Tabular values are presented in the dimensional units of the British system. The tabulations are also available in the dimensional units of the metric system as technical Note No. 120.

The thermodynamic properties of helium from 3 to 300° K between 0.5 and 100 atmospheres, D. B. Mann, *NBS Tech. Note 154 (Jan. 1962) 50 cents.*
The specific volume, enthalpy, entropy, and internal energy values of helium are presented in tabular form as functions of pressure and temperature.
Data are tabulated in one degree Kelvin increments for forty isobars between 0.5 atmospheres and 100 atmospheres. A comparison with previously published data is made where applicable.
An expression is presented which represents the pressure-density-temperature surface based on previously published data.
The tabulation is presented in the dimensional units of the metric system, but is also available in the dimensional units of the British system (Supplement A).

Photosensitized reaction between hydrogen (^{2}P) atoms and molecular nitrogen, I. Tanaka and J. R. McNesby, *J. Chem. Phys.* **36,** *No. 12, 3170–3173 (June 15, 1962).*
The reaction between H(^{2}P) atoms and molecular introgen has been studied. H(^{2}P) atoms were produced by irradiating ground state H(^{2}S) atoms, generated in a microwave discharge, with Lyman alpha radiation at 1216 Å (ca. 10^{14}–10^{15} quanta sec $^{-1}$). The interaction of H(^{2}P) atoms with N_2 produces ammonia but not hydrazine. Two alternative mechanisms of the primary reaction are proposed. The first involves transfer of electronic energy.

$$H(^2P) + N_2(^1\Sigma^+g) \rightarrow H(^2S) + N_2^* \quad (2)$$

$$N_2^* \rightarrow 2N(^4S) \quad (3)$$

The second possibility is a chemical mechanism involving atom transfer.

$$H(^2P) + N_2(^1\Sigma^+g) \rightarrow NH(^3\pi_1) + N(^4S) \quad (4)$$

Ammonia is formed either by reaction of N with H or by reaction of NH with H or H_2.

Effect of particle size on low-temperature heat capacities, A. C. Victor, *J. Chem. Phys.* **36,** *No. 10, 2812–2813 (May 15, 1962).*
A new model is proposed to account for the particle size effect in low temperature heat capacities. As a first approximation a continuum approach is used. The model gives excellent agreement with sodium chloride data. Moderate success is also obtained with magnesium oxide and beryllium oxide.

Effect of molecular oxygen on the emission spectra of atomic oxygen-acetylene flames, S. L. N. G. Krishnamachari and H. P. Broida, *J. Chem. Phys.* **34,** *1709–1711 (1961).*
Studies have been made of the emission (3000 to 6000 A) obtained from low pressure atomic oxygen-acetylene flames diluted with varying amounts of molecular oxygen and molecular nitrogen. Added molecular oxygen greatly increased the OH emission while reducing CH and C_2 emission. It also had an effect on the rotational intensity distribution of OH and on the vibrational intensity distribution of C_2. Nitrogen addition greatly reduced the rotational and vibrational "temperatures" and decreased C_2 emission relative to the other emitters.

The structure of the vibrational-rotational bands of an asymmetric rotor, H. C. Allen, Jr., *Phil. Trans. Roy. Soc. London, Ser. B. Math. and Phys. Sci.* **253,** *No. 1030, 335–357 (Apr. 27, 1961).*
The structure of A- and C-type vibrational-rotational bands of an asymmetric rotor is related to the band types of the two limiting symmetric rotors. The effect of the degree of asymmetry and the change in the effective inertial constants between the two vibrational states on the band structure is shown. The type of information which can be obtained from the analysis of these two types of band is pointed out.

Real representations of coordinate rotations, U. Fano, *J. Math. Phys.* **1,** *No. 5, 417–423 (Sept.–Oct. 1960).*
Since irreducible tensorial sets that represent observables are of integral degree, their transformations under coordinate rotations have real representations. Real representations, with rows and columns classified by eigenvalues of the commuting operators J_z^2 and $\exp(i\pi J_y)$, are given explicitly, so that complex functions of rotation angles need not be used. The addition of angular momenta is worked out for sets in the real representation such as the sets of real orbital wave functions. Applications to the theory of angular distributions are discussed.

Structural and internal state variables in the description of scalar rate processes in fluids, R. E. Nettleton, *Phys. Fluids* **4,** *1488 (1961).*
Arguments are presented to show that the internal energy per molecule in a macroscopically small volume element of an infinite liquid should remain constant, in first approximation, during a sudden fluctuation in liquid structure at constant density and temperature. This result is shown to be consistent with a formulation of non-equilibrium thermodynamics in which the departures of structural parameters from their local equilibrium values appear as thermodynamic variables and in which there is no relaxing structural specific heat. However, it is shown that such a relaxing specific

heat must appear in the thermodynamic treatment of thermal variables, which give the populations of internal vibrational-rotational states; and a new non-equilibrium thermodynamics of thermal relaxation, extending the earlier work of Meixner to include inertial effects, is formulated in such a way as to be consistent with this fact. The new formulation, which replaces a previous theory now shown to be valid only for structural variables, is based on the Pauli equation, generalized to include second-order time-derivatives. It is shown, on plausible assumptions about the molecular transition probabilities, that one can calculate all the rate constants and relaxation times introduced to describe inertial effects, as well as the thermodynamic forces.

Quantum-mechanical calculation of harmonic oscillator transition probabilities in a one-dimensional impulsive collision, K. E. Shuler and R. W. Zwanzig, *J. Chem. Phys.* **33,** *No. 6, 1778–1784 (Dec. 1960).*
The quantum mechanical vibrational transition probabilities $P_{i\to f}(\epsilon)$ for harmonic oscillators, undergoing impulsive hard sphere collisions along the line of centers with an incident atom with relative kinetic energy ϵ, have been computed by a machine (IBM–704) solution of the relevant Schrödinger equation. Curves for $P_{i\to f}(\epsilon)$ over a range of ϵ are presented for initial (i) and final (f) vibrational oscillator states i, f=0, 1, 2 and 3. It is shown that this model of an inelastic collision gives rise to appreciable vibrational transitions $v(i)\to v(f)$ with $|\Delta v|>1$ (in addition to the $|\Delta v|=1$ transitions) in contrast to the Landau-Teller-Herzfeld adiabatic, 1st order perturbation treatment which permits only transitions for which $|\Delta v|=1$. The implication of this result is discussed in relation to the dissociation of diatomic molecules and to the adsorption of atoms on solids. Averaged transition probabilities $\overline{P}_{i\to f}(T)$ are computed for an incident beam of particles with a Maxwellian velocity distribution. It is pointed out that such averaged transition probabilities may give a misleading impression of the efficiency of translational-vibrational energy transfer if the $P_{i\to f}(\epsilon)$ show a resonance type of behavior, i.e. a strong order of magnitude dependence of $P_{i\to f}(\epsilon)$ on ϵ over a small interval of ϵ.

The vapor pressure of 20 °K equilibrium hydrogen, L. C. Weber, Jr., D. E. Diller, H. M. Roder, and R. D. Goodwin, *Cryogenics* **3**, *236–238 (June 1962).*
The vapor pressure of 20 °K equilibrium hydrogen has been measured between the normal boiling point and the critical point. The data are represented analytically for purposes of smoothing and interpolation, and the results are compared with earlier work.

The densities of saturated liquid hydrogen, R. D. Goodwin, D. E. Diller, H. M. Roder, and L. A. Weber, *Cryogenics* **2**, *81–83 (Dec. 1961).*
Densities of para hydrogen from 17° to 32 °K are obtained by extrapolating newly determined compressed liquid isotherms to corresponding vapor pressures. Results are combined with earlier data for the range 14° to 20 °K and compared with normal hydrogen by means of density-temperature relationships.

Reference tables for 40% iridium-60% rhodium versus iridium thermocouples, G. F. Blackburn and F. R. Caldwell, *Book, Temperature, Its Measurement and Control in Science and Industry* **3**, *Pt. 2, 161–175 (Reinhold Publ. Corp., New York, N.Y., 1962).*
In a program to establish reference tables for several alloys of iridium and rhodium against iridium, the work has been completed on 40% iridium-60% rhodium. Tables have been prepared giving emfs for temperatures in degrees Fahrenheit from 32 °F to 3800 °F and in degrees Celsius (centigrade) from 0 °C to 2100 °C, and temperatures in these units with emf in millivolts as the argument. They are based on the average emfs measured on eight thermocouples, made from three lots of wire obtained in 1955, 1958 and 1960.
Measurements at temperatures 32 °F to 2500 °F were made in a platinum-wound furnace of conventional design, using a Pt-10% Rh vs Pt thermocouple to measure temperature. From 1950 °F to 3800 °F (thus overlapping the upper end of the lower range), the furnace used was an iridium block heated by electric induction. Blackbody conditions prevailed in the cavity in which the test thermocouple was inserted, and enabled measurement of the temperature with an optical pyrometer.

Rate of vaporization of refractory substances, J. J. Diamond, J. Efimenko, R. F. Hampson, and R. F. Walker, *(Proc. 4th Intern Symp. Reactivity of Solids), Book, Reactivity of Solids, ed., J. H. de Bower et al., p. 725 (Elsevier Publ. Co., Amsterdam, The Netherlands, 1961).*
The more important factors affecting the rate of vaporization of solid systems are summarized. Techniques for measuring the rates of vaporization of refractory substances at temperatures in the 1600–3000 °C range are briefly described. The techniques pertain to measurements both in vacuum and in the presence of foreign gases. Some of the factors and the experimental techniques are illustrated by brief reference to studies of the vaporization of platinum and aluminum oxide.

Young's modulus of single crystal corundum from 77 °K to 850 °K, J. B. Wachtman, Jr., W. E. Tefft, and D. G. Lam, Jr., *Book, Mechanical Properties of Engineering Ceramics, p. 221–223 (Interscience Publ. Inc., New York N.Y., 1961).*
An equation is proposed to represent the temperature dependence of Young's modulus. This equation fits data on some corundum single crystals very well.

The dynamic compressibility of a rubber-sulfur vulcanizate and its relation to free volume, J. E. McKinney, H. V. Belcher, and R. S. Marvin, *Trans. Soc. Rheology* **4**, *347–362 (1960).*
The dynamic bulk compliance of natural rubber=12% sulfur was measured for varying static pressure (0 to 1000 bar), temperature (−30 to +70 °C), and frequency (50 to 1000 cps). The data can be represented by reduced frequency or temperature plots, assuming viscosity is proportional to $\exp(1/\varphi)$, a fractional free volume which is a linear function of temperature and pressure. The temperature-frequency reduction fits the "universal" WLF constants, and the temperature-pressure reduction term is practically the same as that found by Singh and Holle for polyisobutylene.

Absorption spectrum of CF_2 trapped in an argon matrix, A. M. Bass and D. E. Mann, *J. Chem. Phys.* **36**, *No. 12, 3501–3502 (June 15, 1962).*
The products of a discharge through a mixture of C_4F_8 and argon were condensed on a liquid-helium cooled surface. The absorption spectrum of the condensate shows a series of broad bands in the region 2300 to 2700A, and appears to correspond to the spectrum of the CF_2 radical.

Thermocouple materials, F. R. Caldwell, *Book, Temperature, Its Measurement and Control in Science and Industry* **3,** *Pt. 2, 81–134 (Reinhold Publ., Corp., New York, N.Y., 1962).*
Thermocouple materials are considered that are used primarily as immersion temperature sensors in the range from 0 °C up. Included are the conventional thermocouples that have survived since the beginnings of the art of thermoelectric temperature measurement, newer noble metal thermocouples, and thermocouples of refractory metals for use in the extreme range for immersed sensors. Because of the wide use and increasing popularity of ceramic-packed thermocouples in metal sheaths, they are included.
Limitations of the thermocouple wires are given as to range, stability, environment included atmosphere, magnitude of thermoelectric emf, and accuracy of commercially available materials of standard and extra quality. In addition, properties of the separate elements that are pertinent to the selection or use of thermocouples have been compiled.
In the case of the ceramic-packed thermocouples the following properties are presented: temperature range of the sheath, mechanical properties of the sheath, kinds of packed insulation, resistance between thermocouple wires and between wires and sheath, minimum bending radius of the packed stock, gas-tightness of the packed insulation, and types of measuring junctions available, i.e. grounded, ungrounded, bare, totally enclosed, stagnation mounting, etc.

Thermal radiation standards and measurements of the Radiometry Section at the National Bureau of Standards, A. G. Maki, (*Proc. conf. Radiative Transfer from Solid Materials, Boston, Mass., Dec. 12–13, 1960*), *Book, Radiative Transfer from Solid Materials, ed., H. H. Blau, Jr., and H. Fischer, Sec. III, p. 135–141* (*The Macmillan Co., New York, N.Y., 1962*).
A discussion was given of two aspects of the work of the Radiometry Section at the National Bureau of Standards. Two standards of thermal radiation were described and the method of their calibration detailed. The latter half of this paper will include a description of some work currently being carried on with the aim of obtaining the normal spectral emissivity of gold, aluminum, and platinum in the infrared.

The ammonia beam maser as a standard of frequency, J. A. Barnes, D. W. Allan, and A. E. Wainwright, *IRE Trans. Instrumentation* **I-11,** *26–30* (*June 1962*).
It has been suggested that an error in tuning of the resonant cavity in an ammonia beam maser could be detected by observing a frequency shift of the maser with the application of a magnetic field. Following this suggestion, an oscillatory magnetic field was applied to the NBS double beam maser and a low noise phase demodulator was constructed to detect any phase modulation present in the maser signal. With this equipment, a servo-loop was completed to constantly control the tuning of the maser's resonant cavity. Not only did this result in the elimination of the most critical parameter of the maser's frequency dependence, but improvement of the frequency dependence upon other parameters was also observed.

The radiative formation and destruction of negative ions, L. M. Branscomb, *Proc. Fifth Intern. Conf. Ionization Phenomena in Gases, Munich, Germany, I, 1–18* (*North Holland Publ. Co., Amsterdam, The Netherlands, 1961*).
Recent advances in our understanding of the formation and destruction of negative ions by radiative processes are reviewed. Photodetachment spectra of four atomic ions, H^-, O^-, S^- and C^- have been studied experimentally in crossed beams. Agreement between theory and experiment on H^- is now excellent, except in the threshold region, where the theoretical values are about 10% low, presumably because of neglect of polarization effects. The C^- spectrum is consistent with that expected for a $C^{-4}S$ ground state, about 1.25 ev below the continuum, and a weakly bound metastable (presumably ^2D) state which gives rise to a weak absorption on the infrared side of the 1.25 volt threshold. Metastable states of other atomic ions are predicted. Radiative attachment cross sections and rate coefficients are discussed. The difficulties in interpretation of molecular photodetachment spectra are emphasized.

Group theory and crystal field theory, C. M. Herzfeld and P. H. E. Meijer, *Book, Solid State Physics* **12,** *1–91* (*Academic Press, Inc., New York, N.Y., 1961*).
A survey of the principal group theoretical principles and methods used in crystal field theory.

Ferroelectricity in the compound $Bi_4Ti_3O_{12}$ P. H. Fang and C. R. Robbins, *Phys. Rev.* **126,** *No. 3, 892* (*May 1962*).
Some ferroelectric and crystallographical properties of the compound $Bi_4Ti_3O_{12}$ are presented. The compound has a dielectric maximum at 685°C on increasing temperature and at 670°C on decreasing temperature. At these temperatures, temperatures, an endothermic peak and an exothermic peak, respectively, occur. Ferroelectricity was observed along the *c* axis of the single crystal of this compound.

Linear thermal expansion of aluminum oxide and thorium oxide from 100° to 1100° K, J. B. Wachtman, Jr., T. G. Scuderi, and G. W. Cleek, *J. Am. Ceram. Soc.* **45,** *310–323* (*July 1962*).
The linear thermal expansion of single crystal and polycrystalline aluminum oxide and polycrystalline thorium oxide was measured from 100° to 1100° K with an interferometric technique. For each substance the results are well described by Grüneisen's equation using a Nernst-Lindemann energy function.

Dielectric loss in "non-polar" polymers, A. J. Curtis, *J. Chem. Phys.* **36,** *No. 12, 3500* (*June 15, 1962*).
Using published values of dipole moments of some saturated hydrocarbons, obtained from microwave spectroscopy, we have shown that the dielectric dispersion and loss observed in hydrocarbon polymers may be reasonably accounted for in large part in terms of asymmetry in structure. These calculations show that it is not necessary to propose impurities, oxidation products such as carbonyl groups, or catalyst fragments to account for much of the dielectric relaxation in these materials. These calculations also predict considerably lower dielectric loss in a completely linear polymer such as polyethylene than in a branched material such as polypropylene.

Mobilities of positive ions in argon, E. C. Beaty, *Proc. Conf. Ionization Phenomena in Gases, Aug. 28–Sept. 1, 1961, Munich, Germany, p. 183* (*North Holland Publ. Co., Amsterdam, The Netherlands, 1962*).
Ions of three different mobilities are observed in the afterglow of a pulsed discharge in pure argon. The low field mobilities are: $1.535 \pm .007$, $1.833 \pm .008$, $2.60 \pm .02$ ($cm^2\ volt^{-1}\ sec^{-1}$). The lowest value is associated with A^+. The identities of the other two are uncertain; however, semi-quantitative data are presented which indicate that each of the three are argon ions and are not the products of charge exchange with a contaminant. The ion of intermediate mobility was called A^+ by Munson and Tyndall, and A_2^+ by Hornbeck. The fastest ion was called A_2^+ by Biondi and Chanin.

Infrared spectrum of dideuteroacetylene (C_2D_2), E. D. Tidwell and E. K. Plyler, *J. Opt. Soc. Am.* **52,** *No. 6, 656–664* (*June 1962*).
Thirty bands of C_2D_2 have been observed and measured between 1900 and 3300 cm^{-1}. Twenty of these have been resolved well enough to permit extraction of rotational constants. The Δ_2F values up to J35 for three Σ_g ground state bands were averaged and correlated with other data for a more reliable $B_o = 0.84794 \pm 0.00005$ and $D_o = 7.85 \times 10^{-7} \pm 0.4 \times 10^{-7}$ where the indicated uncertainties are the probable errors of the coefficients. Better resolution and higher J values have reduced the uncertainty derived from other sources. The l-type doubling constants for v_4^1 and v_5^1 have been obtained from resolved Q branches and split P and R branches; they are $q_4 = .00316$ cm^{-1} and $q_5 = .00314$ cm^{-1}.

Other NBS Publications

Journal of Research 66B (Math. and Math. Phys.), No. 4 (Oct.–Dec. 1962), 75 cents.
Reliability of a system in which spare parts deteriorate in storage. G. H. Weiss. (See above abstracts.)
Estimation of dispersion parameters. W. A. Thompson, Jr.
Laguerre expansions for successive generations of a renewal process. G. H. Weiss. (See above abstracts.)
Bounds on ratios of means. G. T. Cargo and O. Shisha.
A model for the viscoelastic behavior of rubberlike polymers including entanglement effects. R. S. Marvin and H. Oser.
Black box maximization of circular coverage. C. T. Zahn, Jr.
An application of information theory to the analysis of contingency tables, with a table of $2n\ 1n\ n$, $n = 1(1)10{,}000$. S. Kullback, M. Kupperman, and H. H. Ku. See above abstracts.)

Journal of Research 67D (Radio Prop.), No. 1 (Jan.–Feb. 1963), 70 cents.
A lunar theory reasserted—a rebuttal. J. V. Evans.
Point-to-point communication on the moon. L. E. Vogler.
HF communication during ionospheric storms. G. E. Hill.
Use of surface refractivity in the empirical prediction of total atmospheric refraction. W. R. Iliff and J. M. Holt. (See above abstracts.)
Effective sunspot numbers. W. B. Chadwick.
On the theory of radio wave propagation over inhomogeneous earth. K. Furutsu.
Fields of electric dipoles in sea water (a correction). W. Anderson.
Composition of reflection and transmission formulae. J. Heading. (See above abstracts.)

Titheridge coefficients for the polynomial method of deducing electron density profiles from ionograms. A. R. Long and J. O. Thomas. (See above abstracts.)

Input admittance of linear antennas driven from a coaxial line. T. T. Wu.

A survey of the techniques for measuring the radio refractive index, R. E. McGavin, NBS Tech. Note 99 (May 1962), 30 cents.

Required signal-to-noise ratios, RF signal power, and bandwidth for multichannel radio communications systems, E. F. Florman and J. J. Tary, NBS Tech. Note 100 (Jan. 1962), $1.00.

Mode conversion in the earth-ionosphere waveguide, J. R. Wait, NBS Tech. Note 151 (June 8, 1962) 20 cents.

A general survey of the semiconductor field, G. W. Reimherr, NBS Tech. Note 153 (Aug. 1962) 30 cents.

Information selection systems retrieving replica copies: A state-of-the-art report, T. C. Bagg and M. E. Stevens, NBS Tech. Note 157 (Dec. 31, 1961) $1.25.

Efficient use of the radio spectrum, K. A. Norton, NBS Tech. Note 158 (Apr. 1962) 45 cents.

A Fortran code for calculation of eigenvalues and eigenfunctions in real potential wells, R. S. Casewell, NBS Tech. Note 159 (August 1962) 25 cents.

A procedure for estimating eigenvalues, N. W. Bazley and D. Fox, J. Math. Phys. **3,** 469–471 (May–June 1962).

Physical standards of emittance and reflectance, J. C. Richmond, (Proc. Conf. Radiative Transfer from Solid Materials, Boston, Mass., Dec. 12–13, 1960), Book, Radiative Transfer from Solid Materials, ed. H. H. Blau, Jr., and H. Fischer, Sec. III, p. 142–153 (The Macmillan Co., New York, N.Y., 1962).

Tchebycheff approximations by exponentials, J. R. Rice, J. Soc. Ind. Appl. Math. **10,** No. 1, 149–161 (Mar. 1962).

Signs of nuclear resonance coupling constants in saturated aliphatic systems, H. Finegold, Proc. Chem. Soc. p. 213–214 (June 1962).

The morphology of mid-latitude 6300 angstrom arcs, T. Tohmatsu and F. E. Roach, J. Geophys. Res. **67,** No. 5, 1817–1821 (May 1962).

Some electrical properties of the porous graphite contact on p-type silicon, G. G. Harman, T. H. Higier, and O. L. Meyer, J. Appl. Phys. **33,** 2206 (July 1962).

A combined analog-digital differential analyzer (CADDA), W. D. Urban, W. R. Hahn, Jr., and H. K. Skramstad, Proc. Combined Analog Digital Computer Systems Symp., Phila., Pa., Dec. 1960, 2d item (1960).

The types of blackout, their time variations, and the mechanisms producing them, V. Agy, J. Phys. Soc. Japan **17,** 93–97 (Sept. 1961).

Some properties of dirty contacts on semi-conductors and resistivity measurements by a two terminal method, G. G. Harman and T. Higier, J. Appl. Phys. **33,** 2198 (July 9 62).

A property of linear frequency modulation, A. J. Goldman, Proc. IRE **50,** No. 7, 1711 (July 1962).

Programming for a closed-loop manned-machine combined system, D. C. Friedman, Proc. Combined Analog Digital Computer Systems Symp., Phila., Pa., Dec. 1960, 12th item (1960).

Studies in non-equilibrium rate processes. V. The relaxation of moments derived from a master equation, K. E. Shuler, K. Anderson, and G. H. Weiss, J. Math. Phys. **3,** No. 3, 550–556 (May–June 1962).

The thermal properties of powder insulators in the temperature range 300°–4 °K, D. Cline and R. H. Kropschot (Proc. Conf. Radiative Transfer from Solid Materials, Boston, Mass., Dec. 12–13, 1960), Book, Radiative Transfer from Solid Materials, ed. H. H. Blau, Jr., and H. Fischer, Sec. I, p. 61–81 (The Macmillan Co., New York, 1962).

Kineties of the hydrolysis of acetal in N-methylpropionamide-water and N, n-dimethylformamide-water solvents at 20, 25, 30, and 40°, R. K. Wolford and R. G. Bates, J. Phys. Chem. **66,** No. 8, 1496–1500 (1962).

Symposium on spectroscopic excitation, B. F. Scribner, Am. Soc. Testing Materials Spec. Tech. Publ. 259, 1 (Oct. 1960).

Path loss measurements versus prediction for long distance tropospheric scatter circuits, A. F. Barghausen and C. F. Peterson, IRE Trans. Commun. Systems **CS–9,** No. 4, 439–445 (Dec. 1961).

Introduction to the theory of V.L.F. propagation, J. R. Wait, Proc. IRE **50,** 1624–1647 (July 1962).

Some experimental aspects of nuclear orientation, E. Ambler, Proc. Tenth Intern. Congress of Refrigeration, Copenhagen, Denmark, **I,** 195–198 (1959).

The cement reference laboratory (1929–1959), J. R. Dise, Am. Soc. Testing Materials Proc. **59,** 369 (1959).

International coordination of measurement, A. G. McNish, McNish, Sci. Math. Weekly **2,** No. 3, 28–29 & 35 (Sept. 1961).

The calibration at the National Bureau of Standards of mass standards for ultramicroanalysis, L. B. Macurdy, Book, Vacuum Microbalance Techniques, ed. R. F. Walker, **2,** 165–175 (Plenum Press, Inc., New York, N.Y., 1962).

Post office mechanization, B. M. Levin, M. C. Stark and P. C. Tosini, Elec. Eng. **80,** No. 2, 105–110 (Feb. 1961).

Irreversible processes in liquids and the density matrix: monatomic molecules, R. E. Nettleton, Phys. Fluids **5,** No. 6, 687–700 (June 1962).

Switching properties in ferroelectrics of the family $Bi_4Ba_{m-2}Ti_{m+1}O_{3(m+2)}$, P. H. Fang and E. Fatuzzo, J. Phys. Soc. Japan **17,** 238 (1962).

A derivation of the relaxation spectrum representation of the mechanical response function, R. S. Marvin, Repts. Progr. Polymer Phys. Japan **5,** 56–58 (1962).

Thermal isomerization of isopropyl-1,1,1-d_3 radicals, W. M. Jackson and J. R. McNesby, J. Chem. Phys. **36,** No. 9, 2272–2275 (May 1, 1962).

Research on light metals in the Metallurgy Division, National Bureau of Standards, T. G. Digges, (Symp. Light Metal Industry, Jamshedpur, India) Indian Construction News, p. 68 (Aug. 1961).

A nomograph for selecting light balancing filters for camera exposure of color films, C. S. McCamy, Med. Biol. Illustration, London, England **11,** No. 1, 13–15 (Jan. 1961).

Attempts to eliminate fatigue damage by heat treatment, J. A. Bennett, Am. Soc. Metals, Trans. Quart. (Tech. Notes) **55,** No. 2, 362–363 (June 1962). Graphs for bivariate normal probabilities, M. Zelen and N. C. Severo, Ann. Math. Stat. **31,** No. 3, 619–624 (Sept. 1960).

A controller for maintaining a constant rate of vaporization in fractional distillation, E. C. Kuehner and R. T. Leslie, Anal. Chem. **34,** No. 9, 1155–1156 (Aug. 1962).

Nuclear moment of NI^{61}, L. H. Bennett and R. L. Streever, Jr., Phys. Rev. Letters **121,** No. 6, 2141–2142 (June 15, 1962).

A method for determining mechanical resonance frequencies and for calculating elastic moduli from these frequencies, S. Spinner and W. E. Tefft, Am. Soc. Testing Materials Proc. **61,** 1221–1238 (1961).

New uses of microfilm with electronic scanners, a progress report on FOSDIC III, M. L. Greenough, Proc. 8th Annual Meeting Natl. Microfilm Assoc., Wash. D.C. Apr. 2–4, 1959, p. 278 (Annapolis, Md., 1959).

Susceptor elements for high temperature induction heating, S. Hasko and H. S. Parker, Am. Ceram. Soc. Bull. **41,** No. 7, 467 (July 1962).

Relation of solar active regions at central meridian passage to ionospheric disturbance, C. S. Warwick and J. V. Lincoln, AGARDograph Proc. Sixth AGARD Ionospheric Research Committee Meeting (Rome, Italy, May 15–18, 1961).

Suggested arrangement of mirrors to form multiple reference angles, J. B. Saunders, J. Opt. Soc. Am. **51,** No. 8, 859–862 (Aug. 1961).

Radiolysis of ethane-1,1,1-d_3, L. J. Stief and P. Ausloos, J. Chem. Phys. **36,** No. 11, 2904 (June 1, 1962).

D-C differential current meter, E. Niesen, Rev. Sci. Instr. **32,** No. 12, 1407–1408 (Dec. 1961).

Radiowave propagation during world war II, K. L. Norton, Proc. IRE **50,** No. 5, 698–704 (May 1962).

Development directions to keep leather apace, J. R. Kanagy, Leather & Shoes **142,** 34–35 (Aug. 12, 1961).

High-energy X-ray spectrometer using large anticoincidence sodium iodide crystals, J. M. Wycoff, Proc. Total Absorp-

tion Gamma-Ray Spectrometry Symp., Gatlinburg, Tenn., May 10, 1960, p. 201–210 (1960).

Radio propagation quality in the North Atlantic area 1953–1960, M: E. Nason, AGARDograph Proc. 6th AGARD Ionospheric Research Committee Meeting (Rome, Italy, May 15–18, 1961).

Discussion of Feldman's and Sereda's Paper "Characteristics of sorption and expansion isotherms of reactive limestone aggregate," C. M. Hunt, L. A. Tomes, R. G. Pike, and D. Hubbard, J. Am. Concrete Inst. **59,** 815–818 (Mar. 1962).

The National Bureau of Standards Library, S. A. Jones, D. C. Libraries **32,** 7–10 (Jan. 1961).

Systematic errors, W. J. Youden, Ordnance XLVI, No. 248, 299–301 (Sept.-Oct. 1961).

Determination of the dissociation equilibria of water by a conductance method, H. C. Duecker and W. Haller, J. Phys. Chem. **66,** No. 2, 225–229 (Feb. 1962).

Heat of formation of the most stable form of metaboric acid, HBO_2(c,I), M. V. Kilday and E. J. Prosen, J. Am. Chem. Soc. Commun. to Editor 82, 550 (1960).

The scientific contributions of William Weber Coblentz, E. K. Plyler, J. Appl. Spect. **16,** No. 3, 73–77 (1962).

The rapid selector and other NBS document retrieval studies, J. L. Pike and T. C. Bagg, Proc. National Microfilm Assoc., Annual Meeting, Wash. D. C., Apr. 25–27, 1962, XI, 213–227 (Annapolis, Md., 1962).

A test method for air-entrainment of standard Ottawa sand, M. R. DeFore and H. J. Corah, ASTM Bull. No. 248, 48–56 (TP162–166) (Sept. 1960).

The angular distribution of beta particles from oriented cerium- 141 nuclei, D. D. Hoppes, Proc. Seventh Inter. Conf. Low Temperature Physics, University of Toronto, Canada, Aug. 1960, p. 186 (University of Toronto Press, Toronto, Canada, 1960).

Die radiometeorologie and ihre bedeutung fur die ausbreitung der m-, dm- and cm- wallen auf grosse entfernungen, B. R. Bean, L. Fehlhaber, and J. Grosskopf, Nachr. Z (NTZ), p. 9–16 (Jan. 1962).

The program at the National Bureau of Standards, L. M. Branscomb, Book, Optical Spectroscopic Measurements High Temperatures, ed. P. J. Dickerman, p. 235 (Univ. of Chicago Press, Chicago, Ill. 1961).

Determination of oxidation rates of air-blown asphalts by infrared spectroscopy, J. R. Wright and P. G. Campbell, J. Appl. Chem. **12,** 256–266 (June 1962)

Study of "valley problem" with a ray tracing program, K. Davies and A. K. Saha, Electron Density Profiles, p. 162–166 (1962).

The extrapolation of the orthorhombic N-paraffin melting properties to very long chain lengths, M. G. Broadhurst, J. Chem. Phys. **36,** No. 10, 2578 (May 15, 1962).

An equation of state for calculating the thermodynamic properties of helium at low temperatures, R. D. McCarty and R. B. Stewart, Book, Progress in International Research on Thermodynamic and Transport Properties, p. 107–117 (Academic Press, Inc., New York, N.Y., 1962).

Oscillatory phenomena, A. H. Kahn (Proc. Conf. High Magnetic Field, Mass. Inst. Tech. Cambridge, Mass., Nov. 1–4, 1961), Book, High magnetic fields, p. 480–488 (Mass. Inst. Tech. Press, Cambridge, Mass., and John Wiley and Sons, Inc., New York, N.Y., 1962).

Thermal expansion of some engineering materials from 20 °K to 293 °K, V. Arp, J. H. Wilson, L. Winrich, and P. Sikora, Cryogenics **3**, 230 (June 1962).

Interlaboratory evaluation of a method for indicated brightness of papers containing fluorescent brighteners, T. W. Lashof and J. M. Patek, Tappi **45,** No. 7, 566 (July 1962).

An intermediate size automatically controlled hydrogen refrigeration system, D. B. Chelton, D. B. Mann, and B. W. Birmingham, Suppl. Bull. Inst. Intern du Froid, Eindhoven, Comm. 1, Annexe 1960–61, 169–178 (1960).

Absolute microwave refractometer, M. J. Vetter and M. C. Thompson, Jr., Rev. Sci. Instr. **33,** 656–660 (June 1962).

The information problem in government, S. N. Alexander, Proc. Engineering Information Symp. (Sponsored by the Engineers Joint Council), p. 15–16 (Jan. 17, 1962).

Problems in the temperature calibration of an X-ray diffractometer furnace, F. A. Mauer and L. H. Bolz, (Proc. Tenth Annual Conf. Applications of X-ray Analysis, Denver, Colo., Aug. 7–9, 1961), Book, Advances in X-ray analysis, p. 229 (Plenum Press, Inc., New York, N.Y., 1962).

The detection and study of solar cosmic rays by radio techniques, D. K. Bailey, (Intern. Conf. on Cosmic Rays and the Earth Storm), J. Phys. Soc. Japan **17,** Suppl. A–1, Pt. I, 106–112 (1962).

Precision and accuracy—experiment design aspects, C. Eisenhart, Conf. on Applications of Statistical Methods in the Chemical Industry, Feb. 4, 1961, (Sponsored by Am. Soc. for Quality Control, Metropolitan Section, Seaton Hall University, South Orange, N.J.), p. (1961).

Games associated with a renewal process, M. M. Siddiqui, Ann. Math. Stat. **33,** 697–701 (June 1962).

Purification and vapor pressure of pure nitric oxide, E. E. Hughes, J. Chem. Phys. Letter to Editor 35, No. 4, 1531–1532 (Oct. 1961).

Ultrasounds induce flaking of ceramics from metals, J. W. Pitts, Metal Progr. **82,** No. 2, 114–115 (Aug. 1962).

Ferroelectricity in the compound $Ba_2Bi_4Ti_5O_{18}$, P. H. Fang and B. Aurivillius, Phys. Rev. **126,** No. 3, 893 (May 1962).

Use of gas phase chromatography for rapid determination of carbonate at low levels, F. G. Carpenter, Anal. Chem. **34,** 66 (Jan. 1962).

An experimental investigation of the scintillation of radio stars observed at frequencies of 223 and 456 megacycles per second from a location close to the auroral zone, C. G. Little, G. C. Reid, E. Stiltner, and R. P. Merritt, J. Geophys. Res. **67,** No. 5, 1763–1784 (May 1962).

A computer for weather data acquisition, P. Meissner, J. A. Cunningham, and C. A. Kettering, Proc. Eastern Joint Computer Conf., Dec. 13–15, 1960, p. 57 (New York, N.Y., 1960).

Position titles of chemists, W. K. Wilson, Capital Chemist **10,** 145 (May 1960).

Corrected calculations of sound absorption in non-associated liquids, R. E. Nettleton, J. Acoust. Soc. Am. **34,** No. 3, 350 (Mar. 1962).

International comparisons of radioactivity standards, W. E. Perry and W. B. Mann, Proc. Ninth Intern. Congress on Radiology, Munich, Germany, July 1959, 23, VII–30. VII, 1338–1342 (Urban and Schwarzenberg, Munich, Germany, 1960).

Criteria for the reality of matrix eigenvalues, M. P. Drazin and E. V. Haynsworth, Z. Math. **78,** 449–452 (Mar. 1962).

A rapid simple method of estimating the order of chemical reactions, J. H. Flynn, Chem. Eng. **69,** No. 17, 137–140 (Aug. 20, 1962).

Paramagnetic resonance phenomena, H. E. Radford, Encyclopaedic Dictionary of Physics **5,** 293 (Pergamon Press Inc., New York, N.Y., 1962).

Chilled-air-distribution in refrigerated trailers, P. R. Achenbach, Suppl. Bull. Intern. Inst. of Refrigeration, p. 9 (1961–1962).

Mass spectrum and appearance potentials of tetrafluorohydrazine, J. T. Herron and V. H. Dibeler, J. Chem. Phys. **33,** No. 5, 1595–1596 (Nov. 1960).

Large longitudinal retarded elastic deformation of rubberlike network polymers, H. Leaderman, J. Polymer Sci. **59,** No. 168, S42 (June 1962).

A survey of polar cap absorption events (solar proton events) in the period 1952 through 1960, D. K. Bailey and J. M. Harrington, (Intern. Conf. on Cosmic Rays and the Earth Storm), J. Phys. Soc. Japan **17,** Suppl. A–II, Pt. II, 334–337 (1962).

Magnifications of a telescope, R. E. Stephens, J. Opt. Soc. Am. **51,** No. 7, 803–804 (July 1961).

Isotope effect in an electric field and jump frequencies for diffusion in ionic crystals, J. R. Manning, J. Appl. Phys. **33,** No. 7, 2145–2151 (July 1962).

Determination of isotope effects by "double labeling" oxidation of d-glucose with iodine, H. S. Isbell, L. T. Sniegoski, and H. L. Frush, Anal. Chem. **34,** No. 8, 982–984 (July 1962).

Methods of nuclear orientation, E. Ambler, Book, Progress in Cryogenics, ed., K. Mendelssohn III, 235–280 (Heywood and Co., Ltd., London, England, 1960).

Molecular collision models and transition probabilities in liquids, R. E. Nettleton, J. Chem. Phys. **38,** 2226–2227 (Apr. 1962).

Electronic development and production in the USSR, C. P. Marsden, Encylcopedia on Russia and the Soviet Union, p. 158–160 (McGraw-Hill Book Co., Inc., New York, N.Y., 1961).

Microwave spectrum of trimethylarsine, D. R. Lide, Jr., Spectrochem. Acta **15,** 473 (1959).

Lattice frequencies and rotational barriers for inorganic carbonates and nitrates, R. A. Schroeder, C. E. Weir, and E. R. Lippincott, J. Chem. Phys. **36,** No. 10, 2803–2804 (May 1962).

Environmental characteristics of a small underground fallout shelter, P. R. Achenbach, F. J. J. Drapeau, and C. W. Phillips, ASHRAE J. **4,** No. 1, 21 (Jan. 1962).

Opportunities in dental research, G. C. Paffenbarger, J. Am. Dental Assoc. **60,** No. 3, 413–414 (Mar. 1960).

On the nature of equatorial slant sporadic E, R. Cohen, K. L. Bowles and W. Calvert, J. Geophys. Res. **67,** No. 3, 965–972 (Mar. 1962).

Elementary statistical design, W. J. Youden, Conf. on Applications of Statistical Methods in the Chemical Industry, Feb. 4, 1961 (Sponsored by Am. Soc. for Quality Control, Metropolitan Section, Seaton Hall University, South Orange, N.J), p. 43 (1961).

Blue-glass filters to approximate the blackbody at 6500° K, D. B. Judd, Farbe **10,** No. 1–4, 31 (1961).

Correction to "doppler studies of the ionosphere with vertical incidence," K. Davies, Proc. IRE **50,** No. 6, 94 (June 1962).

Electron photo-detachment from ions and elastic collision cross sections for O, C, Cl and F, J. W. Cooper and J. B. Martin, Phys. Rev. **126,** No. 4, 1482 (May 15, 1962).

The following articles were presented before the 1961 Cryogenic Engineering Conference and published in the Book, Advances in Cryogenic Engineering **7** (Plenum Press, Inc., New York, N.Y., 1962):

A cryostat for tensile tests in the temperature range 300° to 4° K, R. P. Reed, Paper K–3, 448–454.

A method of measuring shear modulus from −424° to 70° F, R. P. Mikesell and R. M. McClintock, Paper K–11, 509–513.

An electrically controlled guarded flat plate calorimeter, D. Cline and R. H. Kropschot, Paper L–5, 534–538.

An experimental investigation of the individual boiling and condensing heat transfer coefficients for hydrogen, D. E. Drayer and K. D. Timmerhaus, Paper J–6, 401–412.

Dry gas operation of ball bearings at cryogenic temperatures, L. E. Scott, D. B. Chelton, and J. A. Brennan, Paper G–3, 273–276.

Low temperature characteristics of some commercial thermocouples, R. L. Powell and L. P. Caywood, Jr., Paper L–2, 517–521.

Martensitic transformation products and mechanical properties of austenitic stainless steels at low temperatures, C. J. Guntner and R. P. Reed, Paper K–9, 500–502.

On the bulk density of boiling liquid oxygen, R. W. Arnett, Paper F–4, 214–218.

Temperature dependence of magnetic losses, J. J. Gniewek and R. L. Powell, Paper H–1, 303–310.

Testing of ball bearings with five different separator materials at 9200 RPM in liquid nitrogen, J. A. Brennan, W. A. Wilson, R. Radebaugh, and B. W. Birmingham, Paper G–2, 262–272.

The application and behavior of elastomers at cryogenic temperatures, R. F. Robbins, D. H. Weitzel, and R. N. Herring, Paper H–6, 343–352.

The application of gas-lubricated bearings to a miniature helium expansion turbine, B. W. Birmingham, H. Sixsmith, and W. A. Wilson, Paper A–4, 30–42.

The efficiency of an ideal refrigerator, R. B. Jacobs, Paper L–11, 567–571.

Application of reflectometer techniques to accurate reflection measurements in coaxial systems, R. W. Beatty and W. J. Anson, Proc. Inst. Elec. Engr. B, **109,** 345–348 (July 1962).

Chemically induced vibrational excitation: Hydroxyl radical emission in the 1-3-micron region produced by the $H+O_3$ atomic flame, D. Garvin, H. P. Broida, and H. J. Kostkowski, J. Chem. Phys. **37,** No. 1, 193 (July 1962).

Gas-phase radiolysis of propane, P. Ausloos and S. Lias, J. Chem. Phys. **36,** No. 12, 3163–3170 (July 15, 1962).

Four methods for predicting the durability of roofing asphalts, S. H. Greenfeld and J. R. Wright, Mater. Res. Std. **2,** No. 9, 738–745 (Sept. 1962).

The absolute simplest form in digital circuit design, R. S. Ledley, Book, Digital Computers and Control Engineering, 835 pgs., (McGraw-Hill Book Co., Inc., New York, N.Y., 1960).

Coring an electroform, W. H. Metzer, Jr., Plating **49,** No. 8, 880 (Aug. 1962).

The standards challenge, A. H. Scott, Insulation **8,** No. 2, 48–50 (Feb. 1962).

A system for generating "pronounceable" names using a computer, A. L. Leiner and W. W. Youden, J. Assoc. Computing Mach **8,** No. 1, 97–103 (Jan. 1961).

Using digital computers in the design and maintenance of new computers, A. L. Leiner, A. Weinberger, H. Loberman, and C. Coleman, IRE Trans. Electronic Computers **EC–10,** No. 4, 680–690 (Dec. 1961).

Surface preparation of solid metallic samples for X-ray spectrochemical analysis, R. E. Michaelis and B. A. Kilday, Book, Advances in X-ray Analysis **5,** 405–411 (Plenum Press, Inc., New York, N.Y., 1962).

Infrared wavelength dependence of the total absorptivity of electroplated silver, D. Cline, J. Appl. Phys. **33,** 2310–2311 (July 1962).

Simple stain gauge-based load controller, L. Mordfin and R. L. Bloss, Rev. Sci. Instr. **33,** No. 7, 772–773 (July 1962).

Quantum-mechanical calculation of harmonic oscillator transition probabilities. II. Three-dimensional impulsive collisions, F. H. Mies and K. E. Shuler, J. Chem. Phys. **37,** No. 1, 177–181 (July 1, 1962).

Remote phase control of station WWV, R. F. Fey, J. B. Milton, and A. H. Morgan, Nature **193,** No. 4820, 1063–1064 (Mar. 17, 1962).

Melting and contractility of feather keratin, L. Mandelkern, J. C. Halpin, and A. F. Diorio, J. Polymer Sci. Letter to Editor 60, No. 169, S31–S33 (July 1962).

Wave propagation around a curved boundary which contains an obstacle, J. R. Wait, Can. J. Phys. **40,** 1010–1016 (Aug. 1962).

Four-place table decibels return loss to magnitude of voltage reflection coefficient, R. W. Beatty, Microwave Eng. Hanb. & Buyers Guide, p. TD188–192 (Nov. 1961).

Duration and spacing of sferic pulses, R. F. Linfield and C. A. Samson, Proc. IRE **50,** 1841–1842 (Aug. 1962).

VHF and UHF signal characteristics observed on a long knife-edge, A. P. Barsis and R. S. Kirby, IRE Natl. Conv. Record, p. 17–34 (1961).

Some observations on growing crystals of argon, L. H. Bolz, H. P. Broida, and H. S. Peiser, Acta Cryst. **15,** No. 8, 810–812 (Aug. 1962).

Methods and techniques of low and very low frequency monitoring at Boulder Laboratories, A. H. Morgan and D. H. Andrews, Consultative Committee for Definition of the Second Intern. Comm. on Weights and Measures, Apr. 11–12, 1961, p. 1–10 (June 1961).

Insulation resistance measurements, A. H. Scott, Proc. 4th Electrical Insulation Conf., Materials and Application, Wash. D. C., p. 115–117 (Feb. 19–22, 1962).

Physical measurement: Pilot of progress, A. V. Astin, Steel, p. 112 (July 23, 1962).

Some tensile properties of amalgam, M. S. Rodriguez and G. Dickson, J. Dental Res. **41,** No. 4, 840–852 (July–Aug. 1962).

Vacuum photolysis of solid ethane at 77°K, M. D. Scheer, J. McNesby, and R. Klein, J. Chem. Phys. **36,** No. 12, 3504–3505 (June 1962).

Geomagnetic and solar data, J. V. Lincoln, J. Geophys. Res. **67,** No. 5, 2035–2038 (May 1962).

A study of the chemical and physical properties of magnetic recording tape, F. Nesh and R. F. Brown, Jr., IRE Trans. Audio **AU–10,** No. 3, 70–71 (May–June 1962).

Supporting evidence for solar flare effects in the F region of the ionosphere, R. W. Knecht and K. Davies, Nature **192,** No. 4800, 348–350 (Oct. 28, 1961).

Measurement of effect of moisture on heat transfer through insulated flat-roof constructions, F. J. Powell and H. E. Robinson, Am. Soc. Testing Materials Spec. Tech. Publ. **312,** 35–66 (1961).

Dependence of interval between flare and associated sudden commencement storm on prestorm conditions, M. W. Haurwitz, J. Geophys. Res. Letter **67,** 2979–2982 (July 1962).

The application of NMR in determination of the structure of cyclanols. I. The structures of cyclohexane-1,3-diols, H. Finegold and H. Kwart, J. Organic Chem. **27,** 2361–2365 (1962).

APPA–TAPPI reference material program. I. Interlaboratory investigation of TAPPI standard T 414 m-49, internal tearing resistance of paper, T. W. Lashof, Tappi **45,** No. 8, 656 (1962).

Spectrophotofluorometric studies of degraded cotton cellulose, S. D. Toner and K. F. Plitt, Tappi **45,** No. 8, 681–688 (Aug. 1962).

Algorithm and rapid binary division, R. S. Ledley and J. B. Wilson, IRE Trans. Electronic Computers **EC–10,** No. 4, 662–670 (Dec. 1961).

Properties of dental amalgams made from spherical alloy particles, N. C. Demaree and D. F. Taylor, J. Dental Res. **41,** No. 4,890–906 (July–Aug. 1962).

Emission spectra of solids condensed at very low temperatures from the electrical discharge products of nitrogen and carbon monoxide or acetylene, S. L. N. G. Krishnamachari, R. W. Nicholls, and H. P. Broida, Proc. Indian Acad. Sci. **LIV,** 61–68 (1961).

Excitation of the red and green coronal lines, C. Pecker and R. N. Thomas, Ann. Astrophys. **25,** 100–108 (Mar.–Apr. 1962).

Dependence of the ionospheric F. region on the solar cycle, J. W. Wright, Nature **194,** No. 4827, 461–462 (May 1962).

Fast-melting alloy forms water jacket for small klystrons, W. J. Anson and E. Niesen, Electron. Design, p. 42–45 (Mar. 1962).

Boolean matrix equations in digital circuit design, R. S. Ledley, IRE Trans. Electronic Computers **EC–8,** No. 2, 131–139 (June (1959).

**Publications for which a price is indicated are available from the Superintendent of Documents, U.S. Government Printing Office, Washington 25, D.C. (foreign postage one-fourth additional). Reprints from outside journals or the NBS Journal of Research may often be obtained from the authors.*

U.S. GOVERNMENT PRINTING OFFICE: 1963

UNIVERSITY MICROFILMS
313 NORTH FIRST STREET
ANN ARBOR, MICHIGAN
SJR-A-OCT

UNITED STATES
GOVERNMENT PRINTING OFFICE
DIVISION OF PUBLIC DOCUMENTS
WASHINGTON 25, D.C.

OFFICIAL BUSINESS

PENALTY FOR PRIVATE USE TO AVOID PAYMENT OF POSTAGE, $300 (GPO)

JOURNAL OF RESEARCH of the National Bureau of Standards Vol. 67A, No. 1 January–February 1963
A. Physics and Chemistry

Contents

Page

Heat of formation of calcium aluminate monosulfate at 25 °C. H. A. Berman and E. S. Newman. 1

2,3-Dimethylpentane and 2-methylhexane as a test mixture for evaluating highly efficient fractionating columns. Edwin C. Kuehner. 15

Phase equilibrium relations in the Sc_2O_3-Ga_2O_3 system. S. J. Schneider and J. L. Waring. 19

Analysis of two infrared bands of CH_3D_3. Wm. Bruce Olson, Harry C. Allen, Jr., and Earle K. Plyler. 27

Precise coulometric titrations of halides. George Marinenko and John K. Taylor. 31

Radial distribution study of vitreous barium borosilicate. G. J. Piermarini and S. Block. 37

Dynamic compressibility of poly(vinyl acetate) and its relation to free volume. John E. McKinney and Harriet Vera Belcher. 43

An investigation of the constitution of the mercury-tin system. Duane F. Taylor and Claire L. Burns. 55

Effect of methyl bromide additions on the flame speed of methane. Carl Halpern. 71

Publications of the National Bureau of Standards. 79

For sale by the Superintendent of Documents, U.S. Government Printing Office, Washington 25, D.C. Price 70 cents (single copy)
Subscription price: $4 a year; 75 cents additional for foreign mailing.
UNITED STATES GOVERNMENT PRINTING OFFICE, WASHINGTON : 1963

6